p75 Neurotrophin Receptor Modulates the Development and Post-Infarct Remodeling of Cardiac Sympathetic Neurons

By

Christina U. Lorentz

A DISSERTATION

Presented to the Department of Physiology & Pharmacology
and the Oregon Health and Science University
School of Medicine
In partial fulfillment of
the requirements for the degree of

Doctor of Philosophy

April 2010

School of Medicine

Oregon Health & Science University

CERTIFICATE OF APPROVAL

This is to certify that the Ph.D. dissertation of

Christina U. Lorentz

has been approved

_____
Mentor/ Advisor: Beth A. Habecker, Ph.D.

_____
Committee Chair/ Member: Virginia Brooks, Ph.D

_____
Member: Pamela Lein, Ph.D

_____
Member: Philip Stork, M.D.

_____
Member: Sue Aicher, Ph.D

_____
Member: Michael Andresen, Ph.D.

TABLE OF CONTENTS

List of figures ……v

List of abbreviations……x

Acknowledgements xiii

Abstract……1

Chapter 1: Background and Introduction……3

I. Introduction……3

II. Neurotrophins and the Development of the Sympathetic Nervous System……..4

A. History……4

1. The Discovery of Nerve Growth Factor……4

2. The Neurotrophic Factor Hypothesis……7

B. The Neurotrophins……..8

C. Neurotrophin Receptors……9

1. The Neurotrophin Receptors: Binding and Affinity……9

2. Trk Signaling……..12

2.1. TrkA Signaling in Neuron Survival and Axon Outgrowth……..13

3. p75NTR Signaling……17

3.1. p75NTR and Cell Death……18

3.2. p75NTR and Axon Outgrowth……22

D. Development of the Sympathetic Nervous System……..27

1. *The Neural Crest and Early Sympathetic Development*……..27

2. *Sympathetic Target Innervation*……..30

3. *Patterning of Cardiac Sympathetic Innervation*……..34

III. Cardiac Anatomy, Function and Innervation……35

A. Anatomy of the Heart……35

B. Basic Cardiac Function……39

1. *The Heart as a Pump*……...39

2. *The Cardiomyocyte*……...39

3. *Cardiac Electrical Conduction and the ECG*……41

3.1. Cardiac Action Potentials……....41

3.2. The Intrinsic Cardiac Conduction System……43

3.3. The Electrocardiogram (ECG)……44

4. *Excitation-Contraction Coupling*……46

5. *Cardiac Muscle Cell Mechanics*……48

6. *Cardiac function*……53

C. Innervation of the Heart……57

1. *Autonomic Innervation of the Heart*……..58

2. *Sensory Cardiac Innervation*……...60

3. *Autonomic Neurotransmission*……...61

D. Autonomic Regulation of Cardiac Function……..64

1. *Chronotropy*……..64

2. *Inotropy*……..66

3. *Lusitropy*……68

4. *Dromotropy*……69

IV. Sympathetic Remodeling after Myocardial Infarction……70

A. Post-MI Cardiac Remodeling and Heart Failure……70

B. Post-MI Sympathetic Remodeling and Ventricular Arrhythmias……...72

C. Molecular Mechanisms Underlying Sympathetic Remodeling……...76

V. Purpose of Thesis, Hypothesis, and Summary of Results.....79

Chapter 2: Manuscript 2: Cardiac sympathetic denervation after myocardial infarction is mediated by p75NTR……81

Chapter 3: Manuscript 1: Heterogeneous ventricular sympathetic innervation, altered β-adrenergic receptor expression, and rhythm instability in mice lacking the p75 neurotrophin receptor……110

Chapter 4: Summary and Discussion……...143

A. Summary of Results……143

B. The Many Roles of p75NTR in Development and Disease……...146

1. *The Role of p75NTR is Context Dependent*……146

2. *p75NTR, Cardiac Sympathetic Heterogeneity, and Arrhythmias*……148

3. *p75NTR in Disease and Injury-Related Neuroplasticity* ……151

4. *Clinical Considerations*……...153

C. Limitations and Future Directions……...155

D. Concluding Remarks……..……159

Chapter 5: Detailed Methods……....160

Chapter 6: Appendices……181

References……196

LIST OF FIGURES

Chapter 1: Background and Introduction

Fig. 1.1: NGF induces axon outgrowth……6

Fig. 1.2: Neurotrophin- neurotrophin receptor interactions……11

Fig. 1.3: Trk receptor signaling……14

Fig. 1.4: p75NTR receptor signaling……20

Fig. 1.5: The many interaction partners of p75NTR……25

Fig. 1.6: Sympathetic neurons are derived from the neural crest……28

Fig. 1.7: Development of sympathetic neurons……...29

Fig. 1.8: Sympathetic innervation of the heart……32

Fig. 1.9: Anatomy of the heart……36

Fig. 1.10: Cardiac conduction system……...38

Fig. 1.11: The structure of the sarcomere……40

Fig. 1.12: The cardiomyocyte action potential……42

Fig. 1.13: ECG: normal sinus rhythm……45

Fig. 1.14: Excitation-contraction coupling……47

Fig. 1.15: Length-tension relationship for an isometric contraction……..49

Fig. 1.16: Length-tension relationship for an isotonic contraction……50

Fig. 1.17: Length-tension relationship for an afterloaded contraction……51

Fig. 1.18: Relationship between muscle length-tension and cardiac pressure-volume loops……55

Fig. 1.19: The effect of afterload and preload on cardiac function……56

Fig. 1.20: Autonomic innervation of the heart……59

Table 1.1: Adrenergic receptors……63

Fig. 1.21: Autonomic influence of heart rate……...65

Fig. 1.22: Sympathetic influence of contractility……67

Fig. 1.23: Affect of sympathetic blockade on ventricular arrhythmias after MI……74

Fig. 1.24: Factors that conrtibute to arrhythmias after MI……77

Chapter 2: Manuscript 1

Table 2.1: Ventricular sympathetic innervation density 3 days and 7 days after MI……...99

Fig. 2.1: Infarct size compared with area at risk is not different between WT and p75NTR-/- mice……100

Fig. 2.2: Method for sympathetic innervation density quantification.....101

Fig. 2.3: Sympathetic innervation density of the infarct 24h, 3d, and 7d after ischemia-reperfusion……..103

Fig. 2.4: Sympathetic innervation density of the peri-infarct region 24h after ischemia-reperfusion……...104

Fig. 2.5: Sympathetic innervation density of the peri-infarct region 3d after ischemia-reperfusion……..106

Fig. 2.6: Sympathetic innervation density of the peri-infarct region 7d after ischemia-reperfusion……108

Fig. 2.7: BDNF protein is elevated in the left ventricle 24

hours after ischemia/ reperfusion……..……...109

Chapter 3: Manuscript 2

Table 3.1: Left ventricular size and function……...133

Fig. 3.1: Fiber distribution is altered in the p75NTR-/- left Ventricle……..…..134

Fig. 3.2: Innervation density is normal in the p75NTR-/- Subepicardium……..136

Fig. 3.3: p75NTR-/- sympathetic axons are more sensitive to sema3a growth cone collapse/inhibition……..137

Fig. 3.4: p75NTR−/− mice have increased spontaneous ventricular arrhythmias……138

Fig. 3.5: dP/ dt_{MAX} and dP/dt_{MIN} are low in p75NTR-/- mice……..139

Fig. 3.6: p75NTR-/- mice have enhanced response to β_1AR stimulation in the denervated subendocardium……...140

Fig. 3.7: β_1AR expression is low and distribution is altered in the p75NTR-/- left ventricle……..…..141

Fig. 3.8: NE content, NE uptake and TH levels in the left ventricle……142

Chapter 4: Summary of Results and Conclusions:

Fig. 4.1: Summary and model for the role of p75NTR in sympathetic remodeling after myocardial infarction……144

Chapter 5: Detailed Methods

Fig. 5.1: Dissection of the heart for HPLC and Western analysis…….....163

Fig. 5.2: Ischemia-reperfusion surgery: surgical preparation and needle pass……..170

Fig. 5.3: Ischemia-reperfusion surgery: occlusion and reperfusion……..……171

Fig. 5.4: Representative left ventricular pressure and heart rate traces……...176

Table 5.1: Primary antibodies used in immunoblot and immunohistochemistry……180

Chapter 6: Appendices

Table A.1: Post-MI ventricular arrhythmias under isoflurane (3d post-MI)……..182

Table A.2: Post-MI ventricular arrhythmias under isoflurane (7d post-MI)……183

Fig. B.1: Left ventricular peak systolic pressure (LVP) 3 days after ischemia-reperfusion from WT p75NTR-/- mice……185

Fig. B.2: Left ventricular peak systolic pressure (LVP) 7 days after ischemia-reperfusion from WT p75NTR-/- mice……....186

Fig. B.3: dP/dt_{MAX} 3 days after ischemia-reperfusion from WT and p75NTR-/- mice……187

Fig. B.4: dP/dt_{MAX} 7 days after ischemia-reperfusion

from WT and p75NTR-/- mice……188

Fig. B.5: dP/dt_{MIN} 3 days after ischemia-reperfusion

from WT and p75NTR-/- mice……189

Fig. B.6: dP/dt_{MIN} 7 days after ischemia-reperfusion

from WT and p75NTR-/- mice……190

Fig. C.1: Norepinephrine (NE) content in the left ventricle of WT and

p75NTR-/- mice 3 and 7 days after ischemia-reperfusion……...193

Fig. C.2: Norepinephrine (NE) content in the right ventricle of WT and

p75NTR-/- mice 3 and 7 days after ischemia-reperfusion…….194

Fig. C.3: Norepinephrine (NE) content in the base of WT and

p75NTR-/- mice 3 and 7 days after ischemia-reperfusion…….195

LIST OF ABBREVIATIONS

α_1AR	alpha-adrenergic receptor
ACh	acetylcholine
AV	atrioventricular
BCL2	B-cell lymphoma 2
BDNF	brain derived neurotrophic factor
βAR	beta-adrenergic receptor
BMP	bone morphogenetic protein
cAMP	cyclic adenosine monophosphate
CREB	cyclic-AMP responsive element binding protein
CO	cardiac output
DAG	diacyl glycerol
DBH	dopamine-beta-hydroxylase
dHAND	heart and neural crest derivatives 2
ECG	electrocardiogram
ERK	extracellular signal-regulated kinase
GATA2	GATA binding protein 2
HA	hemagglutanin
HR	heart rate
IP_3	inositol-(1,4,5) triphosphate
IVS	interventricular septum
JNK	c-Jun N-terminal kinase

LA	left atria
LAD	left anterior descending coronary artery
LV	left ventricle
LVEF	left ventricular ejection fraction
LVIDs	left ventricular internal diameter in systole
LVIDd	left ventricular internal diameter in diastole
LVPSP	left ventricular peak systolic pressure
mAChR	muscarinic acetylcholine receptor
MAPK	mitogen activated protein kinase
MASH1	mammalian achaete scute homolog 1
MEK	MAP and ERK kinase kinase
MI	myocardial infarction
nAChR	nicotinic acetylcholine receptor
NE	norepinephrine
NGF	nerve growth factor
NP1	neuropillin 1
NRIF	neurotrophin receptor interacting factor
NT-3	neurotrophin 3
NT-4/5	neurotrophin 4/5
p75NTR	p75 neurotrophin receptor
$p75NTR_{icd}$	p75 neurotrophin receptor intracellular domain
PI3K	phosphoinositide-3-kinase
PKA	protein kinase A

PKB	protein kinase B (Akt)
PKC	protein kinase C
PLCγ	phospholipase C gamma
PVC	premature ventricular complex
RA	right atria
RhoGDI	Rho GDP-dissociation inhibitor
RV	right ventricle
RyR	ryanadine receptor
SA	sinoatrial
Sema3a	semaphorin3a
SERCA	sarco/endoplasmic reticulum $Ca^{2=}$-ATPase
SG	stellate ganglia
SH2	Src homology 2
STAT3	signal transducer and activator of transcription 3
SV	stroke volume
TH	tyrosine hydroxylase
TNFα	tumor necrosis factor
TRAF6	TNF receptor associate factor 6
Trk	tropomyosin-related kinase

Acknowledgements:

I would like to thank the members of my Thesis Advisory Committee/ Exam Committee for their tremendous support and guidance over the years and for sharing their expertise: Dr. Pamela Lein, Dr. Virginia Brooks, Dr. Phil Stork, Dr. Sue Aicher. I would also like to thank Dr. Michael Andresen for his willingness to join my Thesis Exam Committee.

Most especially I would like to thank my mentor Dr. Beth Habecker for guiding me through these formative years of scientific development. In particular, I would like to thank her for her endless patience and kindness during the numerous counseling sessions in which she listened and provided much needed reassurance and advice. I also thank her for reading the countless drafts of poorly written manuscripts and never once complaining. I am extremely grateful to have had her as a mentor.

I have been extremely fortunate to work with so many wonderful people. I would very much like to thank the members of the Habecker Lab, past and present, for providing a work atmosphere that was not only supportive, but enjoyable, even when the science wasn't. I thank you for the lively and helpful discussions and the endless entertainment. I would like to extend special thanks to Diana Parrish who has been the best colleague and friend one could ask for. Thank you for all your help and support, both scientific and emotional, throughout the years. I hope to provide you with the same support and friendship during your time as a graduate student as you have done for me. To my fellow graduate student Xiao Shi, we have traveled this road side by side, and now we

finally see that pigs *can* fly! Many thanks also goes to Eric Alston who put a great deal of work and effort into many of the experiments in this thesis.

I am fortunate to be a member of the best class to ever pass through OHSU, the PMCB matriculating class of 2004. This journey would not have been the same without you. I thank you for your endless support and friendship and look forward to sharing future scientific endeavors (and laughs) with one another! In particular, I would like to thank my fellow PH^2 graduate students Kirsten Verhein and Thomas Keck for all their encouragement, hugs, and coffee. Special thanks also go to Chantelle Rein, Annie Powell, and Carole Kuehl. I would especially like to thank Deanne Tibbitts for the countless times she listened as I cried on her shoulder and for supporting me in my attempt to remove my inner thorn.

I would like to extend my most heartfelt thanks to my Portland family, Bridget Robinson and Dustin Johnsen. Your love, friendship, and support has changed me and made me a better person. Thank you for making me laugh until my belly ached. Thank you for holding me up when I could not stand on my own. Thank you for loving me just as I am.

Lastly, I would like to thank my family without whom this would not have been possible. To my brother Marc Lorentz: Thank you for reminding me to breathe and stay grounded and for teaching me to live in the moment. Finally I would like to thank my parents, James and Hilde Lorentz for their unconditional love and support. They are an inspiration to me and their influence has made me the person I am today. They believed in me even when I did not believe in

myself and always encouraged me to follow my dreams. I dedicate this “little paper” to them.

Abstract:

Each year approximately 1.2 million Americans suffer from a myocardial infarction (MI). The most common complication facing patients that survive myocardial infarction is the development of ventricular arrhythmias and sudden cardiac death. Over the last 30 years remodeling of the sympathetic nervous system has emerged as a major factor contributing to post-MI arrhythmias and sudden cardiac death. In particular, regions of sympathetic hyperinnervation and denervation occur in the viable myocardium beyond the infarcted area, resulting in sympathetic heterogeneity and non-uniform transmission to the heart. While elevated nerve growth factor is implicated in sympathetic hyperinnervation, the mechanisms underlying denervation are unknown. Recent studies show that direct activation of the p75 neurotrophin receptor (p75NTR) by brain derived neurotrophic factor (BDNF) causes axon degeneration of sympathetic neurons *in vitro* and *in vivo*. BDNF mRNA is transiently upregulated after MI. Therefore, I hypothesized that sympathetic denervation occurs through p75NTR.

In the first part of my thesis, I asked whether p75NTR was required for denervation of the viable myocardium adjacent to the infarct (the peri-infarct region) using mice that lack p75NTR (p75NTR-/-). Experiments described in Chapter 2 showed that sympathetic denervation occurred in the peri-infarct region adjacent to the infarct in congenic wildtype mice but not in the p75NTR-/- mice. I also determined that BDNF protein is elevated in the left ventricle after ischemia-reperfusion implicating it as a possible ligand for p75NTR-mediate sympathetic axon degeneration. In addition I found that sympathetic

hyperinnervation was exacerbated in p75NTR-/- mice after ischemia-reperfusion. These results suggest that p75NTR plays multiple roles in the development of sympathetic heterogeneity after MI by mediating denervation and attenuating hyperinnervation.

In the process of performing the experiments outlined above, I discovered an altered pattern of sympathetic innervation of the p75NTR-/- left ventricle in the absence of MI (Chapter 3). Sympathetic fibers were confined to the subepicardium of the left ventricle, and the subendocardium was virtually devoid of sympathetic innervation. I determined that this altered pattern of sympathetic innervation was likely due to enhanced repulsion by semaphorin3a in the absence of p75NTR. Finally, I went on to determine that the altered pattern of sympathetic innervation had functional consequences. While cardiac hemodynamics were generally unaffected, p75NTR-/- mice showed a significantly higher incidence of premature ventricular complexes. In summary, the data presented in this thesis identify p75NTR as an important mediator of cardiac sympathetic innervation pattern during development and in sympathetic remodeling after MI.

Chapter 1

Background and Introduction

I. Introduction

Cardiovascular disease is the number one cause of death worldwide (WHO, 2009). In the United States, it affects one in three Americans and is also the leading cause of death (AHA, 2009). Of those with cardiovascular disease, the American Heart Association estimates that each year approximately 1.2 million Americans suffer from a myocardial infarction (MI). Of these myocardial infarctions approximately 785,000 will be new attacks and approximately 470,000 recurrent attacks (AHA, 2009). Although treatment of myocardial infarction has improved greatly, approximately half of the people who suffer from MI die (NHLBI, 2008). Those that survive remain at substantial risk for further complications. The most common complication facing patients that survive myocardial infarction is the development of ventricular arrhythmias and sudden cardiac death, claiming roughly 300,000 lives in the U.S. annually (Solomon et al., 2005). Research over the last two decades strongly implicates the sympathetic nervous system in the development of these post-MI ventricular arrhythmias. In particular, substantial evidence suggests that changes in sympathetic innervation pattern and density, which result in sympathetic heterogeneity, are largely responsible for post-MI ventricular arrhythmias (Rubart and Zipes, 2005). However, the molecular basis underlying the development of sympathetic heterogeneity is not well understood. This dissertation will focus on

the role of the p75 neurotrophin receptor (p75NTR) in the establishment of sympathetic innervation of the heart and sympathetic remodeling after myocardial infarction.

II. Neurotrophins and the Development of the Sympathetic Nervous System:

Neurotrophins are a class of polypeptides that were identified as survival, or trophic, factors for many different types of neurons, including sympathetic neurons. Much of what is known about neurotrophins and their receptors comes from developmental studies of the sympathetic and sensory nervous systems. These early studies were instrumental in establishing the role of neurotrophins in neuron survival and axon outgrowth. Their role, however, is continuously expanding and it is now well accepted that they are not only critical for development, but that they also play major roles in maintenance of neuronal function, plasticity, and repair in response to injury.

A. History

1. The Discovery of Nerve Growth Factor:

The history of neurotrophins began roughly 60 years ago, in the late 1940s, with the observation that altering the size of a neuronal target had a direct effect on the size of the ganglia of the innervating neurons (Hamburger and Levi-Montalcini, 1949). Around the same time, Elmer Bueker, a former student of Viktor Hamburger at Washington University in Saint Louis, MO, made the

unexpected discovery that transplantation of a mouse sarcoma into a 3-day chick embryo resulted in growth of sensory fibers into the neoplastic tissue and a slight but consistent increase in the size of the dorsal root ganglia compared to that of the control side (Bueker, 1948). Rita Levi-Montaclini and Viktor Hamburger further investigated this phenomenon by daily monitoring of serial sections of embryos that had been implanted with the mouse sarcoma and found that sympathetic fibers also entered the neoplastic tissue, as well as sensory fibers, at a very high density (Levi-Montalcini, 1952). Additionally, the sensory and sympathetic ganglia that innervated the tumor progressively grew larger and larger with time, the sympathetic ganglia reaching a size that was six times larger than control ganglia (Levi-Montalcini and Hamburger, 1951; Levi-Montalcini, 1952). The subsequent discovery that all sympathetic chain ganglia were enlarged whether they were adjacent to or came into direct contact with the implanted tumor led Levi-Montalcini and Hamburger to the hypothesis that the tumor cells were releasing a soluble, diffusible agent that was inducing these dramatic changes in sensory and sympathetic neurons (Levi-Montalcini, 1952).

Levi-Montalcini confirmed the presence of the yet unidentified soluble tumor agent in the laboratory of Professor Carlos Chagas at the University of Brazil in Rio de Janeiro by performing explant co-culture experiments with embryonic chick explants in close proximity to, but not contacting, pieces of mouse sarcoma tumors. After 24 hours in culture, both sensory and sympathetic ganglia produced a halo of neurites growing in the direction of the tumor

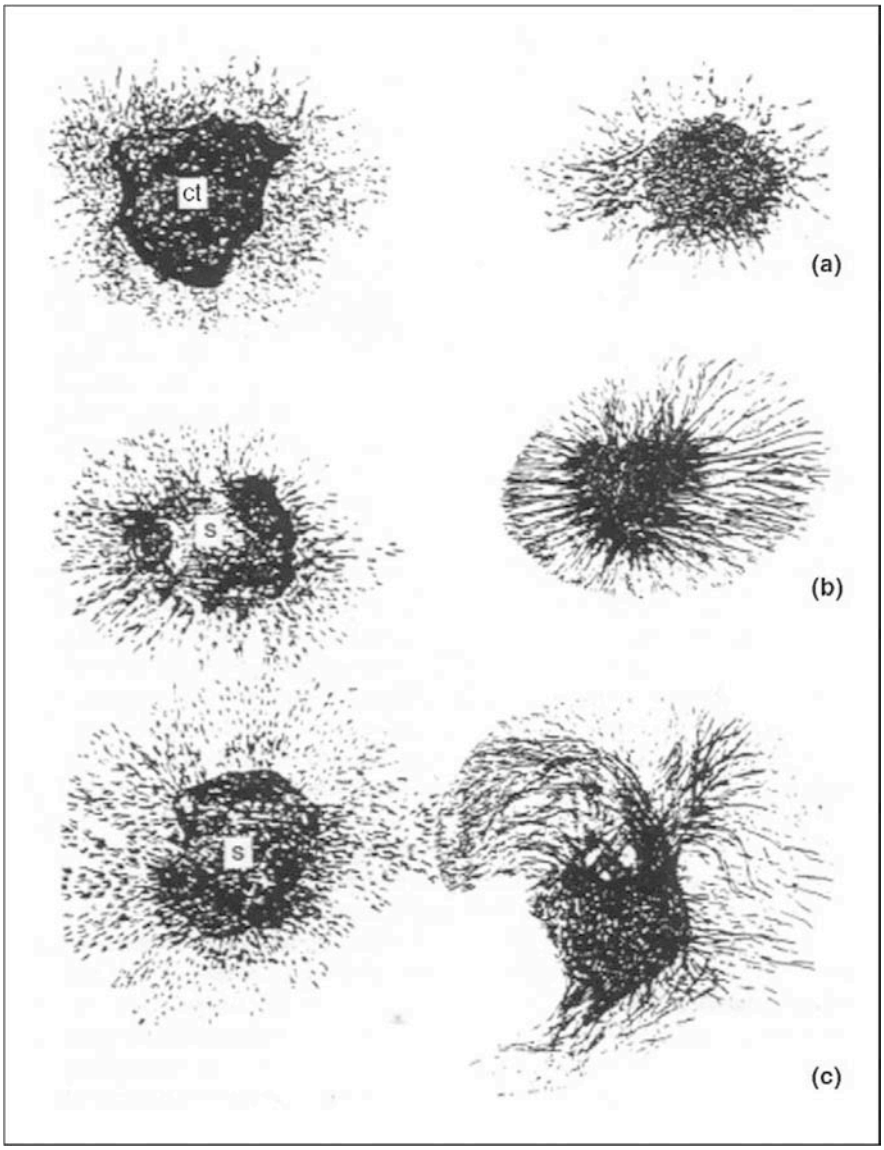

Reprinted from *Trends Cell Biol*: 14 (7) 395-9, Aloe, L. "Rita Levi-Montalcini: the discovery of nerve growth factor and modern neurobiology." 2004, with permission from Elsevier.

Figure 1.1: Nerve growth factor induces axon outgrowth. Sketches of embryonic chick sensory ganglia (right) co-cultured with a) chick embryonic tissue (ct, on left), b) mouse sarcoma for 24 hours, and c) mouse sarcoma for 48 hours. Neurite outgrowth was seen only when ganglia were co-cultured with the mouse sarcoma, later found to contain nerve growth factor.

fragments (Fig 1.1) (Levi-Montalcini et al., 1954). With the help of Stanley Cohen, this soluble "nerve growth factor" was isolated first from the mouse sarcomas (Cohen et al., 1954), followed by snake venom (Cohen and Levi-Montalcini, 1956; Levi-Montalcini and Cohen, 1956), and then from mouse submandibular salivary gland (Cohen, 1960). This identification and isolation of nerve growth factor (NGF) fifty years ago not only revealed the ability of developing neurons to respond to their environment, but also became the pivotal discovery in our understanding of neuronal survival, development and plasticity.

2. The Neurotrophic Factor Hypothesis:

The relationship between the neuronal target size and degree of innervation had already been established before the identification and isolation of NGF. In the late 1940s, Viktor Hamburger and Rita Levi-Montalcini found that removal of a neuronal target, in this case a chick limb bud, resulted in significant reduction of the innervating sensory ganglia. In contrast, addition of a limb bud increased the size of the sensory ganglia, implicating the target tissue as an important regulator in neuronal development (Hamburger and Levi-Montalcini, 1949). A "metabolic exchange between the neurite and the substrate in which it grows" was proposed to explain these data (Hamburger and Levi-Montalcini, 1949). With the discovery of NGF, the "metabolic exchange" was identified and the neurotrophic factor hypothesis emerged. It states that targets of neuronal innervation secrete limiting amounts of survival factors, which function to balance the number of innervating neurons with the size of a target tissue (Korsching and Thoenen, 1983). Therefore, neurons that encounter sufficient survival factor, or

neurotrophins, survive whereas neurons that do not undergo programmed cell death. The neurotrophic factor hypothesis is the basis for proper target innervation by the sympathetic nervous system as well as for most peripheral neurons.

B. The Neurotrophins

Since the discovery of NGF, four additional mammalian neurotrophins have been discovered: brain derived neurotrophic factor (BDNF) (Barde et al., 1982), neurotrophin-3 (NT-3) (Hohn et al., 1990), and neurotrophin-4/5 (NT-4/5) (Berkemeier et al., 1991; Hallbook et al., 1991). Neurotrophins are important for the development of the nervous system and have been identified as critical promoters of neuronal survival, differentiation, target innervation, and plasticity (Chao, 2003; Lu et al., 2005). The biochemical characteristics of the neurotrophins are similar and accordingly, the mature neurotrophins share about 50% sequence homology and are highly conserved across species (Lewin and Barde, 1996). Neurotrophins are secreted proteins that dimerize via highly conserved hydrophobic regions containing cysteine residues. These cysteine residues form “cysteine knot” motifs with other neurotrophin monomers and facilitate homodimerization (McDonald and Blundell, 1991; McDonald and Hendrickson, 1993).

All neurotrophins are synthesized as precursor proteins, or pro-neurotrophins (30-35kDa), which are then cleaved to their mature forms (12-13 KDa). The prodomain is important for proper protein folding and trafficking of

neurotrophins (Chao, 2003) and for many years pro-neurotrophins were thought to be biologically inactive. Pro-neurotrophins are now known to not only bind neurotrophin receptors, but to have very distinct and important biological roles as well (Lu et al., 2005). Some of the activities of the pro-neurotrophins will be discussed further in the next sections.

C. Neurotrophin Receptors:

Neurotrophins bind two structurally distinct receptors: the tropomyosin-related kinase (Trk) receptors and the p75 neurotrophin receptor (p75NTR). Although p75NTR was the first neurotrophin receptor to be discovered (Johnson et al., 1986; Radeke et al., 1987), the Trk receptors mediate the classic cell survival and axon outgrowth effects of neurotrophins (Chao, 2003). p75NTR, on the other hand, can modulate binding of neurotrophins to Trk receptors and downstream signaling, as well as signal independently (Hempstead, 2002; Reichardt, 2006).

1.The Neurotrophin Receptors: Binding and Affinity:

The Trks are a family of receptor tyrosine kinases that are the critical receptors involved in neurotrophin-induced survival and axon outgrowth of neurons (Chao, 2003). The members of the Trk receptor family include TrkA, TrkB, and TrkC (Chao, 2003). TrkA was the first of the Trk receptors to be identified and it received its name from the oncogene derived from a cancer cell line that led to its discovery (Martin-Zanca et al., 1986; Martin-Zanca et al., 1989). Trk receptors consist of an extracellular binding domain, a single

transmembrane domain, and an intracellular tyrosine kinase domain (Campenot, 1994; Reichardt, 2006). For the most part, the Trk receptors selectively bind a single neurotrophin. For example, TrkA selectively binds NGF, TrkB selectively binds BDNF/ NT-4 and TrkC selectively binds NT-3 (Chao, 2003; Reichardt, 2006) (Fig 1.2). Neurotrophins bind their respective Trk receptors with an affinity ranging from 10^{-9} M (Hempstead et al., 1991; Kaplan et al., 1991) to 10^{-10} M (Jing et al., 1992; Klein et al., 1991). Because Trk receptors were reported to bind NGF at higher affinities than p75NTR, they have been termed the "high-affinity" neurotrophin receptors (Chao and Hempstead, 1995). In general, neuronal expression of different Trk receptors determines responsiveness to a particular neurotrophin.

p75NTR was the first neurotrophin receptor to be discovered (Johnson et al., 1986; Radeke et al., 1987) and is expressed at much higher levels than the Trk receptors (Chao and Hempstead, 1995). p75NTR is a member of the TNFα superfamily and its structure consists of an extracellular domain containing four cysteine-rich domains, a single transmembrane domain, and an intracellular domain that, like other members of the TNFα superfamily, contains a death domain (Blochl and Blochl, 2007; Reichardt, 2006). Unlike the Trk receptors, p75NTR binds all neurotrophins with equal affinity (K_D= 10^{-9} M) (Rodriguez-Tebar et al., 1990) and is often called the "low affinity" neurotrophin because it binds neurotrophins with a lower affinity than the Trk receptors. However, p75NTR can interact with Trk receptors to form a high-affinity Trk binding site that binds neurotrophins with an affinity of 10^{-11} M (Hempstead et al., 1991). This occurs

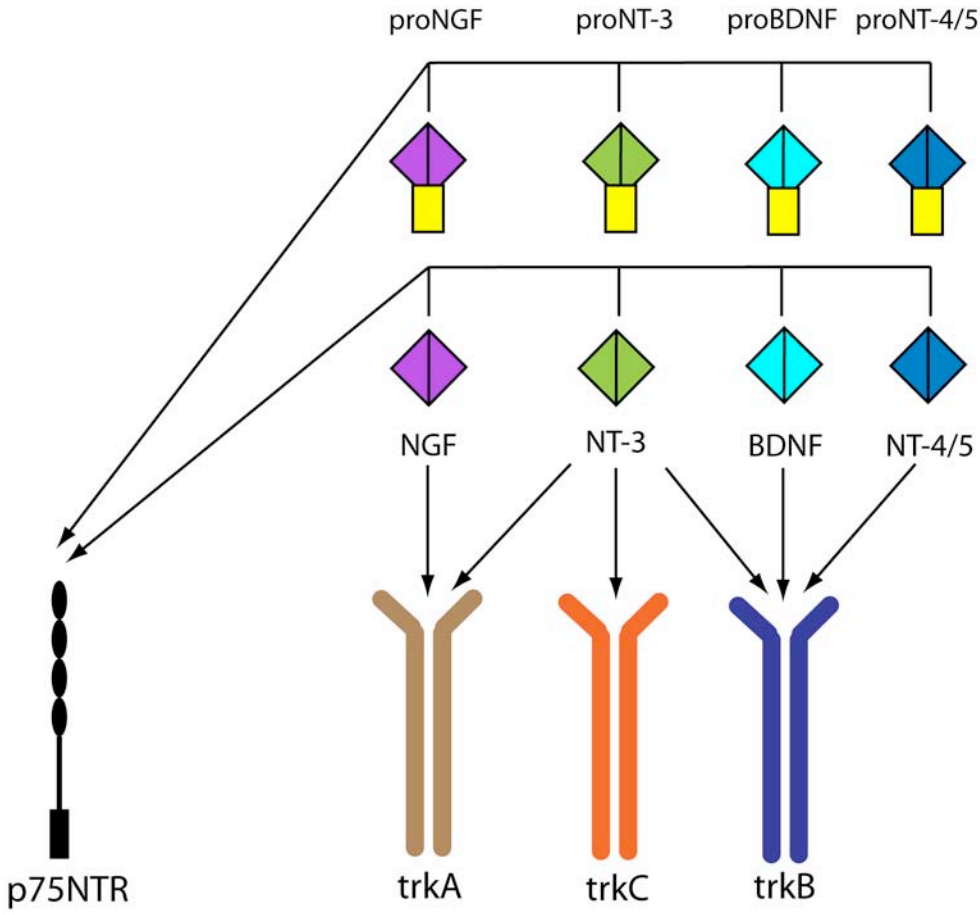

Figure 1.2: Neurotrophin- neurotrophin receptor interactions. Pro-neurotrophins (pro-NGF, pro-BDNF, pro-NT-3, pro-NT-4/5) all bind p75NTR but do not bind Trk receptors. The mature neurotrophins (NGF, BDNF, NT-3, NT-4/5) all bind p75NTR with similar affinity. Each neurotrophin preferentially binds a Trk receptor: NGF preferentially binds TrkA, BDNF and NT-4/5 preferentially bind TrkB, and NT-3 preferentially binds TrkC. However, NT-3 can also bind TrkA and TrkB with lower affinity.

sthrough interaction of p75NTR with Trk receptors at their transmembrane and intracellular domains (Esposito et al., 2001). Recent studies reveal that p75NTR also serves as the preferred receptor for the pro-neurotrophins and binds all pro-neurotrophins with higher affinity than the mature neurotrophins (Lee et al., 2001).

p75NTR interaction with Trk receptors can also modulate the selectivity of Trk receptors for neurotrophins. When p75NTR is present, binding of neurotrophins to Trk receptors becomes restricted. For example, although NGF is the preferred ligand for TrkA, NT-3 can also bind and activate TrkA (Belliveau et al., 1997; Brennan et al., 1999; Davies et al., 1995), but this can only occur when p75NTR is absent. Once p75NTR is co-expressed with TrkA, binding to TrkA is restricted to NGF and NT-3 can no longer bind (Belliveau et al., 1997; Brennan et al., 1999; Kuruvilla et al., 2004). The ability of p75NTR to modulate binding and affinity of neurotrophins to Trk receptors is not restricted to TrkA, but occurs for TrkB as well (Bibel et al., 1999).

2. Trk Signaling:

The discovery of TrkA as a receptor tyrosine kinase (Kaplan et al., 1991) revealed that Trk receptor signaling was similar to other known growth factor receptors such as epidermal growth factor receptor and fibroblast growth factor receptor. Like other receptor tyrosine kinases, neurotrophins activate Trk receptors by inducing Trk dimerization (Jing et al., 1992). Receptor dimerization triggers the intracellular tyrosine kinase domains to trans-autophosphorylate each other on multiple tyrosine residues (Fig. 1.3). This autophosphorylation is

crucial for TrkA activation in two ways. First, phosphorylation of the three tyrosine residues located in the activation loop of the kinase domain (Y670, Y674, and Y675 in the human TrkA sequence) enhances tyrosine kinase activity (Cunningham and Greene, 1998). Second, additional phosphorylated tyrosine residues serve as docking sites for intracellular proteins that contain SH2 (Src homology 2) domains, protein domains that recognize phosphorylated tyrosine residues. Binding of these intracellular proteins provides scaffolds for additional proteins involved in intracellular signaling pathways (Reichardt, 2006).

There are three major signaling pathways that are activated by Trk receptors: the PLCγ (phospholipase Cγ) pathway, the Ras/ Raf/ MAPK pathway (mitogen activated protein kinase), and the PI3K/ Akt pathway (phosphoinositide-3-kinase/ Akt, also called Protein kinase B or PKB) (Fig 1.3). Phosphorylated Y490 on the intracellular TrkA domain serves as a docking site for the adaptor protein Shc, which, through a series of additional adapter proteins, activates the small GTPase Ras. Ras then activates two major signaling pathways, Raf-MEK-ERK, and the PI3K/ Akt. Phosphorylation of Y785 on Trk receptors recruits and activates PLCγ. PLCγ generates diacyl glycerol (DAG) and inositol-(1,4,5) triphosphate (IP_3) from membrane lipids. DAG can activate protein kinase C (PKC) and IP_3 can mobilize Ca^{2+} from internal stores and thereby activate Ca^{2+}-sensitive kinases, such as Calmodulin kinase (CamK) (Reichardt, 2006).

2.1. TrkA Signaling in Neuron Survival and Axon Outgrowth

The survival effects of NGF are mediated by TrkA signaling. This has been shown using gene knock-out studies in which sympathetic and sensory

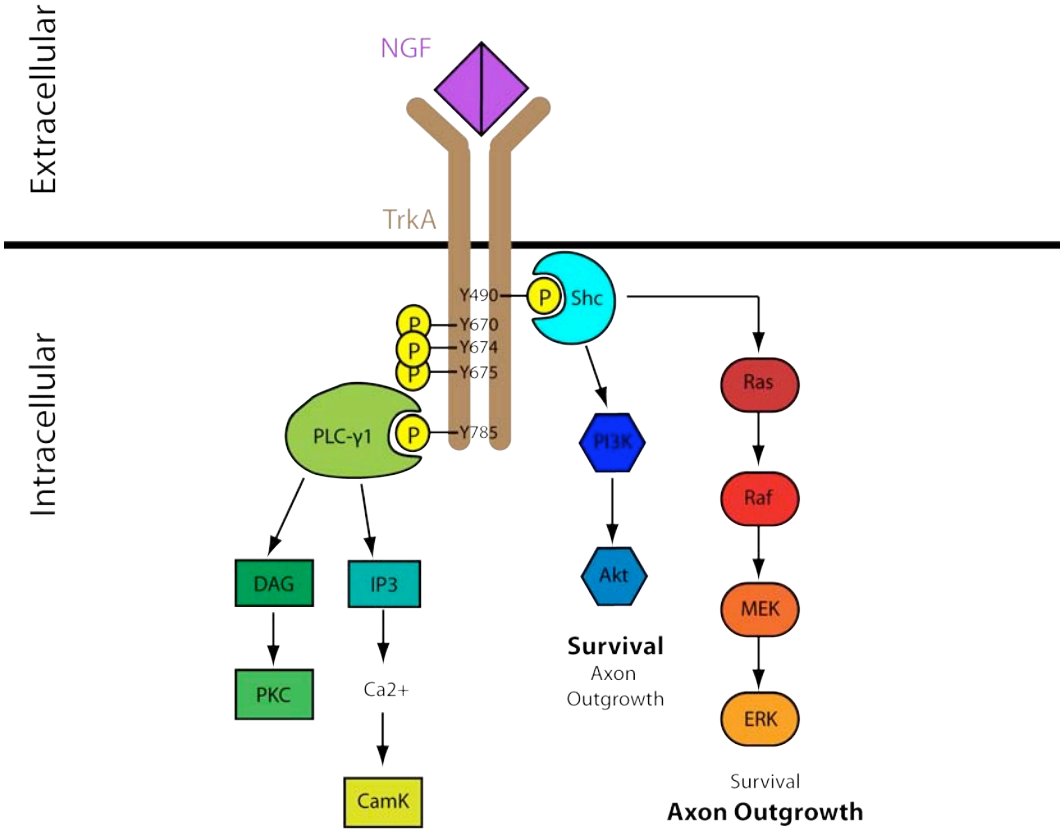

Figure 1.3: A simplified schematic of the major signaling pathways of Trk receptors. Binding of a neurotrophin to Trk receptors induces Trk dimerization and trans-autophosphorylation of tyrosine residues located in the Trk intracellular domain (Y490, Y670, Y674, Y675, Y785 of the human TrkA receptor are shown). Phosphorylation of Y490 and Y785 provide docking sites for adaptor proteins such as Shc and PLCγ. This leads to activation of three major signaling cascades: MAP kinase signaling cascade (Raf/ MEK/ ERK), PI3K/ Akt, and PLCγ/ DAG/ IP3 pathways. PI3K/ Akt is the primary pathway that mediates neuron survival and Raf/ MEK/ ERK is the primary pathway that mediates axon outgrowth.

neurons die in the presence of NGF when TrkA receptors are absent (Smeyne et al., 1994). Trk-mediated survival occurs primarily through activation of PI3K/ Akt (Chao, 2003; Kuruvilla et al., 2000; Lu et al., 2005; Reichardt, 2006), which directly inactivates pro-apoptotic proteins (Brunet et al., 1999; Datta et al., 1997). The secondary pathway is the Raf-MEK-ERK pathway, which activates transcription factors including the cyclic-AMP responsive element binding protein (CREB) to turn on anti-apoptotic proteins such as BCL2 (Bonni et al., 1995; Ginty et al., 1994; Lonze et al., 2002; Pugazhenthi et al., 2000; Riccio et al., 1999).

NGF is produced by target tissues but promotes survival by its actions in the nucleus. Therefore, an important issue is how NGF-mediated survival signals generated at axon terminals reach the cell body. The current hypothesis of how neurotrophin signaling at distal axons can mediate survival signals in the nucleus is the “signaling endosome” hypothesis (Campenot, 1994; Grimes et al., 1996; Ibanez, 2007). Early *in vivo* studies from the 1970s revealed that NGF undergoes retrograde transport from target tissues to sympathetic nuclei by way of their axons (Hendry et al., 1974; Stockel et al., 1974). *In vitro* studies using compartmentalized cultures confirmed these results (Ure and Campenot, 1997) and demonstrated that NGF localized to the axon terminal is sufficient to promote neuronal survival (Campenot, 1977; Riccio et al., 1997). More recent studies provide evidence for the formation of a signaling endosome, created by internalization of the NGF-TrkA complex (Watson et al., 1999) with many signaling components attached (Delcroix et al., 2003; Zweifel et al., 2005). The endosomal complex then undergoes retrograde transport to the nucleus via

cellular motors (Heerssen et al., 2004), and remains active along the way (Zweifel et al., 2005). While neuron survival can occur through both retrograde signaling from the axon and signaling directly at the cell body, evidence from *in vitro* primary cultures of sensory neurons suggest that neurotrophin-induced survival signals can vary according to the location of the stimulus. For example, in sensory neurons, NGF-mediated survival at the distal axon is mediated by ERK5 whereas NGF-induced survival at the cell body is mediated by both ERK5 and ERK1/2 (Watson et al., 2001). While ERK1/2 and ERK5 share some substrate specificity, such as CREB, they both activate distinct transcriptional pathways as well (Pearson et al., 2001). These studies suggest that the location of neurotrophin stimulation can elicit a specific response.

The effect of TrkA signaling on sympathetic axon outgrowth is less well understood than its effects on survival because manipulations inhibiting Trk signaling cause neuronal death. Local NGF-TrkA signaling at axon terminals mediates outgrowth (Campenot, 1994; Glebova and Ginty, 2005) via activation of both MEK/ERK and PI3K signaling pathways (Atwal et al., 2000). A recent study implicated STAT3 as a downstream component of the MEK/ERK pathway that may also be involved in axon outgrowth (Ng et al., 2006). Although the precise mechanisms of axon outgrowth are not understood, experiments in cell lines, sensory and hippocampal neurons suggest that local signaling pathways likely stabilize cytoskeletal elements such as members of the RhoGTPase family, and thereby facilitate axon elongation (Daniels et al., 1998; Estrach et al., 2002;

Nusser et al., 2002; Sebok et al., 1999; Veeranna et al., 1998; Yamaguchi et al., 2001; Zhou et al., 2004a).

In contrast to the effects of NGF on survival, NGF-induced axon outgrowth appears to be predominately mediated by local Trk activation at the growth cone rather than via retrograde signaling. Experimental evidence from compartmentalized cultures suggests that local signaling is necessary for axon outgrowth (Campenot, 1994). Further evidence from Kuruvilla and colleagues suggests that local signaling might actually be sufficient for axon outgrowth because activation of TrkA by NT-3 during proximal sympathetic axon outgrowth does not initiate TrkA internalization and retrograde signaling, unlike NGF-TrkA activation (Kuruvilla et al., 2004). Certainly changes in gene transcription are necessary to sustain axon outgrowth and, indeed, NGF signaling causes upregulation of cytoskeletal elements required for growth (Mathew and Miller, 1990; Zweifel et al., 2005). However the ability of NT-3 to induce axon outgrowth via TrkA in the absence of receptor internalization and retrograde transport (Kuruvilla et al., 2004) reveals possible differential requirements for local vs. retrograde neurotrophin signaling at different developmental time points or even differential mechanisms that mediate axon outgrowth.

3. p75NTR Signaling:

While the role of Trk receptors in neuron survival and outgrowth are well established, the role of p75NTR is much more complex. When p75NTR was first discovered as the NGF receptor, it was surprising that the intracellular domain did not contain a tyrosine kinase catalytic domain like other growth factor

receptors such as epidermal growth factor receptor or the fibroblast growth factor receptor (Johnson et al., 1986). However, it is now understood that p75NTR can interact with and modulate numerous co-receptors and downstream signaling in addition to being able to signal on its own. This "promiscuity" of p75NTR results in a diverse set of functions.

There are several signaling pathways that become activated upon binding of a neurotrophin to p75NTR through interaction with adaptor proteins including the E3 ubiquitin ligase TRAF6, neurotrophin receptor interacting factor (NRIF), and RhoGDI (Rho GDP-dissociation inhibitor) (Reichardt, 2006). The three major signaling pathways activated by p75NTR are Jun N-terminal Kinase (JNK), NFκB, and Rho activation (Kaplan and Miller, 2000; Reichardt, 2006) (Fig 1.4). In addition, recent evidence demonstrates that p75NTR itself undergoes proteolytic processing by γ-secretase at the cell membrane. This results in release of the p75NTR intracellular domain ($p75NTR_{icd}$) and translocation to the nucleus, where it is believed to participate in gene transcription (Jung et al., 2003; Kanning et al., 2003; Kenchappa et al., 2006). These signaling pathways mediate some of the diverse actions of p75NTR and will be discussed in further detail below.

3.1. p75NTR and Cell Death:

One of the best characterized outcomes of p75NTR activation is apoptotic cell death. During development, more than 50% of neurons will undergo apoptosis (Oppenheim, 1991). While much of this developmental cell death is due to insufficient target-derived survival signals received by these neurons,

there is also evidence for pro-death signals as well. Studies using p75NTR function blocking antibodies or mice lacking p75NTR (p75NTR-/-) provide evidence that p75NTR-induced apoptosis is important for early development of some neuronal systems (Frade et al., 1996), including some sympathetic neurons (Bamji et al., 1998). However, the role of p75NTR in sympathetic neuronal death during development is anything but straightforward. While neonatal p75NTR-/- mice have increased number of sympathetic neurons (Bamji et al., 1998), sympathetic neuron number and ganglia size are normal in adult p75NTR-/- mice (Bamji et al., 1998; Brennan et al., 1999). This suggests that while some cell death occurs via p75NTR early in development, other mechanisms are employed at later stages that do not require p75NTR.

The signaling mechanisms involved in p75NTR-induced apoptosis are still not completely understood. In several neuronal cell types, including sympathetic neurons, activation of the JNK signaling cascade stimulates apoptosis via activation of the pro-apoptotic factor p53 (Aloyz et al., 1998; Bamji et al., 1998). Additionally, p75NTR activation elevates intracellular ceramide by cleavage of sphingomyelin in the cell membrane by sphingomyelinases (Dobrowsky et al., 1994; Dobrowsky et al., 1995; Dobrowsky and Carter, 1998) and elevated ceramide is required for p75NTR- induced apoptosis (Blochl and Blochl, 2007; Brann et al., 2002). Although ceramide is central to many apoptotic mechanisms, there is evidence that increased ceramide production facilitates apoptosis by converging with the JNK-p53 signaling pathway (Blochl and Blochl, 2007; Ruvolo, 2003). Many factors mentioned above have been identified as

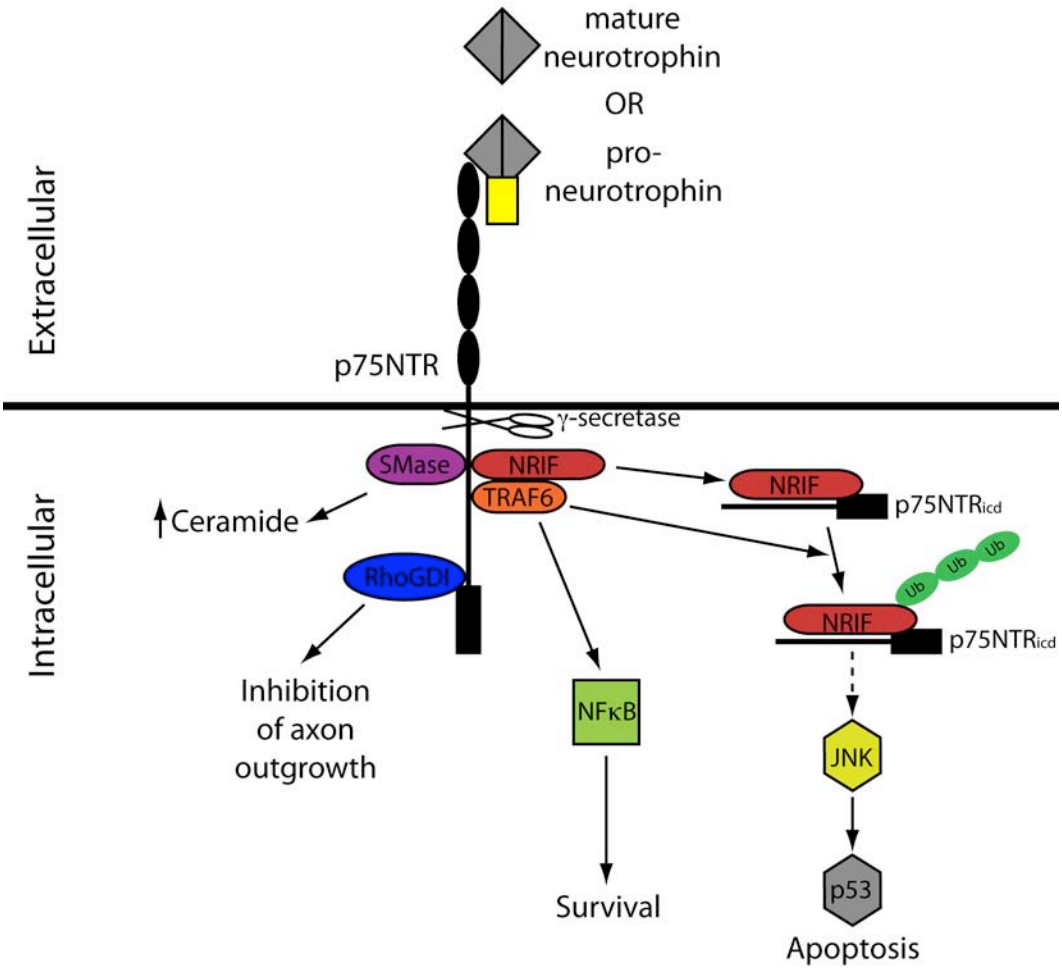

Figure 1.4: A simplified schematic of the major signaling pathways of the p75NTR receptor. Binding of a pro-neurotrophin or mature neurotrophin to p75NTR results in activation of three major signaling pathways by recruitment of adaptor proteins to the p75NTR intracellular domain. Recruitment of RhoGDI to p75NTR activates RhoA and inhibits axon outgrowth. Recruitment of adaptor proteins TRAF6 and NRIF are important for activating NFκB, which promotes survival, and JNK, which promotes apoptosis. Several signaling elements are required for JNK-induced apoptosis. Ligand-dependant cleavage of p75NTR by γ-secretase releases the $p75NTR_{icd}$, which forms a complex with NRIF. TRAF6 polyubiquitinates the NRIF/ $p75NTR_{icd}$ complex, and thereby facilitates nuclear translocation and activation of JNK. Ceramide production by sphingomyelinase (SMase) is necessary for p75NTR-mediated apoptosis and is implicated in functional antagonism of Trk signaling.

necessary for p75NTR/ JNK- induced apoptosis, including NRIF (Linggi et al., 2005), TRAF6 (Yeiser et al., 2004), and the $p75NTR_{icd}$ (Kenchappa et al., 2006). One model of how these signaling factors contribute to p75NTR-JNK-induced apoptosis in sympathetic neurons is that elevated ceramide enhances cleavage of the $p75NTR_{icd}$ and NRIF expression. NRIF then associates with $p75NTR_{icd}$ and the E3 ubiquitin ligase TRAF6, is polyubiquitinated and translocates to the nucleus where it acts as a transcription factor (Blochl and Blochl, 2007; Geetha et al., 2005; Kenchappa et al., 2006; Reichardt, 2006). Interestingly, this p75NTR-JNK-induced apoptosis only occurs in the absence of or at suboptimal levels of Trk signaling (Bamji et al., 1998), likely because activation of Trk silences JNK-p53 mediated neuronal apoptosis (Kaplan and Miller, 2000; Mazzoni et al., 1999). This might occur through inhibition of sphingomyelinase and reduction of ceramide by Trk activation (Blochl and Blochl, 2007; Dobrowsky et al., 1995; Plo et al., 2004).

Recently, the pro-neurotrophins were identified as potent mediators of p75NTR-induced cell death (Lee et al., 2001). Pro-neurotrophins bind p75NTR with five times the affinity as mature neurotrophins and have been identified as the preferred ligands for p75NTR (Lee et al., 2001) (Fig. 1.2). However, interaction of p75NTR with the co-receptor sortilin is necessary for this high-affinity binding by pro-neurotrophins and induction of apoptosis (Nykjaer et al., 2004) (Fig 1.5C). To date, not much is known about the signaling pathways that mediate apoptosis via the p75NTR/ sortilin complex, but some evidence from hippocampal neurons suggests that cleavage of the $p75NTR_{icd}$, polyubiquitination

of NRIF, and nuclear translocation are necessary (Volosin et al., 2008). This suggests that all p75NTR-induced apoptosis may utilize similar signaling pathways and that the presence of sortilin modulates specificity of p75NTR to the pro-neurotrophins. However, unlike apoptosis mediated by p75NTR alone, p75NTR/ sortilin/ proneurotrophin- induced apoptosis is insensitive to Trk activation (Nykjaer et al., 2005). These studies demonstrate that whether a cell survives or undergoes apoptosis in response to neurotrophins can be regulated at two levels: the expression of cell surface receptors and cleavage of the pro-neurotrophins.

3.2. p75NTR and Axon Outgrowth:

In contrast to Trk receptors, the role of p75NTR on axon outgrowth is still unclear. Conflicting reports from mice lacking p75NTR demonstrate a range of outcomes on axon outgrowth from hyperinnervation to decreased innervation in several types of neurons (Ben-Zvi et al., 2007; Dhanoa et al., 2006; Habecker et al., 2008; Hannila and Kawaja, 1999; Hannila and Kawaja, 2005; Jahed and Kawaja, 2005; Kohn et al., 1999; Krol et al., 2000; Lee et al., 1992; Lee et al., 1994), suggesting that the actions of p75NTR are complex.

There are several circumstances in which p75NTR is involved in inhibition of axon outgrowth. For example, p75NTR forms a complex with two known mediators of axon outgrowth inhibition: the NogoR/ Lingo-1 receptor complex (Mi et al., 2004; Wong et al., 2002) and ephrinA (Lim et al., 2008) (Fig 1.5E, F). Members of the myelin-based growth inhibitors such as Nogo-A and myelin-associated glycoprotein (MAG) bind the Nogo receptor and activate the NogoR/

p75NTR/ Lingo-1 receptor complex by recruitment of the RhoA inhibitor Rho-GDI (Yamashita and Tohyama, 2003). Recruitment of Rho-GDI to p75NTR activates RhoA and results in growth cone collapse and axon growth inhibition in postnatal sensory and cerebellar neurons (Schmidt and Hall, 2002; Yamashita et al., 2002). Similarly, p75NTR was found to interact with the membrane-bound signaling molecule ephrinA and is necessary for ephrinA-induced axon repulsion in retinal ganglion cell axons (Lim et al., 2008). EphrinA, like NogoR is a glycophosphatidylinositol (GPI)-linked membrane protein, and requires association with p75NTR to mediate axon repulsion.

In addition to interaction with various co-receptors, direct ligand activation of p75NTR in the presence of Trk activation has also been shown to inhibit axon outgrowth in sympathetic neurons. Direct activation of p75NTR on cultured sympathetic neurons by BDNF dose-dependently inhibits NGF/ TrkA-induced axon outgrowth (Kohn et al., 1999) (Fig 1.5B). Accordingly, sympathetic targets that express BDNF during development, such as the pineal gland, are hyperinnervated in p75NTR-/- mice (Kohn et al., 1999). This is not limited to sympathetic neurons but occurs in sensory neurons as well (Kimpinski et al., 1999). The axonal inhibition caused by direct activation of p75NTR is likely caused by inhibition of Trk signaling. TrkA autophosphorylation is elevated when p75NTR is absent, and activation of downstream effector molecules such as ERK1/2 is enhanced (Hannila et al., 2004). Conversely, direct activation of p75NTR inhibits ERK activation (Kaplan and Miller, 2000). This may occur through p75NTR–induced ceramide elevation, which inhibits signaling pathways

critical for neurotrophin-induced axon outgrowth such as PI3K/ Akt and Ras/ MEK/ ERK (Ruvolo, 2003) and NGF-dependent neurite outgrowth of cultured sympathetic neurons (de Chaves et al., 2001), but the complete mechanism is not fully understood.

In contrast to inhibition of axon outgrowth, p75NTR can also positively influence axon outgrowth. Direct activation of p75NTR facilitates axon outgrowth in ciliary neurons lacking TrkA by inactivation of RhoA (Yamashita et al., 1999). As mentioned previously, p75NTR can interact with Trk receptors to form a high-affinity binding site for neurotrophins (Hempstead et al., 1991) (Fig 1.5A). Another indirect mechanism by which p75NTR facilitates axon outgrowth in sensory neurons is by interacting with the semaphorin3a (sema3a) receptor complex, neuropilin1 (NP1) and plexin A4 (Ben-Zvi et al., 2007) (Fig. 1.5D). Sema3a is a chemorepulsive factor that causes growth cone collapse and inhibition of axon outgrowth (Kawasaki et al., 2002). p75NTR interacts with and disrupts the sema3a receptor complex, thereby blunting sema3a-induced repulsion. Mice lacking p75NTR have severe deficits in sensory innervation of the limbs and crossing p75NTR-/- mice with sema3a-/- mice rescued this phenotype (Ben-Zvi et al., 2007).

Recently, direct activation of p75NTR in sympathetic neurons by BDNF was found to not only inhibit axon outgrowth, but also to cause axon degeneration *in vivo* and *in vitro* (Singh et al., 2008). This p75NTR-mediated axonal degeneration occurs in the presence of NGF and is distinct from axon degeneration caused by NGF withdrawal. The mechanism underlying axonal

Figure 1.5

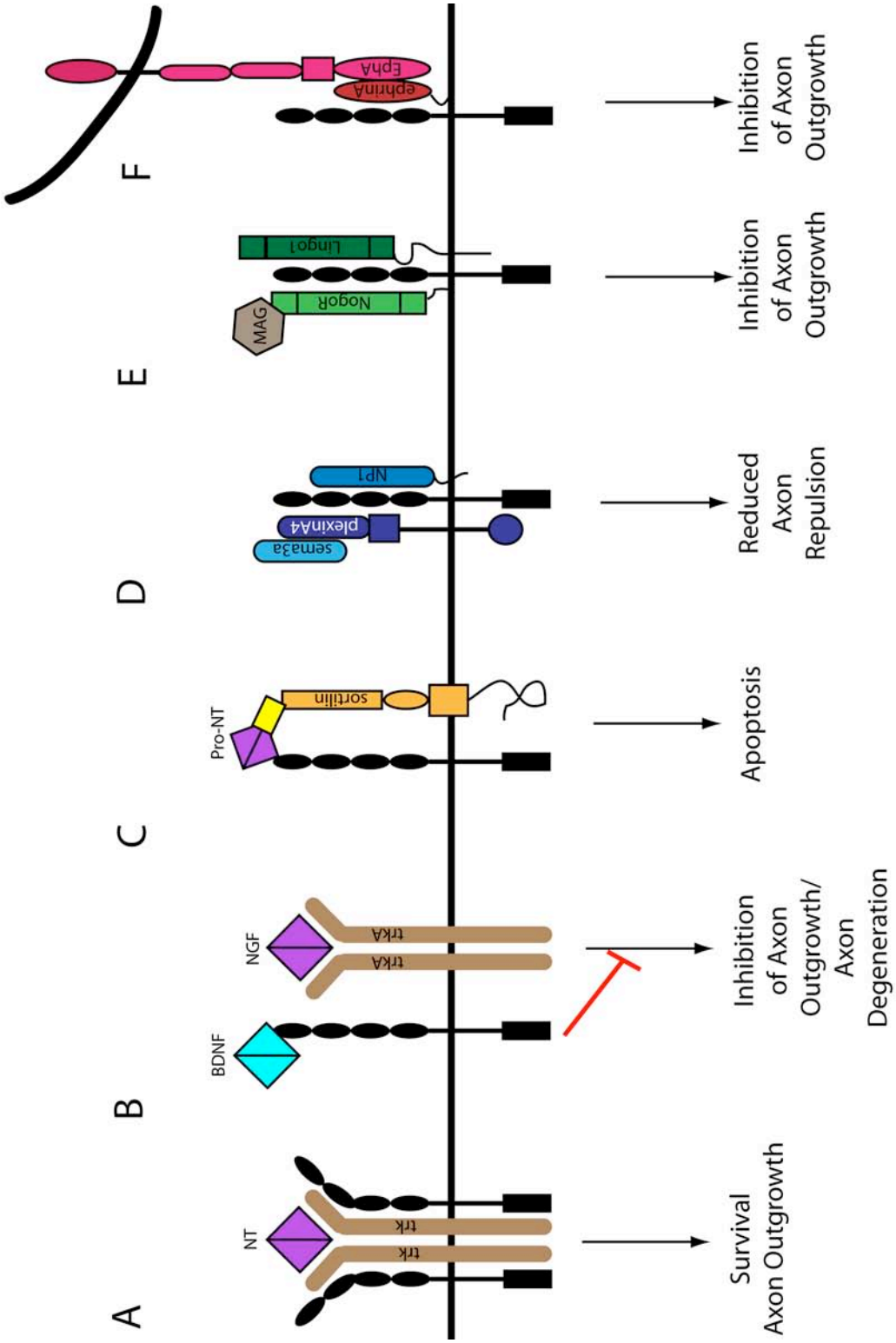
A
B
C
D
E
F
NT
trk
trk
BDNF
NGF
trkA
trkA
Pro-NT
sortilin
sema3a
PlexinA4
NP1
MAG
NogoR
Lingo1
ephrinA
EphA
Survival
Axon Outgrowth
Inhibition
of Axon
Outgrowth/
Axon
Degeneration
Apoptosis
Reduced
Axon
Repulsion
Inhibition
of Axon
Outgrowth
Inhibition
of Axon
Outgrowth

Figure 1.5: The many interaction partners of p75NTR. **A**) p75NTR interacts with Trk receptors to create a high affinity binding site for neurotrophins. This interaction modulates the selectivity of Trk receptors, restricting neurotrophin binding. Binding of a neurotrophin to this complex results in Trk activation and neuronal survival and axon outgrowth. **B**) Selective activation of p75NTR inhibits Trk signaling. This can result in inhibition of axon outgrowth or axonal degeneration. **C**) p75NTR interacts with sortilin. Pro-neurotrophins bind this receptor complex and promote apoptosis. **D**) p75NTR interacts with the sema3a receptor complex NP1/ plexinA4. This disrupts of the NP1/ plexinA4 complex and attenuates sema3a-induced axon repulsion. **E**) p75NTR interacts with the NogoR/ Lingo1 complex. Myelin-based growth inhibitors such as MAG bind the NogoR of the NogoR/ p75NTR/ Lingo1 complex and inhibit axon outgrowth. NogoR is a GPI-linked membrane protein and requires p75NTR for signaling. **F**) p75NTR interacts with ephrinA. Membrane bound ephrinA binds membrane bound protein EphA, which inhibits axon outgrowth. EphrinA is a GPI-linked membrane receptor and requires p75NTR for signaling.

degeneration involves inhibition of NGF/ TrkA signaling. Interestingly, p75NTR-mediated sympathetic axon degeneration requires inhibition of both PI3K *and* MEK/ ERK signaling. Although pharmacological inhibition of either PI3K or MEK/ ERK attenuates axon outgrowth (Atwal et al., 2000; Singh et al., 2008), degeneration only occurs when both signaling pathways are inhibited (Singh et al., 2008).

As demonstrated in the examples above, activation of p75NTR results in a wide range of outcomes from apoptotic cell death to survival and axon outgrowth inhibition, degeneration and promotion. It is, therefore, difficult to create a unifying model for p75NTR signaling. Because p75NTR can bind numerous different ligands and interact with several co-receptors the effect of p75NTR binding and activation is likely to be highly dependent on which stimulating ligands and co-receptors are present.

D. Development of Sympathetic Nervous System:

1. The Neural Crest and Early Sympathetic Development:

The sympathetic nervous system arises from the neural crest, a group of cells derived from the neuroectoderm (Goridis and Rohrer, 2002; Sanes et al., 2005). Neural crest cells migrate from the dorsal portion of the neural tube and differentiate into a wide variety of cell types including most cells in the peripheral nervous system, the endocrine chromaffin cells of the adrenal medulla, smooth muscle cells, melanocytes and cranial cartilage (Sanes et al., 2005). Sympathetic neurons arise from thoracic and lumbar neural crest cells that

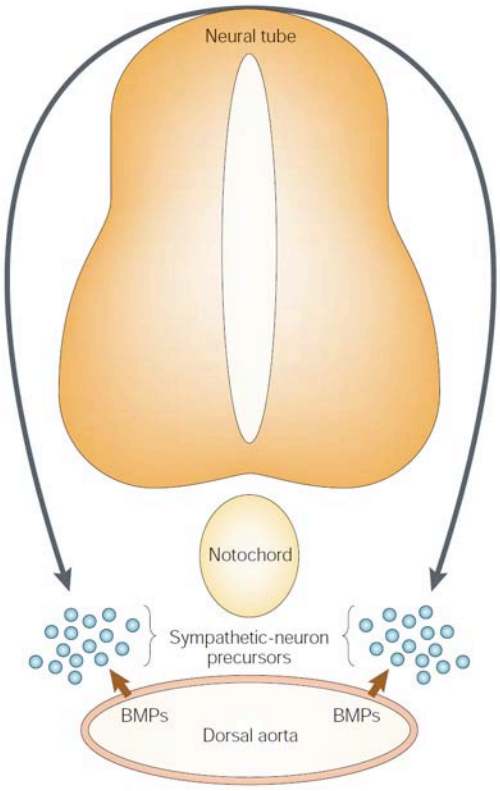

Reprinted by permission from MacMillan Publishers Ltd: Gordis and Rohrer. 2002. *Nat Rev Neurosci*, 3: 531-541.

Figure 1.6: Sympathetic neurons develop from thoracic and lumbar neural crest cells. Neural crest cells migrate from the dorsal portion of the neural tube to the dorsal aorta (black arrows) where they aggregate to form sympathetic ganglia. At the dorsal aorta, neural crest cells encounter BMPs, which promote differentiation to committed neuronal cells.

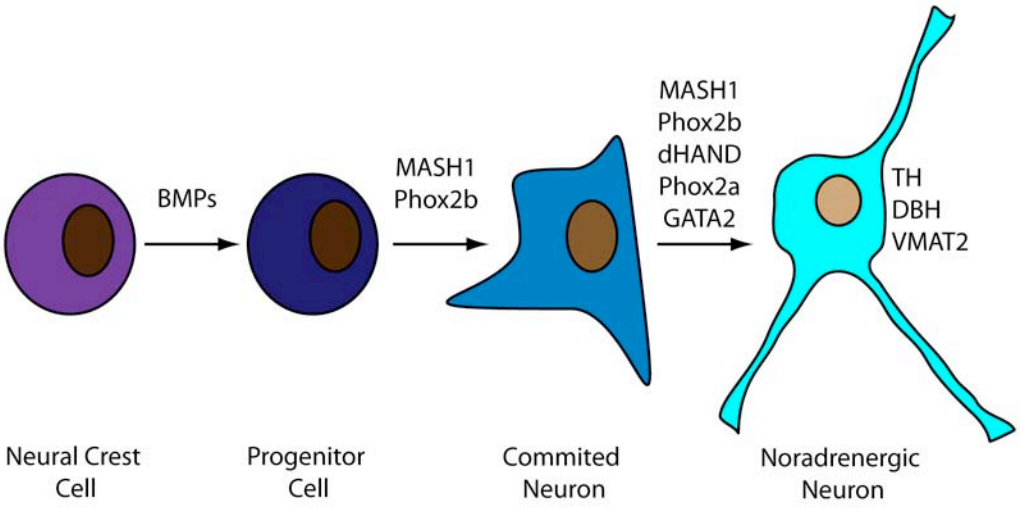

Figure 1.7: Development and differentiation of sympathetic neurons from neural crest cell precursors. When neural crest cells encounter bone morphogenetic proteins (BMPs) at the dorsal aorta they begin to express the transcription factors MASH1 and Phox2b and differentiate into committed neuronal cells. Expression of Phox2b and MASH1 leads to the expression of the transcription factors Phox2a, dHAND and GATA2 and, together, this collection of transcription factors coordinate to promote expression of the noradrenergic markers tyrosine hydroxylase (TH), dopamine-β-hydroxylase (DBH) and the vesicular monoamine transporter 2 (VMAT2).

migrate to the dorsal aorta where they cluster to form what will become sympathetic ganglia (Fig 1.6). There they encounter bone morphogenetic proteins (BMPs) synthesized at the dorsal aorta. BMPs induce expression of transcription factors such as MASH1 and Phox2b and thereby promote differentiation to committed neuronal cells. Committed neuronal cells further differentiate into noradrenergic neurons through expression of the transcription factors MASH1, Phox2b, Phox2a, dHAND and GATA2 which promote expression of the noradrenergic markers Tyrosine Hydroxylase (TH), Dopamine-β-hydroxylase (DBH) and vesicular monoamine transporter 2 (VMAT2) (Howard, 2005) (Fig 1.7).

2. Sympathetic Target Innervation:

Sympathetic axons innervate target tissues that lie at a great distance from their cell bodies in the sympathetic ganglion. Therefore, the precise innervation of these target tissues requires coordination of many signaling factors that instruct the developing neurons which path to follow, which target to innervate and the density of final target innervation. Early initiation of axon outgrowth is not well understood, but sympathetic axon outgrowth is observed soon after the formation of the sympathetic ganglia (Rubin, 1985). The formation of axons at this early stage is thought to coincide with the earliest time point that sympathetic precursors exit the mitotic cycle. Once axon outgrowth begins, the axons generally follow the arterial vasculature as an intermediate target en route to their final destinations (Rubin, 1985). The neurotrophin NT-3 is expressed by the smooth muscle of the arterial vasculature at this intermediate time point

(Francis et al., 1999) and is critical for promoting survival and axon outgrowth towards target tissues in developing sympathetic neurons (Francis et al., 1999; Kuruvilla et al., 2004) (Fig 1.8A). It is important to note that some sympathetic outgrowth along the vasculature occurs in the absence of NT-3, indicating additional factors that may contribute to proximal axon outgrowth. The trophic factor artemin and its receptor complex Ret-GFR3 have also been found to be important mediators of axon extension along intermediate targets (Honma et al., 2002) and likely work in concert with NT-3 to facilitate proximal sympathetic axon outgrowth.

While NT-3 plays a critical role in guiding axons of developing sympathetic neurons, final innervation of the target organ is usually mediated by NGF (Crowley et al., 1994; Glebova and Ginty, 2004). NGF is synthesized by sympathetic target organs, including the heart (Ieda et al., 2004; Glebova and Ginty, 2005). NGF acts as a chemoattractant factor that guides innervating axons to their final destination in addition to promoting sympathetic neuron survival (Fig 1.8B). The two phases of sympathetic target innervation are mediated by distinct guidance cues: proximal axon outgrowth along the intermediate target of the vasculature requires NT-3 and distal axon outgrowth and final target innervation requires NGF. Interestingly, both NT-3 and NGF mediate these effects through activation of TrkA (Fagan et al., 1996; Kuruvilla et al., 2004). Sympathetic neurons predominately express TrkA, although TrkC is present during early stages of development and low levels of TrkC remain in mature sympathetic neurons (Fagan et al., 1996). Although the preferred

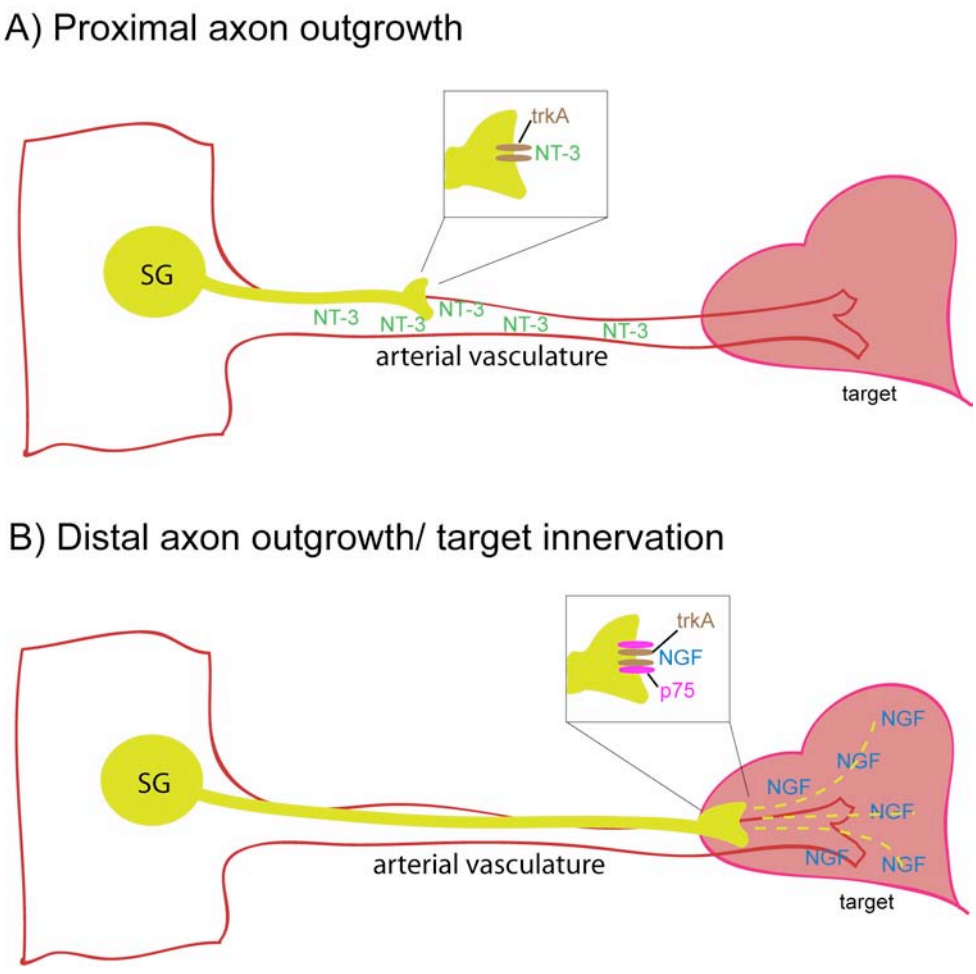

Figure 1.8: Sympathetic innervation of the heart. **A**) Cardiac sympathetic innervation begins with proximal axon outgrowth from developing neurons in the stellate ganglia (SG). Axons travel along the vasculature in response to NT-3, which binds and activates TrkA to promote axon outgrowth. **B**) Once the sympathetic axons reach their target (the heart in this example) they encounter NGF. NGF, the preferred ligand for TrkA, promotes neuron survival and innervation of the target organ. The switch in neurotrophin dependence from NT-3 to NGF is facilitated by the upregulation of p75NTR. Not only does p75NTR form a high-affinity binding site for NGF, but it restricts TrkA binding to NGF, and NT-3 can no longer bind.

receptor for NT-3 is TrkC, NT-3 can also bind and activate TrkA at higher concentrations (Belliveau et al., 1997). Sympathetic axon outgrowth and target innervation is not impaired when TrkC is absent (Tessarollo et al., 1997), indicating that NT-3 acts through TrkA to facilitate proximal axon outgrowth.

Sympathetic axons become dependent upon NGF at the time that they reach their targets (Davies, 1994). NGF preferentially binds TrkA to promote neuron survival and further axon outgrowth (Belliveau et al., 1997) and the switch in neurotrophin dependence from NT-3 to NGF is further facilitated by upregulation of p75NTR expression (Kuruvilla et al., 2004). As mentioned previously, p75NTR interacts with the TrkA receptor to 1) create a high affinity binding site for NGF (Hempstead et al., 1991) and 2) cause a shift in TrkA binding selectivity to NGF and away from NT-3 (Benedetti et al., 1993; Brennan et al., 1999). Interestingly, while activation of TrkA by both NT-3 and NGF results in axon extension, only NGF activation of TrkA at distal axons can promote survival of developing sympathetic neurons because only NGF activation of TrkA causes receptor internalization and retrograde signaling. In contrast, binding of NT-3 to TrkA at distal axons can cause activation of the TrkA receptor, but does not result in internalization or retrograde signaling (Kuruvilla et al., 2004). It is therefore thought that the requirement of developing sympathetic neurons of NT-3 for survival is at least partially due to its role in guiding axons to target tissues where NGF is available (Francis et al., 1999; Kuruvilla et al., 2004).

Sympathetic neurons become less dependent on NGF for survival in the adult (Orike et al., 2001). For example, systemic administration of an antibody to

NGF results in permanent destruction of sympathetic ganglia in neonatal mice (Levi-Montalcini and Angeletti, 1966) but not in adult mice (Angeletti et al., 1971; Bjerre et al., 1975b). However, NGF is still required for the maintenance of NE production in adult animals (Bjerre et al., 1975a; Bjerre et al., 1975b). In addition, adult sympathetic neurons remain responsive to elevated NGF for axon outgrowth (Bjerre et al., 1975a; Kaye et al., 1979; Orike et al., 2001).

3. Patterning of Cardiac Sympathetic Innervation:

While the neurotrophins NT-3 and NGF are critical for guiding sympathetic fibers to the heart during development, final innervation density and pattern involves a balance between chemoattractant factors and chemorepulsive factors. Because developing fibers initially follow the vasculature, cardiac sympathetic innervation projects from the base of the heart down towards the apex (Randall et al., 1968). This sets up a sympathetic gradient in which innervation density is greater at the base than at the apex of the heart. Additionally, innervating fibers primarily travel through the subepicardium of the ventricle and then dive in towards the subendocardial layer of the ventricle (Martins and Zipes, 1980; Randall et al., 1968). Recently, Ieda and colleagues showed that the chemorepellent sema3a is expressed in the subendocardial layer of the ventricle during development and is a critical regulator of ventricular sympathetic innervation density and pattern (Ieda et al., 2007). Sema3a signaling through its receptor complex NP1/ plexinA causes growth cone collapse and inhibition of axon outgrowth in sympathetic and sensory neurons (Kawasaki et al., 2002; Tanelian et al., 1997). Expression of sema3a in the subendocardium creates a

sympathetic gradient in which innervation density is greater in the subepicardium than in the subendocardium (Ieda et al., 2007). Therefore, development of normal cardiac sympathetic innervation density and pattern results from coordination of both chemoattractant signals (NGF) and chemorepulsive factors (sema3a).

III. CARDIAC ANATOMY, FUNCTION, AND INNERVATION:

A. Anatomy of the Heart:

The heart is the center of the cardiovascular system and is responsible for pumping blood throughout the body. This large pump is composed of cardiac muscle, which is involuntary, striated muscle that differs from both skeletal muscle and smooth muscle. Mammalian hearts consist of four chambers: the right atrium (RA), the left atrium (LA), the right ventricle (RV), and the left ventricle (LV) (Fig. 1.9). The interatrial septum separates the right and left atria and the interventricular septum (IVS) separates the left and right ventricles. Valves separate the atria from their corresponding ventricles. For example, the tricuspid valve separates the right atrium from the right ventricle and the mitral valve separates the left atrium from the left ventricle. Additionally, valves separate the ventricular chambers from the connecting arteries: the pulmonic valve separates the right ventricle from the pulmonary artery and the aortic valve separates the left ventricle from the aorta (Fig. 1.9). The structure of the ventricles is helical, consisting of two loops of muscle (Torrent-Guasp et al., 2001). The left ventricle contains both muscle loops, which roughly create the

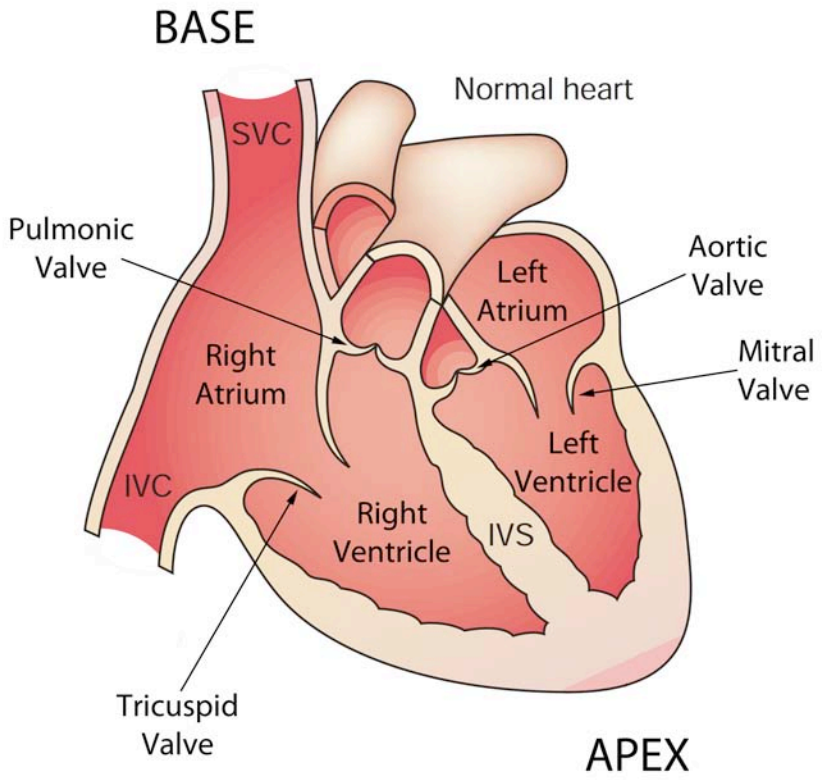

Adapted by permission from MacMillan Publishers Ltd: Towbin and Bowles. 2002. *Nature* 415 (6868) : 227-33.

Figure 1.9: Anatomy of the heart. Deoxygenated blood returns to the heart via the superior and inferior vena cava (SVC and IVC respectively) where it enters the right atrium. From the right atrium, blood passes through the tricuspid valves into the right ventricle. The right ventricle pumps blood through the pulmonic valve to the lungs. Oxygenated blood returns to the heart via the pulmonic veins (not pictured) into the left atrium. From the left atrium blood passes through the mitral valve to the left ventricle. From the left ventricle oxygenated blood is pumped through the aortic valve to the aorta and to the body. IVS = interventricular septum.

subendocardium (inner layer) and the subepicardium (outer layer). The right ventricular free wall, on the other hand, is formed by the outer loop alone (Torrent-Guasp et al., 2001). Papillary muscles located in the right and left ventricles are connected to the tricuspid and mitral valves respectively by fibrous strands, the chordae tendineae, to prevent blood leakage back into the atria. It is important to note that the "top" of the heart is referred to as the *Base* and the "bottom" of the heart is referred to as the *Apex* (Fig. 1.9). This terminology will be used throughout the dissertation.

In addition to cardiac muscle and valves, the heart contains a special internal conduction system to facilitate coordinated electrical conduction through the heart (Fig. 1.10). The cells that make up this special electrical conduction system are specialized myocytes with electrical properties that are distinct from cardiomyocytes and neurons (Mohrman and Heller, 2006). The major components of the cardiac conduction system are the sinoatrial node (SA node), located in the right atrium, the atrioventricular node (AV node), located in the lower region between the right and left atria, the bundle of His, located at the base of the interventricular septum, and the right and left bundle branches, which travel through the interventricular septum in a basal to apical direction. The ability of this internal conduction system to generate electrical impulses and conduct them throughout the heart will be discussed further in section B.3 of this chapter.

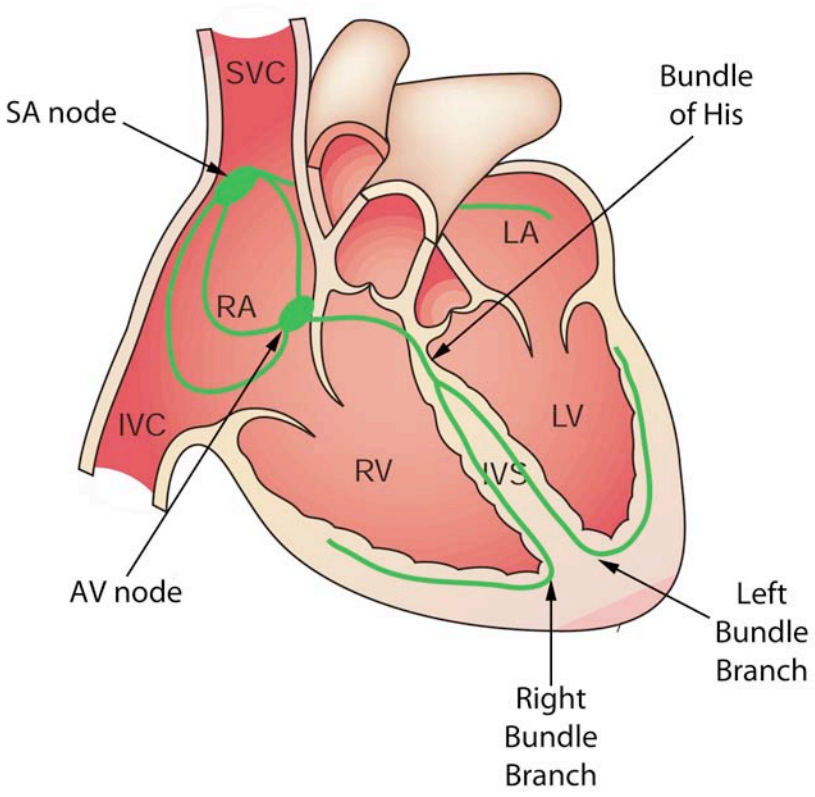

Adapted by permission from MacMillan Publishers Ltd: Towbin and Bowles. 2002. *Nature* 415 (6868) : 227-33.

Figure 1.10: The cardiac conduction system. Electrical impulses are generated by the pacemaker cells of the sinoatrial (SA) node, located in the right atrium (RA). The action potential from the SA node spreads across the right atrium and to the left atrium (LA). The electrical impulse must then pass through the atrioventricular (AV) node. From there it travels through the bundle of His and down the left and right bundle branches and spreads across the left and right ventricles (LV and RV respectively).

B. Basic Cardiac Function:

1. The Heart as a Pump:

The function of the heart is to pump blood throughout the body, delivering oxygen and nutrients. This process begins when deoxygenated blood returns to the right atrium through the vena cava and is then passed through the tricuspid valve into the right ventricle. From the right ventricle, blood is pumped through the pulmonic valve to the lungs via the pulmonary arteries where blood becomes reoxygenated. Oxygenated blood returns to the heart via the pulmonary veins and enters the left atrium. From the left atrium the oxygenated blood passes through the mitral valve into the left ventricle and from there is pumped through the aortic valve into the aorta and to the rest of the body. The period of time within the cardiac cycle in which the cambers are filling up with blood is called *diastole* and the period within the cardiac cycle where the heart is actively pumping blood is called *systole*.

2. The Cardiomyocyte:

Cardiomyocytes are the muscle cells of the heart and contain bundles of myofibrils, tubular organelles that are responsible for cardiac muscle cell contraction. The basic contractile unit of myofibrils is the sarcomere and it is responsible for muscle shortening and tension development. The sarcomere is made up of thick and thin myofilaments. The thick myofilaments are composed of myosin and the thin filaments are mainly composed of actin along with regulatory proteins. Figure 1.11A shows a simplified structure of a sarcomere. Actin filaments are connected to the Z-lines of the sarcomere, and are therefore

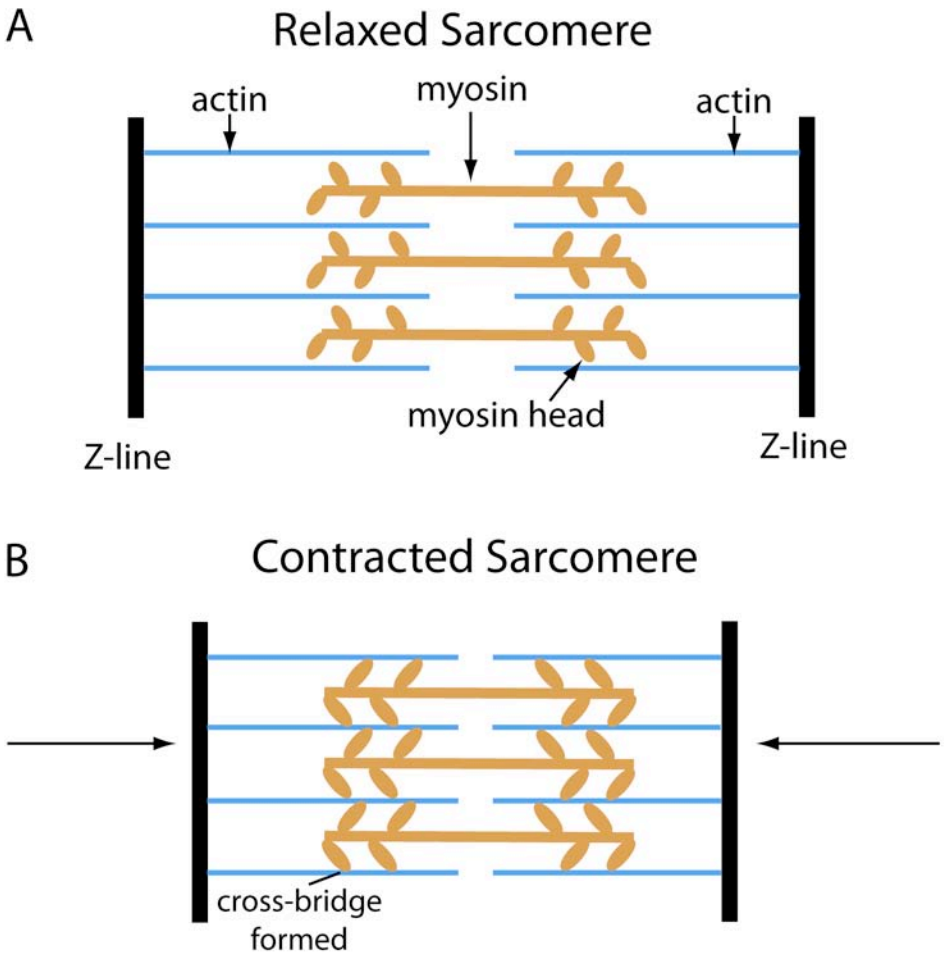

Figure 1.11: Structure of the sarcomere. **A**) The sarcomere is the contractile unit of cardiac muscle and is composed mainly of alternating myosin (thick filaments) and actin (thin filaments). Connection of actin to the Z-lines anchors it in place. **B**) When the myocyte becomes activated, increased intracellular Ca^{2+} allows cross-bridge formation between the myosin heads and actin followed by ATP-hydrolysis. This facilitates a conformational change of the myosin head, causing the actin and myosin filaments to slide past each other and shorten the sarcomere.

anchored in place. Myosin filaments sit in between the actin filaments. Upon excitation, myosin heads bind to actin and undergo a conformational change in response to ATP-hydrolysis. This conformational change results in actin and myosin filaments sliding past each other, shortening the sarcomere, and contracting the muscle (Fig 1.11B) (Mohrman and Heller, 2006). The coordination of excitation and contraction in the cardiomyocyte will be further discussed in section B.4 of this chapter.

3. Cardiac Electrical Conduction and the ECG:

3.1: Cardiac Action Potentials:

There are two types of cardiac action potentials: the fast-response and the slow-response. All cardiomyocytes, except specialized pacemaker cells, undergo fast-response action potentials (Fig 1.12A). Phase 4 of the fast-response action potential is the resting potential of the myocyte. Upon depolarization, by a neighboring cell for example, voltage-gated Na^+ channels open, allowing Na^+ to rapidly enter the cell and rapid depolarization (phase 0) takes place. This is followed by an initial repolarization due to inactivation of Na^+ channels and activation of transient outward K^+ channels (phase 1). However, repolarization is delayed due to opening of L-type Ca^{2+} channels and influx of Ca^{2+} and the action potential enters a plateau phase (phase 2). Repolarization occurs when delayed rectifier K^+ channels open (phase 3) until the cell returns back to its resting potential. During phases 0, 1, 2, and some of 3 the cardiomyocyte cannot be depolarized again, and the cell is said to be refractory.

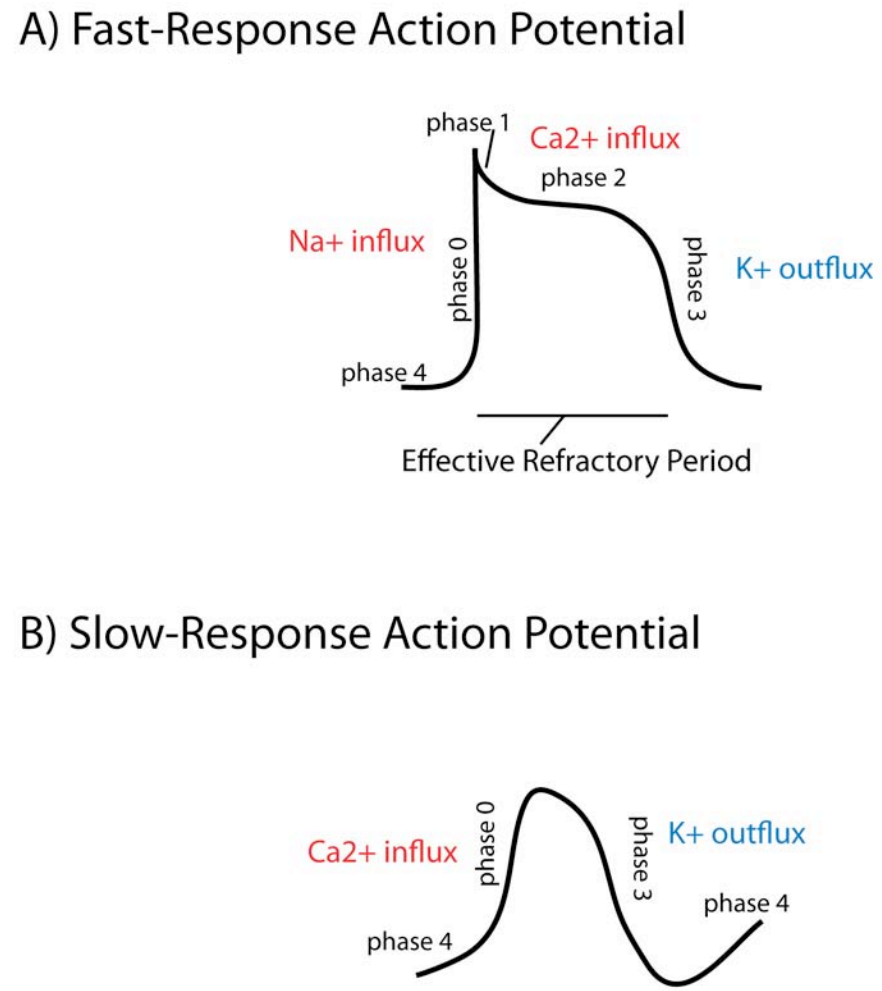

Adapted from Mohrman, D.E., Heller, L.J., 2006. Cardiovascular physiology. In: Lange physiology series. Lange Medical Books/McGraw-Hill, New York.

Figure 1.12: The cardiomyocyte action potential. **A**) The "fast response" action potential of a cardiac myocyte is characterized by rapid depolarization due to influx in Na^+ (phase 0) followed by an initial repolarization (phase 1). The action potential then enters a plateau phase (phase 2) where Ca^{2+} enters the cell. This is followed by increased K^+ permeability and repolarization of the myocyte (phase 3) back to its resting potential (phase 4). The cell is unresponsive during phases 0, 1, 2 and part of 3, also called the effective refractory period. (**B**) The "slow-response" action potential of a pacemaker cell is characterized by the slowly depolarizing membrane potential (phase 4) and a shorter plateau phase. Phase 0 depolarization is less rapid than in the "fast response" action potential and is caused by influx of Ca^{2+}. This is followed by an increase in K^+ permeability and repolarization of the cell.

The period of time that the cell is unresponsive to initiation of an action potential is called the effective refractory period (Mohrman and Heller, 2006).

The slow-response action potential of the pacemaker cells that make up the SA node is remarkably different from the cardiomyocyte fast-response action potential (Fig 1.12B). Pacemaker cells are able to spontaneously depolarize in a rhythmic manner due to their slowly depolarizing membrane potential (phase 4). This slowly depolarizing membrane potential is a result of gradual changes in membrane permeability to ions: a gradual decrease in K^+ permeability, and a gradual increase in Na^+ and Ca^{2+} membrane permeability, all of which slowly depolarize the cell until threshold is reached. Once the threshold potential has been reached, depolarization of the cell is achieved by influx of Ca^{2+} via L-type C^{2+} channels. Repolarization then takes place due to increased K^+ permeability through delayed rectifier K^+ channels and decreased Ca^{2+} permeability (Mohrman and Heller, 2006).

3.2 The Intrinsic Cardiac Conduction System:

In order for the heart to function properly as a pump, precise coordination of all cardiomyocytes is absolutely critical. This coordination is achieved by 1) the presence of the intrinsic cardiac conduction system, 2) by propagating action potentials from one cardiomyocyte to the next via gap junctions and 3) by appropriate phasing of refractoriness. Cardiac conduction begins at the SA node (Fig 1.10), which contains the specialized myocytes that have the ability to spontaneously depolarize and initiate action potentials mentioned above. The action potential generated by the SA node spreads throughout the right and left

atria by cell-to cell conduction via gap junctions. The atria and ventricles are separated by non-conductive connective tissue and therefore the impulse can only continue by passing through the AV node, a bundle of slow-conducting cells that create a delay in conduction between the atria and the ventricles. This delay ensures that the atria have enough time to contract and empty blood into the ventricles before the ventricles contract. From the AV node the action potential travels down the bundle of His and down the left and right bundle branches, depolarizing ventricular myocytes along the way in a subendocardial to subepicardial direction (Klabunde, 2005; Mohrman and Heller, 2006).

3.3: The Electrocardiogram (ECG):

The electrocardiogram is an invaluable tool used to monitor the electrical activity of the heart and for detecting abnormal heart rhythms, or arrhythmias. Using electrodes placed on the body surface, it is possible to measure electrical currents generated by the heart during depolarization and repolarization. Figure 1.13 depicts a normal ECG during one cardiac cycle from a Lead II configuration in which the negative electrode is placed on the right arm and the positive lead is placed on the left leg. There are many different ECG configurations, including the 12- lead configuration used most often clinically. All ECG measurements taken in studies for this dissertation, however, were from Lead II configurations. The ECG represents the sum of all electrical activity from the heart. The major components of the ECG are: the P wave, which corresponds to depolarization of the atria, the QRS complex, which corresponds to ventricular depolarization, and the T wave, which corresponds to ventricular repolarization (Fig 1.13).

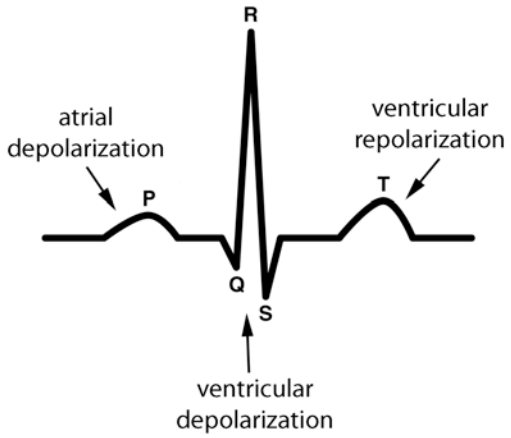

Figure 1.13: Normal lead II ECG from one cardiac cycle. The major components of the ECG are shown above. The P wave represents depolarization of the atria, the QRS complex represents depolarization of the ventricles, and the T wave represents ventricular repolarization.

4. Excitation- Contraction Coupling:

Muscles contract in response to an action potential through a process called excitation- contraction coupling (Fig 1.14). The major event that occurs in excitation- contraction coupling is a dramatic rise in intracellular Ca^{2+}. As mentioned previously, phase 2 of the cardiac action potential includes an influx of Ca^{2+} through voltage-gated L-type Ca^{2+} channels (Klabunde, 2005). This localized influx of Ca^{2+} into the cell triggers release of additional Ca^{2+} from the sarcoplasmic reticulum through Ca^{2+}-sensitive Ca^{2+} channels (ryanodine receptors, RyR). Elevated Ca^{2+} in the cardiac myocyte is critical for contraction of the myocyte in that it facilitates binding of the thick and thin filaments and shortens the sarcomere. Ca^{2+} binds troponin-C, a member of an inhibitory complex that prevents the thick and thin filaments from interacting with each other. Binding of Ca^{2+} to troponin-C causes a conformational change in the inhibitory protein tropomyosin, allowing the thick and thin filaments to interact and shorten the sarcomere. After contraction, Ca^{2+} is quickly sequestered back into the sarcoplasmic reticulum by the ATP-dependent Ca^{2+} pump SERCA (Sarco/ Endoplasmic Reticulum Ca^{2+}-ATPase) or transported out of the myocyte itself (Fig 1.14) (Klabunde, 2005; Mohrman and Heller, 2006). Norepinephrine can modulate Ca^{2+} release and reuptake from the sarcoplasmic reticulum and thereby modulate the contractile ability of the myocyte. This will be discussed in further detail in section D.2 of this chapter.

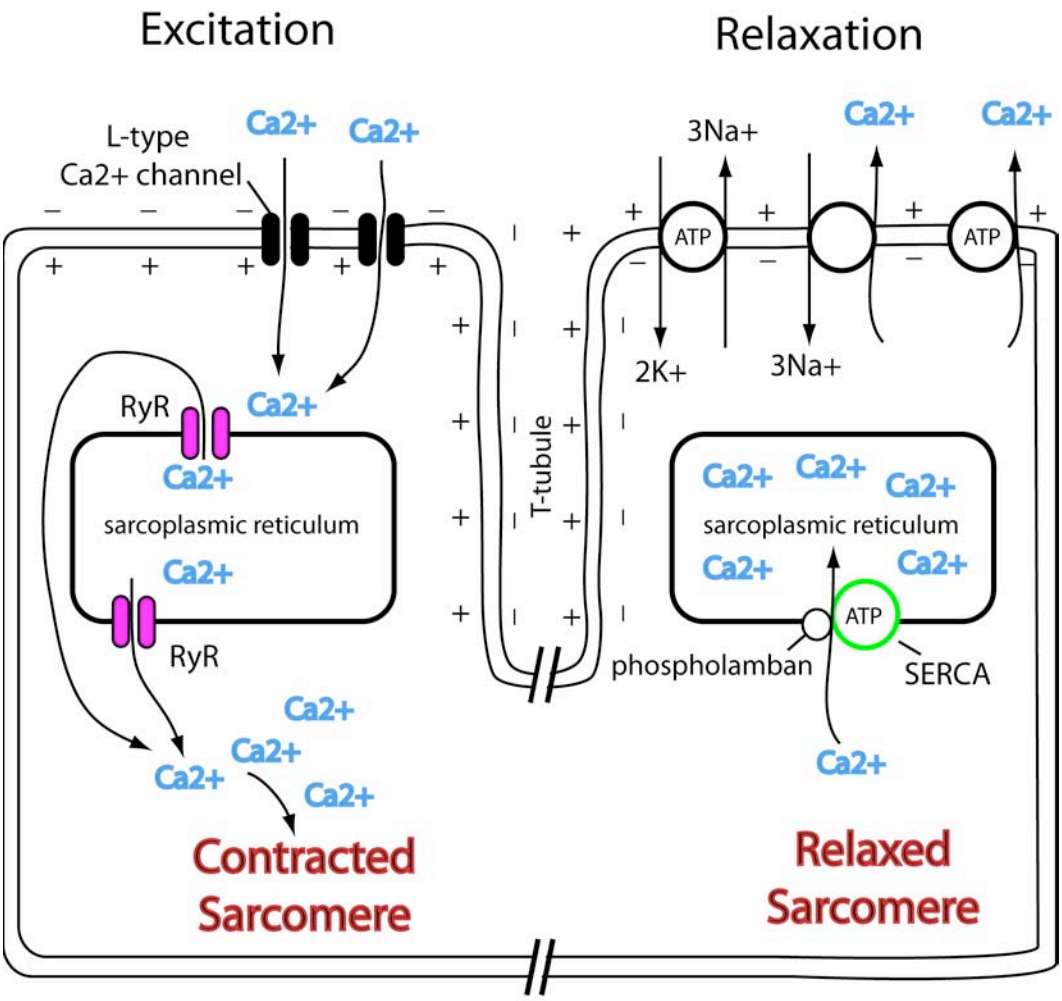

Adapted from Mohrman, D.E., Heller, L.J., 2006. Cardiovascular physiology. In: Lange physiology series. Lange Medical Books/McGraw-Hill, New York.

Figure 1.14: Excitation- Contraction Coupling. Depolarization of the cardiomyocyte (left side of cartoon) results in influx of Ca^{2+} through L-type Ca^{2+} channels. This increase in Ca^{2+} causes release of Ca^{2+} from the sarcoplasmic reticulum through Ca^{2+}- sensitive ryanodine receptors (RyR). Elevated intracellular Ca^{2+} binds to troponin-C (not shown), allows the myosin heads to interact with actin and shortening of the sarcomere. During repolarization of the cardiomyocyte (right side of cartoon), Ca^{2+} is rapidly sequestered back into the sarcoplasmic reticulum via the Ca^{2+}- ATPase pump SERCA. Phospholamban negatively regulates SERCA. Phosphorylation of phospholamban decreases its ability to inhibit SERCA. While most Ca^{2+} is take up into the sarcoplasmic reticulum, some Ca^{2+} is transported back out of the cell by the Na^{+}/ Ca^{2+} exchanger or by Ca^{2+}- ATPase pumps located on the cell surface. Decreased intracellular Ca^{2+} causes relaxation of the sarcomere.

5. Cardiac Muscle Cell Mechanics:

The length-tension relationship establishes the relationship between muscle length and tension and is an inherent property of the muscle itself. Figure 1.15 shows the length-tension relationship for an isometric (fixed length) contraction of cardiac muscle. The bottom curve represents the resting tension of the muscle and the top curve shows the peak tension the muscle can develop. Once the muscle is stimulated to contract, it develops active tension (Fig 1.15, points 1- 2) until the maximum tension is reached (Fig 1.15, point 3). The length of the muscle at rest has a direct effect on the maximum tension it can develop. A cardiac muscle can generate the most tension from an intermediate resting length, L_{Max}. At resting muscle lengths greater or smaller than L_{Max} active tension is reduced (Fig. 1.15).

A muscle that is not fixed in length and works against a fixed load undergoes isotonic contraction (Fig 1.16). In this example, the muscle has a 1g weight attached to it that stretches the muscle to a certain length determined by the resting length-tension curve. This load on the muscle at rest is called preload. When the muscle is stimulated to contract, it generates tension that exceeds the 1g constant load and shortens in length instead of developing additional tension until it reaches a length at which the maximum possible tension is 1g (Fig 1.16, points 1-3).

A more complex and physiologically relevant type of contraction is the afterloaded contraction, where the load on the muscle at rest is different than the load on the muscle during contraction. Figure 1.17 shows an example of an

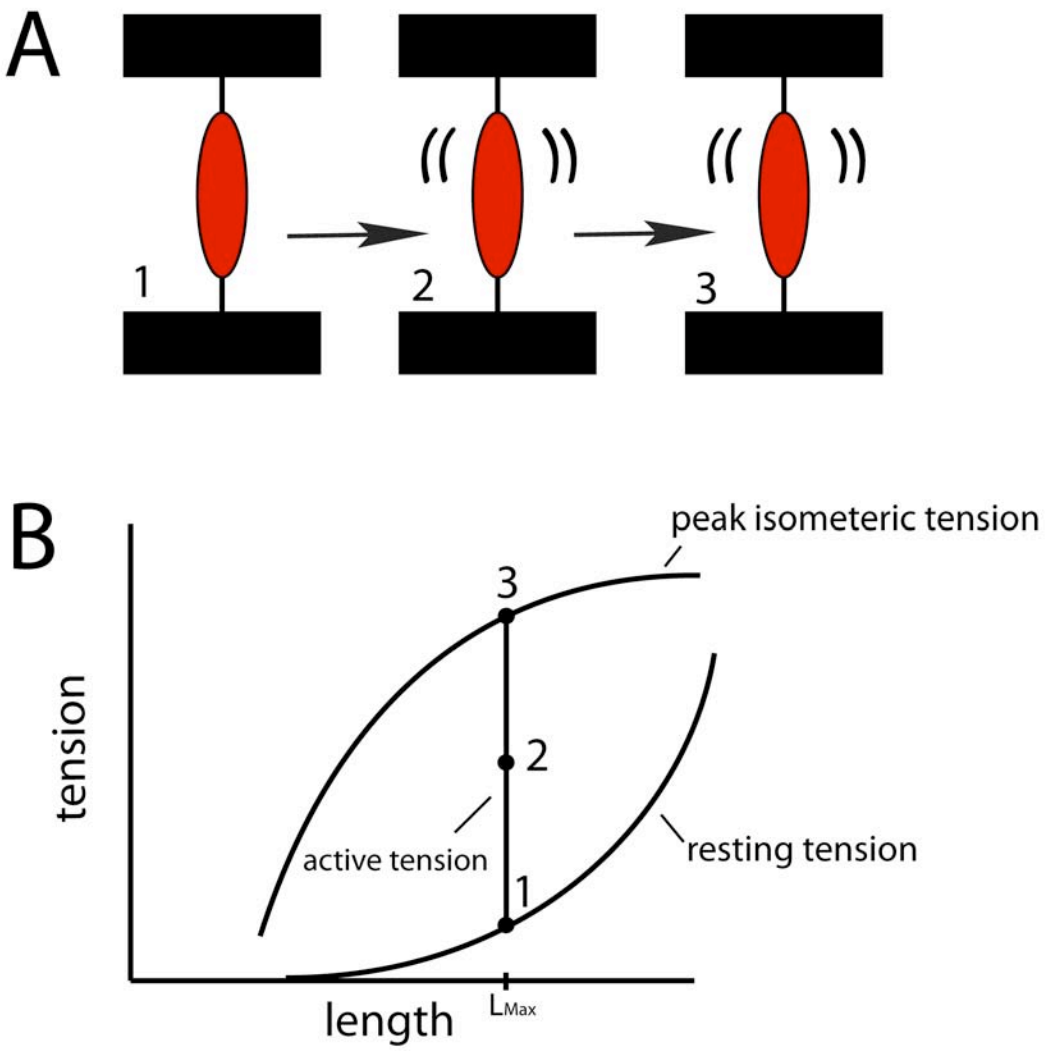

Adapted from Mohrman, D.E., Heller, L.J., 2006. Cardiovascular physiology. In: Lange physiology series. Lange Medical Books/McGraw-Hill, New York.

Figure 1.15: Length-tension relationship of an isolated cardiac muscle for an isometric contraction. **A**) Cartoon representation of an isolated cardiac muscle maintained at a fixed length. At point 1 the muscle is at rest and stretched to a fixed length. Points 2 and 3 depict the muscle contracting while the length is held constant. **B**) Length-tension curve for an isometric contraction. The bottom curve in the resting tension curve and the top curve is the peak isometric curve for the muscle. Stretching the muscle at rest generates some tension (point 1) called resting tension. The resting length that generates the maximum isometric tension is called L_{Max}. When a muscle that is fixed in length contracts tension is developed (active tension, points 2 and 3) until the maximum isometric tension is reached (point 3).

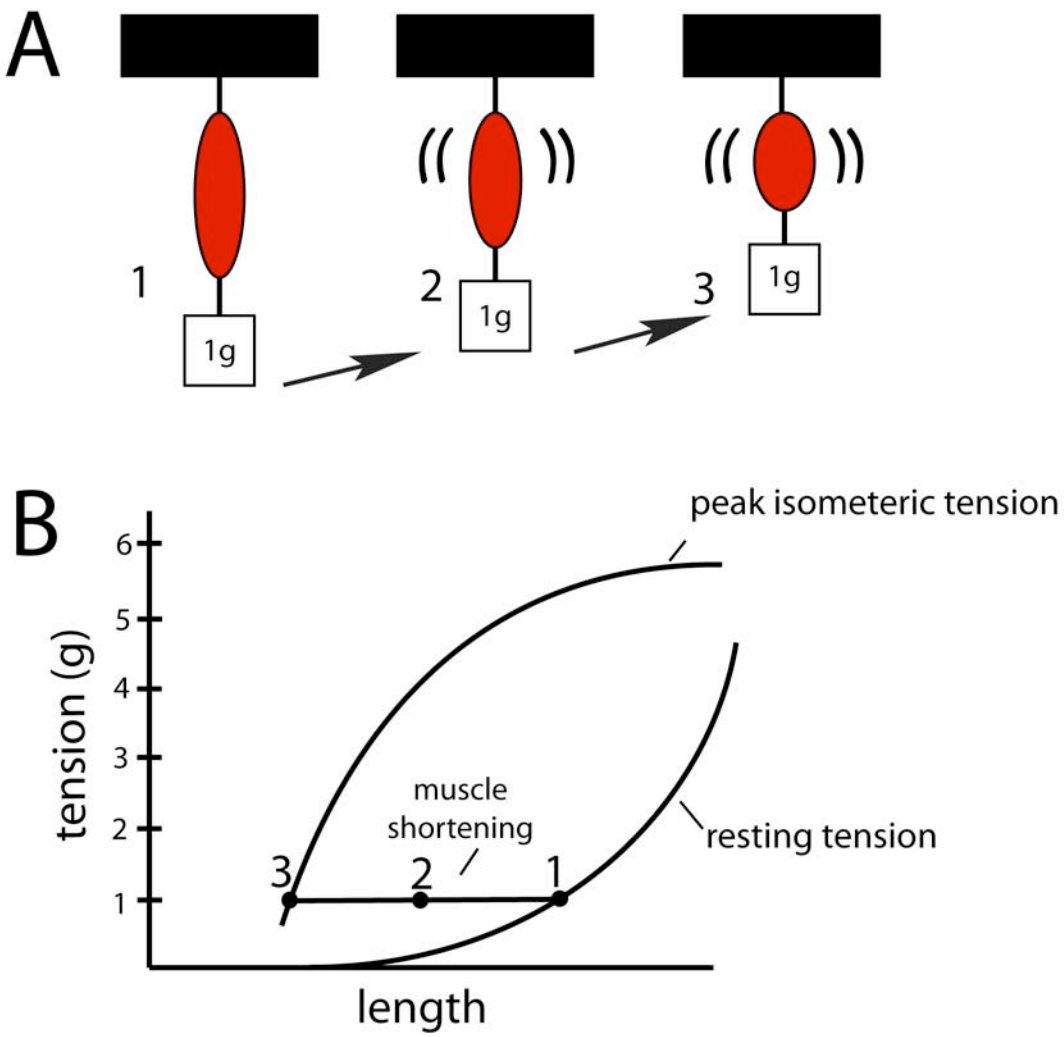

Adapted from Mohrman, D.E., Heller, L.J., 2006. Cardiovascular physiology. In: Lange physiology series. Lange Medical Books/McGraw-Hill, New York.

Figure 1.16: Length-tension relationship of an isolated cardiac muscle for an isotonic contraction. **A**) Cartoon representation of an isolated cardiac muscle working against a fixed load. In this cartoon, a 1g weight is attached to the muscle (load). At point 1 the muscle is at rest and stretched by the 1g weight. Points 2 and 3 depict the muscle contracting while the load is held constant. When the muscle contracts, and the tension generated exceeds the load on the muscle, it shortens (points 2 and 3). **B**) Length-tension curve for an isotonic contraction. The bottom curve in the resting tension curve and the top curve is the peak isometric curve for the muscle. The 1g weight stretches the muscle, generating 1g of resting tension (point 1). When the muscle contracts, the active tension generated exceeds the 1g load the muscle must work against and the muscle shortens (points 2 and 3). The muscle will shorten until it reaches the length for which the maximum possible tension is 1g on the peak isometric tension curve (point 3).

Figure 1.17

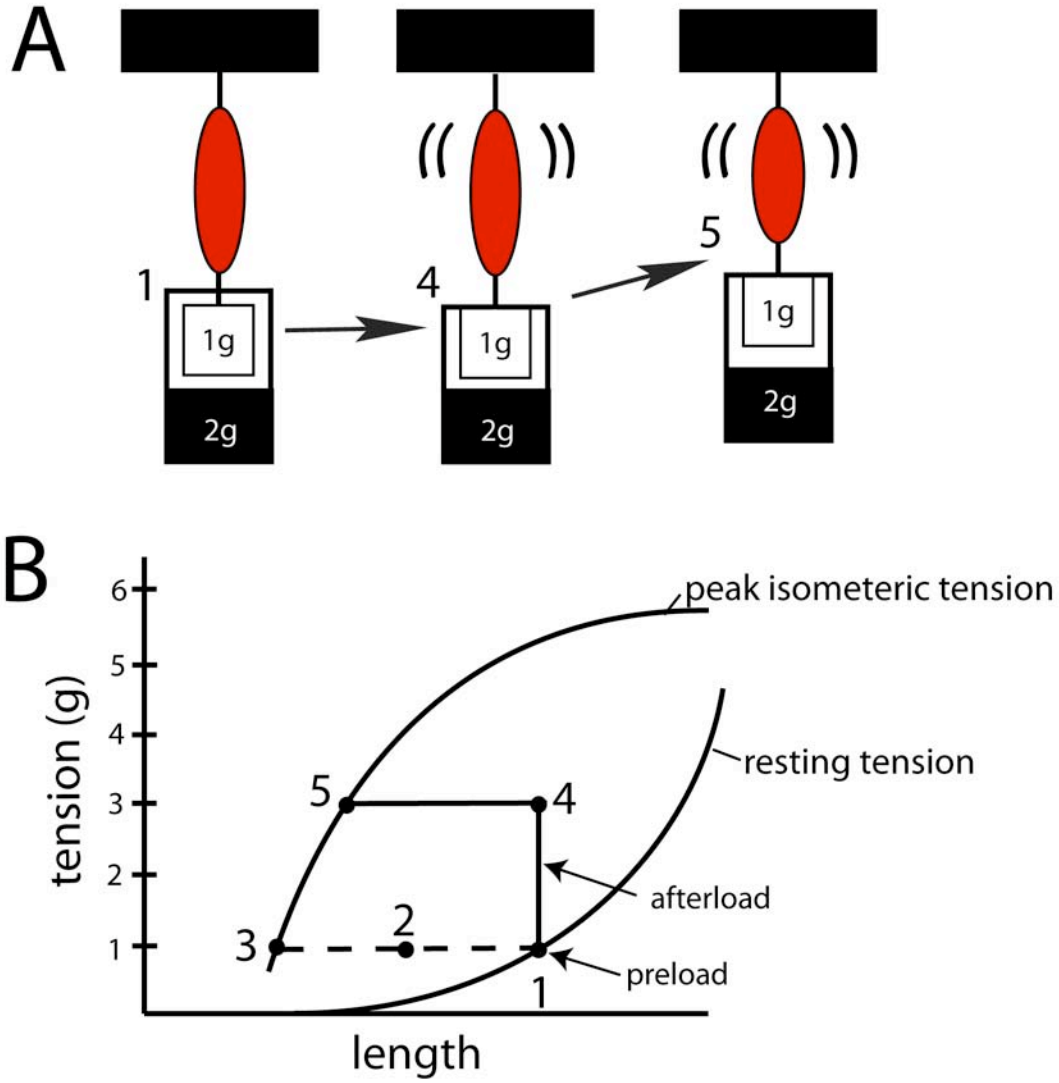

Adapted from Mohrman, D.E., Heller, L.J., 2006. Cardiovascular physiology. In: Lange physiology series. Lange Medical Books/McGraw-Hill, New York.

Figure 1.17: Length-tension relationship of an isolated cardiac muscle for an afterloaded contraction. **A**) Cartoon representation of an isolated cardiac muscle undergoing an afterloaded contraction, where the load on the muscle at rest (preload) is different than the load on the muscle during contraction (afterload). In this cartoon, a 1g weight is attached to the muscle, stretching the muscle at rest (point 1, preload). Points 4 and 5 depict the muscle during contraction. When the muscle contracts, it must work against an additional 2g load (the afterload, point 4). Once the muscle generates enough tension to overcome the 2g afterload (3g total) it will shorten (point 5). **B**) Length-tension curve for an afterloaded contraction. The bottom curve in the resting tension curve and the top curve is the peak isometric curve for the muscle. The 1g weight stretches the muscle, generating 1g of resting tension (point 1). When the muscle contracts, the active tension generated must exceed 2g to overcome the afterload (point 4) before the muscle shortens. The muscle will shorten until it reaches the length for which the maximum possible tension is 3g on the peak isometric tension curve (point 5). The dashed line (points 1-3) is an isotonic contraction shown for comparison.

afterloaded muscle contraction in which the load on the muscle at rest (the preload) is 1g but the afterload on the muscle is an additional 2g, making the total load on the muscle 3g. When the muscle is stimulated to contract in this scenario, it must initially generate enough tension to overcome the total load (Figure 1.17, point 1-4). Once the muscle has generated enough tension to overcome the 3g total load, it shortens until it reaches the length at which the maximum possible tension is 3g (Figure 1.17, point 4-5). It is important to note that the afterloaded contraction shortens less than the non-afterloaded contraction even though they start at the same initial length (Fig 1.17, points 4-5 vs. points 1-3) (Mohrman and Heller, 2006).

6. Cardiac Function:

The best indicator of cardiac function is cardiac output (CO) and it is defined as the amount of blood pumped by the left ventricle per minute. CO is continuously adjusted in order to meet the needs of the body. The factors that determine CO are heart rate (HR) and stroke volume (SV).

$$CO = HR \times SV$$

As mentioned previously, HR is determined by the pacemaker cells of the SA node, but it can be modulated by neural input from the autonomic nervous system. SV is the volume of blood that is ejected from the heart with each cardiac cycle. There are many determinants of SV and these will be discussed below. What is important to note from the above equation is that modulation of CO must come from changes in HR, SV, or both (Klabunde, 2005; Mohrman and Heller, 2006).

The length-tension relationship of individual cardiomyocytes is the underlying basis for cardiac function. However, the heart consists of many cardiomyocytes working together as a cohesive unit. Therefore, in order to understand how the principles of the myocyte length-tension relationship applies to the heart as a whole, one must look at the heart's pressure-volume relationship. Figure 1.18 shows the pressure-volume relationship of the left ventricle with the length-tension relationship from one cardiac cycle and illustrates that each event of the cardiac cycle has a corresponding event in the length-tension relationship. For example, during diastole, when the mitral valve is open, blood flows into the ventricle, causing the muscle to stretch, and generates increasing resting tension in the cardiac muscle. The end-diastolic volume establishes the muscle resting length before it contracts and is called ventricular *preload*. When systole begins the cardiac muscle starts generating isometric tension. At this point in the cardiac cycle both the mitral valve and the aortic valve are closed and so the ventricles are contracting against a constant volume (isovolumetric contraction). Ventricular pressure therefore increases until it overcomes aortic pressure, at which time the aortic valve opens and the muscle begins to shorten, ejecting the blood out of the ventricular chamber. The aortic pressure therefore is called ventricular afterload because it determines the amount of force needed to overcome aortic pressure. Note that this is precisely the same phenomenon that occurs in the afterloaded contraction example of an isolated cardiac muscle: the muscle must generate enough tension to overcome

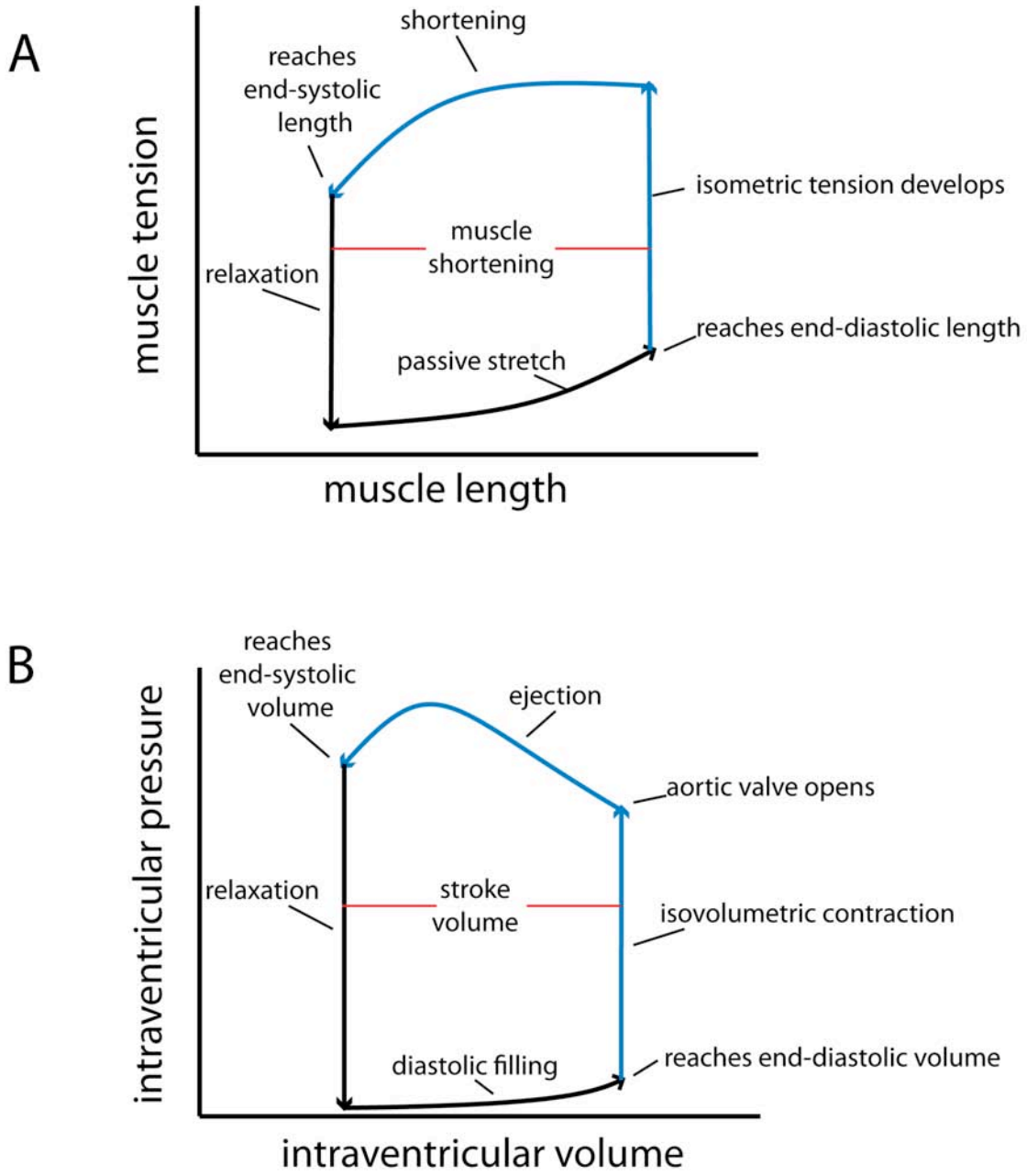

Adapted from Mohrman, D.E., Heller, L.J., 2006. Cardiovascular physiology. In: Lange physiology series. Lange Medical Books/McGraw-Hill, New York.

Figure 1.18: The relationship between muscle length-tension and cardiac pressure-volume curves. Each point on the length- tension curve **A**) corresponds to an event of the pressure- volume relationship of the left ventricle **B**).

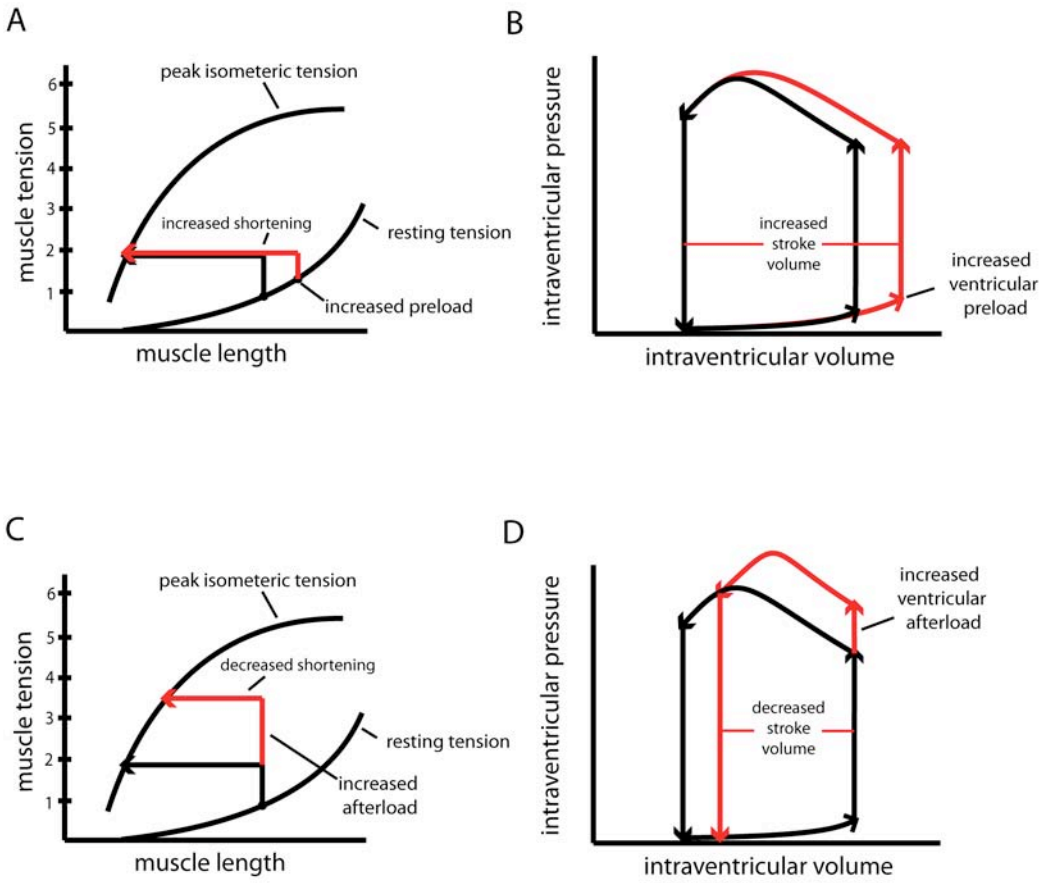

Adapted from Mohrman, D.E., Heller, L.J., 2006. Cardiovascular physiology. In: Lange physiology series. Lange Medical Books/McGraw-Hill, New York.

Figure 1.19: The effect of preload and afterload on the muscle length-tension relationship and the cardiac pressure-volume relationship. **A**) The effect of increased preload on the muscle length-tension relationship. Increased preload (load on the muscle at rest, shown in red) increases the shortening of the muscle. However, if preload continues to increase and stretches the muscle beyond L_{Max}, the muscle will shorten less. **B**) The effect of increased preload on the left ventricular pressure-volume relationship. Increased end diastolic volume (preload, shown in red) stretches the ventricular muscle, which in accordance with to the length-tension relationship, causes increased muscle shortening, and therefore increased stroke volume. **C**) The effect of increased afterload, with constant preload, on the muscle length-tension relationship. Increased afterload (load on the muscle during contraction, shown in red) has a negative effect on muscle shortening. **D**) The effect of increased afterload on the left ventricular pressure-volume relationship. Increased aortic pressure (afterload, shown in red) increases the amount of isovolumetric pressure (isometric tension) that must be generated to open the aortic valve and therefore allows less muscle shortening and decreased stroke volume.

the afterload before it can begin shortening (Fig 1.18). Once the muscle has finished shortening, ventricular pressure begins to drop and the muscle relaxes.

An important concept illustrated in figure 1.18 is that the volume of blood ejected during one cardiac cycle, the stroke volume (SV), is dependent on the ability of the muscle to shorten. Numerous factors can influence the shortening ability of a muscle and SV such as a change in preload, or end diastolic volume (Fig 1.19A-B), and afterload, or arterial pressure (Fig 1.19C-D), but these factors can only influence SV in the context of the muscle's length-tension curve. Altering the intrinsic ability of the muscle to shorten requires a shift in the length-tension curve itself. Sympathetic activity can modulate this property and this will be further discussed in D.2 of this chapter.

C. Innervation of the Heart:

The mammalian nervous system is divided into the central nervous system, including the brain and the spinal cord, and the peripheral nervous system. The peripheral nervous system can be further subdivided into the somatic nervous system, consisting of sensory and motor neurons, and the autonomic nervous system, consisting of the sympathetic and parasympathetic nervous systems. While the somatic nervous system transmits sensory input and mediates voluntary motor control, the autonomic nervous system modulates the function of internal organs that are involuntary. Some examples of organ systems that are controlled by the autonomic nervous system are cardiovascular,

respiratory, digestive, and thermoregulatory, and proper balance between these two branches is critical for maintaining homeostasis.

1. Autonomic Innervation of the Heart:

The autonomic nervous system consists of two branches: the sympathetic and the parasympathetic. Although these two branches often have different biochemical properties and opposing actions on their targets, their differentiation is primarily anatomical (Fig. 1.20). Parasympathetic cardiac innervation begins in the medulla of the brainstem, where the cell bodies of the pre-ganglionic cardiac neurons are located. Cardiac pre-ganglionic neurons exit the medulla at the tenth cranial nerve and project their axons toward the heart via the vagus nerve. The cardiac parasympathetic ganglia are located on top of the atria forming a network of cell bodies that send axons throughout the atria. Parasympathetic neurons modulate heart rate at the SA node and conduction velocity through the AV node but rarely project to the ventricles (Fig. 1.20) (Klabunde, 2005).

In contrast, the cardiac sympathetic preganglionic neurons originate in the thoraco-lumbar segments of the spinal cord, their cell bodies located in the intermediolateral cell column. From the spinal cord, sympathetic preganglionic neurons project their axons to sympathetic ganglia that are organized into two bilateral chains that run parallel to the spinal column, also referred to as the paravertebral ganglia. These sympathetic ganglia contain the cell bodies of the post-ganglionic neurons that project towards and innervate the heart (Klabunde, 2005) (Fig. 1.20).

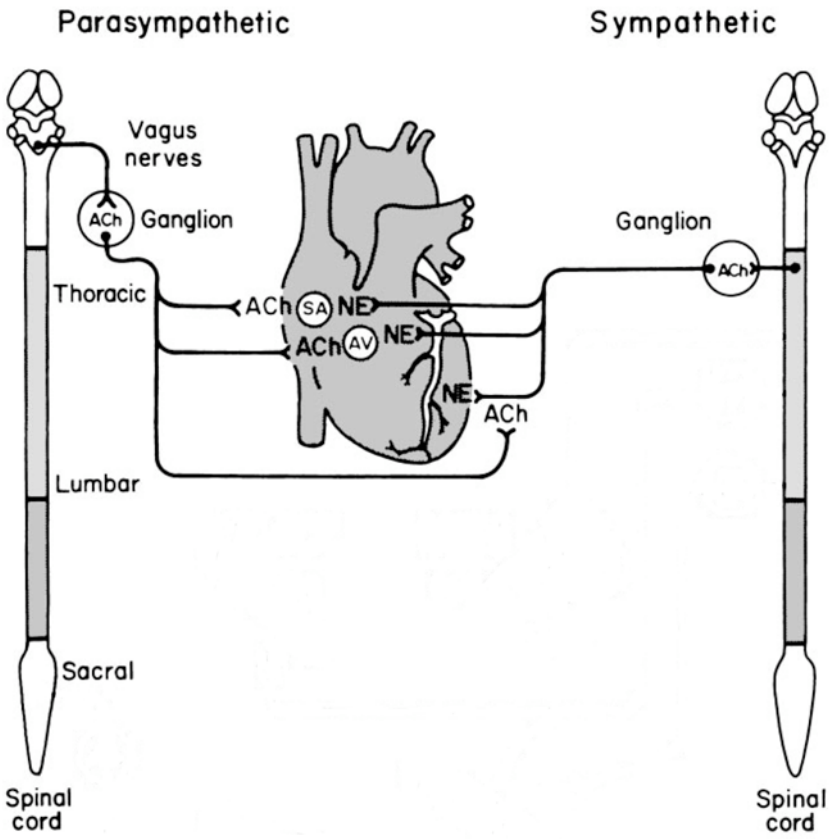

Adapted from Sparks and Rooke 1987. *Essentials of Cardiovascular Physiology.* Minneapolis, MN: Univ. of Minnesota Press, 1987.

Figure 1.20: Autonomic innervation of the heart. ACh = acetylcholne, NE = norepinephrine. The parasympathetic preganglionic nerves originate in the brainstem and project their axons towards the heart via the vagus nerve. They synapse with the parasympathetic post-ganglionic neurons in the cardiac ganglion, which lie close to the heart. Post-ganglionic parasympathetic neurons primarily innervate the SA node and the AV node in the heart. The post-ganglionic parasympathetic neurons also form pre-synaptic connections with post-ganglionic sympathetic neurons and modulate NE release. The cardiac sympathetic preganglionic neurons originate in the thoracic spinal cord. From there they project to the stellate ganglia where they synapse with post-ganglionic sympathetic neurons. Post-ganglionic sympathetic neurons project to the heart and innervate the SA node, the AV node, and the ventricular myocardium.

The paravertebral ganglia that project to the heart are variable within and across species (Janes et al., 1986a; Janes et al., 1986b; Pardini et al., 1989). However, for the most part, cardiac innervation arises from post-ganglionic nerves originating in the middle and inferior cervical ganglia (also known as the stellate ganglia) (Janes et al., 1986a; Janes et al., 1986b; Pardini et al., 1989). Several studies report cardiac sympathetic innervation arising from the superior cervical ganglion as well, however, this is not consistent across species and, in species where this has been observed, accounts for less than 8% of cardiac sympathetic innervation (Pardini et al., 1989).

In contrast to the parasympathetic nervous system which primarily innervates the atria, the sympathetic nervous system innervates all chambers of the heart and the intrinsic cardiac conduction system. Cardiac sympathetic fibers project to the heart from the base towards the apex, and are predominantly located in the subepicardium (Crick et al., 1994; Martins and Zipes, 1980; Randall et al., 1968). From the subepicardium sympathetic fibers project inwards towards the subendocardium. This pattern of innervation forms a basal to apical innervation gradient along with an innervation gradient across the left ventricle where sympathetic innervation is greater in the subepicardium than the subendocardium (Crick et al., 1994; Ieda et al., 2007; Martins and Zipes, 1980; Randall et al., 1968).

2. Sensory Cardiac Innervation:

The heart is also innervated by sensory afferent neurons, mainly comprised of myelinated Aδ-fibers and unmyelinated C-fibers (Ieda et al., 2006).

Cardiac sensory afferents innervate the ventricular myocardium as well as the epicardium (Ieda et al., 2006) and project to the upper thoracic dorsal horn via the dorsal root ganglion, where the cell bodies are located (Foreman, 1999). These chemosensitve sensory afferents transmit stretch and pain signals in response to ischemia in the heart (Foreman, 1999; Schultz and Ustinova, 1998).

3: Autonomic Neurotransmission:

Neurotransmission by pre-ganglionic sympathetic and parasympathetic neurons is mediated by the neurotransmitter Acetylcholine (ACh). Upon release, ACh binds to postsynaptic nicotinic acetylcholine receptors (nAChR) located on post-ganglionic neurons. Binding of ACh to post-synaptic nAChRs depolarizes the post-synaptic neuron and allows further propagation of the action potential. ACh is synthesized by the transfer of the acetyl group from acetyl coenzyme A to choline by the enzyme choline acetyl transferase. ACh is then packaged into vesicles by the vesicular ACh transporter and is ready for release. Parasympathetic transmission is terminated by enzymatic breakdown of ACh by acetylcholinesterase found in the bloodstream and within synapses, and choline is taken back up by the high affinity choline transporter to be recycled (Squire, 2003).

The neurotransmitter phenotype of post-ganglionic neurons is very distinct between sympathetic and parasympathetic neurons. Post-ganglionic parasympathetic neurons release ACh at the site of contact between a neuron and the cardiomyocyte or pacemaker cell, where it binds M_2 muscarinic acetylcholine receptors (mAChR), and slows heart rate. In contrast sympathetic

post-ganglionic neurons primarily release norepinephrine (NE) at the neuro-effector junction. NE synthesis begins with the conversion of the amino acid tyrosine to L-Dopa by tyrosine hydroxylase (TH), the rate-limiting enzyme of NE synthesis. L-Dopa is converted to dopamine by L-aromatic amino acid decarboxylase. Dopamine is packaged into vesicles by the vesicular monoamine transporter 2 where it is converted to NE by dopamine-β-hydroxylase. Upon release, NE primarily binds β_1-adrenergic receptors (β_1AR) on cardiomyocytes and stimulates heart rate, conduction velocity and contractility. Muscarinic and adrenergic receptors are 7 transmembrane G-protein coupled receptors. There are 3 classes of adrenergic receptors, α1ARs, α2ARs, and βARs, each of which have 3 subtypes (Goodman et al., 2001; Rockman et al., 2002) (Table 1). In the heart, there are ten fold more βARs than α_1ARs. The predominant βAR subtype in the heart is the β_1AR, comprising of 75-80%, and approximately 25% are β_2ARs (Bristow et al., 1986). Sympathetic transmission is terminated by re-uptake of NE by the NE transporter, which is located on the pre-junctional membrane of the post-ganglionic sympathetic neuron.

In addition to the classic neurotransmitters ACh and NE, parasympathetic and sympathetic neurons can express and release neuropeptides (Cane and Anderson, 2009). In particular, most cardiac sympathetic neurons express and release neuropeptide Y (Richardson et al., 2006) and parasympathetic neurons can express vasoactive intestinal peptide (Henning and Sawmiller, 2001).

Table 1.1: Adrenergic Receptors

Receptor	G-protein	Tissue Distribution	Endogenous Agonist
β_1	G_S	heart	NE = Epi
β_2	G_S/ G_i	heart, lungs, vessels, kidney	NE < Epi
β_3	G_S/ G_i	adipose tissue, heart	NE > Epi
$\alpha_{1A,\ 1B,\ 1D}$	G_q	heart, vessels, smooth muscle, liver, CNS	NE ≤ Epi
$\alpha_{2A,\ 2B,\ 2C}$	G_q/ G_i	smooth muscle, presynaptic terminals, pancreas, CNS	NE ≤ Epi

D. Autonomic Regulation of Cardiac Function:

The autonomic nervous system can regulate cardiac function by modulating four properties: chronotropy (heart rate), inotropy (contractility), lusitropy (relaxation), and dromotropy (conduction velocity).

1. Chronotropy:

Both the parasympathetic and sympathetic nervous systems can modulate heart rate. This is achieved by changing the slope of the slowly depolarizing membrane potential of pacemaker cells (phase 4), altering the threshold for triggering an action potential (phase 0) and/ or altering the degree of hyperpolarization at the end of phase 3. Activation of the sympathetic nervous system increases heart rate, i.e. has a positive chronotropic effect. NE activation of β_1ARs at the SA node stimulates accumulation of intracellular cyclic adenosine monophosphate (cAMP), which activates the enzyme protein kinase A (PKA). PKA phosphorylates L-Type Ca^{2+} channels, and increases flow of Ca^{2+} into the cell, increasing the rate of depolarization of the pacemaker cells. In contrast, activation of the parasympathetic nervous system decreases heart rate, i.e. has a negative chronotropic effect. This occurs through activation of M_2 muscarinic receptors at the SA node. M_2 receptors decrease intracellular cAMP and Ca^{2+} influx, thereby decreasing the rate of depolarization of pacemaker cells. In addition, activation of M_2 receptors increases K^+ influx into the cell, resulting in hyperpolarization (Fig 1.21). Heart rate is an important modulator of cardiac output. Therefore the ability of the autonomic nervous system to influence HR is

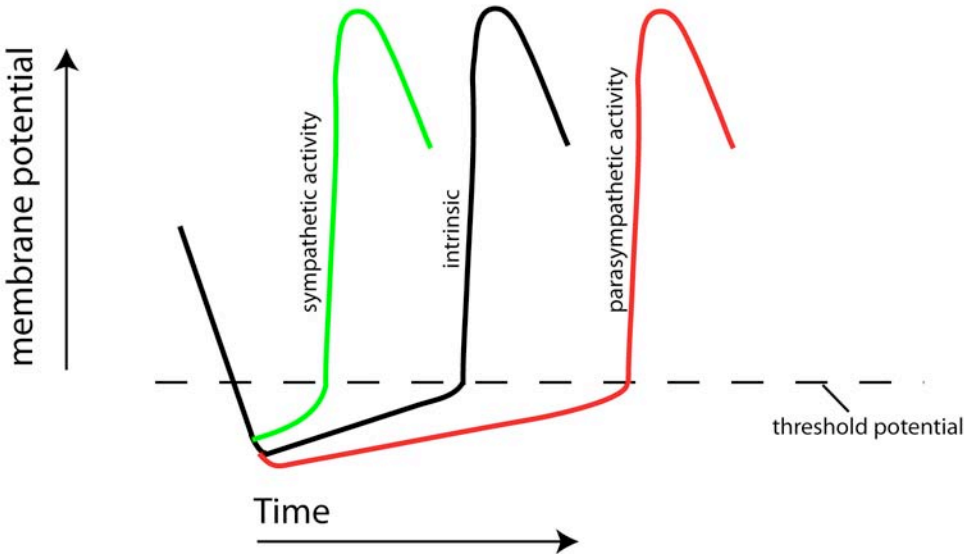

Adapted from Mohrman, D.E., Heller, L.J., 2006. Cardiovascular physiology. In: Lange physiology series. Lange Medical Books/McGraw-Hill, New York.

Figure 1.21: The effect of the autonomic nervous system on heart rate. Intrinsic pacemaker action potential is shown in black. Activation of the parasympathetic nervous system has a negative chronotropic effect (red) by decreasing the slope of the depolarizing membrane potential (phase 4) and increasing hyperpolarization after phase 3. In contrast, the sympathetic nervous system has a positive chronotropic effect (green) by increasing the slope of the depolarizing membrane potential (phase 4 of the action potential) and decreasing hyperpolarization after phase 3 of the action potential.

a critical mechanism for modulating cardiac output (Klabunde, 2005; Mohrman and Heller, 2006).

2: Inotropy:

Inotropy, or contractility, is the ability of the heart muscle to change its contractile strength without changes in preload. In response to sympathetic activation and NE release, cardiomyocytes contract 1) more forcefully and 2) more rapidly. Therefore, NE has a positive inotropic effect. Parasympathetic input has moderate influence on the atria and weak direct influence on the ventricles and therefore only sympathetic influence on contractility will be considered here.

Contractility of cardiac muscle is directly related to the muscle's length-tension relationship. Sympathetic activation results in an increase in the maximum possible tension (or force) the cardiac muscle can generate at any given length. In other words, activation of the sympathetic nervous system shifts the peak isometric tension curve upwards (Fig 1.22A). In afterloaded contractions, this shift in the peak isometric tension curve results in increased shortening of the muscle at a fixed preload (Fig 1.22A). In the intact heart, this increased ability to shorten in response to NE therefore results in an increased stroke volume (Fig 1.22B) and therefore increased cardiac output.

The ability of NE to modulate contractility occurs through activation of β_1AR and subsequent elevation of intracellular Ca^{2+}. β_1AR stimulates cyclic AMP accumulation, activating PKA. PKA in turn can modulate several factors involved in intracellular Ca^{2+}. First, phosphorylation of the L-type Ca^{2+} channels results in

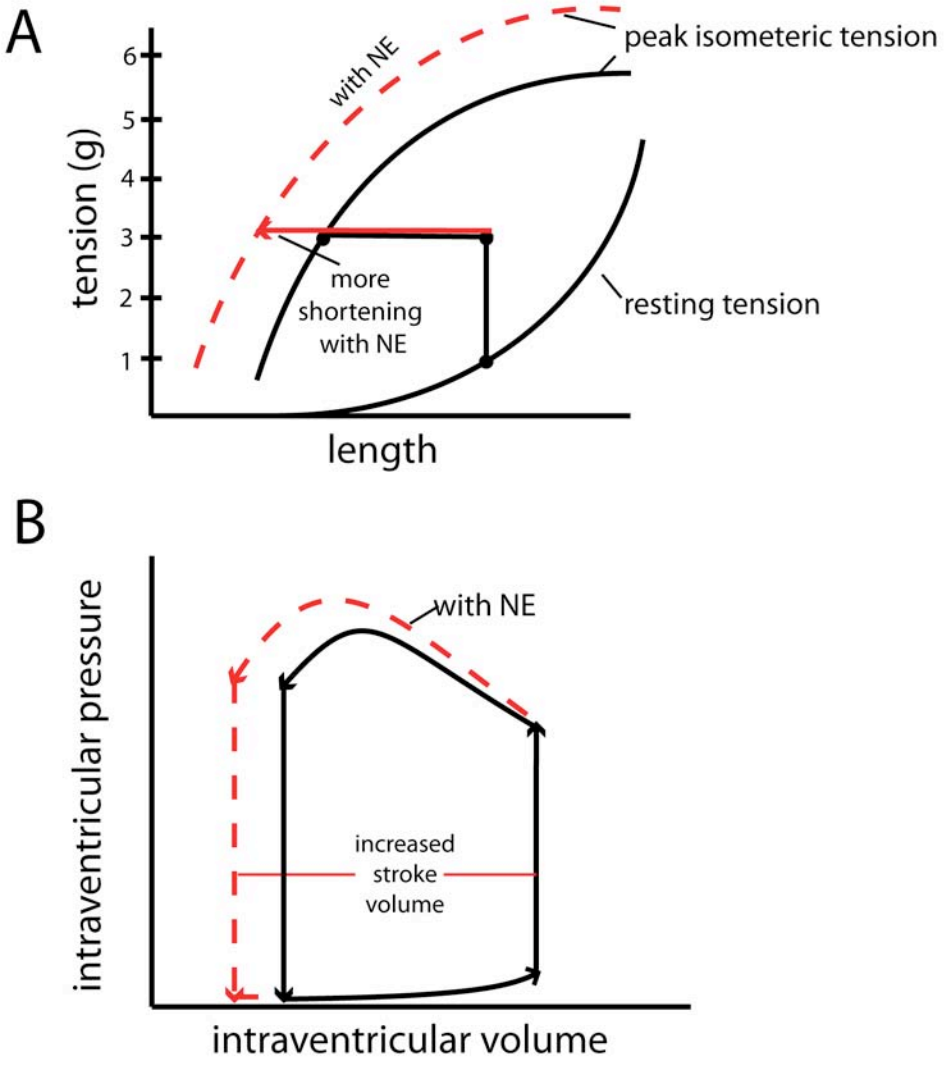

Adapted from Mohrman, D.E., Heller, L.J., 2006. Cardiovascular physiology. In: Lange physiology series. Lange Medical Books/McGraw-Hill, New York.

Figure 1.22: Sympathetic influence on muscle contractility. NE= norepinephrine. **A**) Sympathetic input (NE) shifts the peak isometric length-tension curve upwards (red dashed line). This results in increased muscle shortening when preload and total load are constant. **B**) Sympathetic influence on the left ventricular pressure-volume relationship. The increased ability of the muscle to shorten in response to NE results in greater stroke volume.

an increased influx of Ca^{2+} during an action potential. This elevated Ca^{2+} influx causes enhanced Ca^{2+} release from the sarcoplasmic reticulum and results in more cross-bridge formation between the thick and thin filaments of the sarcomere. Second, this increased influx of Ca^{2+} into the cardiomyocyte elevates the amount of Ca^{2+} that will be re-loaded into the SR, and released in response to future action potentials (Klabunde, 2005; Mohrman and Heller, 2006).

Contractility can be measured by a variety of techniques. The most accurate method is by echocardiography, which has the advantage of being non-invasive. Echocardiography uses ultrasonic waves to generate a continuous image of the heart. These images can be used to measure cardiac wall dimensions and many parameters of cardiac function, including cardiac output in addition to cardiac contractility via fractional shortening. Another technique used to assess contractility is to calculate dP/dt_{MAX} from ventricular pressure measurements. dP/dt_{MAX} is the maximum rate of pressure development during the isovolumetric phase of cardiac contraction and can be measured by placing a pressure transducer into the left ventricle. While measurement of dP/dt_{MAX} can function as an index of contractility, dP/dt_{MAX} is dependant on loading conditions placed on the heart such as arterial pressure (afterload) (Boudoulas et al., 1982; Mason, 1969). Therefore, while measurement of dP/dt_{MAX} provides some insight into the inotropic state of the heart, interpretation should be made with caution.

3. Lusitropy:

Sympathetic input to the heart can also accelerate the rate of cardiac relaxation. This is called a positive lusitropic effect. β_1AR activation of PKA can also phosphorylate phospholamban (Fig. 1.14), the regulatory subunit of SERCA. Phosphorylation of phospholamban removes inhibition of SERCA and enhances Ca^{2+} re-trapping. In addition to enhanced Ca^{2+} re-uptake into the sarcoplasmic reticulum, NE enhances relaxation by shortening the action potential duration. This occurs through modification of K^+ channel activity by both elevated intracellular Ca^{2+} and direct modification of the K^+ channels (Thomas et al., 2004). The positive lusitropic effect of NE is an important mechanism by which NE can shorten the systolic interval by shortening action potential duration of myocytes when HR is elevated (Klabunde, 2005; Mohrman and Heller, 2006).

4. Dromotropy:

Both the parasympathetic and sympathetic nervous systems can modulate the conduction velocity, or dromotropy, of action potentials at the AV node. As mentioned previously, the AV node contains specialized, slow-conducting cells that create a delay in conduction between the atria and the ventricles. Sympathetic activation accelerates conduction velocity at the AV node and this is referred to as a positive dromotropic effect. In contrast, the parasympathetic nervous system slows conduction at the AV node and this is referred to as negative dromotropy (Klabunde, 2005; Mohrman and Heller, 2006).

IV. SYMPATHETIC REMODELING AFTER MYOCARDIAL INFARCTION:

Each year approximately 1 million Americans will suffer from a myocardial infarction (MI). Myocardial infarction occurs when blood flow to the heart is disrupted. As a consequence, the cardiomyocytes are deprived of oxygen and die. The most common cause of coronary obstruction is atherosclerosis, or plaque build up in the coronary arteries. Therefore, treatment of myocardial infarction begins by reopening the obstructed coronary artery and allowing blood flow to return back to the ischemic myocardium. Although reperfusion of the myocardium dramatically improves survival and cardiac function, numerous changes continue to take place within the heart. These include remodeling of the myocardium and the cardiac sympathetic nervous system, both of which may lead to serious life-threatening complications such as heart failure and development of ventricular arrhythmias and sudden cardiac death (Dobaczewski et al., 2010; Rubart and Zipes, 2005).

A. Post-MI Cardiac Remodeling and Heart Failure:

During myocardial infarction, ischemia of the heart causes necrotic death of cardiomyocytes. Because the heart does not possess the ability to regenerate, the dead cardiomyocytes are replaced with a collagen scar. The formation of this scar occurs in three overlapping phases: the inflammatory phase, the proliferative phase, and the maturation phase (Dobaczewski et al., 2010; Frangogiannis, 2006). Cardiomyocyte injury and death by necrosis triggers a cascade of inflammatory events including expression of cytokines,

chemokines and adhesion molecules by cardiac fibroblasts (Porter and Turner, 2009). This initial inflammation recruits inflammatory cells such as neutrophils and macrophages to the site of injury (Nian et al., 2004). During the inflammatory phase, fibrinogen and plasma fibronectin extravasate out of the microvasculature and form a temporary matrix network to guide infiltrating immune cells to the injury (Dobaczewski et al., 2010). The proliferative phase begins as neutrophils and macrophages clean up the injured area by phagocytosing cellular and extracellular matrix debris while fibroblasts differentiate into myofibroblasts. The temporary matrix network is broken down and replaced with cellular fibronectin, collagen, and other matricellular proteins produced by myofibroblasts and macrophages (Porter and Turner, 2009). As the scar matures, more and more collagen is deposited and cross-linked together, and myofibrobasts begin to undergo apoptosis (Dobaczewski et al., 2010; Porter and Turner, 2009). This forms a dense collagen scar that provides mechanical strength and support to the infarcted heart (Dobaczewski et al., 2010). Although the formation of a scar in the injured myocardium during infarction is important for initial wound healing, in the long run it may becomes maladaptive and contributes to cardiac dysfunction (Porter and Turner, 2009). These phases of scar formation are similar in different animal models, however, a more accelerated time course is observed in smaller animals (Dobaczewski et al., 2006).

In addition to scar formation, many changes occur in the heart after myocardial infarction that eventually may lead to heart failure (Rockman et al., 2002). Although many myofibroblasts involved in scar formation undergo

apoptosis, there is evidence that some remain in the heart long after scar formation is complete (Porter and Turner, 2009). Continued remodeling of the cardiac extracellular matrix by these myofibroblasts leads to fibrosis of the heart, decreased elasticity, and eventually heart failure. Myocardial infarction and the formation of a scar affect the ability of the heart to function efficiently. In response to this, the sympathetic nervous system becomes hyperactive in order to maintain cardiac output (Bristow, 1997; Graham et al., 2002; Graham et al., 2004b; Karlsberg et al., 1979). However, chronically elevated sympathetic drive and NE become pathological and cause changes in the adrenergic receptor expression profile in the ventricular myocardium. In the failing myocardium, β_1ARs are downregulated (Bristow et al., 1986). Although no changes in β_2AR or α_1AR occur (Bristow et al., 1986; Bristow et al., 1988), downregulation of β_1AR changes the ratio of myocardial adrenergic receptor expression. These changes in the adrenergic receptor profile eventually lead to pathological cardiac hypertrophy and accelerated development of heart failure, characterized by ventricular dysfunction and inadequate perfusion of tissues (Bristow, 1997; Rockman et al., 2002).

B. Post-MI Sympathetic Remodeling and Ventricular Arrhythmias:

People who have had a myocardial infarction remain at substantial risk for developing ventricular arrhythmias and sudden cardiac death. There is striking evidence that links the sympathetic nervous system to these post-MI arrhythmias (Barber et al., 1983; Dorian, 2005; Du et al., 1999; Inoue and Zipes, 1988;

Nademanee et al., 2000; Rubart and Zipes, 2005; Solomon et al., 2005; Zipes, 1990). This becomes most apparent when looking at the survival of patients suffering from post-MI ventricular arrhythmias that are treated with sympathetic blockade vs. conventional anti-arrhythmia treatment. Treatment with sympathetic-blockade, either via administration of βAR antagonists (beta blockers) or by stellate ganglia blockade results in a much higher survival rate than conventional standard anti-arrhythmia treatment alone (Nademanee et al., 2000) (Fig. 1.23). In addition, the onset of post-MI ventricular arrhythmias occurs more frequently in the morning when there is a sympathetic surge (Cao et al., 2000a; Lampert et al., 1994; Muller et al., 1987a; Muller et al., 1987b), further implicating the sympathetic nervous system. These studies provide substantial evidence that changes in the cardiac sympathetic nervous system post-MI are linked to development of post-MI ventricular arrhythmias.

The current model explaining the link between the sympathetic nervous system and ventricular arrhythmias is that sympathetic heterogeneity develops in the ventricles (Rubart and Zipes, 2005). This occurs at two levels: regional changes in norepinephrine content and noradrenergic properties and changes in sympathetic innervation density and pattern (Rubart and Zipes, 2005). Early studies first identified heterogeneous denervation of the left ventricle post-MI. Because sympathetic fibers innervate the heart in a general basal to apical direction, denervation occurs in the viable myocardium apical to,

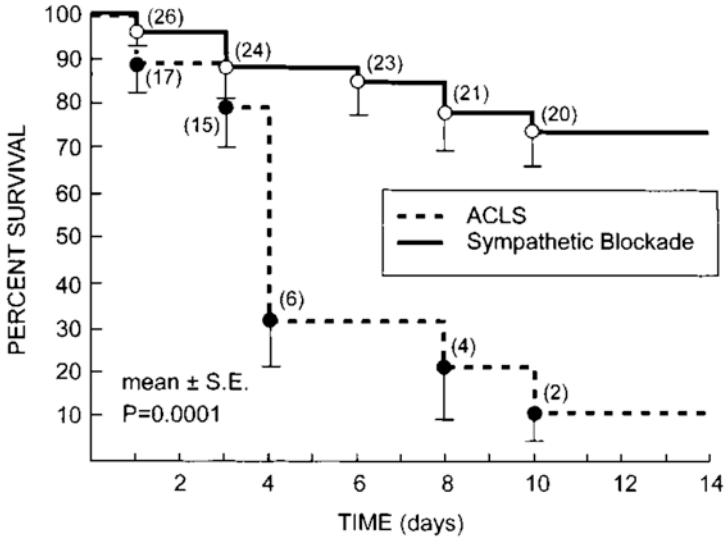

Adapted with permission from Wolters Kluwer Health. Nademanee et al., 2000 *Circulation:* 102(7):742-7.

Figure 1.23: Affect of sympathetic blockade on fatal ventricular arrhythmias after myocardial infarction. The group that received sympathetic blockade (either beta-blockers or stellate ganglia blockade) had a higher rate of survival compared to those that received standard advanced cardiac life support (ACLS). Thus the cardiac sympathetic nervous system is linked to development of post-MI ventricular arrhythmias.

or below, the infarct (Barber et al., 1983; Inoue and Zipes, 1987; Inoue and Zipes, 1988; Minardo et al., 1988; Stanton et al., 1989). In canine models, the post-infarct loss of functional sympathetic fibers in viable myocardium occurs as early as 5-20 minutes after ischemia (Inoue and Zipes, 1988) and persists up to three weeks after infarction (Barber et al., 1983). Other labs have also reported sympathetic denervation in the viable myocardium next to the infarct, the peri-infarct region, in both humans and animal models (Cao et al., 2000b; Hasan et al., 2006; Li et al., 2004b). In addition to sympathetic denervation, recent studies identify regions of significant hyperinnervation in the peri-infarct regions in humans and numerous animal models (Cao et al., 2000b; Hasan et al., 2006; Li et al., 2004b; Oh et al., 2006; Zhou et al., 2004c). Taken together these localized areas of sympathetic denervation and hyperinnervation in the peri-infarct region create a highly heterogeneous sympathetic innervation pattern in the post-MI ventricle. This development of sympathetic heterogeneity results in non-uniform sympathetic transmission to the heart and, along with sympathetic hyperactivity, is directly correlated with enhanced susceptibility to ventricular arrhythmias (Cao et al., 2000a; Cao et al., 2000b; Rubart and Zipes, 2005).

The exact mechanism of how sympathetic heterogeneity causes ventricular arrhythmias is not fully understood but disruption of repolarization gradients are implicated. Depolarization and repolarization of the heart during one cardiac cycle is tightly regulated. Basal to apical and transmural gradients of K^+ ion channels involved in cardiomyocyte repolarization exist in order to precisely coordinate contraction and relaxation of the ventricles (Brunet et al.,

2004; Costantini et al., 2005b; Nabauer et al., 1996; Wang et al., 2006). The differential K^+ ion channel expression results in a repolarization gradient in which repolarization, and therefore action potential duration, is longer in the subendocardium vs. the subepicardium (Antzelevitch et al., 1991; Brunet et al., 2004; Wang et al., 2006). This ensures that the subendocardium does not depolarize again before the subepicardium is repolarized. Because action potential duration/ repolarization is modulated by sympathetic activity (Mohrman and Heller, 2006; Thomas et al., 2004), a transmural gradient of sympathetic innervation also exists across the ventricles (Ieda et al., 2007; Randall et al., 1968). Myocardial infarction and heart failure cause changes in ion channel expression and function (Kaprielian et al., 2002; Lukas and Antzelevitch, 1993; Rozanski et al., 1998; Wang et al., 2006; Zicha et al., 2004). This electrical remodeling, in combination with development of sympathetic heterogeneity, disrupts the tightly coordinated action potential duration and repolarization gradient of the ventricles (Jiang et al., 2007), allowing early depolarization to occur out of sync with the pacemaker-controlled cardiac cycle. When this happens, non-pacemaker cells can spontaneously depolarize and develop an ectopic focus, leading to ventricular arrhythmia (Rubart and Zipes, 2005) (Fig. 1.24).

C. Molecular Mechanisms Underlying Sympathetic Remodeling:

Despite the increasing evidence that post-MI sympathetic remodeling results in enhanced susceptibility to ventricular arrhythmias, the mechanisms

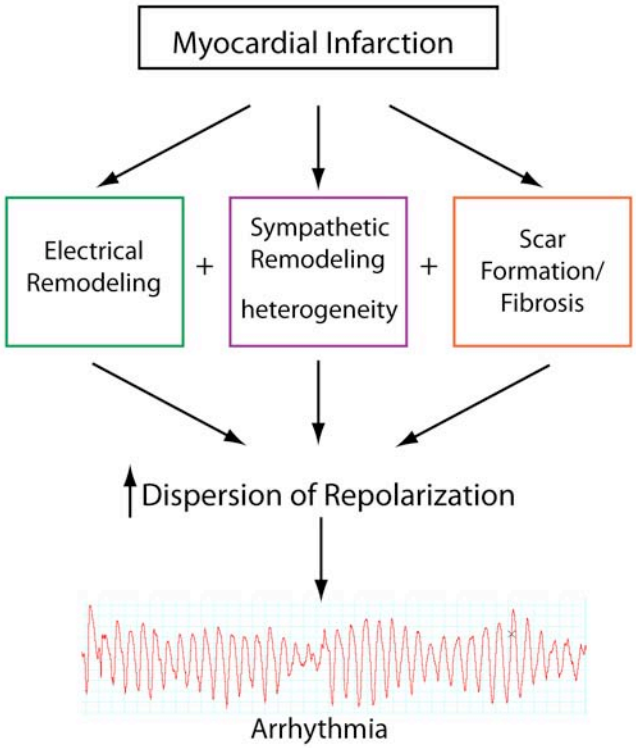

Adapted from Rubart, M., Zipes, D.P., 2005. Mechanisms of sudden cardiac death. J Clin Invest. 115**,** 2305-15.

Figure 1.24: Factors that contribute to ventricular arrhythmias after myocardial infarction. Myocardial infarction causes remodeling of the myocardium and the sympathetic nervous system. Myocardial remodeling includes the formation of the scar and fibrosis of the viable myocardium and electrical remodeling, changes in electrophysiological properties of the myocardium. In addition, sympathetic remodeling occurs. Regions of sympathetic denervation and regions of sympathetic hyperinnervation lead to sympathetic heterogeneity in the left ventricle. These three factors lead to disruption of the tightly regulated repolarization gradients (also known as increased dispersion of repolarization), which can lead to development of ventricular arrhythmias.

underlying generation of heterogeneous sympathetic innervation are still not fully understood. Recent studies implicate the neurotrophin NGF in sympathetic hyperinnervation after myocardial infarction (Hasan et al., 2006; Hiltunen et al., 2001; Zhou et al., 2004c). NGF stimulates sympathetic axon outgrowth during development (Crowley et al., 1994; Glebova and Ginty, 2004; Kuruvilla et al., 2004) and can also cause axon outgrowth and hyperinnervation in the adult with or without injury (Bjerre et al., 1975a; Cao et al., 2000a; Kaye et al., 1979). In particular, infusion of NGF at the stellate ganglia results in cardiac sympathetic hyperinnervation with increased incidence of ventricular arrhythmias in dogs (Cao et al., 2000a). NGF mRNA and protein are elevated in the heart after myocardial infarction induced by chronic ischemia (Hasan et al., 2006; Oh et al., 2006; Zhou et al., 2004c) and ischemia-reperfusion (Hiltunen et al., 2001; Zhou et al., 2004c). Elevated NGF mRNA and protein are detected in the peri-infarct region as early as 3 hours post-infarct (Hiltunen et al., 2001; Oh et al., 2006; Zhou et al., 2004c) and can remain elevated for up to 1 month (Zhou et al., 2004c), however these time courses can vary according to species and surgical model of myocardial infarction. The source for elevated NGF is not clear but evidence from chronic ischemia studies suggests that infiltrating inflammatory cells such as myofibroblasts and macrophages are a major source for NGF (Hasan et al., 2006). However, because cardiac myocytes produce NGF during development to facilitate sympathetic innervation of the heart (Ieda et al., 2004), they cannot be ruled out as a possible source of post-MI NGF.

While some aspects of the mechanism behind post-MI sympathetic

hyperinnervation have been elucidated, the mechanisms underlying post-MI sympathetic denervation are unknown. Recent studies show that selective activation of p75NTR by BDNF in the presence of TrkA signaling not only inhibits sympathetic axon outgrowth (Kohn et al., 1999), but can cause sympathetic axon degeneration both *in vitro* and *in vivo* (Singh et al., 2008). BDNF mRNA is elevated in the peri-infarct region after myocardial infarction (Hiltunen et al., 2001). Because TrkB, the preferred receptor for BDNF, is not present on sympathetic neurons (Fagan et al., 1996) the only neurotrophin receptor BDNF can activate is p75NTR. Therefore BDNF activation of p75NTR is a possible mechanism of post-MI denervation of the peri-infarct region.

V. PURPOSE OF THESIS, HYPOTHESIS, and SUMMARY OF RESULTS:

Development of sympathetic heterogeneity post-MI correlates with increased susceptibility to ventricular arrhythmias. Elevated NGF is likely responsible for cardiac sympathetic hyperinnervation but the mechanism for post-MI sympathetic denervation is unknown. Selective activation of p75NTR in sympathetic neurons leads to axon degeneration.

Therefore, I hypothesize that post-MI peri-infarct sympathetic denervation occurs through activation of p75NTR.

To test this hypothesis I quantified sympathetic innervation density using mice that lack functional p75NTR receptor (Lee et al., 1992). I found that both

sympathetic hyperinnervation and denervation occur in the peri-infarct myocardium after ischemia-reperfusion in wildtype mice. Peri-infarct sympathetic denervation was absent in p75NTR-/- mice, while sympathetic hyperinnervation was exacerbated in p75NTR-/- mice. BDNF protein increases 24 hours after ischemia-reperfusion, implicating it as a possible ligand for p75NTR-mediate sympathetic axon degeneration (Chapter 2).

In the process of performing the experiments for Chapter 2, I discovered an altered pattern of sympathetic innervation of the p75NTR-/- left ventricle in the absence of MI. Sympathetic fibers were confined to the subepicardium of the left ventricle, and the subendocardium was virtually devoid of sympathetic innervation. I determined that this altered pattern of sympathetic innervation was likely due to enhanced repulsion by semaphorin3a in the absence of p75NTR. Finally, I went on to determine if this altered pattern of sympathetic innervation had functional consequences. While cardiac hemodynamics was generally unaffected, p75NTR-/- mice showed a significantly higher incidence of premature ventricular complexes (Chapter 3).

Chapter 2

Manuscript 1:

Cardiac sympathetic denervation after myocardial infarction is mediated by p75NTR

Christina U. Lorentz[1], Eric N. Alston[1], Chia-Jen Siao[2], Barbara L. Hempstead,[2] and Beth A. Habecker[1]

[1] Department of Physiology and Pharmacology, Oregon Health and Science University, Portland, Oregon 97239, [2] Weill Cornell Medical College, New York, New York 10065

Abstract:

Development of cardiac sympathetic heterogeneity after myocardial infarction (MI) contributes to ventricular arrhythmias and sudden cardiac death. Regions of sympathetic hyperinnervation and denervation occur in the viable myocardium beyond the infarcted area. While elevated nerve growth factor is implicated in sympathetic hyperinnervation, the mechanisms underlying denervation are unknown. Recent studies show that direct activation of the p75 neurotrophin receptor (p75NTR) by brain derived neurotrophic factor (BDNF) causes axonal degeneration of sympathetic neurons. BDNF mRNA is elevated in the heart after myocardial infarction. Therefore, we tested the hypothesis that p75NTR causes sympathetic denervation using mice that lack p75NTR in an ischemia-reperfusion model of myocardial infarction. Sympathetic denervation occurred adjacent to the infarct in wildtype hearts 24 hours after ischemia-reperfusion and persisted for 3 days post-MI. Peri-infarct sympathetic denervation did not occur in p75NTR-/- mice 24 hours or 3 days after ischemia-reperfusion. Sympathetic hyperinnervation was found in the distal peri-infarct myocardium of both wildtype and p75NTR-/- mice, but hyperinnervation was exacerbated in the p75NTR-/- mice. By 7 days after ischemia-reperfusion, cardiac sympathetic innervation density returned back to sham-operated levels in both genotypes. Finally, we demonstrated that BDNF protein increases in the heart after ischemia-reperfusion using *HA-Bdnf* mice. These results suggest that peri-infarct sympathetic denervation is mediated by p75NTR, while sympathetic nerve sprouting is attenuated by p75NTR.

Introduction:

Myocardial infarction (MI) leads to increased risk of ventricular arrhythmias and sudden cardiac death (Solomon et al., 2005). The sympathetic nervous system is a major contributor to the development of these post-MI arrhythmias (Cao et al., 2000a; Cao et al., 2000b; Nademanee et al., 2000). Cardiac sympathetic drive is increased after MI (Graham et al., 2004a; Karlsberg et al., 1979; Lombardi et al., 1983) and sympathetic axons undergo remodeling that includes areas of hyperinnervation (Cao et al., 2000a; Hasan et al., 2006; Oh et al., 2006; Zhou et al., 2004c) and areas of denervation in the viable myocardium beyond the infarcted tissue (Barber et al., 1983; Inoue and Zipes, 1988; Li et al., 2004b; Minardo et al., 1988; Stanton et al., 1989). The resulting non-uniform sympathetic innervation and transmission to the heart contributes to ventricular arrhythmias (Rubart and Zipes, 2005).

Recent studies implicate neurotrophins such as nerve growth factor (NGF) in sympathetic remodeling after myocardial infarction (Hasan et al., 2006; Hiltunen et al., 2001; Zhou et al., 2004c). NGF stimulates sympathetic axon outgrowth (Levi-Montalcini, 1987) and is important for normal sympathetic cardiac innervation (Crowley et al., 1994; Glebova and Ginty, 2004). NGF is upregulated in the heart after myocardial infarction caused by ischemia-reperfusion (Hiltunen et al., 2001; Zhou et al., 2004c) and chronic ischemia (Hasan et al., 2006; Oh et al., 2006; Zhou et al., 2004c). Elevated NGF is thought to be responsible for the hyperinnervation that occurs after MI (Hasan et al., 2006; Zhou et al., 2004c). For example, areas of sympathetic

hyperinnervation co-localize with NGF-producing inflammatory cells after chronic ischemia (Hasan et al., 2006). While this suggests a mechanism for hyperinnervation after MI, the cause of sympathetic denervation is not known.

Neurotrophins bind two structurally distinct neurotrophin receptors, the Trk receptors and the p75 neurotrophin receptor (p75NTR) (Chao, 2003). In sympathetic neurons, activation of TrkA is required for NGF to stimulate axon outgrowth and target innervation (Smeyne et al., 1994). In contrast, selective activation of p75NTR by brain derived neurotrophic factor (BDNF), which binds only p75NTR on sympathetic neurons (Fagan et al., 1996), causes sympathetic axon degeneration *in vitro* and *in vivo* (Singh et al., 2008). BDNF mRNA is elevated at the infarct border zone after ischemia-reperfusion (Hiltunen et al., 2001) raising the possibility that BDNF might be a ligand for p75NTR-mediated sympathetic denervation. Therefore, we hypothesized that activation of p75NTR causes sympathetic denervation of the peri-infarct region after ischemia-reperfusion and tested this hypothesis using mice lacking p75NTR (p75NTR-/-)(Lee et al., 1992). We found that sympathetic denervation requires p75NTR, and that p75NTR also attenuates post-MI sympathetic hyperinnervation. Finally, we found that BDNF protein is elevated in the heart after ischemia-reperfusion, making it a potential ligand for p75-mediated sympathetic denervation.

Methods:

Animals and Experimental Group: Wildtype C57BL/6J and p75NTR-/- mice (B6.129S4-Ngfr^{tm1Jae}/J) (Lee et al., 1992) were obtained from Jackson

Laboratories. Homozygous *Bdnf-HA* mice in which the endogenous *Bfnf* coding exon was replaced with the murine *Bdnf* sequence fused to a C-terminal hemagglutinin (HA) epitope tag were generated as described by Yang et al., 2009 (Yang et al., 2009). Mice were kept on a 12h:12h- light dark cycle with ad libitum access to food and water. Age- and gender-matched male and female mice between 12-18 weeks old were used for all experiments. All procedures were approved by the Institutional Animal Care and Use Committee and comply with the *Guide for the Care and Use of Laboratory Animals* published by the United States National Institutes of Health (NIH publication No. 85-23, revised 1996). The experimental groups used were sham-operated animals and animals that underwent ischemia-reperfusion surgery. A minimum of four animals were assigned to each group for each experiment, and tissue from all groups was processed together for each type of molecular or biochemical analysis.

Ischemia-reperfusion Surgery: Anesthesia was induced with 4% inhaled isoflurane and maintained with 2% isoflurane. Mice were then intubated and mechanically ventilated. Core body temperature was monitored with a rectal probe and maintained at 37° C and two-lead ECG was monitored throughout the surgery using a PowerLab data acquisition system. A left thoracotomy was performed in the 4^{th} intercostal space and the pericardium was opened. The left anterior descending coronary artery (LAD) was reversibly ligated with an 8-0 suture for 30 minutes and then reperfused by release of the ligature. Occlusion was confirmed with ST segment elevation on the ECG, regional cyanosis, and

wall motion abnormalities. Reperfusion was confirmed by return of color to the myocardium distal to the ligation and disappearance of ST elevation. The suture remained within the wound for identification of the ligature site, and the chest and skin were closed in layers. After surgery, animals were returned to individual cages and given regular food and water for 24h, 3 days or 7 days before euthanasia and tissue harvest. Buprenex (0.1 mg/kg) was administered to ensure that the animals were comfortable following surgery. All surgical procedures were performed under aseptic conditions. Sham animals underwent the procedure described above except for the LAD ligation.

Infarct/ Area at Risk Analysis: 24 hours after the onset of reperfusion, the mice were anesthetized with 4% isoflurane, intubated, and mechanically ventilated, and anesthesia was maintained with 2% inhaled isoflurane. The chest cavity was re-opened and the LAD was re-occluded using the same suture from the ischemia-reperfusion procedure. Fluorescent particles (4 mg/ml in deionized water with 0.01% Tween 20; Duke Scientific no. 34 –1, 2- to 8-μm size) were infused through a polyethelyne tube (PE10) with a 30-gauge needle tip in the left ventricle of the heart. Microspheres were infused at a rate of 400μL/min for 4 minutes to delineate the area at risk. The heart was then excised for infarct size analysis and cut into transverse sections 1mm thick using a cutting block. Both sides of each tissue section were photographed under ultraviolet light for measurement of area at risk. The slices were then placed in 2,3, 5-triphenyltetrazolium chloride solution (TTC, 1% wt/vol in a sodium phosphate

buffer at 37° C, pH 7.4) for 20 minutes. TTC is commonly used as an indicator of cellular respiration. TTC is a white compound that can be enzymatically reduced by mitochondrial dehydrogenases giving rise to the red compound1,3,5-triphenylformazan. Thus live tissue is stained red and dead tissue, or infarct, remains white. The staining procedure was carried out in the dark to prevent break down of the TTC by the light. The slices were then placed in 10% neutral buffered formalin overnight to increase the contrast of the stained and unstained tissue. Myocardium that did not stain red was presumed to be infarcted. Both sides of each 1mm section were photographed under white light and total area, area at risk and infarct areas for each slice were traced in Photoshop. The volume of myocardium at risk and infarcted myocardium were calculated from the measured areas and slice thickness. Infarct size was normalized as a fraction of the area at risk or as a percent of the entire ventricle. All analyses were performed in a blinded fashion by two people. The data presented are the average of the two independent determinations of infarct/ risk. Infarct normalized to risk area was identical in both wildtype and p75NTR-/- mice (Fig. 2.1A-B).

Immunohistochemistry: Tyrosine Hydroxylase (TH) immunohistochemistry was performed as previously described (Lorentz et al., 2010). Briefly, sections were placed in 2% B.S.A/ 0.3% Triton X-100 in PBS for 1 h and then incubated with rabbit anti-TH (1:300, Chemicon) overnight. The following day the slides were incubated 1.5 h with AlexaFluor 488-conjugated rabbit IgG-specific antibody

(1:300, Molecular Probes) and visualized by fluorescence microscopy. For HA immunohistochemistry heart tissue was fixed for 2h in 3% paraformaldehyde, rinsed in PBS, cryoprotected in 30% sucrose overnight and 10 µm transverse sections were thaw-mounted onto charged slides. Sections were then placed in 5% B.S.A/ 0.1% Triton X-100 in PBS for 1 h followed by blocking with AvidinD blocking buffer (Vector Laboratories) for 15 min. Slides were briefly rinsed with PBS and blocked with Biotin solution (Vector Laboratories) for 15 min. Slides were rinsed again with PBS and incubated with rabbit anti-HA (1:500, Sigma) overnight at 4°C. Slides were then rinsed in PBS and incubated with biotinylated goat anti-rabbit (1:400, Jackson ImmunoResearch) for 1h at room temperature. Slides were washed with PBS and incubated with Cy3-streptavidin (1:800, Jackson ImmunoResearch) for 45 min. Slides were rinsed with PBS, coverslipped and visualized by fluorescence microscopy.

Innervation Density Analysis: Immunohistochemical staining was visualized on a Zeiss (Axiophot II) fluorescent microscope with the 20X objective. Photos were taken of 11 fields of view (A-K) from each section (Fig. 2.2A). Five sections approximately 150 µm apart were analyzed from each heart. Each picture occupied an area of 710 µm x 530 µm, which was defined as one field of view. Pictures A and B were taken in the right ventricle. C was taken at the border between the right ventricle and the left ventricle and each successive picture (D-J) was directly adjacent to the previous picture without overlap. K was taken from the interventricular septum. p75NTR-/- mice lack subendocardial

sympathetic innervation (Lorentz et al., 2010). Therefore, all pictures from the left ventricle were confined to the subepicardial layer of muscle. Innervation density was determined by threshold discrimination (ImageJ) as previously described (Lorentz et al., 2010) and each image was quantified by two independent blinded observers and averaged together.

Initially, each field of view (A-K) was averaged across the five sections from each heart in order to obtain an unbiased analysis of sympathetic innervation density after MI. Table 2.1 shows innervation density from WT hearts 3 days and 7 days after ischemia-reperfusion surgery. However, the position of the infarct in the left ventricle was not the same in all 5 sections analyzed from one heart (Fig. 2.2B), nor was it the same between animals due to anatomical variability of LAD morphology and surgical variability (Scherrer-Crosbie et al., 2007). Therefore, the data were also analyzed by segregating the infarct from peri-infarct myocardium. Once the infarct was identified for each section (Fig. 2.2C), three regions of the left ventricle emerged as areas of interest: the infarct, the proximal peri-infarct region (peri-infarct 1 or P1) and distal peri-infarct region (peri-infarct 2 or P2) (Fig. 2.2D). Pictures containing any infarcted myocardium were considered infarct. Peri-infarct 1 was defined as the field of view adjacent to the infarct and peri-infarct 2 was defined as the field of view adjacent to peri-infarct 1. Analyzing these three regions allowed us to control for variable positioning of the infarct within the individual animals. Innervation density from the fields of view that corresponded to peri-infarct 1 and peri-infarct 2 were averaged together and were compared to the corresponding region from sham-

operated animals (regions E, D and H respectively, Fig 2.2A, E). Because the infarct usually occupied more than one field of view, one representative infarct picture from each section was chosen and averaged across the five sections from one heart.

Statistics: Student's t-test was used for a single comparison between two groups (WT vs. p75NTR). One-way ANOVA with a Neuman-Keuls post-test was used to compare across multiple groups within the same genotype. Two-way ANOVA with a Bonferroni post-test was used to compare across genotypes and treatment groups.

Results:

TH+ innervation density was similar in the subepicardium of sham-operated wildtype (WT) and p75NTR-/- mice in regions corresponding to the infarct and peri-infarct in mice undergoing cardiac ischemia-reperfusion (Fig. 2.2E, 4C-D). Sympathetic innervation densities of sham-operated hearts collected 3 days and 7 days after surgery were identical and were pooled into one sham group.

To test the hypothesis that cardiac sympathetic denervation occurs through p75NTR, we analyzed sympathetic fiber density in wildtype (WT) and p75NTR-/- mice 24 hours, 3 days and 7 days after ischemia-reperfusion surgery. The infarct was significantly denervated in both genotypes by 24 hours (Fig 2.3A), and this sympathetic denervation persisted through 3 and 7 days after

surgery (Fig 2.3B-C). The infarct remained substantially denervated 7 days after ischemia-reperfusion but occasional TH+ fibers were observed within the infarct of mice from both genotypes (data not shown).

In contrast to the infarct, innervation density in the peri-infarct region was dynamic. Twenty-four hours after MI, sympathetic innervation trended down in the proximal peri-infarct region of WT mice, although the change was not statistically significant (Fig 2.4A, C, E). This did not occur in the p75NTR-/- mice (Fig. 2.4B, D, F). No change in sympathetic innervation density was detected in the distal peri-infarct region of WT hearts 24 hours after ischemia-reperfusion (Fig 2.4A, C, G) but significant sympathetic hyperinnervation was present in the distal peri-infarct region of p75NTR-/- mice (Fig. 2.4B, D, H).

Three days after MI significant sympathetic denervation was observed in the proximal peri-infarct region in WT mice (Fig. 2.5A, C, E) but no decrease in innervation density was observed in the same region from p75NTR-/- mice (Fig. 2.5B, D, F). At the same time, significant hyperinnervation was observed in the distal peri-infarct region of both the WT mice (Fig. 2.5A, C, G) and the p75NTR-/- mice (Fig. 2.5B, D, H). Sympathetic hyperinnervation was significantly greater in the p75NTR-/- distal peri-infarct region compared to WT ($p < 0.01$, two-way ANOVA with Bonferroni post-test). Sympathetic innervation density was also elevated in the p75NTR-/- right ventricle 3 days after MI (RV region A: p75NTR-/-: 207 ± 85% vs. WT 118 ± 51%, mean ± SD, $p < 0.01$, n=6-8; RV region B: p75NTR-/-: 190 ± 57% vs. WT 106 ± 69.24%, mean ± SD, $p < 0.05$, n=6-8),

suggesting that post-infarct hyperinnervation in the p75NTR-/- may extend beyond the left ventricle.

One week after ischemia-reperfusion surgery, there were no significant differences in peri-infarct innervation density compared to surgical sham animals. Sympathetic innervation in the WT proximal peri-infarct region continued to trend low, although it was not significantly different than sham (Fig 2.6A). In addition, the sympathetic hyperinnervation observed 3 days after myocardial infarction was no longer present in either genotype (Fig. 2.6A-B). Despite this, the distribution of the sympathetic fibers was altered compared to sham-operated animals. Instead of the even distribution of sympathetic fibers throughout the myocardium seen in the sham operated animals, sympathetic fibers were unevenly distributed, with areas of denervation and adjacent areas containing clusters of TH+ fibers (Fig. 2.6C).

The loss of sympathetic nerve fibers adjacent to the infarct required p75NTR. These data suggest that a ligand acting through p75NTR stimulated degeneration of axons outside of the infarct. BDNF binds only p75NTR on sympathetic neurons (Fagan et al., 1996) and BDNF mRNA is transiently elevated in the peri-infarct border zone 2-5 hours after ischemia-reperfusion (Hiltunen et al., 2001). To determine if BDNF protein was also increased in the myocardium after ischemia-reperfusion, we used homozygous *Bdnf-HA* mice (Yang et al., 2009). Immunohistochemistry to detect HA-BDNF revealed an increase in HA-BDNF 24 hours after MI compared to sham operated control animals (Fig 2.7). Interestingly, HA-BDNF immunohistochemistry revealed

punctate staining, suggesting that the source of BDNF might be from infiltrating immune cells rather than cardiomyocytes.

Discussion:

Previous studies examining innervation density in the heart following myocardial infarction have analyzed only regions of sympathetic hyperinnervation or denervation, excluding large areas of analysis (Hasan et al., 2006; Oh et al., 2006; Zhou et al., 2004c). Here, we sought to perform a systematic analysis of the whole left ventricle after ischemia-reperfusion. We found that simply analyzing the same region at different levels of the ventricle was not the best way to assess changes in cardiac innervation after ischemia-reperfusion. Thus, we identified the infarct and analyzed innervation density within each section based on proximity to the infarct within that section. This method revealed significant sympathetic denervation adjacent to the infarct combined with significant hyperinnervation in the distal peri-infarct myocardium. This is the first study to analyze total innervation density and identify both hyperinnervation and loss of innervation in the heart after myocardial infarction.

We found that p75NTR is required for the peri-infarct sympathetic denervation that occurs after ischemia-reperfusion. Sympathetic fibers that innervate the ventricles travel from the base to the apex (Randall et al., 1968), and numerous studies have shown that sympathetic denervation occurs both in the infarct and in the viable myocardium (Barber et al., 1983; Inoue and Zipes, 1987; Inoue and Zipes, 1988; Kammerling et al., 1987; Li et al., 2004b; Minardo et al., 1988; Stanton et al., 1989). In canine models, loss of functional

sympathetic fibers in the post-MI viable myocardium occurs within minutes after ischemia (Inoue and Zipes, 1988) and persists up to three weeks after infarction (Barber et al., 1983). In human patients, post-MI denervation can persist for years (Stanton et al., 1989). While peri-infarct denervation was detected in the WT mice 24 hours and 3 days after ischemia-reperfusion, denervation did not occur in the p75NTR-/- mice, suggesting that peri-infarct denervation is p75NTR-dependent. Selective activation of p75NTR can induce axon degeneration in sympathetic neurons (Singh et al., 2008), and a mechanism was recently proposed for p75NTR-mediated degeneration that involves a p75NTR-Rho-GDI-Rho- caspase-6 pathway (Park et al., 2010). This p75NTR-mediated axon degeneration pathway requires myelin, and therefore, it is unclear whether this particular signaling pathway is responsible for denervation in the left ventricle after myocardial infarction since myelin is not found in the heart.

p75NTR-mediated sympathetic axon degeneration *in vitro* is ligand dependent (Singh et al., 2008). One ligand that selectively binds p75NTR and causes sympathetic axon degeneration is BDNF (Singh et al., 2008). BDNF mRNA is transiently elevated in myocytes located at the infarct border zone 2-5 hours after ischemia-reperfusion and is back down to baseline by 120 hours (Hiltunen et al., 2001). We found elevated BDNF protein in the left ventricle 24h after MI. However BDNF protein was detected in cells that resemble infiltrating immune cells and not myocytes. These data suggest that there may be two phases of BDNF expression: an early phase in which BDNF is upregulated in cardiac myocytes that we were unable to detect at 24 hours after ischemia-

reperfusion followed by a later phase in which the source of BDNF may be infiltrating immune cells. These data suggest that BDNF is a likely candidate for triggering axon degeneration through p75NTR. However we cannot rule out a role for other p75NTR ligands, particularly pro-NGF and pro-BDNF (Lee et al., 2001). Pro-neurotrophins are the predominant form of neurotrophins found in peripheral tissues, including the heart (Bierl et al., 2005), and therefore are likely to be present after MI. Further investigation will be necessary to identify the ligand(s) responsible for p75NTR-mediated sympathetic denervation after myocardial infarction.

Our results suggest that p75NTR attenuates sympathetic outgrowth after ischemia-reperfusion in addition to enhancing axon degeneration. This is consistent with the observation that NGF stimulates greater axon outgrowth in cultured sympathetic neurons that lack p75NTR (Kohn et al., 1999). How p75NTR attenuates NGF-induced axon outgrowth after ischemia-reperfusion is unclear, but studies done in cultured sympathetic neurons provide some clues. p75NTR can functionally antagonize NGF-stimulated TrkA signaling, including downstream activation of ERK1/2 (Hannila et al., 2004). These studies implicate p75NTR as a negative regulator of NGF/ TrkA signaling. An alternative explanation for increased sympathetic hyperinnervation in p75NTR-/- mice is enhanced signaling by NT-3. NT-3 typically binds the TrkC receptor (Chao, 2003), but NT-3 can also bind and activate TrkA in the absence of p75NTR (Belliveau et al., 1997; Francis et al., 1999). Therefore, sympathetic neurons lacking p75NTR maintain the ability to respond to both NT-3 and NGF through

TrkA. It is possible that the exacerbated axon sprouting of p75NTR-/- sympathetic fibers after MI is a result of the response to elevated NGF and NT-3. However, NT-3 mRNA is not increased in the myocardium after ischemia-reperfusion (Hiltunen et al., 2001), suggesting that enhanced NGF signaling is the primary mechanism. Taken together, these data suggest multiple roles for p75NTR in sympathetic remodeling after myocardial infarction.

Peri-infarct sympathetic innervation changes in the week following ischemia-reperfusion. Sympathetic remodeling starts within 24 hours and continues over weeks and even months in both chronic ischemia (Hasan et al., 2006; Oh et al., 2006; Zhou et al., 2004c) and ischemia-reperfusion (Zhou et al., 2004c). The time course appears to differ depending on the animal and surgical model of myocardial infarction. We found that average peri-infarct sympathetic innervation density in the mouse returned to sham operated levels by 7 days after ischemia-reperfusion surgery, although sympathetic distribution remained heterogeneous. Similar results are observed in a rat model of chronic ischemia, but the time course was extended over four weeks (Hasan et al., 2006). The shortened time course of sympathetic remodeling in the mouse is paralleled by the accelerated time course of cardiac remodeling compared to larger species (Dobaczewski et al., 2006). This suggests that, although a similar pattern of sympathetic remodeling occurs, the time frame in which this takes place is dependent on the model. The hyperinnervation of the distal peri-infarct of both WT and p75NTR-/- mice was no longer present 7 days after ischemia-reperfusion, suggesting that sympathetic pruning took place. This occurred in

both genotypes, indicating that the sympathetic pruning did not require p75NTR. The mechanisms of axonal pruning are not well understood but factors responsible for axon retraction during development such as ephrins or semaphorins are expressed in the heart and may play a role (Ieda et al., 2007; Luo and O'Leary, 2005; Mansson-Broberg et al., 2008). For example, ephrinB2 mRNA is elevated in the peri-infarct region 5 days after chronic ischemia (Mansson-Broberg et al., 2008). Further investigation is necessary to determine what factors are present in models of ischemia-reperfusion vs. chronic ischemia and whether they play a role in sympathetic axonal pruning after MI.

Myocardial reperfusion is standard care for coronary artery blockade and myocardial infarction (Prasad et al., 2009). Therefore, ischemia-reperfusion in animals is the model that most closely mimics the human condition. However, this method of generating myocardial infarction has some drawbacks. Unlike chronic ischemia, which affects and causes thinning of the entire left ventricular free wall, ischemia-reperfusion produces a more variable infarct in terms of its placement in the left ventricle. Wall thinning does not occur after ischemia-reperfusion and infarct shape and placement are variable as a result. Some of the infarcts produced by ischemia-reperfusion in our study were transmural, occupying the entire left ventricular free wall, and some were not. Therefore, for consistency, pictures that contained any infarct were considered infarcted myocardium. An additional complication of the model is that nerve branches follow the vasculature and, therefore, nerve damage occurs during the LAD occlusion. However, this nerve crush would occur equally in both genotypes and

is unlikely to have affected our results. In larger animal models this can be avoided by obstructing the coronary artery with a balloon (Zhou et al., 2004c) but in the mouse model LAD ligation is the only feasible method to induce myocardial infarction.

In conclusion, our results identify the p75 neurotrophin receptor as a key player in the establishment of sympathetic heterogeneity after ischemia-reperfusion by mediating peri-infarct sympathetic denervation as well as attenuating distal peri-infarct hyperinnervation. Sympathetic heterogeneity promotes ventricular arrhythmias (Rubart and Zipes 2005) and therefore, understanding the mechanisms that underlie the development of post-MI sympathetic heterogeneity might provide novel insights to future treatments.

Grants:

Supported by AHA 0715669Z & 09PRE2110052 (C.U.L), AHA 0555553Z (B.A.H) and NIH HL093056 (B.A.H.).

Disclosures:

None

Table 2.1: Ventricular Sympathetic Innervation Density 3 days and 7 days after MI

Region	**WT 3d MI (%) (n=6)**	**WT 7d MI (%) (n=7)**
A	118.5 ± 50.6	56.67 ± 31.25 *
B	106.1 ± 69.24	65.08 ± 46.1
C	111.7 ± 36.55	91.45 ± 42.89
D	84.84 ± 31.75	71.01 ± 33.96
E	72.81 ± 26.48	68.66 ± 48.38
F	57.75 ± 35.64 *	73.24 ± 38.57
G	33.57 ± 21.07 ***	53.43 ± 29.88 **
H	9.24 ± 12.66 ***	30.62 ± 36.12 ***
I	8.28 ± 8.454 ***	12.7 ± 16.89 ***
J	41.31 ± 36.08 *	17.95 ± 21.56 **
K	87.72 ± 28.37	93.39 ± 53.43

Values are % sham operated control, mean ± SD.
* $p < 0.05$, ** $p < 0.01$, ***$p < 0.001$

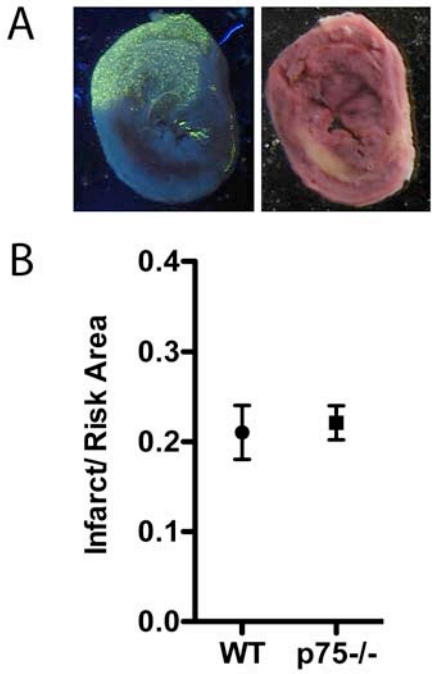

Figure 2.1: Infarct size compared with area at risk is not different between WT and p75NTR-/- mice. A) Area at risk (left) and infarct (right) in a representative section. The area at risk is devoid of fluorescent microspheres. The infarct is yellow/ white after 2,3,5-triphenyltetrazolium chloride staining, whereas viable tissue is stained red. B) Comparison of infarct size normalized to the area at risk quantified from 5 mice of each genotype (mean ± SEM, n=5).

Figure 2.2:

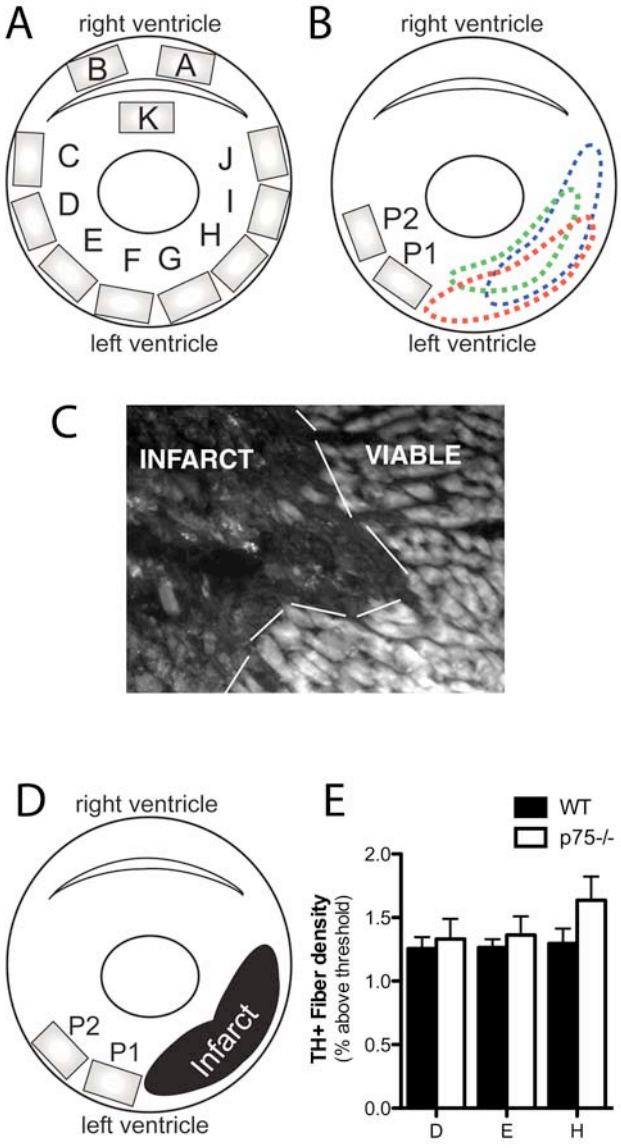
A
right ventricle
B
A
K
C
J
D
I
E
H
F G
left ventricle
B
right ventricle
P2
P1
left ventricle
C
INFARCT
VIABLE
D
right ventricle
P2
P1
Infarct
left ventricle
E
WT
p75-/-
TH+ Fiber density
(% above threshold)
2.0
1.5
1.0
0.5
0.0
D
E
H

Figure 2.2: Method for sympathetic innervation density quantification. A) Cartoon cross section of the left and right ventricles showing the 11 fields of view analyzed (A-K). Pictures A and B were taken from the right ventricle, C-J were taken from the subepicardium of the left ventricle, and K was taken from the interventricular septum. B) Cartoon cross section of the left and right ventricles showing the variable location of the infarct after ischemia-reperfusion. The proximal peri-infarct region (P1) was defined as the field of view adjacent to the infarct and the distal peri-infarct region (P2) was defined as the field of view adjacent to P1. C) Photomicrograph depicting the infarct 7 days after ischemia-reperfusion and the adjacent viable myocardium. D) Cartoon cross section of the regions quantified. One representative picture within the infarct was averaged over the five sections analyzed. E) Quantification of sympathetic fiber density in 3 sample regions (D, E, and H) from sham-operated animals from WT (black bars) and p75NTR-/- mice (white bars) that correspond to P2, P1, and infarct regions after MI respectively, mean ± SEM, n=8.

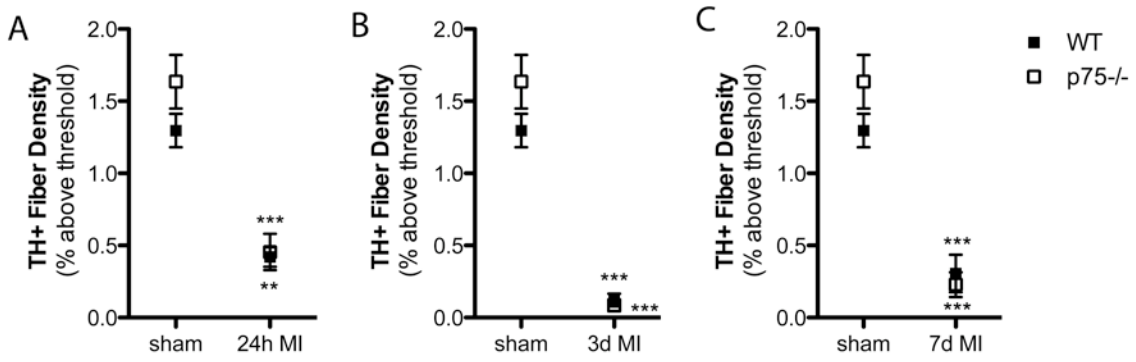

Figure 2.3: Sympathetic denervation occurs in the infarct 24 hours, 3 days, and 7 days after ischemia-reperfusion. A) Quantification of sympathetic fiber density in the infarct 24 hours B) 3 days, and C) 7 days after ischemia-reperfusion from WT (black squares) and p75NTR-/- mice (open squares) compared to sham operated animals, mean ± SEM, **p< 0.01, ***p< 0.001, n=4-8.

Figure 2.4

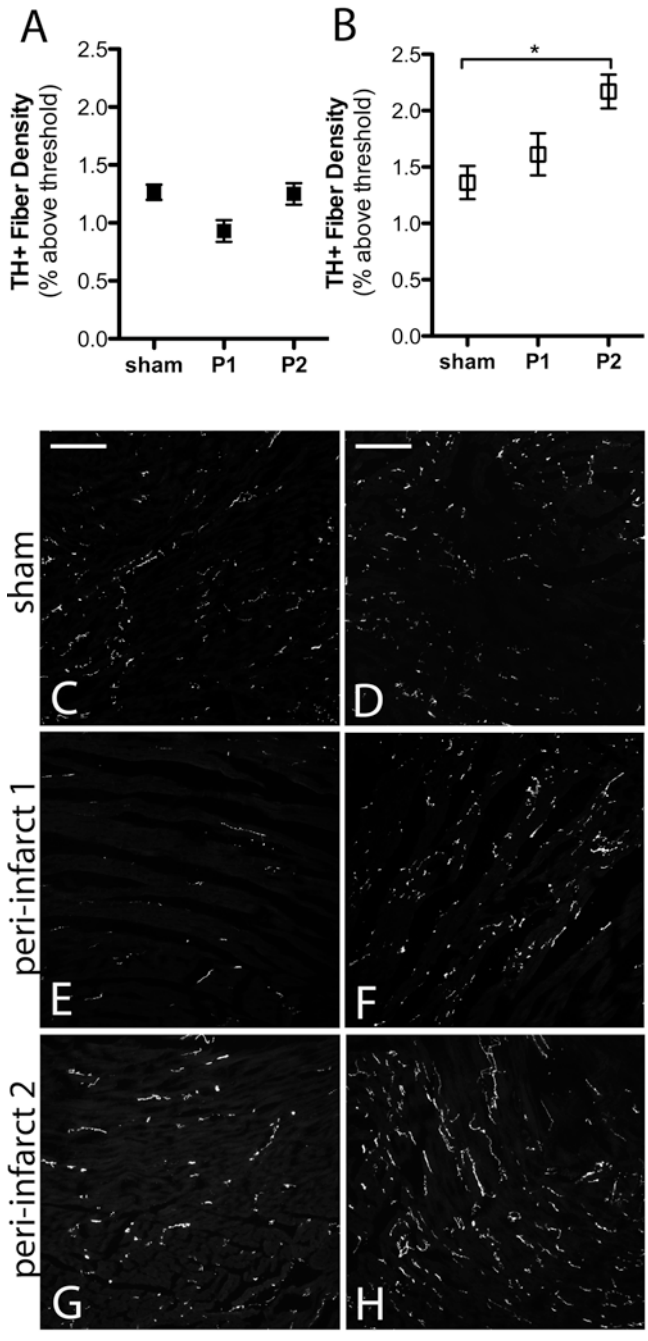
A
B
TH+ Fiber Density
(% above threshold)
2.5
2.0
1.5
1.0
0.5
0.0
sham
P1
P2
*
sham
peri-infarct 1
peri-infarct 2
C
D
E
F
G
H

Figure 2.4: Sympathetic innervation density 24 hours after ischemia-reperfusion in WT and p75NTR-/- peri-infarct left ventricle. A) Quantification of sympathetic fiber density in the proximal peri-infarct region (P1) and distal peri-infarct region (P2) 24 hours after ischemia-reperfusion from WT (black squares) and B) p75NTR-/- mice (open squares), mean ± SEM, *p< 0.05, n=4-8. C) Representative picture from WT sham operated left ventricle D) and from p75NTR-/- left ventricle, scale bar= 100μm. E) Representative picture from the proximal peri-infarct region (peri-infarct 1, P1) from WT mice and F) from p75NTR-/- mice. G) Representative picture from the distal peri-infarct region (peri-infarct 2, P2) from WT mice and H) p75NTR-/- mice.

Figure 2.5:

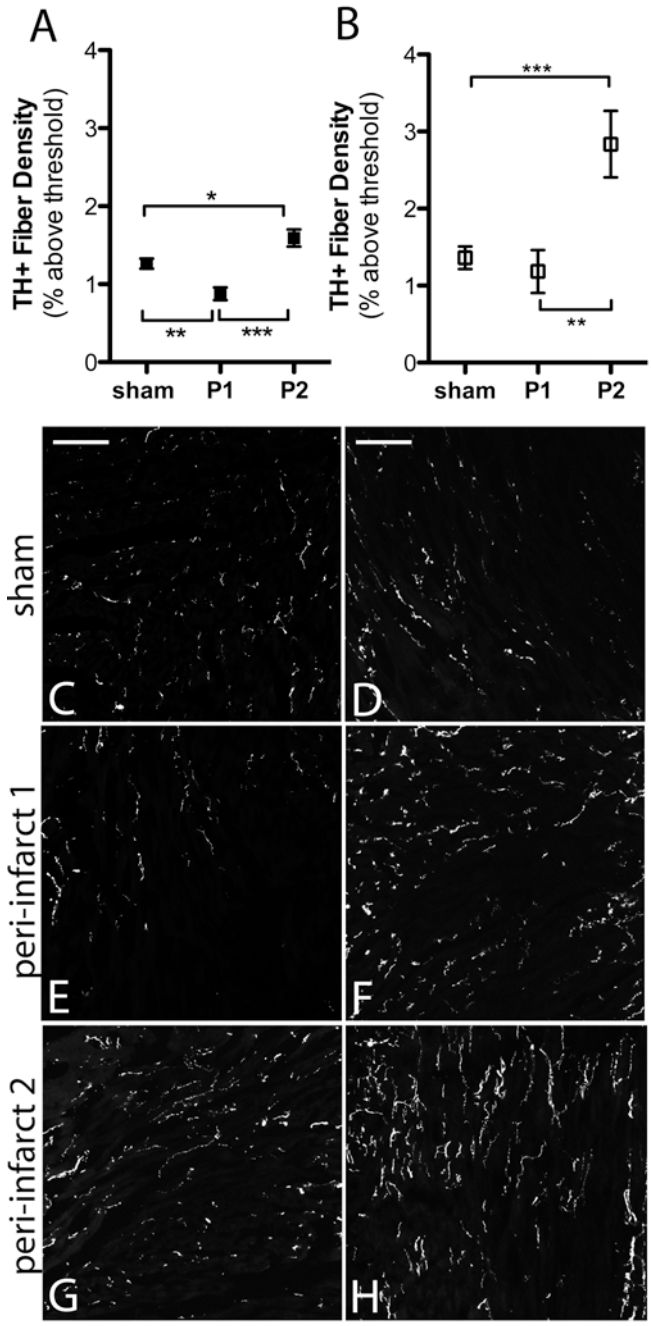
A
B
TH+ Fiber Density
(% above threshold)
sham
P1
P2
*
**
***
sham
peri-infarct 1
peri-infarct 2
C
D
E
F
G
H

Figure 2.5: Sympathetic innervation density 3 days after ischemia-reperfusion in WT and p75NTR-/- peri-infarct left ventricle. A) Quantification of sympathetic fiber density in the proximal peri-infarct region (P1) and distal peri-infarct region (P2) 3 days after ischemia-reperfusion from WT (black squares) and B) p75NTR-/- mice (open squares), mean ± SEM, *p< 0.05, **p< 0.01, ***p< 0.001, n=6-8. C) Representative picture from WT sham operated left ventricle D) and from p75NTR-/- left ventricle, scale bar= 100μm. E) Representative picture from the proximal peri-infarct region (peri-infarct 1, P1) 3 days after ischemia-reperfusion from WT mice and F) from p75NTR-/- mice. G) Representative picture from the distal peri-infarct region (peri-infarct 2, P2) 3 days after ischemia-reperfusion from WT mice and H) p75NTR-/- mice.

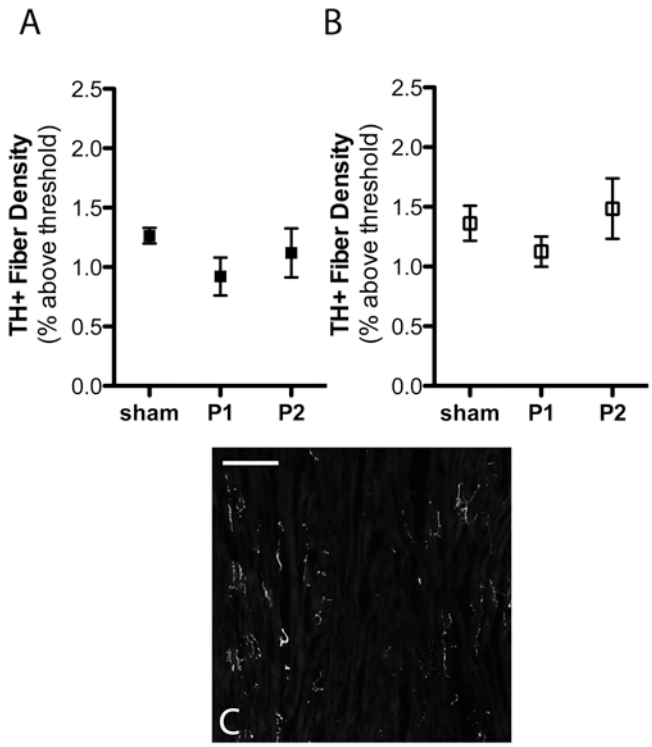

Figure 2.6: Sympathetic innervation density 7 days after ischemia-reperfusion in WT and p75NTR-/- peri-infarct left ventricle. A) Quantification of sympathetic fiber density in the proximal peri-infarct region (P1) and distal peri-infarct region (P2) 7 days after ischemia-reperfusion from WT (black squares) and B) p75NTR-/- mice (open squares), mean ± SEM, n=6-8. C) Representative picture from WT peri-infarct region 7 days after ischemia-reperfusion shows heterogeneous sympathetic innervation with distinct regions of denervated myocardium next to hyperinnervated regions, scale bar= 100μm.

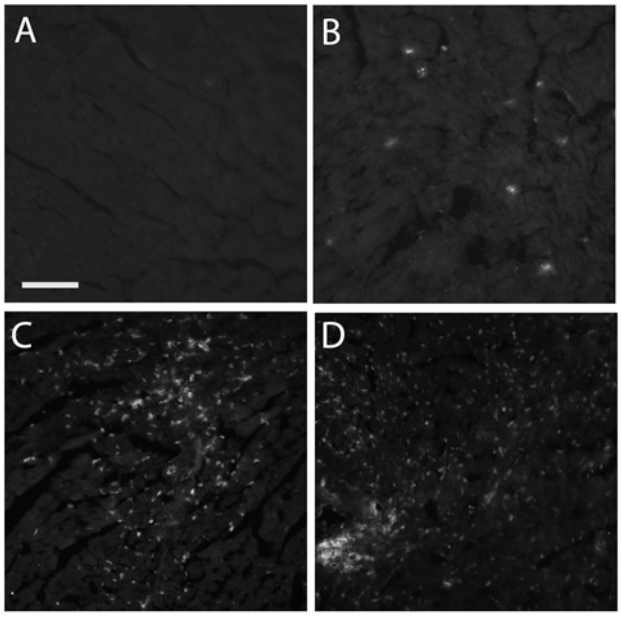

Figure 2.7: BDNF protein is elevated in the left ventricle 24 hours after ischemia-reperfusion. Representative pictures of immunofluorescence detection of BDNF using an antibody to HA in the left ventricle from *Bdnf-HA* mice that underwent sham operation (A-B) or 24 hours after ischemia-reperfusion (C-D), scale bar= 100μm.

Chapter 3

Manuscript 2:

Heterogeneous ventricular sympathetic innervation, altered β adrenergic receptor expression, and rhythm instability in mice lacking the p75 neurotrophin receptor

Christina U. Lorentz[1], Eric N. Alston[1], Todd Belcik[2], Jonathan R. Lindner[2], George D. Giraud[2,3] , and Beth A. Habecker[1]

[1] Department of Physiology and Pharmacology, and [2] Division of Cardiovascular Medicine, Oregon Health and Science University, Portland, Oregon 97239 [3] Department of Hospital and Specialty Medicine, Portland VA Medical Center, Portland, OR 97201, USA

American Journal of Physiology, Heart and Circulatory Physiology, 2010 Feb 26. [Epub ahead of print]

Abstract

Sympathetic nerves stimulate cardiac function through release of norepinephrine and activation of cardiac β1-adrenergic receptors (β_1AR). The sympathetic innervation of the heart is sculpted during development by chemoattractive factors including Nerve Growth Factor (NGF) and the chemorepulsive factor semaphorin3a. NGF acts through the TrkA receptor and the p75 neurotrophin receptor (p75NTR) in sympathetic neurons. NGF stimulates sympathetic axon extension into the heart through TrkA, but p75NTR modulates multiple co-receptors that can either stimulate or inhibit axon outgrowth. In mice lacking p75NTR the sympathetic innervation density in target tissues ranges from denervation to hyperinnervation. Recent studies revealed significant changes in the sympathetic innervation density of p75NTR -/- atria between early postnatal development and adulthood. We examined the innervation of adult p75NTR-/- ventricles and discovered that the subendocardium of the p75NTR-/- left ventricle was essentially devoid of sympathetic nerve fibers, while the innervation density of the subepicardium was normal. This phenotype is similar to that seen in mice over-expressing semaphorin3a, and we found that sympathetic axons lacking p75NTR are more sensitive to semaphorin3a *in vitro* than control neurons. The lack of subendocardial innervation was associated with decreased dP/dt, altered cardiac β_1 adrenergic receptor (β_1AR) expression and sensitivity, and a significant increase in spontaneous ventricular arrhythmias. The lack of p75NTR also resulted in increased tyrosine hydroxylase content in cardiac sympathetic

neurons and elevated norepinephrine in the right ventricle, where innervation density was normal.

Key Words: sympathetic innervation, p75 neurotrophin receptor, nerve growth factor, semaphorin3a, ventricular arrhythmias

Introduction:

The sympathetic innervation of the heart regulates cardiac function by stimulating heart rate, contractility, and conduction velocity through release of norepinephrine (NE) and activation of cardiac β_1-adrenergic receptors (β_1AR). Sympathetic innervation of the heart is sculpted during development by chemoattractive and chemorepulsive factors (Glebova and Ginty, 2004; Ieda et al., 2007). For example, Nerve Growth Factor (NGF) supports sympathetic neuron survival and promotes cardiac axon outgrowth during development (Crowley et al., 1994; Glebova and Ginty, 2004), while the chemorepulsive factor semaphorin3a (sema3a) attenuates sympathetic axon extension in the heart (Ieda et al., 2007) and in the peripheral vasculature (Long et al., 2009).

Neurotrophins such as NGF act through two distinct types of receptors: the Tropomyosin-related tyrosine kinase (Trk) receptors, and the lower affinity p75 neurotrophin receptor (p75NTR)(Glebova and Ginty, 2005; Zampieri and Chao, 2006). The actions of these receptors have been most thoroughly characterized in the context of development. NGF acts through TrkA to promote the extension of sympathetic axons into the heart (Glebova and Ginty, 2004;

Kuruvilla et al., 2004), while the role of p75NTR is more complicated because p75NTR modulates signaling by co-receptors that can either stimulate or inhibit axon outgrowth (Bandtlow and Dechant, 2004; Kaplan and Miller, 2003). Thus, in mice lacking p75NTR the sympathetic innervation density in target tissues ranges from denervation to hyperinnervation, with many tissues exhibiting normal innervation (Jahed and Kawaja, 2005; Kohn et al., 1999; Kuruvilla et al., 2004; Lee et al., 1994).

Developmental studies have examined the cardiac innervation in p75NTR -/- mice, but neurotrophins also maintain neurotransmitter production and little is known about the role of p75NTR in the adult cardiac innervation. The lack of p75NTR delays sympathetic innervation of the heart (Kuruvilla et al., 2004), but despite this delay sympathetic innervation in the ventricle is qualitatively normal soon after birth (Jahed and Kawaja, 2005; Lee et al., 1994). It is unknown if the lack of p75NTR impacts the sympathetic cardiac innervation of the adult ventricles, and recent studies raise the possibility that the cardiac innervation might be altered in adult ventricle. First, sympathetic innervation density in p75NTR -/- atria is elevated 4 weeks after birth but decreased in adults (Habecker et al., 2008), while parasympathetic innervation is normal at both ages despite parasympathetic expression of p75NTR (Hoard et al., 2008). This suggests that p75NTR plays a role in both establishment and maintenance of sympathetic, but not parasympathetic, neurons. Second, sema3a expression in the left ventricle (LV) subendocardium retards the growth of sympathetic fibers, generating a gradient of sympathetic innervation across the ventricle with more

fibers in the subepicardium than the subendocardium (Ieda et al., 2007; Randall et al., 1968). p75NTR attenuates sema3a signaling in sensory neurons (Ben-Zvi et al., 2007) and therefore we hypothesized that the lack of p75NTR would result in decreased sympathetic innervation in the LV subendocardium due to enhanced susceptibility to sema3a repulsion. To test this hypothesis, we used tyrosine hydroxylase immunohistochemistry to determine sympathetic innervation density and pattern in the p75NTR -/- adult LV and used ganglia explants to determine the susceptibility of sympathetic axons to sema3a. Furthermore, we used ECG telemetry to determine if potential sympathetic heterogeneity would be associated with increased ventricular arrhythmias as seen in mice overexpressing sema3a (Ieda et al., 2007).

Materials and Methods:

Materials: ± Dobutamine hydrochloride was from Hospira Inc., mouse β-NGF was from Austral Biologicals, and semaphorin-3A/Fc Chimera was from R&D Systems. TH-specific antibody was from Chemicon; the PGP9.5-specific antibody was from Accurate Chemicals; the β1AR-specific antibody was from Affinity Bioreagents; the HRP-conjugated rabbit IgG-specific antibody was from Pierce; the AlexaFluor 488-conjugated rabbit IgG-specific antibody was from Molecular Probes. DMEM/F12 media was obtained from Life Technologies.

Animals: Wild type C57BL/6J and p75NTR -/- mice (B6.129S4-Ngfr^{tm1Jae}/J) were obtained from Jackson Laboratories. The B6.129S4-Ngfr^{tm1Jae}/J mice contain

two mutated exon III alleles, which removes the coding region for the last three of four cysteine–rich repeats in the extracellular domain, and prevents the expression of functional p75NTR (Lee et al., 1992; Welcher et al., 1991; Yan and Chao, 1991). The $p75^{NTR}$-/- mice were genotyped upon arrival (Dhanoa et al., 2006) and a colony was maintained using homozygous breeder pairs, with additional genotyping every 6 months. All mice were kept on a 12h:12h- light dark cycle with ad libitum access to food and water. Age and gender-matched male and female mice between 12-18 weeks old were used for all experiments. All procedures were approved by the Institutional Animal Care and Use Committee and comply with the Guide for the Care and Use of Laboratory Animals published by the United States National Institutes of Health (NIH publication No. 85-23, revised 1996).

Axon Outgrowth: To test the role of p75NTR in modulating sema3a inhibition of axon outgrowth, we used explants of stellate ganglia which contain most of the sympathetic neurons that project to the heart. Ganglia were desheathed to facilitate axon outgrowth, embedded in reduced growth factor Matrigel™, and covered with serum-free DMEM/F12 with penicillin/ streptomycin (1:10,000) and 10 ng/mL NGF. Explants were maintained at 37 °C with 5% CO_2. 20 hr after plating (t=0) explants were photographed, treated with vehicle or sema3a-Fc and then photographed again 6 hours later (t=6). Axon length was measured at each time point using Nikon Elements AR 3.0, and the rate of axon growth/hour was calculated. For each treatment group, 6-10 axon measurements were obtained

and averaged from a minimum of 3 different sites. The experiment was repeated 3 times and data from a single representative experiment are shown.

Immunohistochemistry: Hearts were fixed for 1h in 4% paraformaldehyde, rinsed in PBS, cryoprotected in 30% sucrose and 10 µm transverse sections were thaw-mounted onto charged slides. To reduce fixative-induced autofluorescence, sections were rinsed in 10 mg/mL sodium borohydride 3X10 minutes and then rinsed in PBS 3X10 minutes. Sections were then blocked in 2% B.S.A/ 0.3% Triton X-100 in PBS for 1 h, incubated with a TH-specific antibody (1:300) overnight, rinsed 3 x 10 minutes in PBS, and incubated 1.5 h with the AlexaFluor 488-conjugated rabbit IgG-specific antibody (1:300). Sections were rinsed 3 x 10 minutes in PBS, coverslipped and visualized by fluorescence microscopy. Sections from WT and P75NTR-/- hearts were always stained and photographed side by side to minimize variation between the groups due to the immunohistochemistry procedure.

Imaging and Analysis of Ventricles:

Composite analysis. Immunohistochemical staining was visualized on a Zeiss (Axiophot II) fluorescent microscope with the 10X objective. Composite images were used to generate a representative heart section from each mouse that included the left and right ventricles. The composite was divided into right ventricle, subepicardium or subendocardium (includes interventricular septum) of the left ventricle, and quantified using ImageJ software (NIH). In order for two

observers to analyze endo- vs. epi-cardium consistently, we measured the ventricle wall and identified half as endocardium and half as epicardium rather than trying to follow the border between the two layers of muscle. Innervation density was determined by threshold discrimination using ImageJ (Figure 3.1C). All photos were treated in an identical manner. Black and white photos were opened in ImageJ and the brightness/contrast tool was used to adjust each image so that the minimum was set at the left side of the histogram. The threshold tool was then used to identify nerve fibers. The automated function set a beginning threshold level, but this did not reliably include all sympathetic fibers while excluding all non-neuronal tissue. The threshold was then manually adjusted to ensure that only specific TH staining was identified. The ventricle has two layers of muscle set at different angles, so each section included some nerve fibers cut longitudinally along the plane of the section and other fibers cut in cross-section and appearing as small round dots. Thus, specific criteria for size and shape were not used in our analysis. Innervation density was expressed as the percent of area that was above the threshold (TH+ fibers). Each image was quantified by two independent observers. The coefficient of variance between the two independent analyses averaged 10±8.3%, mean± SD.

Analysis of specific regions: TH staining was visualized using the 20X objective, and pictures were obtained for areas A-E as shown in Figure 3.2C. Innervation density was determined by threshold discrimination (ImageJ), and each image was quantified by two independent observers. 5 sections at least 150 μm apart were analyzed from each heart and averaged together. The data shown are the

average of the two independent determinations. The coefficient of variance between the two independent analyses averaged 9.8±7.8%, mean± SD.

HPLC: NE was measured by high-performance liquid chromatography (HPLC) with electrochemical detection as described previously (Li et al., 2004b; Parrish et al., 2008). Detection limits were ~0.05 pmol with recoveries from the alumina extraction >60%.

Immunoblot Analysis: TH and β_1AR were quantified via western blot as previously described (Li et al., 2004b; Parrish et al., 2008). For biochemical analysis of subendocardium vs subepicardium, the inner vertical loop was dissected from the outer transverse loop. The pan-neuronal marker PGP9.5 (1:1000) was used to normalize TH content to the total amount of neuronal protein in each sample. Actin (1:1000) was quantified as a loading control for β_1AR expression in cardiac myocytes. Data were analyzed using LabWorks Software (UVP, Upland, CA).

Real-time PCR: Hearts and ganglia were stored in RNAlater®. RNA was isolated and real-time PCR performed as described previously (Parrish et al., 2008). Samples were assayed using prevalidated Taqman gene expression assays for mouse β_1AR, NP1, Plexin4A, actin and GAPDH. β_1AR was normalized to actin, and NP1 and PlexinA4 were normalized to GAPDH.

Hemodynamics and Ventricular Function: Ventricular function was measured in isoflurane anesthetized mice using both transthoracic echocardiography and a micromanometer-tipped pressure transducer (SPR1000, Millar Instruments) inserted retrograde into the ventricle. Left ventricular dimensions and function were evaluated using transthoracic echocardiography at a transmission frequency of 40 MHz (Vevo 770, VisualSonics Inc.) and a cycle length of 1. Parasternal imaging was performed in the mid-papillary short-axis and parasternal long-axis imaging planes. Image sequences were acquired with ECG gating of sequential M-mode sweeps (EKV mode) for an effective 2-D frame rate of 1,000 Hz. Left ventricular anteroseptal and posterolateral wall thickness in the short-axis were measured at end-systole and end-diastole and used to calculate thickening fraction. Left ventricular cavity dimensions in the anterior-posterior dimension at end-systole (LVIDs) and at end-diastole (LVIDd) were measured and used to calculate shortening fraction by: 100(LVIDd-LVIDs)/LVIDd, left ventricular volumes by: $([7.0/(2.4+LVID)]XLVID^3$ and ejection fraction (LVEF). Stroke volume was measured by the product of the proximal aortic area and time-velocity integral derived from pulsed-wave Doppler at the same level. The product of stroke volume and heart rate was used to calculate cardiac output. Tissue Doppler imaging was performed to determine peak radial endocardial velocities in systole (S') and early diastole (E') in the anterior wall. (±)-dobutamine hydrochloride (32μg/ kg) was injected intra-peritoneally to assess β_1AR responsiveness.

Ventricular pressure and arterial pressure were monitored with a microtipped pressure transducer (1.0 French; Millar). Anesthesia was induced with 4% inhaled isoflurane. Mice were intubated, ventilated and anesthesia was maintained with 2-3% inhaled isoflurane. Body temperature was maintained at 37±0.2 ºC. The microtipped pressure transducer was inserted into the right carotid artery for arterial pressure measurements and then advanced into the left ventricle for measurement of left ventricular pressure using a PowerLab data acquisition system. Left ventricular peak systolic pressure (LVPSP), dP/dt_{MAX}, and dP/dt_{MIN} were analyzed using ChartPro software.

NE Uptake: Uptake of [^{3}H]-NE into sympathetic nerve terminals was assayed as previously described (Parrish et al., 2009). Mouse ventricles were separated into sections 1 mm thick. Each section contained RV, LV, and septum. Two sections from each heart were used for total uptake and two for background uptake (defined by addition of 1 mM desipramine). Ten minutes after addition of 50 nmol/L [^{3}H]-NE, reactions were terminated by adding ice cold KRH buffer.

ECG Telemetry Recordings and Analysis: ECGs were obtained from conscious adult mice using telemetry implants and were analyzed with Dataquest ART software (Data Sciences International). Mice were anaesthetized with 4% inhaled isofluorane and maintained on 2% inhaled isoflurane. The transmitter was implanted into the abdominal cavity in a lead II configuration, with the negative lead placed in the right pectoral muscle and the positive lead to the left

of the xyphoid process. A sub-cutaneous injection of 0.1mg/kg buprenorphine was administered post-operatively for analgesia. Mice recovered for at least 72 h before data acquisition. ECG recordings were collected for 24 hr and were analyzed at 4 time points within the circadian cycle (6 pm-7 pm, 12 am-1 am, 6 am-7 am, and 12 pm-1 pm) to determine heart rate and the presence of spontaneous premature ventricular complexes (PVCs). PVCs were defined as a single premature QRS complex in relation to the P-wave.

Statistics: Student's t-test was used for a single comparison between two groups (WT vs. p75NTR). Two-way ANOVA with a Bonferroni post-test was used to compare across genotypes and treatment groups.

Results:

We used tyrosine hydroxylase immunohistochemistry to determine sympathetic innervation density in the right and left ventricles of WT and p75NTR -/- mice. We discovered a consistent and profound alteration in the pattern of sympathetic nerve fibers in the p75NTR -/- left ventricle (LV; Fig. 3.1A). Few sympathetic nerve fibers projected into the subendocardium of the p75NTR -/- LV, but many fibers were present in the subepicardium and the right ventricle (RV) innervation appeared normal (Fig. 3.1B). We generated composite images of ventricle sections and quantified innervation density in the low magnification images using threshold discrimination (Fig. 3.1C). Density in the subendocardium and right ventricle were not significantly different than control,

but there was a significant deficit in sympathetic fiber density in the LV subendocardium and septum (Fig. 3.1D, E). To confirm this striking result, we carried out additional experiments quantifying pictures taken at a higher magnification that sampled a smaller number of specific sites throughout the RV, LV, and septum (Fig. 3.2). This confirmed the initial assessment that innervation density in the p75NTR -/- RV and subepicardium of the LV were normal, while the septum was essentially devoid of sympathetic fibers (Fig. 3.2).

The altered innervation pattern in the adult p75NTR -/- LV raised the question of why sympathetic fibers are excluded from the subendocardium. Sema3a expression in the subendocardium decreases sympathetic innervation density in that part of the heart (Ieda et al., 2007), and p75NTR disrupts a neuropilin 1/plexin sem3a receptor complex in sensory neurons and attenuates sema3a signaling (Ben-Zvi et al., 2007). We evaluated the growth of cardiac sympathetic axons lacking p75NTR using stellate ganglion explants (Fig. 3.3A). Addition of sema3a into solution, rather than from a point source, causes axon collapse and essentially inhibits axon outgrowth (He and Tessier-Lavigne, 1997; Kolodkin et al., 1997). We found that sema3a (at 120 ng/mL and 240 ng/mL) did not inhibit axon outgrowth from wildtype (WT) ganglia, but dose-dependently inhibited outgrowth from p75NTR-/- ganglia (Fig. 3.3B). Neuropilin1 and plexin mRNA were identical in both genotypes (Fig. 3.3C), suggesting that sema3a receptor expression is normal in p75NTR -/- mice, and the lack of p75NTR increased sensitivity to sema3a in cardiac sympathetic neurons.

Experimental manipulations and pathologies that cause heterogeneous sympathetic innervation in the left ventricle increase the occurrence of ventricular arrhythmias (Cao et al., 2000a; Cao et al., 2000b; Ieda et al., 2007; Rubart and Zipes, 2005). To determine if aberrant development of sympathetic innervation was sufficient to trigger arrhythmias, we examined heart rhythm in conscious mice. ECGs were monitored for 24 hours and rhythm abnormalities were quantified during four 1-hour periods throughout the circadian cycle. p75NTR null mice had significantly more spontaneous premature ventricular complexes (PVCs) than WT mice during the 4 hours that were analyzed in detail (Fig. 3.4A, B). However, there was significant circadian variability in the presence of PVCs so that the difference between genotypes was significant during the wake phase but not significant during the sleep phase (Fig 3.4C). Analysis of heart rate in conscious mice confirmed the previous observation in anesthetized mice (Habecker et al., 2008) that heart rates are lower in p75NTR -/- mice compared to wild type mice (HR midnight-1AM: WT 618±52 bpm vs. p75NTR 551±27 bpm, mean±SD $p<0.01$, n=7-8).

To determine if the absence of sympathetic innervation in the subendocardium altered cardiac function, we measured ventricular dimensions and function by transthoracic echocardiography. Ventricle size, fractional shortening, ejection fraction, stroke volume and cardiac output at rest were not significantly different in p75NTR -/- mice (Table 3.1), suggesting that absence of sympathetic innervation in the subendocardium of the left ventricle had no effect on ventricular function. This was surprising, and we asked if the lack of p75NTR

had other effects on sympathetic nerves that might contribute to normal stroke volume and cardiac output.

Afterload affects stroke volume, and a recent study revealed that sema3a impacts the sympathetic innervation density of vascular beds (Long et al., 2009). Thus, vessels with high sema3a expression have lower innervation density resulting in decreased arterial pressure. Since p75NTR-/- sympathetic fibers are more sensitive to sema3a, we asked if arterial pressure was low in p75NTR-/- mice. Mean arterial pressure was normal in C57Bl6/J control mice under isoflurane anesthesia (Zuurbier et al., 2002) but was decreased significantly in p75NTR-/- mice compared to the controls (Table 3.1). Left ventricular peak systolic pressure (LVPSP) trended lower in the p75NTR nulls (WT: 93 ± 2.1 mmHg vs. p75NTR-/-: 83± 5.4 mmHg; mean±sem, n=6-7, p=0.1) and both dP/dt_{Max} and dP/dt_{Min} were decreased significantly in p75NTR-/- mice (Fig. 3.5A-B).

One drawback of measuring stroke volume or LVPSP is that these values reflect function of the entire left ventricle, and do not allow specific analysis of the innervated p75NTR-/- subepicardium separate from the denervated subendocardium. To specifically examine the function of each layer of the heart, spectral tissue Doppler was used to compare subendocardial and subepicardial radial thickening velocities under basal conditions and following stimulation of beta-1 adrenergic receptors (β_1AR) with the agonist dobutamine. No differences were observed between the genotypes in basal or stimulated systolic thickening velocities (Basal S': Endo WT 12.8±1.7 vs. KO 11.8±0.9 cm/s; Epi WT 8.±1.5 vs.

KO 7.8±0.4 cm/s; Dobutamine Stimulated S': Endo WT 13.3±1.4 vs. KO 15.7±0.5 cm/s; Epi WT 9.8±0.6 vs. KO 8.9±0.4 cm/s; all values are mean± SEM, n=4). Under basal conditions there were no differences in diastolic thickening velocity (E') between the genotypes in either layer of cardiac muscle (Fig. 3.6A, C). However, the denervated subendocardium of p75NTR-/- null mice exhibited a significantly greater peak diastolic thickening velocity following stimulation with dobutamine than the wild type subendocardium (Fig. 3.6D). In contrast, the normally innervated subepicardium of p75NTR-/- mice did not respond differently than wild type subepicardium to β_1AR stimulation (Fig. 3.6B).

Given the enhanced responsiveness of denervated p75NTR-/- subendocardium to beta agonists, we suspected that β_1AR levels were increased in that layer of the p75NTR-/- left ventricle. We examined β_1AR levels by western blot and found that β_1ARs were significantly higher in the denervated subendocardium than the subepicardium of p75NTR-/- left ventricle, but were evenly distributed across the WT left ventricle (Fig 3.7A). However, overall β_1AR levels in the p75NTR-/- left ventricle were only 50% of wild type controls (Fig 3.7B). β_1AR mRNA was also lower in p75NTR-/- left ventricle compared to wild type (data not shown). Therefore, β-receptor responsiveness was high in the subendocardium and normal in the subepicardium despite significantly fewer receptors.

The significant lack of cardiac β-receptors in p75NTR-/- mice raised additional questions about the normal ventricular function observed in those mice. Norepinephrine (NE) can regulate β_1AR expression, and NGF signaling

through TrkA and p75NTR can modulate NE production in addition to axon outgrowth (Bjerre et al., 1975a; Chun and Patterson, 1977). Therefore, we measured cardiac NE content in the left ventricle and found that NE levels in the p75NTR-/- ventricle were identical to wild type mice despite the decreased sympathetic innervation density (Fig 3.8A). NE was elevated in the p75NTR-/- right ventricle where innervation density was normal (Fig. 3.8B). These data suggest that sympathetic neurons lacking p75NTR produce more NE, and are consistent with elevated NE previously reported in p75NTR-/- atria (Habecker et al., 2008). [^{3}H]-NE uptake was similar in WT and p75NTR-/- ventricles (Fig. 3.8C), but tyrosine hydroxylase, the rate-limiting enzyme in NE synthesis, was elevated in p75NTR-/- left ventricle (Fig. 3.8D). Thus, increased tyrosine hydroxylase may lead to higher NE synthesis in sympathetic neurons lacking p75NTR.

Discussion

Sympathetic innervation of target tissues is critically dependent on NGF activation of TrkA (Crowley et al., 1994; Glebova and Ginty, 2004; Smeyne et al., 1994), but the precise role of p75NTR has been less clear (Jahed and Kawaja, 2005; Kohn et al., 1999; Lee et al., 1994). p75NTR interacts with, and modulates, several signaling pathways involved in cell survival, axon outgrowth and axon degeneration and repulsion (Ben-Zvi et al., 2007; Chao, 2003; Singh et al., 2008). For example, in the pineal gland, activation of p75NTR inhibits NGF-induced axon outgrowth and the absence of p75NTR results in sympathetic

hyperinnervation (Kohn et al., 1999). Likewise, p75NTR comprises part of a Nogo-R/Lingo/p75NTR complex that mediates Nogo inhibition of axon regeneration after injury (Nykjaer et al., 2005), and Nogo is present in the heart (Bullard et al., 2008; Huber et al., 2002) where it might interact with p75NTR on sympathetic neurons. p75NTR blunts axon outgrowth in both of these scenarios, although the receptors and signaling involved are quite distinct, and the absence of p75NTR would be expected to enhance axon outgrowth. Indeed, the absence of p75NTR enhances NGF stimulated sympathetic axon outgrowth *in vivo* (Dhanoa et al., 2006; Kohn et al., 1999) and *in vitro* (Hannila et al., 2004). Sema3a inhibits sympathetic axon extension into the LV subendocardium (Ieda et al., 2007), and p75NTR disrupts sema3a signaling in sensory neurons by breaking up its neuropilin 1- plexin receptor complex. Thus, the absence of p75NTR results in decreased sensory innervation to the skin, which expresses sema3a (Ben-Zvi et al., 2007). We found that the absence of p75NTR renders adult sympathetic axons more susceptible to inhibition by sema3a. The doses of sema3a that we used did not inhibit axon outgrowth in wildtype neurons, but we expect that using higher doses of sema3a would inhibit WT outgrowth since sema3a is clearly able to cause growth cone collapse and axon repulsion in embryonic sympathetic neurons (Yaron et al., 2005). Given the clear role identified for sema3a in controlling sympathetic innervation density in the subendocardium (Ieda et al., 2007), we think it likely that the lack of subendocardial innervation in p75NTR nulls is due to enhanced sensitivity to sema3a. Thus, the ability of p75NTR to modulate multiple different signaling

pathways can explain the variable degree of sympathetic organ innervation when p75NTR is absent (Jahed and Kawaja, 2005; Kohn et al., 1999; Lee et al., 1994).

Sympathetic heterogeneity in the heart contributes to the generation of ventricular arrhythmias in pathological conditions (Kjekshus, 1990; Rubart and Zipes, 2005; Stevens et al., 1998), and our data support the model that sympathetic heterogeneity in the ventricle is arrhythmogenic even in the absence of pathology. p75NTR-/- mice exhibited significantly more PVCs than age-matched control mice, and the circadian variation in the number of PVCs implicated the sympathetic nervous system as a contributor (Aronow et al., 1994; Jung et al., 2006; Muller et al., 1987a) despite other alterations in autonomic transmission that normally prevent arrhythmias. First, the atria of adult p75NTR-/- hearts exhibit a relative increase in cholinergic parasympathetic nerve fibers compared to sympathetic fibers, which are decreased in number (Habecker et al., 2008). Enhanced parasympathetic transmission in the atria typically protects against arrhythmias (Jouven et al., 2005; Tsuji et al., 1996). Second, there is a lower overall density of sympathetic nerve fibers in the p75NTR-/- ventricle, and decreased expression of β_1AR. Inhibition of noradrenergic transmission by beta-blockers normally prevents arrhythmias (Haverkamp et al., 1990; Lopez-Sendon et al., 2004). Although total cardiac β_1AR were low in p75NTR-/- left ventricle, the distribution was altered compared to WT hearts, with significantly higher β_1AR in the denervated p75NTR-/- subendocardium. Transmural gradients of ion channel expression and myocyte repolarization are tightly regulated across the left ventricle (Brunet et al., 2004; Costantini et al., 2005b; Kuo et al., 2001;

Nabauer et al., 1996; Wang et al., 2006). Disruption of these gradients can destabilize cardiac rhythm (Costantini et al., 2005b; Kuo et al., 2001), and aberrant distribution of sympathetic nerve fibers and β_1AR may alter regulation of repolarization across the left ventricle (Thomas et al., 2004), resulting in enhanced susceptibility to ventricular arrhythmias despite the overall lower number of β_1AR and sympathetic fibers. These findings have significant clinical implications since neurotrophins are critical regulators of neuronal remodeling after cardiac injury (Cao et al., 2000a; Zhou et al., 2004c).

The uneven distribution of sympathetic nerves in the p75NTR-/- ventricle may contribute to the gradient in β_1AR expression. The lack of p75NTR enhances NGF-induced TrkA signaling in sympathetic neurons (Hannila et al., 2004; Kohn et al., 1999) and NGF stimulates TH expression and NE synthesis in the superior cervical ganglion (Max et al., 1978; Thoenen et al., 1971). Our data confirmed that cardiac p75NTR-/- sympathetic neurons produced more TH *in vivo*, and the right ventricle exhibited increased NE content. NE content in the LV was normal in p75NTR nulls, but we expect that if we dissected the subendocardium and subepicardium separately, we would detect little NE in the denervated endocardium and elevated NE in the epicardium. β_1AR expression is regulated by NE release (Mann, 1998; Wallukat, 2002) and heterogeneity of NE release in the heart may contribute to the corresponding gradient in β_1AR.

While alterations in sympathetic innervation pattern and density seem to affect arrhythmogenic potential, basal LV function determined by echocardiography was normal in the p75NTR-/- mice. The impact of aberrant

sympathetic innervation on cardiovascular function only becomes evident upon direct activation of βAR, which is consistent with other animal models that have altered ventricular sympathetic innervation (Ieda et al., 2007; Kiriazis et al., 2005). Although basal stroke volume and cardiac output were normal in the p75NTR-/- mice, catheterization experiments revealed some differences not detected via echocardiography, including decreased mean arterial pressure and decreased dP/dt_{MAX}. Sema3a is a critical regulator of sympathetic innervation density in the vasculature (Long et al., 2009), so low arterial pressure might result from decreased sympathetic innervation of the vasculature due to enhanced sema3a signaling. Arterial pressure can affect dP/dt_{MAX}, so the low dP/dt_{MAX} may result from decreased afterload rather than denervation of endocardial muscle. It is not possible to do these experiments in conscious mice, but the need for anesthesia is a limitation of our study as it likely impacts our results. For example, p75NTR-/- heart rate in the echo study trended higher than control mice, even though heart rate in conscious p75NTR-/- mice was significantly lower than wild type. This discrepancy may be a combination of isoflurane anesthesia and handling during the echo procedure, since p75NTR-/- mice anesthetized with isoflurane but maintained in the dark without disruption have a significantly lower heart rate than wild type mice (Habecker et al., 2008), similar to conscious animals.

Tissue Doppler analysis revealed additional functional consequences in the heart, even though stroke volume and cardiac output were normal. Tissue Doppler allowed us to examine separately the tissue velocities of the normally

innervated subepicardium and the denervated subendocardium. Basal tissue velocities in the p75NTR-/- heart were normal, but treatment with the β_1AR agonist dobutamine stimulated a significantly greater peak diastolic thickening velocity in the p75NTR-/- subendocardium compared to wild type, despite lower β_1AR levels. Thus, significant differences in muscle function only become apparent using techniques that allow for separate analysis of the subendocardium and subepicardium. These mice provided a unique opportunity to examine the responsiveness of cardiac muscle that had developed in the absence of sympathetic innervation, and we completed *in vivo* studies in order to examine cardiac function in the context of the other hemodynamic changes in these animals. However, a limitation of this approach is that it does not allow us to examine fractional shortening of isolated myocytes *in vitro* and to identify molecular differences in cardiac cells that develop in the presence of sympathetic nerves vs. those that develop without innervation.

We have focused on the role of p75NTR in controlling the sympathetic innervation of the left ventricle, but p75NTR is expressed in cardiac interstitial cells as well, and its expression in those cells is increased after injury (Zhou et al., 2004b). There is no evidence that p75NTR is expressed in cardiac myocytes *in vivo* (Zhou et al., 2004b) or *in vitro* (Caporali et al., 2008; Caporali and Emanueli, 2009), but we cannot rule out the possibility that some of the changes observed in p75NTR-/- mice are due in part to an effect of non-neuronal cells within the heart. Nevertheless, given the lack of p75NTR in cardiac myocytes and the profound changes in the distribution and NE content of p75NTR-/-

sympathetic nerves, it seems reasonable to attribute many of the changes observed in p75NTR-/- hearts to altered innervation.

Our results identify the p75NTR neurotrophin receptor as a key player in the establishment of ventricular sympathetic innervation, and are consistent with the model that heterogeneous sympathetic innervation enhances susceptibility to ventricular arrhythmias. We found that p75NTR has a greater functional impact on the cardiovascular system and cardiac rhythm stability than previously understood. Our findings are particularly relevant to myocardial infarction, heart failure and diabetic autonomic neuropathy where heterogeneous sympathetic innervation is correlated with altered neurotrophin expression and the development of ventricular arrhythmias (Kjekshus, 1990; Rubart and Zipes, 2005; Stevens et al., 1998).

Acknowledgements

The authors thank Dr. William Woodward and Laura Pahlmeyer for technical assistance, and Dr. Susan Birren for helpful discussions.

Grants

Supported by AHA 0715669Z & 09PRE2110052 (C.U.L), AHA 0555553Z (B.A.H) and NIH HL093056 (B.A.H.).

Disclosures:

None

Table 3.1: Left ventricular size and function

Heart Dimensions	**WT (n=4)**	**P75-/- (n=4)**
IVSd (mm)	0.68 ± 0.1	0.68 ± 0.05
LVIDd (mm)	3.3 ± 0.27	3.1 ± 0.12
LVPWd (mm)	0.64 ± 1.12	0.64 ± 0.06
IVSs (mm)	1.16 ± 0.1	1.18 ± 0.04
LVIDs (mm)	2.06 ± 0.24	1.87 ± 0.07
LVPWd (mm)	1.11 ± 0.09	1.15 ± 0.03
Ventricular Function		
Heart Rate (bpm)	432 ± 22	463 ± 30
Fractional Shortening (%)	38.2 ± 10.8	39.7 ± 3.7
LV ejection Fraction (%)	68.4 ± 13.8	71.6 ± 4.3
Stroke Volume (ml)	38.8 ± 8.7	42.9 ± 6.5
Cardiac Output (ml/min)	16.9 ± 2.8	20.5 ± 4.8
Arterial Pressure	**WT (n=7)**	**P75-/- (n=6)**
Mean (mm Hg)	76.0 ± 4.1	60.1 ± 4.5*
Systolic (mm Hg)	88.6 ± 4.4	74.5 ± 4.3*
Diastolic (mm Hg)	64.0 ± 3.9	47.7 ± 4.3*

Values are mean ± SD.; d=diastole, s=systole; IVS, Interventricular Septum; LVID, Left Ventricular Internal Dimension; LVPW, Left Ventricular Posterior Wall. *p<0.05 vs. WT

Figure 3.1

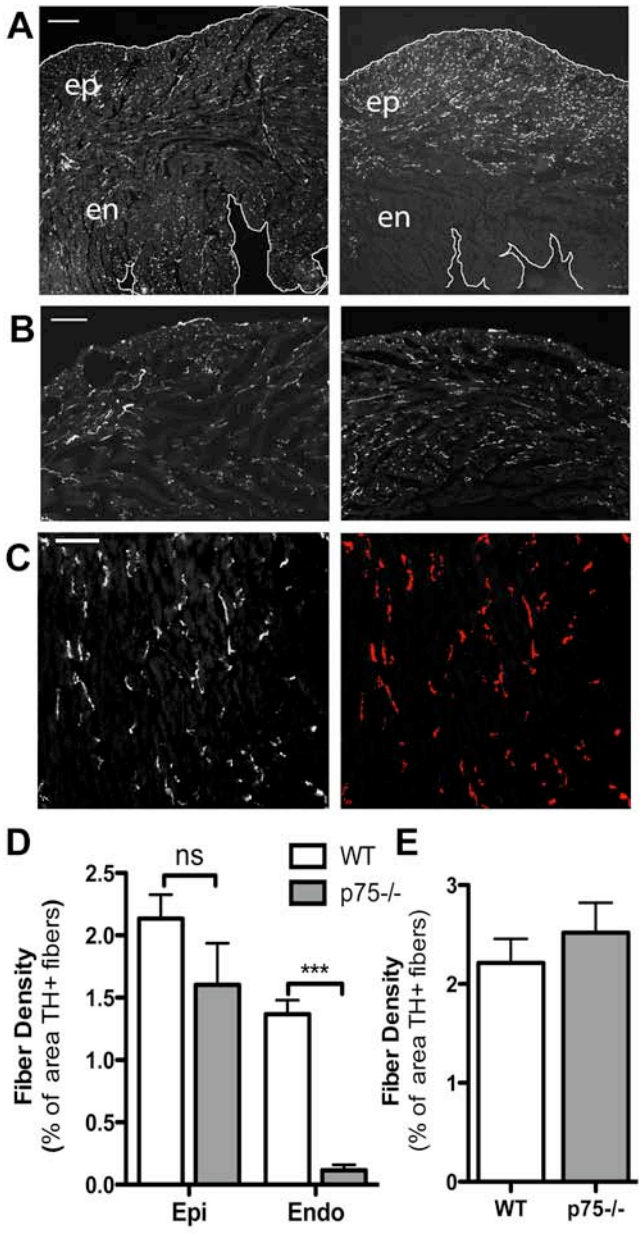
A
ep
en
ep
en
B
C
D
ns
WT
p75-/-
***
Fiber Density
(% of area TH+ fibers)
2.5
2.0
1.5
1.0
0.5
0.0
Epi
Endo
E
Fiber Density
(% of area TH+ fibers)
3
2
1
0
WT
p75-/-

Figure 3.1: Fiber distribution is altered in the p75NTR-/- left ventricle. Sympathetic fiber distribution was identified by TH immunoreactivity. **A)** Representative pictures taken at 5x showing the entire width of the LV free wall reveal altered pattern of sympathetic innervation in p75NTR-/-mice (right) compared to WT mice (left). This low magnification was not used for quantitative analysis. The edges of the tissue have been outlined for clarity. Scale bar = 0.25 mm. ep = subepicardium, en = subendocardium. **B)** Sympathetic fiber distribution in the right ventricle of WT mice (left) and p75NTR-/- mice (right). Scale bar = 0.1 mm. **C)** Example of threshold discrimination used to determine innervation density in which the TH+ nerves above the threshold are highlighted. Innervation density is then expressed as the percent of area that is above the determined threshold (TH+ fibers). Scale bar = 0.05mm. **D)** Quantification of sympathetic fiber density in the subendocardium (endo) and the subepicardium (epi) of WT (white bars) and p75NTR-/- mice (grey bars), mean ± SEM., ***p< 0.001, n=4. **E)** Quantification of sympathetic fiber density of the right ventricle in WT and p75NTR-/- mice, mean ± SEM, n=4.

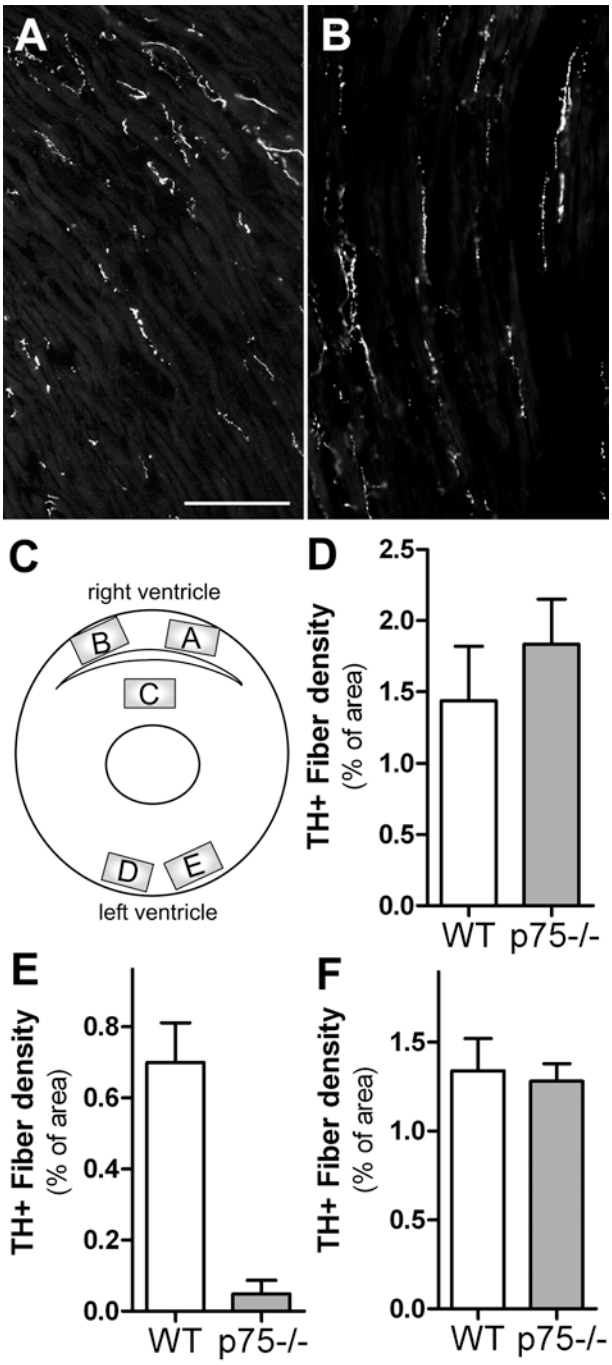

Figure 3.2: Innervation density is normal in the p75NTR-/- subepicardium. **A, B)** Representative 20X pictures of TH+ fibers in WT (A) mice and (B) p75NTR-/- subepicardium that were used for quantitative analysis. Scale bar = 0.1mm. **C)** Cartoon diagram depicting regions analyzed to further characterize innervation density of WT and p75NTR-/- ventricles. **D-F)** Quantification of sympathetic fiber density in WT and p75NTR-/- right ventricle **(D)**, interventricular septum **(E),** and left ventricle **(F)**, mean ± SEM, n=7.

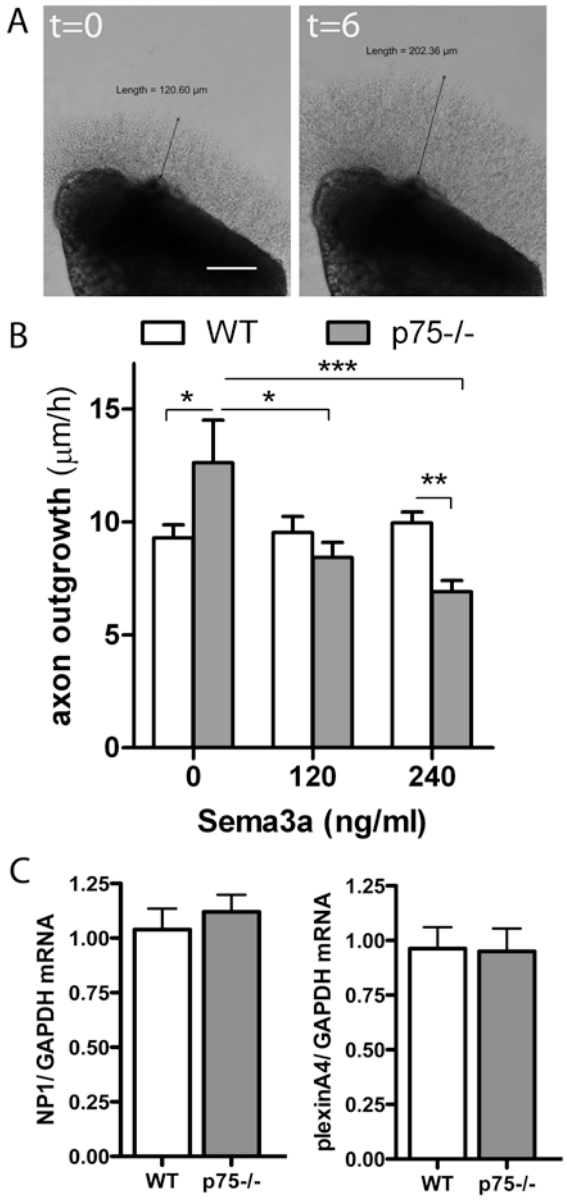

Figure 3.3: p75NTR-/- sympathetic axons are more sensitive to sema3a growth cone collapse/inhibition. **A)** Representative stellate ganglia explants at time zero (t=0, left) and six hours later (t=6, right)**,** scale bar = 0.1 mm. **B)** Quantification of axon growth rate from WT (white bars) and p75NTR-/- (grey bars) sympathetic ganglia in the presence of 0, 120, or 240 ng/mL sema3a (mean ± SEM, n= 3, *p<0.05, **p<0.01). **C)** Neuropilin1 (NP1) mRNA normalized to GAPDH (left) in WT (clear bars) and p75NTR-/- (grey bars) stellate ganglia, and plexinA4 mRNA normalized to GAPDH (right) in WT and p75NTR-/- stellate ganglia (mean ± SEM, n=5).

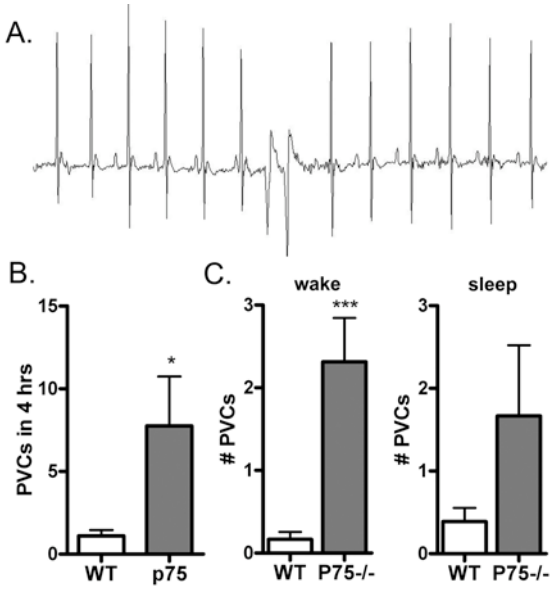

Figure 3.4: Mice lacking p75NTR have increased spontaneous ventricular arrhythmias. **A)** Representative ECG depicting spontaneous premature ventricular complexes (PVCs) in a p75NTR-/- mouse. **B)** p75NTR-/- mice experienced more than spontaneous PVCs than WT mice (mean ± SEM, *p< 0.05, n= 8–9). **C)** Number of PVCs in WT and p75NTR-/- mice during two hours of the awake phase and the sleep phase (mean ± SEM, *p< 0.05, n= 8–9).

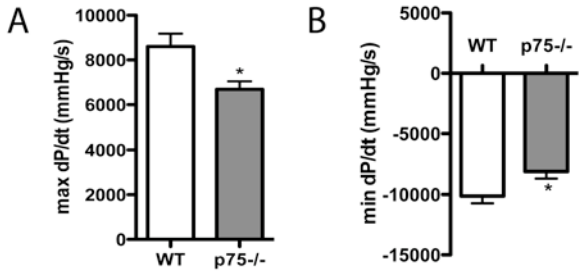

Figure 3.5: dP/ dt_{MAX} and dP/dt_{MIN} are low in p75NTR-/- mice. **A)** Baseline dP/dt_{MAX} in WT (open bars) and p75NTR-/- (grey bars) mice. **B)** dP/dt_{MIN} min in WT (open bars) and p75NTR-/- (grey bars) mice (mean ± SEM, *p<0.05, n=6–7).

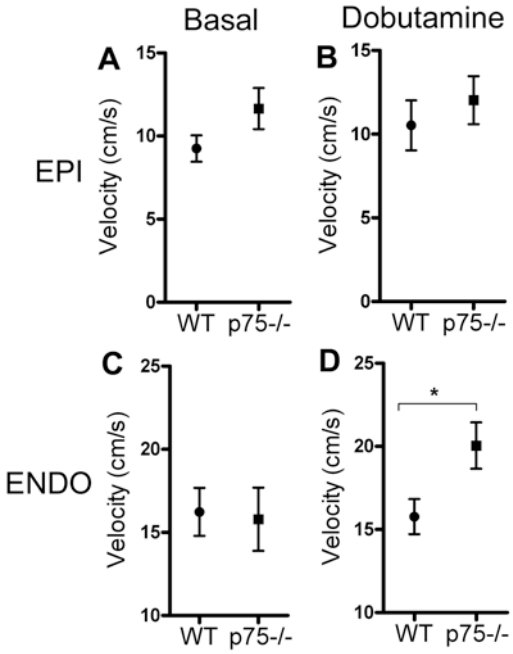

Figure 3.6: p75NTR-/- mice have enhanced response to β_1AR stimulation in the denervated subendocardium. **A, B)** Peak radial thickening velocity of the subepicardium at early diastole in WT and p75NTR-/- mice determined by tissue Doppler analysis before (**A**) and after (**B**) i.p. injection of dobutamine (32μg/ kg). **C, D)** Peak radial thickening velocity of the subendocardium in WT and p75NTR-/- mice determined at early diastole before (**C**) or after (**D**) i.p. injection of dobutamine (32μg/ kg)(mean ± SEM, *$p<0.05$, n=4).

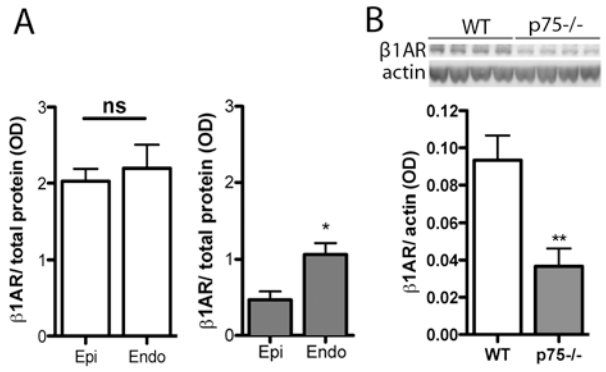

Figure 3.7: β_1AR expression is low and distribution is altered in the p75NTR-/- left ventricle. **A)** β_1AR protein the subendocardium (endo) and subepicardium (epi) of WT (left, white bars) and p75NTR-/- mice (right, grey bars) normalized to total protein (mean ± SEM, *p< 0.05, n=4). **B)** Representative western blot (top) and quantification (below) of β_1-AR and actin in WT and p75NTR-/- left ventricle (mean ± SEM, *p<0.05, **p< 0.01, n=6).

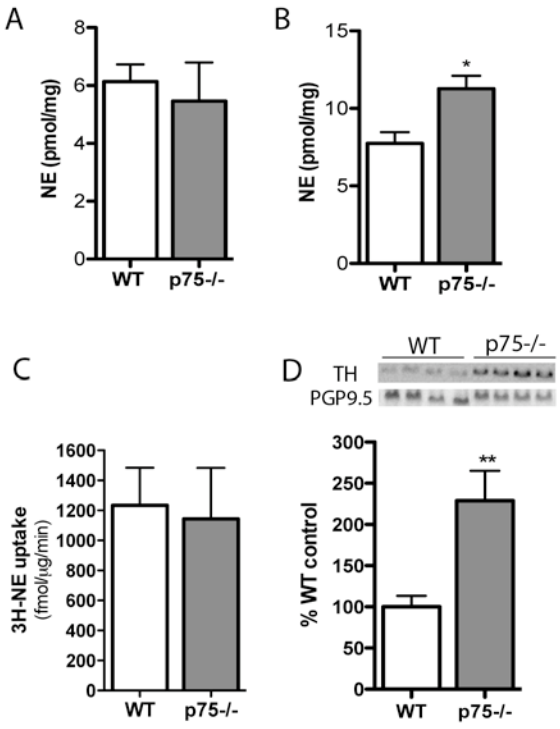

Figure 3.8: NE content, NE uptake and TH levels in the left ventricle. **A)** NE content in the p75NTR-/- left ventricle is not significantly different than WT (mean ± SEM, n=5–6). **B)** NE is elevated in the right ventricle of p75NTR-/- mice (mean ± SEM, *p< 0.05, n=5–6). **C)** NE uptake in p75NTR-/- mouse ventricles is identical to uptake in WT ventricles (mean ± SEM, n=6). **D)** TH protein, normalized to the pan-neuronal marker PGP9.5, is elevated in the left ventricle of p75NTR-/- mice compared to WT. (mean ± SEM, *p< 0.05, **p< 0.01, n=5–6).

Chapter 4

Summary of Results and Discussion:

A. Summary of Results:

The studies presented in this thesis identify the p75 neurotrophin receptor as an important regulator in the patterning of sympathetic innervation of the ventricles during development (Chapter 3) and after ischemic injury (Chapter 2). Data from Chapter 3 demonstrated an altered sympathetic innervation pattern in the p75NTR-/- left ventricle, where the subendocardium was devoid of sympathetic fibers in the p75NTR-/- mice but sympathetic innervation of the subepicardium and RV were normal (Chapter 3). Using sympathetic ganglion explants I showed that neurons lacking p75NTR are more sensitive to sema3a repulsion, which likely explains the lack of sympathetic innervation in the sema3a expressing subendocardium (Ieda et al., 2007). Cardiac function and rhythm were further investigated to determine if the altered pattern of innervation had functional consequences. Although echocardiography showed no differences in left ventricular wall dimensions or cardiac output, mean arterial pressure, dP/dt_{MAX}, and dP/dt_{MIN} were decreased. Most interestingly, p75NTR-/- mice had more spontaneous premature ventricular complexes than WT mice, consistent with the model that sympathetic heterogeneity is arrhythmogenic (Chapter 3). In addition, I found that p75NTR was required for peri-infarct sympathetic denervation after myocardial infarction (Chapter 2). BDNF is a possible ligand for this p75NTR-mediated denervation because BDNF mRNA is transiently

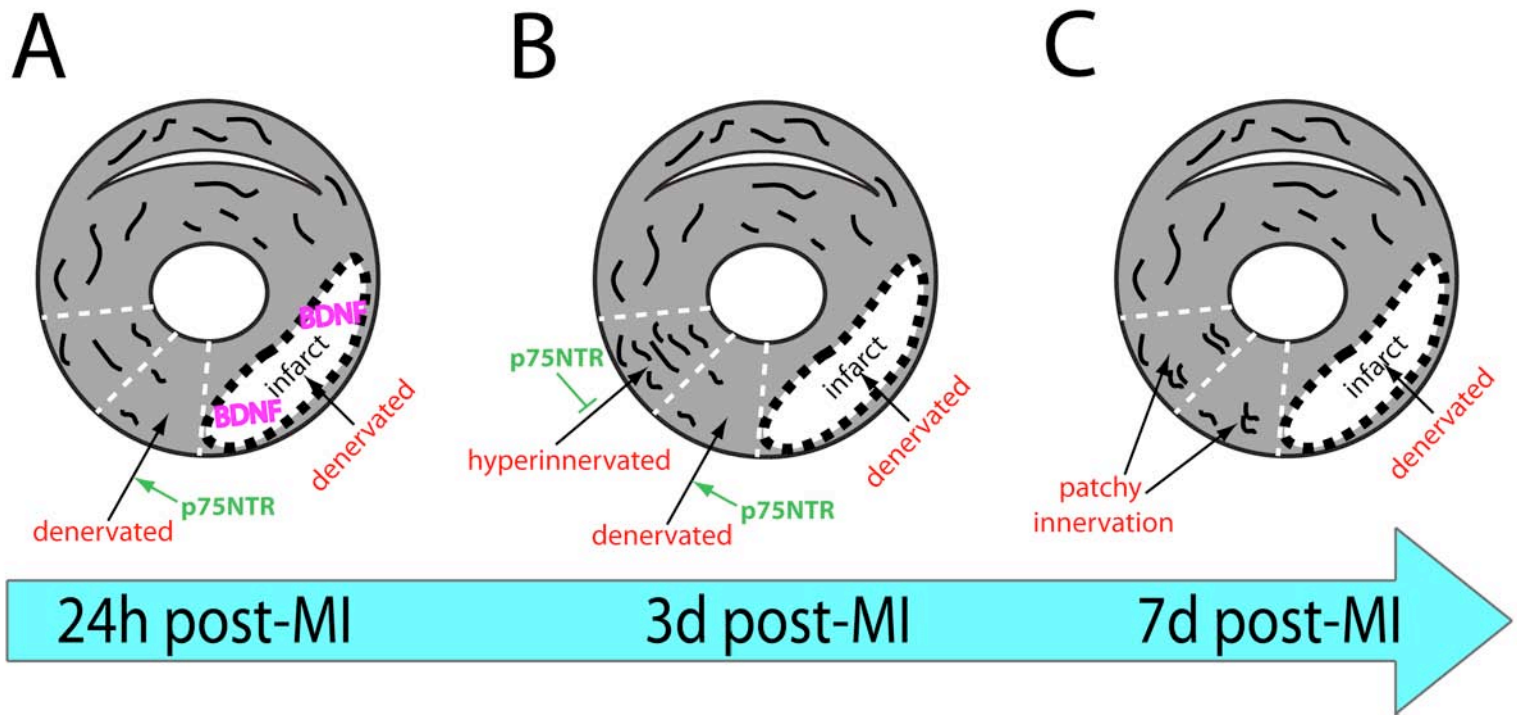
A
B
C
BDNF
BDNF
infarct
denervated
denervated
p75NTR
p75NTR
hyperinnervated
infarct
denervated
denervated
p75NTR
patchy
innervation
infarct
denervated
24h post-MI
3d post-MI
7d post-MI

Figure 4.1: Summary and model for the role of p75NTR in sympathetic remodeling after myocardial infarction. A) 24 hours after ischemia-reperfusion surgery, sympathetic denervation occurs in the proximal peri-infarct region via a p75NTR-dependent mechanism. BDNF protein is elevated in the infarct 24 hours after ischemia-reperfusion surgery and might be the ligand for p75NTR-mediated denervation of the proximal peri-infarct region. Finally, the infarct is denervated 24 hours after ischemia-reperfusion surgery, but this denervation is not mediated by p75NTR. B) 3 days after ischemia-reperfusion surgery, sympathetic denervation is still present in the proximal peri-infarct region and occurs via a p75NTR-dependent mechanism. In contrast, sympathetic hyperinnervation occurs in the distal peri-infarct region 3 days after ischemia-reperfusion, which is attenuated by p75NTR. The infarct remains denervated 3 days after ischemia-reperfusion surgery. C) 7 days after ischemia-reperfusion surgery, sympathetic innervation density in the proximal peri-infarct region returns back to sham-operated levels, suggesting sympathetic regrowth. Sympathetic hyperinnervation is no longer present in the distal peri-infarct region, suggesting sympathetic pruning is taking place. This pruning is not mediated by p75NTR because it occurs whether p75NTR is present or not. The infarct continues to be denervated 7 days after ischemia-reperfusion surgery.

upregulated in the heart after ischemia-reperfusion (Hiltunen et al., 2001) and experiments presented in Chapter 2 showed increased BDNF protein after ischemia-reperfusion. In addition, sympathetic hyperinnervation was exacerbated in the p75NTR-/- mice after myocardial infarction, suggesting that p75NTR plays a role in both denervation and hyperinnervation (Chapter 2; Figure 4.1).

B. The Many Roles of p75NTR in Development and Disease:

1. The Role of p75NTR is Context Dependent:

The role that p75NTR plays in establishing sympathetic innervation of target organs is anything but straightforward. This is illustrated by the highly variable degrees of sympathetic target innervation reported in p75NTR-/- mice, which range from hyperinnervated to hypoinnervated (Jahed and Kawaja, 2005; Kohn et al., 1999; Lee et al., 1994). The multifaceted role for p75NTR in axon outgrowth was first understood with regard to its interaction with Trk receptors. On the one hand, p75NTR can interact with TrkA receptors to create a high-affinity binding site for NGF and promote axon outgrowth (Hempstead et al., 1991). On the other hand, selective activation of p75NTR can functionally antagonize TrkA signaling and even result in axon degeneration (Kohn et al., 1999; Singh et al., 2008). Recent discoveries identifying novel interaction partners of p75NTR beyond Trk receptors reveal multiple roles for p75NTR in axon outgrowth and target innervation. Some of p75NTR partners, such as NogoR/ Lingo1 and ephrinA, form a receptor complex that inhibits axon

outgrowth (Lim et al., 2008; Mi et al., 2004; Wong et al., 2002). Conversely, interaction of p75NTR with the NP1/ plexin sema3a receptor complex, attenuates sema3a repulsion and promotes axon outgrowth (Ben-Zvi et al., 2007). Taken together, these studies, along with work from this thesis, suggest that the role p75NTR plays is dependent on environmental context. It is clear by the nature of its binding partners that p75NTR plays an important role in patterning of the nervous system. Nervous system development involves a tightly orchestrated coordination of growth factors and guidance cues in order to form precise and appropriate connections with targets that often lie far away. Perhaps the ability of p75NTR to modulate a number of these growth and guidance factors provides a means of coordinating and fine-tuning these signals.

The multiple actions of p75NTR on sympathetic target innervation are illustrated in the heart. In particular, data in this thesis illustrate two distinct and opposite roles for p75NTR in cardiac sympathetic innervation: promotion and inhibition of axon outgrowth. During development, p75NTR promotes sympathetic axon outgrowth via two mechanisms. First, through its interaction with TrkA, p75NTR facilitates the switch in neurotrophin dependence from NT-3 to NGF, thereby promoting innervation of the heart (Kuruvilla et al., 2004). p75NTR continues to promote axon outgrowth later in development by disrupting the sema3a receptor complex and putting a brake on sema3a axon repulsion (Ben-Zvi et al., 2007; Ieda et al., 2007; Chapter 3). In contrast, the role of p75NTR on sympathetic innervation after injury induced by ischemia-reperfusion is primarily inhibitory. p75NTR mediates sympathetic denervation and inhibits

NGF- induced sympathetic hyperinnervation after ischemia-reperfusion injury, possibly through elevated BDNF (Chapter 2).

These examples from the heart illustrate that the particular role p75NTR plays is dependent on the molecular environment. It is important to note that the molecular context of the heart after ischemia-reperfusion is not fully elucidated. It is unclear whether ligands for other p75NTR-binding partners, such as sema3a, are upregulated in the heart after ischemia-reperfusion. Therefore, further investigation is necessary to determine the complete molecular environment after ischemia-reperfusion in order to fully understand the role of p75NTR in post-MI sympathetic remodeling.

2. p75NTR, Cardiac Sympathetic Heterogeneity, and Arrhythmias:

The work presented in this thesis links p75NTR with cardiac function and rhythm for the first time. While the altered sympathetic innervation pattern had little effect on hemodynamic function before or after MI (Chapter 2 and Appendix B) we found that p75NTR-/- mice had a higher incidence of premature ventricular complexes. These results support data from other labs that sympathetic heterogeneity alone, in the absence of injury, is sufficient to promote abnormal heart rhythms (Ieda et al., 2007). Although the mechanisms underlying arrhythmogenensis by sympathetic heterogeneity are not fully understood, disruption of normal gradients that coordinate the electrical activity of the heart is probably involved (Antzelevitch et al., 1991; Jiang et al., 2007; Rubart and Zipes, 2005; Wang et al., 2006). Evidence of β-supersensitivity in the subendocardium

and the presence of a transmural β_1AR gradient in the p75NTR-/- mice further support this and suggest that the normal transmural repolarization gradient might be disrupted in these mice (Chapter 3). Another method to further test this would be to examine the QT interval of p75NTR-/- ECGs. Because sympathetic transmission shortens myocyte repolarization (Mohrman and Heller, 2006), the lack of sympathetic innervation of the p75NTR-/- subendocardium might result in increased subendocardial repolarization and action potential duration. Increased subendocardial repolarization would be reflected in a longer QT interval, which is known to be arrhythmogenic. Alternatively, action potential duration of subepicardial and subendocardial myocytes from p75NTR-/- left ventricles could be directly measured by electrophysiology. These studies would further explore the effect of altered sympathetic innervation pattern on the electrical properties of cardiac myocytes, such as ionic currents and refractoriness, and might explain the susceptibility of p75NTR-/- mice to ventricular arrhythmias.

Sympathetic remodeling and heterogeneity are also correlated with fatal ventricular arrhythmias after myocardial infarction. The data presented in this thesis demonstrate that p75NTR plays multiple roles in development of post-MI sympathetic heterogeneity: by facilitating axonal degeneration and inhibiting hyperinnervation. A question that emerges from this data is whether p75NTR-/- mice exhibit more or less ventricular arrhythmias after myocardial infarction than WT mice. This is a difficult question to answer since both WT and p75NTR-/- demonstrate sympathetic heterogeneity after ischemia-reperfusion. While both sympathetic hyperinnervation and denervation occurred after ischemia-

reperfusion in WT mice, only hyperinnervation occurred in p75NTR-/- mice. However, the p75NTR-/- subendocardium remained denervated after ischemia-reperfusion, resulting in sympathetic heterogeneity in both WT and p75NTR-/- mice. Therefore, there may be little difference in ventricular arrhythmias between the genotypes. Indeed, the results presented in Appendix A, in which I monitored the ECGs under anesthesia from WT and p75NTR-/- mice 3 and 7 days after sham surgery or ischemia-reperfusion surgery, showed no difference between the genotypes nor was there a difference between surgical groups. However, those experiments were performed under isoflurane anesthesia, which blunts sympathetic transmission and epinephrine-induced ventricular arrhythmias (Seagard et al., 1984; Tucker et al., 1974), and therefore, are difficult to interpret. In light of this, measuring spontaneous ventricular arrhythmias after myocardial infarction via ECG telemetry in conscious mice would provide a more accurate assessment of post-MI ventricular arrhythmias.

Differences in relative parasympathetic tone in p75NTR-/- mice provide an additional level of complication when assessing post-MI ventricular arrhythmias. The balance between parasympathetic and sympathetic input to the heart has proven to be a powerful indicator of arrhythmia susceptibility and sudden cardiac death after myocardial infarction in that a relative or absolute decrease in parasympathetic, or vagal, activity increases risk of sudden cardiac death (Jouven et al., 2005; La Rovere et al., 1988; La Rovere et al., 2001; Schwartz et al., 1988). In contrast to this, previous studies show p75NTR-/- mice might exhibit increased parasympathetic tone compared to WT mice. While

sympathetic innervation is decreased in the p75NTR-/- right atria, parasympathetic innervation is unchanged, suggesting a relative increase in parasympathetic tone (Habecker et al., 2008). The lower heart rate in conscious p75NTR-/- mice further supports this idea (Chapter 3). In humans, the risk of developing fatal arrhythmias and sudden cardiac death is elevated in individuals with a higher resting heart rate (Jouven et al., 2005). While it is unknown what changes occur in parasympathetic and sympathetic crosstalk, or innervation of the p75NTR-/- atria after myocardial infarction, or if autonomic imbalance occurs, the relative increase in parasympathetic tone before myocardial infarction may be protective against ventricular arrhythmias and sudden cardiac death. This would further complicate the analysis of post-MI arrhythmias and it is therefore important to evaluate autonomic tone of p75NTR mice compared to WT. Several analyses can be performed using the ECG telemetry system mentioned above to assess autonomic balance before and after myocardial infarction including heart rate variability analysis, heart rate turbulence, and heart rate recovery after an exercise stress test (Ghuran et al., 2002; Jouven et al., 2005; Kleiger et al., 1987). In addition, baroreflex sensitivity, which measures vagal reflexes, can also be used as a strong indicator of autonomic balance and risk for sudden cardiac death after myocardial infarction (La Rovere et al., 1988). The results from these experiments will be important for interpretation of any post-MI ECG analysis performed in p75NTR-/- and WT mice.

3. p75NTR in Disease and Injury-Related Neuroplasticity:

Remodeling of the sympathetic nervous system is not limited to myocardial infarction. Changes in sympathetic drive, innervation and neurotransmitter expression occur as a result of several diseases such as heart failure, cardiac hypertrophy, diabetes and some forms of neuropathic pain (Kanazawa et al.; Kimura et al., 2007; Kimura et al., 2010; Kreusser et al., 2008; Stevens et al., 1998; Yen et al., 2006). A common feature of these diseases is abnormal neurotrophin expression, which is thought to underlie many aspects of sympathetic remodeling in these pathologies (Kaye et al., 2000; Kreusser et al., 2008; Yen et al., 2006). The work done in this thesis demonstrates that p75NTR plays multiple key roles in sympathetic remodeling post-MI and suggests that these roles are dependent on environmental context. In light of this, it is likely that p75NTR is also an important mediator of sympathetic remodeling that occurs in other diseases in which neurotrophin signaling is altered, although its precise role is probably determined by the unique molecular environment of each pathological condition.

p75NTR is expressed in many types of neurons (Chao and Hempstead, 1995) and it is, therefore, likely that the context dependent roles p75NTR plays in cardiac development and cardiac neuronal remodeling after injury can be extrapolated to a broad spectrum of neuronal diseases. p75NTR is indeed implicated in several neurodegenerative diseases of the central nervous system as well as failure to regenerate axons after traumatic brain and spinal cord injury (Costantini et al., 2005a; Costantini et al., 2006; Kokaia et al., 1998; Ramos et al., 2007). However, despite upregulation of p75NTR in these pathological

states, the role of p75NTR in each condition is likely to be distinct and determined by the local molecular environment. For example, it is well known that upregulation of a host of inhibitory factors is responsible for the failure to regenerate axons after spinal cord injury (Lee and Zheng, 2008). p75NTR is known to interact with and modulate two of these inhibitory pathways: myelin/ NogoR/ Lingo1 and sema3a/ NP1/ plexin. While selectively targeting either pathway promotes increased axonal regeneration across spinal cord lesions, p75NTR-/- mice showed no improvement of axon regeneration (Kaneko et al., 2006; Li et al., 2004a; Song et al., 2004). This is likely because p75NTR plays opposing roles in axon outgrowth via NogoR/ Lingo1 and sema3a/ NP1/ plexin pathways, on the one hand promoting axon outgrowth while inhibiting outgrowth on the other. These opposing effects may explain why p75NTR-/- axons of the spinal cord still fail to regenerate after injury. This example, again, underscores the importance of understanding the molecular environment in determining the role that p75NTR will play.

4. Clinical Considerations:

The potential role of p75NTR in so many diseases presents a number of clinical considerations. First, the range of interactions and multiple roles p75NTR plays complicates consideration of p75NTR as a therapeutic target. For example, as seen in p75NTR-/-mice, removal of p75NTR rescued one aspect of post-MI sympathetic heterogeneity but exacerbated another. Therapeutically targeting p75NTR after myocardial infarction, therefore, would be unlikely to

prevent the development of sympathetic heterogeneity. A more effective approach might be to target ligands of p75NTR, such as BDNF, or interaction partners in order to achieve a more selective effect.

A second clinical consideration that has largely been ignored is whether the several p75NTR polymorphisms identified correlate to development of disease or disease severity (Gau et al., 2008; McGregor et al., 2007). One particularly intriguing polymorphism results in a missense residue change from serine to leucine in the fourth exon of p75NTR, a region highly conserved across species (Gau et al., 2008). Although the effect of this polymorphism on p75NTR function is not known, it is linked to major depression and decreased responsiveness to selective serotonin reuptake inhibitors (SSRIs) (Gau et al., 2008; Kunugi et al., 2004). Because exon 4 codes for the p75NTR transmembrane domain, which is involved in interactions with some co-receptors (Esposito et al., 2001) it is possible that this polymorphism may affect protein-protein interactions or even cellular localization. In light of the recent understanding of p75NTR's numerous interactions and binding partners this could have significant developmental and disease-related consequences. For example, do individuals with this polymorphism have normal cardiac sympathetic innervation or a higher susceptibility to ventricular arrhythmias? Do they show a higher or lower incidence of neurodegenerative disease? It will be interesting to know if this polymorphism affects p75NTR function, or interaction with binding partners, and whether this polymorphism has any clinical consequences.

C. Limitations and Future Directions:

The work presented in this thesis has begun to identify the many roles of p75NTR in cardiac sympathetic innervation both during development and after cardiac injury such as myocardial infarction. However, several study limitations exist and several questions remain unanswered. One limitation is the use of TH immunohistochemistry as a method of sympathetic fiber detection used in Chapters 2 and 3. Although TH is commonly used as a marker to detect sympathetic fibers in vivo (Dhanoa et al., 2006; Jahed and Kawaja, 2005; Kohn et al., 1999; Lee et al., 1994) it is possible that this method did not identify all sympathetic fibers, particularly in the p75NTR-/- mice. An important follow-up study would be to ensure that most sympathetic fibers are detected using TH immunohistochemistry. This could be done by labeling the stellate ganglia from WT and p75NTR-/- mice with a fluorescent anterograde lipophilic label to identify cardiac sympathetic fibers that originate from the stellate. Using this technique one could confirm the altered pattern of sympathetic innervation in the p75NTR-/- left ventricle detected by TH immunohistochemistry.

A second limitation of this thesis is the lack of direct evidence showing that the altered pattern of sympathetic innervation in the p75NTR-/- left ventricle is caused by enhanced sensitivity to sema3a (Chapter 3). Sema3a is developmentally expressed in the subendocardium and is responsible for generating the normal transmural gradient of sympathetic innervation (Ieda et al., 2007). Data presented in this thesis showed that sympathetic neurons lacking p75NTR are more susceptible to sema3a repulsion, suggesting a mechanism for

the altered pattern of innervation in the p75NTR-/- left ventricle. To directly test this mechanism one could perform a rescue experiment by crossing p75NTR-/- mice with sema3a-/- mice (Taniguchi et al., 1997) to determine whether p75NTR-/- sympathetic neurons would innervate the subendocardium in the absence of sema3a. This technique has been shown to rescue sensory innervation deficits of p75NTR-/- mice caused by enhanced sema3a repulsion of sensory neurons lacking p75NTR (Ben-Zvi et al., 2007). If the altered pattern of sympathetic innervation in the p75NTR-/- left ventricle is indeed caused by enhanced sema3a repulsion one would expect this genetic cross to result in sympathetic innervation of the subendocardium despite lack of p75NTR.

Finally, the work presented in this thesis has begun to dissect the mechanisms that underlie sympathetic denervation after myocardial infarction and demonstrate that this occurs via a p75NTR-dependent mechanism. Despite this, a limitation of this study is that the ligand for p75NTR-mediated sympathetic axon degeneration remains unidentified. The finding that BDNF protein was elevated in the left ventricle 24 hours after ischemia-reperfusion surgery (Chapter 2), along with results from David Kaplan and Frieda Miller's group demonstrating that sympathetic axon degeneration occurs via a BDNF-p75NTR mediated mechanism (Singh et al., 2008), identify BDNF as an attractive candidate. However, determining whether BDNF is required for p75NTR-mediated denervation involves many considerations. Firstly, because global knock out of BDNF is generally lethal (Ernfors et al., 1994), a conditional BDNF knockout would be a preferred method. However, in order to generate a conditional BDNF

knockout the source of post-MI BDNF must be identified. The data presented here suggest that the source for BDNF at 24 hours post-MI might be immune cells in the infarct, possibly macrophages, neutrophils or myofibroblasts. In contrast, elevated BDNF mRNA 2-5 hours after ischemia-reperfusion was found in myocytes at the infarct border zone (Hiltunen et al., 2001). Taken together these data suggest there may be multiple sources of BDNF post-MI that occur in at least two distinct phases: an early phase 2-5 hours post-MI in which myocytes express BDNF followed by a later phase 24 hours post-MI by infiltrating immune cells. To confirm this, an important future study then will be to identify the precise timeline for BDNF protein upregulation and the various sources. If multiple sources for BDNF are identified and a conditional knockout is not possible, an alternative experiment to test if BDNF is necessary for p75NTR-mediated denervation would be to neutralize BDNF post-MI by administration of a function-blocking antibody.

Although BDNF is an interesting and likely candidate for p75NTR-mediated sympathetic denervation post-MI, other possible candidates, such as the pro-neurotrophins, should also be considered. Pro-neurontrophins have been found to be the preferred ligands for p75NTR, having a five-fold higher affinity for p75NTR than mature neurotrophins (Lee et al., 2001). The relative expression of pro-neurotrophins compared to mature neurotrophins after ischemia-reperfusion or chronic ischemia is unknown and it will be important to determine these expression levels in order to identify the ligand(s) for p75NTR. Neither the immunohistochemistry performed in this thesis nor the *in situ*

hybridization used to detect BDNF mRNA rule out pro-BDNF since these methods of detection cannot distinguish between pro- and mature forms (Hiltunen et al., 2001; Chapter 2). Similarly, it is not known whether pro-NGF levels increase after MI. One way to distinguish between the pro- and mature forms of NGF or BDNF would be to perform ischemia-reperfusion on HA-BDNF mice (Yang et al., 2009) and HA-NGF mice (unpublished) and immunoprecipitate all forms of neurototrophins from the post-MI left ventricle using an antibody to the HA tag. The presence of pro- and mature neurotrophins could then be detected by size fractionation and immunoblot analysis. Determining which p75NTR ligand or ligands are present after MI and their sources are critical future experiments for understanding the mechanism of post-MI sympathetic denervation.

While mechanisms of sympathetic axon degeneration through p75NTR are often ligand dependent (Park et al., 2010; Singh et al., 2008), the interaction of p75NTR with several different co-receptors suggests p75NTR-mediated sympathetic denervation post-MI might be neurotrophin independent. For example, as mentioned above, p75NTR plays an essential role in a variety of axon growth inhibitory signals such as ephrinA and NogoR/ Lingo1. It is not known whether the ligands that mediate repulsion by these receptor complexes are expressed in the heart after ischemia-reperfusion and these will be important future points of investigation. The expression of the chemorepulsive agent sema3a during development suggests it may also be upregulated in the heart after myocardial infarction. However, it is unlikely that sema3a is responsible for

p75NTR-dependent denervation since p75NTR attenuates sema3a axon repulsion (Ben-Zvi et al., 2007; Chapter 3). Sema3a expression, however, still may play a role in the sympathetic pruning that occurs 7 days after ischemia-reperfusion. Sympathetic innervation of the distal peri-infarct region returned back to sham-operated levels that were comparable between genotypes 7 days after MI, despite exacerbated hyperinnervation in p75NTR-/- mice. This increased pruning of p75NTR-/- sympathetic neurons could possibly be explained by enhanced sema3a repulsion if sema3a is expressed in the heart after MI. Taken together, determining what chemorepulsive factors and p75NTR ligands are present in the heart after ischemia-reperfusion and their spatio-temporal expression pattern are critical future directions necessary for understanding the mechanisms that underlie post-MI sympathetic denervation.

D. Concluding Remarks:

Cumulatively, the data presented in this thesis contribute to our understanding of p75NTR in development and disease. Previous studies demonstrate that sympathetic heterogeneity develops after myocardial infarction and that this heterogeneity increases susceptibility to fatal ventricular arrhythmias. The work done in this thesis further supports the link between sympathetic heterogeneity and ventricular arrhythmias. More importantly, this study furthers our understanding of the mechanisms underlying the generation of sympathetic heterogeneity after myocardial infarction and identifies p75NTR as an important mediator of this process.

Chapter 5

Detailed Methods

Animals: Wild type C57BL/6J and p75NTR -/- mice (B6.129S4-Ngfr^{tm1Jae}/J) were obtained from Jackson Laboratories. The homozygous knock-in mice in which the endogenous *Bfnf* coding exon was replaced with the murine *Bdnf* sequence with a C-terminal hemagglutinin (HA) epitope tag (*Bdnf-HA)* were generated as described by Yang et al., 2009 (Yang et al., 2009). The B6.129S4-Ngfr^{tm1Jae}/J mice contain two mutated exon III alleles, which removes the coding region for the last three of four cysteine–rich repeats in the extracellular domain, and prevents the expression of functional p75NTR (Lee et al., 1992; Welcher et al., 1991; Yan and Chao, 1991). The p75NTR -/- mice were genotyped upon arrival (NEO+1: 5' CTTGGGTGGAGAGGCTATTC 3'; NEO-: 5' AGGTGAGATGACAGGAGATC 3'; p75 exon3+: 5' TGTTACGTTCTCTGACGTGGTGAG 3'; p75 exon3-: 5' TCAGCCCAGGGTGTGCACTC 3') and a colony was maintained using homozygous breeder pairs, with additional genotyping every 6 months. All mice were kept on a 12h:12h- light dark cycle with ad libitum access to food and water. Age and gender-matched male and female mice between 12-18 weeks old were used for all experiments. All procedures were approved by the Institutional Animal Care and Use Committee and comply with the Guide for the Care and

Use of Laboratory Animals published by the United States National Institutes of Health (NIH publication No. 85-23, revised 1996).

Axon Outgrowth: To test the role of p75NTR in modulating sema3a inhibition of axon outgrowth, we used explants of stellate ganglia, which contain most of the sympathetic neurons that project to the heart. Both left and right ganglia were gently dissected from adult wildtype and p75NTR animals, taking care not to crush or damage ganglia. Immediately upon dissection the ganglia were placed in ice cold Hank's Balanced Saline Solution (HBSS, Sigma) and desheathed to facilitate axon outgrowth, cut in half, and embedded in 30μL reduced growth factor Matrigel™ (BD Biosciences), and covered with 650 μL serum-free DMEM/F12 with penicillin/ streptomycin (1:10,000) and 10 ng/mL NGF. Explants were maintained at 37 °C with 5% CO_2. 20 hr after plating (t=0) explants were photographed, treated with vehicle or 120 or 240ng/mL sema3a-Fc (R & D Systems) and then photographed again 6 hours later (t=6). Axon length was measured at each time point using Nikon Elements AR 3.0, and the rate of axon growth/hour was calculated. For each treatment group, 6-10 axon measurements were obtained and averaged from a minimum of 3 different sites. These experiments were repeated 3 times.

Dissection of Tissue for Western and HPLC analyses: Following euthanasia, hearts were removed from the chest cavity of the mice and placed in saline. Any remaining blood in the heart was gently expelled with forceps. Hearts from unoperated, sham or MI mice were dissected into four sections (Fig. 5.1). First,

the atria were removed. Next the base was separated from the ventricles at the point of ligation using a razor blade. In the case of unoperated animals the base was defined as the top 3mm of the heart (Figure 5.1). The apex (bottom 1mm of tissue) was then removed and discarded. The LV was then dissected away from the RV, splitting the interventricular septum along the natural division of the muscle, which was identified visually. All dissected regions of the heart were immediately flash frozen (HPLC) or placed in RNAlater (Western).
For immunoblot analysis of subendocardium vs. subepicardium, the ventricles were sectioned into 1mm sections using a heart block and the inner vertical loop of the left ventricle was dissected from the outer transverse loop.

HPLC: Norepinephrine was measured by high-performance liquid chromatography (HPLC) with electrochemical detection. Hearts were dissected as described above and frozen. The frozen hearts were pulverized using a ceramic mortar and pestle chilled on dry ice. The frozen tissue was weighed out in pre-weighed 1.5mL microcentrifuge tubes immediately followed by homogenization of the tissue in 250μL 0.1M perchloric acid containing 0.5μM of the internal standard, 3,4-Dihydroxybenzylamine (DHBA), to correct for sample recovery. The homogenates were centrifuged and the catechols were pre-purified by adsorption onto alumina as follows: 200μL of supernatant was neutralized with 1.0M Tris buffer, pH 8.6, and 15 mg acid-washed alumina was added. NE standards (0.25μM) were processed similarly. The alumina was washed twice with mqH_2O and the catechols were desorbed with 100μL 0.1M

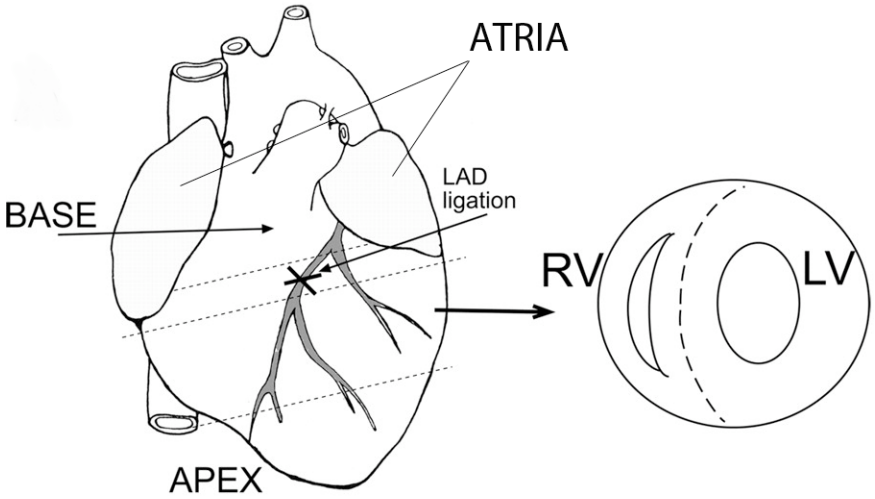

Figure 5.1: Dissection of the heart for HPLC and Western analysis.

perchloric acid. Fifty microliters of sample were injected onto the HPLC and the catecols were fractionated by reverse-phase HPLC on a C_{18} column (5μm, 4.5 mm x 15 cm) using a mobile phase that consisted of 75mM $NaH_2PO_4 \bullet H_2O$, 1.7mM sodium octane sulfonate, 0.01% triethylamine, and 3.0% acetonitrile, pH=3.0. A coulometric electrochemical detector was used (Coulochem III, ESA) with an electrode voltage set at 180mV, fullscale 200nA. Detection limits for NE were ~0.05 pmol with recoveries from the alumina extraction >60%.

TH Immunohistochemistry: Hearts were fixed for 1h in 4% paraformaldehyde, rinsed in PBS (5 x 5min), cryoprotected in 30% sucrose overnight and 10 μm transverse sections were thaw-mounted onto charged slides. To reduce fixative-induced autofluorescence, sections were rinsed in 10 mg/mL sodium borohydride 3X10 minutes and then rinsed in PBS 3X10 minutes. Sections were then blocked in 2% B.S.A/ 0.3% Triton X-100 in PBS for 1 h, incubated with a TH-specific antibody (1:300) overnight, rinsed 3 x 10 minutes in PBS, and incubated 1.5 h with the AlexaFluor 488-conjugated rabbit IgG-specific antibody (1:300). Sections were rinsed 3 x 10 minutes in PBS. To reduce lipofuscin-induced autofluorescence sections were dipped briefly in mqH_2O followed by treatment with 10mM $CuSO_4$ in 50mM $NH_4C_2H_3O_2$ for 30 minutes. Slides are then again briefly dipped in mqH_2O and placed in PBS, coverslipped and visualized by fluorescence microscopy. Sections from WT and p75NTR-/- hearts were always stained and photographed side by side to minimize variation between the groups due to the immunohistochemistry procedure.

HA Immunohistochemistry: Heart tissue was fixed for 2h in 3% paraformaldehyde rinsed in PBS (5 x 5min), cryoprotected in 30% sucrose overnight and 10 µm transverse sections were thaw-mounted onto charged slides. Sections were then blocked in 5% B.S.A/ 0.1% Triton X-100 in PBS for 1 h followed by blocking with AvidinD blocking buffer (Vector Laboratories) for 15 min. Slides were briefly rinsed with PBS and blocked with Biotin solution (Vector Laboratories) for 15 min. Slides were rinsed again 3 x 5 min with PBS and incubated with rabbit anti-HA IgG (1:500, Sigma) overnight at 4°C. Slides were then rinsed 5 x 6 min in PBS and incubated with biotinylated goat anti-rabbit IgG (1:400, Jackson ImmunoResearch) for 1h at room temperature. Slides were then washed 3 x 5 min with PBS and incubated with Cy3-streptavidin (1:800, Jackson ImmunoResearch) for 45 min. Slides were washed 3 x 5 min with PBS, coversliped and visualized by fluorescence microscopy.

Imaging and Analysis of Ventricles:

Composite analysis. Immunohistochemical staining was visualized on a Zeiss (Axiophot II) fluorescent microscope with the 10X objective. Composite images were used to generate a representative heart section from each mouse that included the left and right ventricles. The composite was divided into right ventricle, subepicardium or subendocardium (includes interventricular septum) of the left ventricle, and quantified using ImageJ software (NIH). In order for two observers to analyze endo- vs. epicardium consistently, we measured the ventricle wall and identified half as endocardium and half as epicardium rather

than trying to follow the border between the two layers of muscle. Innervation density was determined by threshold discrimination using ImageJ. All photos were treated in an identical manner. Black and white photos were opened in ImageJ and the brightness/contrast tool was used to adjust each image so that the minimum was set at the left side of the histogram. The threshold tool was then used to identify nerve fibers. The automated function set a beginning threshold level, however, this sometimes included non-specific areas or did not include sympathetic fibers. The threshold was then manually adjusted to ensure that only TH staining was identified by the threshold tool. The ventricle has two layers of muscle with fibers running at different angles, thus each section included some nerve fibers cut longitudinally along the plane of the section and other fibers cut in cross-section and appearing as small round dots. Thus, specific criteria for size and shape were not used in our analysis. Innervation density is expressed as the percent of area that is above the determined threshold (TH+ fibers). Each image was quantified by two independent observers. The coefficient of variance between the two independent analyses averaged 10±8.3%, mean± SD.

Analysis of specific regions: TH staining was visualized using the 20X objective, and pictures were obtained for areas A-K as shown in Figure 3.2. Pictures taken occupied an area of 710 μm x 530 μm and this area is referred to as one field of view. Pictures A and B in the right ventricle were taken first. C was taken at the border between the right ventricle and the left ventricle and each successive picture (D-J) was approximately one field of view adjacent to the previous picture.

K was taken from the interventricular septum. Innervation density was determined by threshold discrimination as described above (ImageJ). Each image was quantified by two independent observers. 5 sections at least 150 μm apart were analyzed from each heart and averaged together. The data shown are the average of the two independent determinations.

Analysis at 24h Post-MI: Tissue sections from 24 hours post-MI were analyzed in the following manner. Pictures of five areas were taken: the infarct, peri-infarct 1 (one field of view directly adjacent to the infarct), peri-infarct 2 (one field of view directly adjacent to peri-infarct 1), the RV and the IVS. Innervation density was analyzed using threshold discrimination using ImageJ as described above.

Immunoblot Analysis: Hearts were dissected as described above. Tissue was homogenized in lysis buffer (20mL lysis buffer per 1g of tissue) (lysis buffer: 1% Igepal, 20mM Tris HCl (pH 8.0), 137mM NaCl, 10% glycerol, 2mM EDTA, 10mM NaF, protease inhibitor cocktail (Roche, 1 tablet/ 50mL lysis buffer) using ground glass homogenizers and protein content was quantified using the Pierce bicinchoninic acid protein assay kit. 20 μg of cardiac protein were added to 4x XT Sample Buffer and 20x XT Reducing Agent (Biorad), heated at 95°C for 5 min, sized fractionated on 4-12% Bis-Tris precast gels (Biorad), and transferred to nitrocellulose membranes. Membranes were blocked in 5% nonfat dry milk diluted in TBST (100 mM NaCl, 10 mM Tris (pH 7.5), and 0.1% Tween 20), incubated overnight at 4°C with primary antibody (Table 5.1) in TBST and 5% nonfat dry milk. The blots were then washed 3 x 10 min with TBST, and

incubated for 1 h at room temperature with secondary antibody in TBST and 5% nonfat dry milk (goat anti-mouse-horseradish peroxidase IgG (1:10,000; Pierce Cat# 32460), and immunoreactive bands were visualized by chemiluminescence. Band intensity was recorded by a 40°C charge coupled device camera and analyzed using LabWorks software (UVP, Upland, CA). In order to probe for a second protein as a loading control, blots were stripped for 1 h at room temperature in stripping solution (62.5 mM Tris (pH 6.8), 2% SDS, and 0.7% (vol/vol) β-mercaptoethanol) and washed extensively in TBST. Blots were then incubated with primary antibody () in TBST and 5% nonfat dry milk at 4°C overnight and incubated with appropriate secondary antibodies, and immunoreactive bands were visualized by chemiluminescence. TH band density was normalized to PGP from the same sample. β_1AR was normalized to actin or total protein and TH was normalized to PGP9.5. Total and mean band density gave similar results.

Infarct/ Area at Risk Analysis: 24 hours after the onset of reperfusion, the mice were anesthetized with 4% isoflurane. Once unconscious, the mice were intubated and mechanically ventilated and anesthesia was maintained with 2% inhaled isoflurane. The chest cavity was then re-opened and the LAD was re-occluded using the same suture from the ischemia-reperfusion procedure. Fluorescent particles (4 mg/ml in deionized water with 0.01% Tween 20; Duke Scientific no. 34 –1, 2- to 8-μm size) were infused through a polyethelyne tube (PE10) with a 30-gauge needle tip in the left ventricle of the heart. Microspheres

were infused at a rate of 400μL/min for 4 minutes to delineate the area at risk. The heart was then excised for infarct size analysis and cut into transverse sections 1mm thick using a cutting block. Both sides of all slices were photographed under ultraviolet light and saved in Photoshop for measurement of area at risk. The slices were then placed in 2,3, 5-triphenyltetrazolium chloride solution (TTC, 1% wt/vol in a sodium phosphate buffer at 37° C, pH 7.4) for 20 minutes. The staining procedure was carried out in the dark to prevent break down of the TTC by the light. The slices were then placed in 10% neutral buffered formalin overnight to increase the contrast of the stained and unstained tissue. Myocardium that did not stain red was presumed to be infarcted. Both sides of each 1mm section was photographed under white light and the Images were saved in Photoshop. Total area, area at risk and infarct areas for each slice were traced and digitized. The volume of myocardium at risk and infarcted myocardium was calculated from the measured areas and slice thickness. Infarct size was normalized as a fraction of the area at risk or as percent of the entire ventricle. All analyses were performed in a blinded fashion by two people. The data presented are the average of the two independent determinations of infarct/ risk.

Ischemia-reperfusion Surgery: Myocardial infarction was generated using ischemia-reperfusion surgery because reperfusion of occluded coronary arteries is standard treatment for humans. Anesthesia was induced with 4% inhaled isoflurane and maintained with 2% isoflurane. Mice were then intubated and

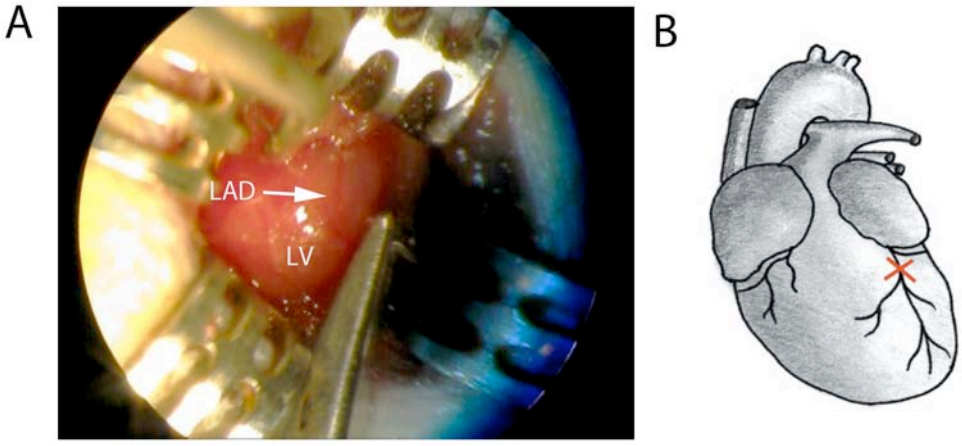

Figure 5.2: Ischemia-reperfusion surgery: surgical preparation and needle pass. **A**) A needle pass is shown. After thoracotomy and pericardotomy the left ventricle (LV) of the heart is exposed. A needle with an 8-0 suture is passed underneath the left anterior descending coronary artery (LAD). Contrast has been enhanced in order to see the LAD more clearly. **B**) Cartoon showing approximately where the LAD is occluded for ischemia-reperfusion.

Figure 5.3

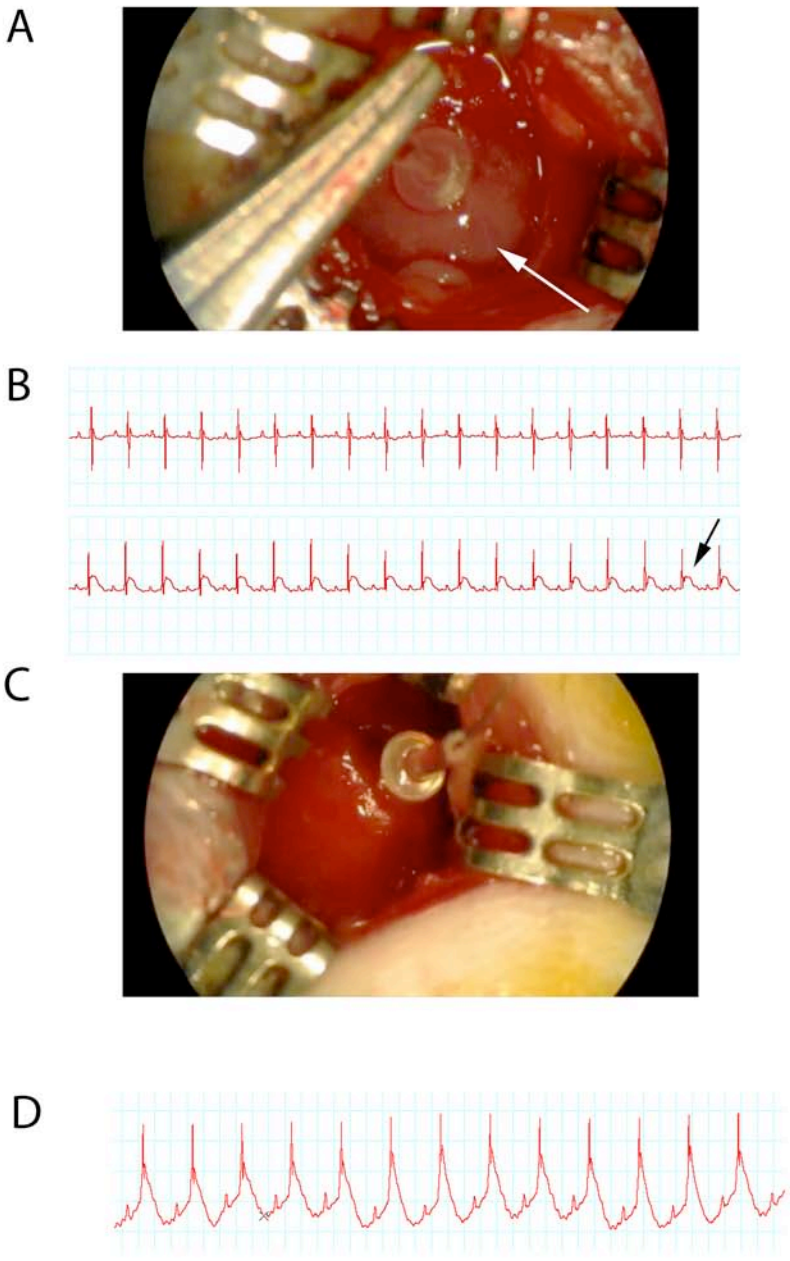

Figure 5.3: Ischemia-reperfusion surgery: occlusion and reperfusion. **A**) Representative picture showing an LAD occlusion. Note the blanched tissue below the ligation (white arrow). **B**) Representative ECG traces from before LAD occlusion (top trace, normal sinus rhythm) and after LAD occlusion (bottom trace, arrow shows ST elevation). **C**) Representative picture showing reperfusion. Note the return of color to the myocardium. **D**) Representative ECG trace from reperfusion.

mechanically ventilated (Fig. 5.2A). Core body temperature was monitored with a rectal probe and maintained at 37° C and ECG (lead II configuration) was monitored throughout the surgery using a PowerLab data acquisition system. A left thoracotomy was performed in the 4th intercostal space and the pericardium was opened. The left anterior descending coronary artery (LAD) (Fig 5.2B-C) was reversibly ligated with an 8-0 suture for 30 minutes and then reperfused by release of the ligature. Occlusion was confirmed with ST segment elevation (Fig. 5.3B), regional cyanosis, blanching, (Fig. 5.3A) and wall motion abnormalities. Reperfusion was confirmed by return of color to the myocardium distal to the ligation (Fig. 5.3C) and the appearance of accelerated idioventricular rhythm (Fig. 5.3D). The suture remained within the wound for identification of the ligature site and the chest and skin were closed in layers. After surgery, animals were returned to individual cages and given regular food and water for 24h, 3 days or 7 days before death and tissue harvest. Buprenex (0.1 mg/kg) was administered as needed to ensure that the animals were comfortable following surgery. All surgical procedures were performed under aseptic conditions. Unoperated control animals did not undergo any surgical procedures, whereas sham-operated animals underwent the procedure described above except for the LAD ligature.

Real-time PCR: Ganglia were dissected out from wildtype and p75NTR-/- mice and stored in RNAlater®. RNA was isolated using an RNAqueous micro kit (Ambion). Total RNA was treated with DNase, quantified by determining

optical density at 260 nm and 100ng of RNA was reverse transcribed (42°C for 1h followed by 95°C for 5 min to kill enzyme). An RNA alone control was included for each sample to test for genomic DNA contamination. Each sample was then diluted 1:4 with PCR-grade H_2O. Real-time PCR was performed with either ABI TaqMan Universal PCR master mix ABI 7500. Samples were assayed using using ABI prevalidated TaqMan gene expression assays for mouse NP1, plexinA4, GAPDH, β_1AR, and actin. For the PCR amplification, 4 μL of reverse transcription reactions were used in a total volume of 20 μL, and each sample was assayed in duplicate. Standard curves were generated with known amounts of mouse brain RNA or mouse heart ranging from 0.8 to 100ng. β_1AR was normalized to actin, and NP1 and PlexinA4 were normalized to GAPDH.

Echocardiography: Ventricular function was measured in isoflurane anesthetized mice using both transthoracic echocardiography and a micromanometer-tipped pressure transducer (SPR1000, Millar Instruments) inserted retrograde into the ventricle. Left ventricular dimensions and function were evaluated using transthoracic echocardiography at a transmission frequency of 40 MHz (Vevo 770, VisualSonics Inc.) and a cycle length of 1. Parasternal imaging was performed in the mid-papillary short-axis and parasternal long-axis imaging planes. Image sequences were acquired with ECG gating of sequential M-mode sweeps (EKV mode) for an effective 2-D frame rate of 1,000 Hz. Left ventricular anteroseptal and posterolateral wall thickness in the short-axis were measured at end-systole and end-diastole and used to calculate thickening fraction. Left

ventricular cavity dimensions in the anterior-posterior dimension at end-systole (LVIDs) and at end-diastole (LVIDd) were measured and used to calculate shortening fraction by: 100(LVIDd-LVIDs)/LVIDd, left ventricular volumes by: ([7.0/(2.4+LVID)]XLVID^3 and ejection fraction (LVEF). Stroke volume was measured by the product of the proximal aortic area and time-velocity integral derived from pulsed-wave Doppler at the same level. The product of stroke volume and heart rate was used to calculate cardiac output. Tissue Doppler imaging was performed to determine peak radial endocardial velocities in systole (S') and early diastole (E') in the anterior wall. (±)-dobutamine hydrochloride (32μg/ kg) was injected intra-peritoneally to assess β_1AR responsiveness.

Left Ventricular Peak Systolic Pressure, dP/dt$_{MAX}$ and dP/dt$_{MIN}$: Left Ventricular Pressure, dP/dtMAX and dP/dtMIN: Ventricular pressure and arterial pressure were measured with a microtipped pressure transducer (1.0 French; Millar) which was calibrated daily with a manometer before use. Anesthesia was induced with 4% inhaled isoflurane. Mice were intubated, ventilated and anesthesia was maintained with 2-3% inhaled isoflurane. Body temperature was maintained at 37±0.2 ºC. The right carotid artery was isolated by blunt dissection and the microtipped pressure transducer was inserted into the right carotid artery for arterial pressure measurements, then advanced into the left ventricle. The left jugular vein was cannulated for intravenous (i.v.) access. Baseline parameters were monitored for 5 minutes. In order to block ganglionic transmission hexamethonium (5 mg/kg) was infused i.v. and a new baseline was measured.

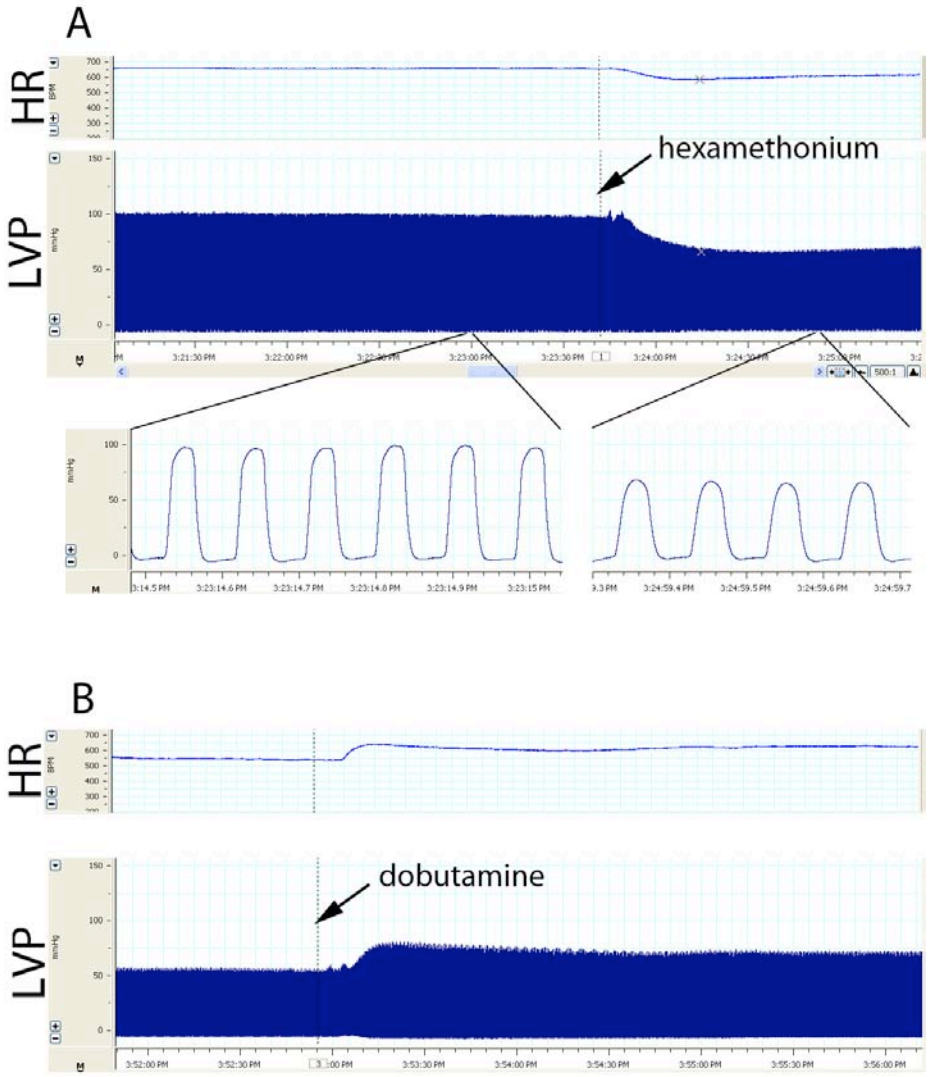

Figure 5.4: Representative left ventricular pressure and heart rate traces. **A)** Traces showing heart rate and left ventricle pressure after i.v. administration of hexamethonium to block ganglionic transmission. The top panel shows the heart rate. The middle trace shows 4 minutes and 30 seconds of left ventricular peak systolic pressure and the bottom trace shows approximately 1s of the top trace. **B**) Traces showing heart rate and left ventricular pressure after i.v. infusion of the β_1AR agonist dobutamine. The top trace shows the heart rate and the bottom trace shows left ventricular pressure.

In order to assess β1-responsiveness of the heart, a maximal dose of the short-acting β1AR agonist dobutamine (32 µg/kg) was infused i.v. Because dobutamine has a half-life of about 2.5 minutes, at least 10 minutes were allowed to pass before the next drug infusion. Tyramine (200 µg/kg) was then infused i.v. to trigger non-exocytotic release of endogenous NE from sympathetic terminals. Mean arterial pressure (MAP) and left ventricular peak systolic pressure (LVPSP) were monitored using a PowerLab data acquisition system (AD Instruments) (Fig. 5.4). dP/dt_{MAX} and dP/dt_{MIN} were calculated using LabPro software (AD Instruments).

NE Uptake: Uptake of 3H-NE into sympathetic nerve terminals was assayed essentially as described by Sharma and Benerjee (Sharma and Banerjee, 1977) and Liang et. al.(Liang et al., 1989). Mouse ventricles were separated into sections 1 mm thick, with two sections from each heart used for total uptake and two for background uptake (defined by addition of 1 mM desipramine). The high concentration of desipramine is comparable to what is needed in binding assays to fully block non-specific NET binding in the heart (Backs et al., 2001). Samples were preincubated for 10 minutes at 37ºC in KRH buffer (KRH; 120 mM NaCl, 4.7 mM KCl, 2.2 mM $CaCl_2$, 1.2 mM KH_2PO_4, 1.2 mM $MgSO_4$, 10 mM HEPES, 5 mM Tris Base pH 7.4) with or without desipramine, and then 50 nM ^{3}H-NE was added. 10 or 20 minutes after addition of ^{3}H-NE, reactions were stopped by placing the samples on ice and adding 1 mL of ice-cold KRH buffer. Tissue was rinsed 3 times in cold KRH, weighed, placed into ice-cold 0.4 M perchloric acid,

minced, and extracted in the acid for 21 hours at 4ºC (Sharma and Banerjee, 1977). 0.5 mL of the supernatant was quantified by liquid scintillation counting. Both time points generated similar results when calculated as the amount of uptake per minute.

ECG Telemetry Recordings and Analysis: ECGs were obtained from conscious adult mice using telemetry implants and were analyzed with Dataquest ART software (Data Sciences International). Mice were anaesthetized with 4% inhaled isofluorane and maintained on 2% inhaled isoflurane. The transmitter was implanted into the abdominal cavity in a lead II configuration, with the negative lead placed in the right pectoral muscle and the positive lead placed to the left of the xyphoid process. A sub-cutaneous injection of 0.1mg/kg buprenorphine was administered post-operatively for analgesia. Mice recovered for at least 72 h before data acquisition. ECG recordings were collected at a sampling rate of 1000Hz for 24 hr and were analyzed at 4 time points within the circadian cycle (6 pm-7 pm, 12 am-1 am, 6 am-7 am, and 12 pm-1 pm) to determine heart rate and the presence of spontaneous premature ventricular complexes (PVCs). PVCs were defined as a single premature QRS complex in relation to the P-wave (Walker et al., 1988).

Quantification of post-MI arrhythmias: 24 hours after the onset of reperfusion, the mice were anesthetized with 4% isoflurane, intubated, and mechanically ventilated, and anesthesia was maintained with 2% inhaled isoflurane. ECG

leads were attached to the mouse in a lead II configuration and ECG was monitored for 10 minutes using a PowerLab data acquisition system (AD Instruments). After baseline measurements were taken epinephrine was injected (2mg/kg, i.p.) and the ECG was monitored for an additional 10 minutes. ECG traces were analyzed using LabPro Software (AD Instruments). Abnormal ventricular rhythms were classified according to the standards of the Lambeth Conventions where a premature ventricular complex (PVC) was defined as a single premature QRS complex in relation to the P-wave and ventricular tachycardia was defined as more than 4 sequential PVCs (Walker et al., 1988).

Table 5.1: Primary Antibodies Used in Immunoblot and Immunohistochemical Analyses

Antibody	Dilution	Company	Catalog #
rabbit anti-b_1AR IgG	1:500	Affinity BioReagents	PA1-049
rabbit anti-TH IgG	1:1000	Millipore	AB 152
rabbit anti-PGP9.5 IgG	1:1000	Accurate Chemicals	RA 95101
rabbit anti-actin IgG	1:500	Sigma	A2066
rabbit anti-trkA IgG	1:500	Upstate	06-574
rabbit anti-HA IgG	1:500	Sigma	H6908

Appendix

Appendix A:

Quantification of post-MI arrhythmias: 24 hours after ischemia-reperfusion surgery, the mice were anesthetized with 4% isoflurane, intubated, and mechanically ventilated, and anesthesia was maintained with 2% inhaled isoflurane. ECG leads were attached to the mouse in a lead II configuration and ECG was monitored for 10 minutes using a PowerLab data acquisition system (AD Instruments). After baseline measurements were taken epinephrine was injected (2mg/kg, i.p.) and the ECG was monitored for an additional 10 minutes. ECG traces were analyzed using LabPro Software (AD Instruments). Abnormal ventricular rhythms were classified according to the standards of the Lambeth Conventions where a premature ventricular complex (PVC) was defined as a single premature QRS complex in relation to the P-wave and ventricular tachycardia was defined as more than 4 sequential PVCs (Walker et al., 1988).

Table A.1: Post-MI Ventricular Arrhythmias Under Isoflurane (3d post-MI)

				PRE-EPI (5min)			POST-EPI (5min)		
Animal	***Genotype***	***Gender***	***Surgery***	***# of PVCs***	***Vtach Episodes***	**Duration**	***# of PVCs***	***Vtach Episodes***	**Duration**
9093.1	WT	m	3d sham	0	0	N/A	4	0	N/A
9093	WT	m	3d sham	0	0	N/A	0	0	N/A
9145	WT	m	3d sham	0	0	N/A	0	0	N/A
9128	WT	f	3d sham	0	0	N/A	0	0	N/A
9194.1	WT	f	3d sham	1	0	N/A	0	0	N/A
9194.2	WT	f	3d sham	0	0	N/A	0	0	N/A
9145.1	C57Bl6	m	3d MI	0	0	N/A	3	0	N/A
9159.1	C57Bl6	m	3d MI	0	0	N/A	4	0	N/A
9174.0	C57Bl6	m	3d MI	0	0	N/A	5	2	6s, 2s
9122.0	C57Bl6	f	3d MI	0	0	N/A	0	0	N/A
9166.0	C57Bl6	f	3d MI	0	0	N/A	0	0	N/A
9194.0	C57Bl6	f	3d MI	2	0	N/A	0	0	N/A
9114.2	p75	m	3d sham	0	0	N/A	0	0	N/A
9177.0	p75	m	3d sham	0	0	N/A	0	1	8s
9177.1	p75	m	3d sham	0	0	N/A	25	0	N/A
9117.1	p75	f	3d sham	0	0	N/A	0	0	N/A
9160.1	p75	f	3d sham	0	0	N/A	0	0	N/A
9170.1	p75	f	3d sham	0	0	N/A	0	0	N/A
9163.0	p75	m	3d MI	0	0	N/A	0	0	N/A
9163.1	p75	m	3d MI	0	0	N/A	0	0	N/A
9170.0	p75	m	3d MI	0	0	N/A	0	0	N/A
9117.0	p75	f	3d MI	0	0	N/A	0	0	N/A
9129.1	p75	f	3d MI	0	0	N/A	0	0	N/A
9160.0	p75	f	3d MI	0	0	N/A	0	0	N/A

Table A.2 Post-MI Ventricular Arrhythmias Under Isoflurane (7d post-MI)

				PRE-EPI (5min)			POST-EPI (5min)		
Animal	***Genotype***	***Gender***	***Surgery***	***# of PVCs***	***Vtach Episodes***	**Duration**	***# of PVCs***	***Vtach Episodes***	**Duration**
9131.0	C57Bl6	m	7d sham	0	0	N/A	0	0	N/A
9118.1	C57Bl6	m	7d sham	0	0	N/A	0	0	N/A
9153.0	C57Bl6	m	7d sham	0	0	N/A	0	0	N/A
9142.2	C57Bl6	f	7d sham	0	0	N/A	0	0	N/A
9161.0	C57Bl6	f	7d sham	0	0	N/A	0	0	N/A
9204.1	C57Bl6	f	7d sham	0	0	N/A	0	0	N/A
9118.0	C57Bl6	m	7d MI	2	0	N/A	8	2	1s, 2s
9161.1	C57Bl6	m	7d MI	0	0	N/A	0	0	N/A
9196.0	C57Bl6	m	7d MI	0	0	N/A	0	0	N/A
9120.0	C57Bl6	f	7d MI	0	0	N/A	0	0	N/A
9134.1	C57Bl6	f	7d MI	0	0	N/A	0	0	N/A
9196.1	C57Bl6	f	7d MI	0	0	N/A	0	0	N/A
9146.0	p75	m	7d sham	0	0	N/A	6	1	2s
9146.2	p75	m	7d sham	2	0	N/A	6	0	N/A
9204.2	p75	m	7d sham	0	0	N/A	0	0	N/A
9112.2	p75	f	7d sham	1	0	N/A	0	0	N/A
9154.0	p75	f	7d sham	1	0	N/A	0	0	N/A
9154.1	p75	f	7d sham	1	0	N/A	0	0	N/A
9141.1	p75	m	7d MI	0	0	N/A	0	0	N/A
9201.0	p75	m	7d MI	0	0	N/A	2	0	N/A
9204.0	p75	m	7d MI	0	0	N/A	4	0	N/A
9112.1	p75	f	7d MI	0	0	N/A	0	0	N/A
9142.1	p75	f	7d MI	0	0	N/A	5	0	N/A

Appendix B:

Left Ventricular Peak Systolic Pressure, dP/dt_{MAX} and dP/dt_{MIN}: Ventricular pressure was measured with a microtipped pressure transducer (1.0 French; Millar) which was calibrated daily with a manometer before use. Anesthesia was induced with 4% inhaled isoflurane. Mice were intubated, ventilated and anesthesia was maintained with 2-3% inhaled isoflurane. Body temperature was maintained at 37±0.2 ºC. The right carotid artery was isolated by blunt dissection and the microtipped pressure transducer was inserted into the right carotid artery for arterial pressure measurements, then advanced into the left ventricle. The left jugular vein was cannulated for intravenous (i.v.) access. Baseline parameters were monitored for 5 minutes. In order to block ganglionic transmission hexamethonium (5 mg/kg) was infused i.v. and a new baseline was measured. In order to assess β1-responsiveness of the heart, a maximal dose of the short-acting β1AR agonist dobutamine (32 µg/kg) was infused i.v. Because dobutamine has a half-life of about 2.5 minutes, at least 10 minutes were allowed to pass before the next drug infusion. Tyramine (200 µg/kg) was then infused i.v. to trigger non-exocytotic release of endogenous NE from sympathetic terminals. Left ventricular peak systolic pressure (LVPSP) was monitored using a PowerLab data acquisition system (AD Instruments). dP/dt_{MAX} and dP/dt_{MIN} were calculated using LabPro software (AD Instruments). All data were analyzed using a two-way ANOVA with a Bonferroni post-test to compare across genotypes and treatment groups.

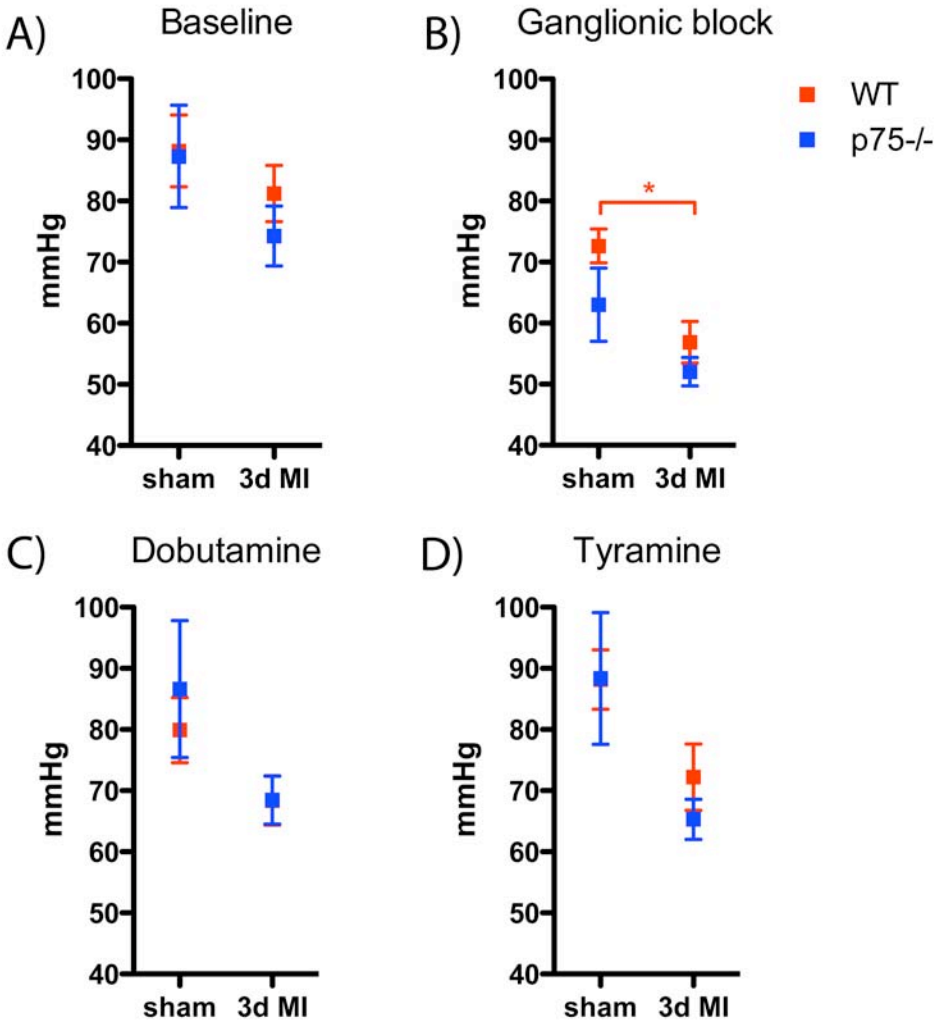

Figure B.1: Left ventricular peak systolic pressure (LVPSP) 3 days after ischemia-reperfusion from WT (red squares) and p75NTR-/- mice (blue squares). **A**) Baseline LVPSP taken from WT and p75NTR-/- mice 3 days after sham or ischemia-reperfusion surgery. **B**) LVPSP after ganglionic block induced by i.v. infusion of hexamethonium (5mg/ kg) from WT and p75NTR-/- mice 3 days after sham or ischemia-reperfusion surgery. **C**) LVPSP in response to the β_1-adrenergic receptor agonist dobutamine (32 μg/ kg) from WT and p75NTR-/- mice 3 days after sham or ischemia-reperfusion surgery. **D**) LVPSP in response to tyramine (200 μg/ kg) from WT and p75NTR-/- mice 3 days after sham or ischemia-reperfusion surgery. (Mean ± SEM, *p< 0.05, n=6).

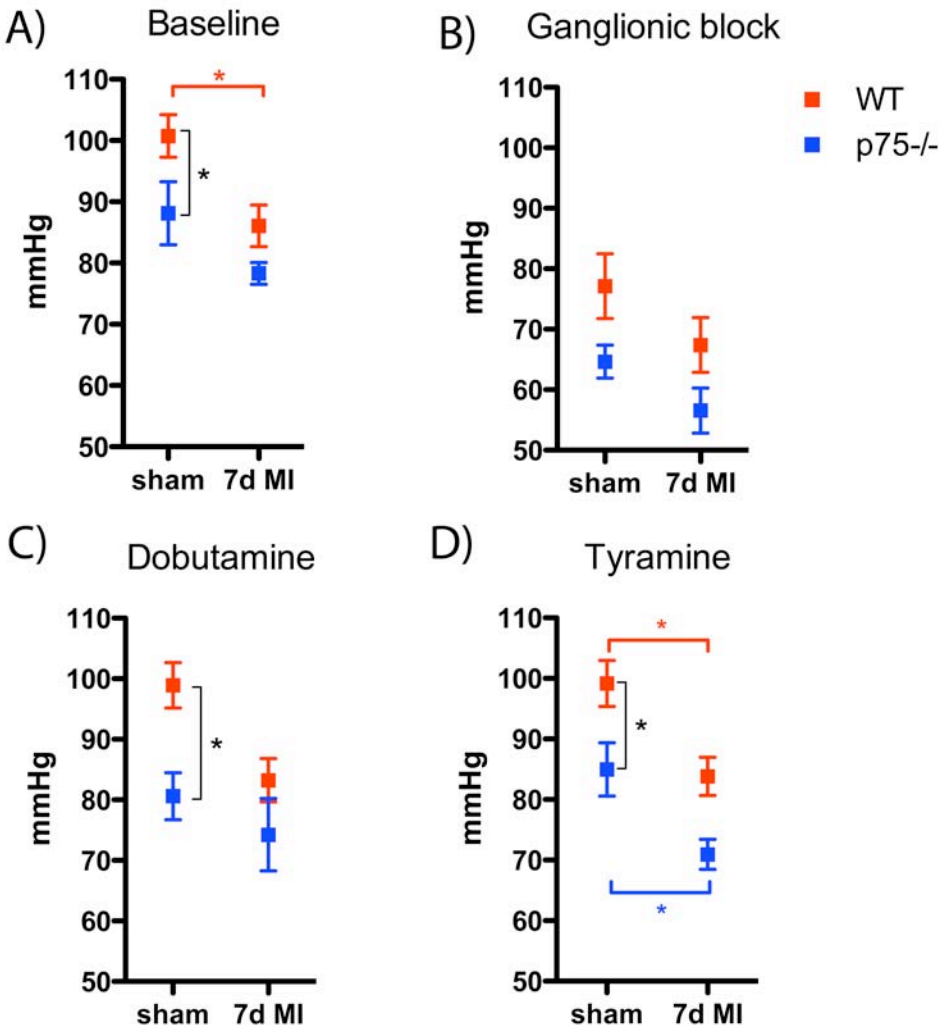

Figure B.2: Left ventricular peak systolic pressure (LVPSP) 7 days after ischemia-reperfusion from WT (red squares) and p75NTR-/- mice (blue squares). **A**) Baseline LVP taken from WT and p75NTR-/- mice 7 days after sham or ischemia-reperfusion surgery. **B**) LVPSP after ganglionic block induced by i.v. infusion of hexamethonium (5mg/ kg) from WT and p75NTR-/- mice 7 days after sham or ischemia-reperfusion surgery. **C**) LVPSP in response to the β_1-adrenergic receptor agonist dobutamine (32 μg/ kg) from WT and p75NTR-/- mice 7 days after sham or ischemia-reperfusion surgery. **D**) LVPSP in response to tyramine (200 μg/ kg) from WT and p75NTR-/- mice 7 days after sham or ischemia-reperfusion surgery. (Mean ± SEM, *p< 0.05, n=4-6).

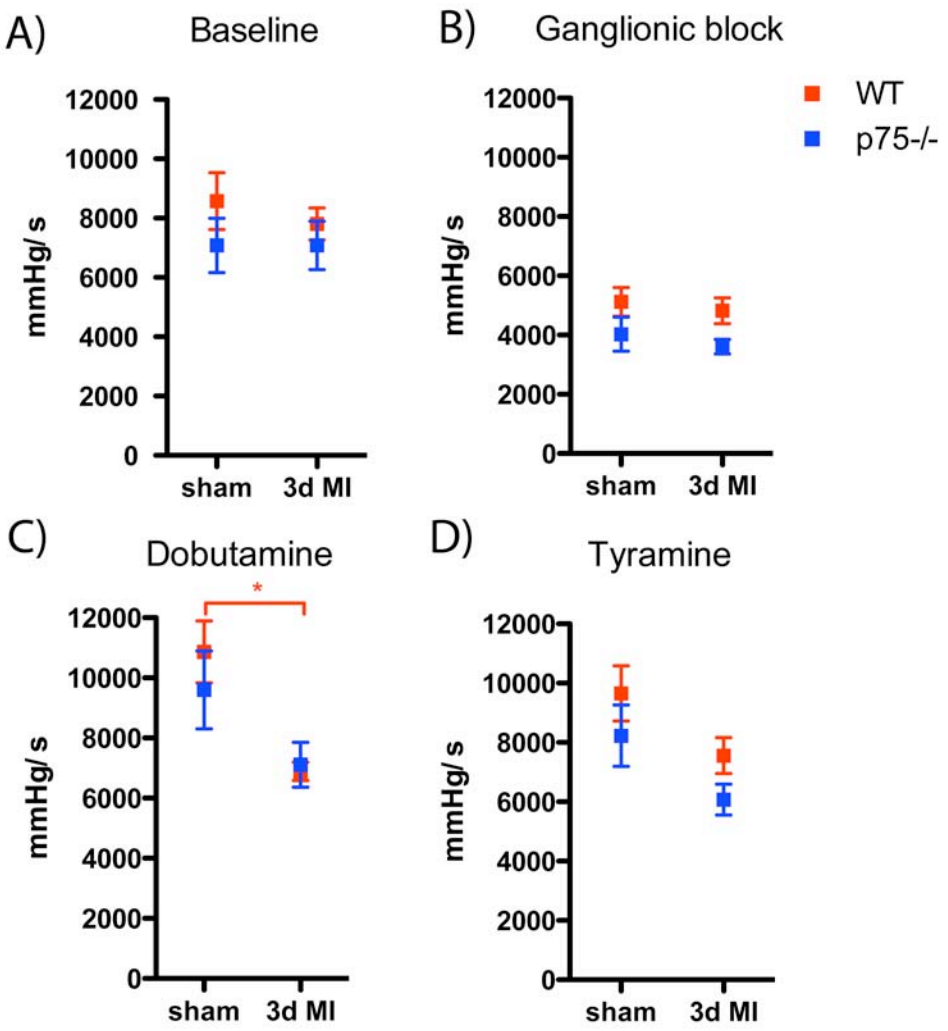

Figure B.3: dP/dt_{MAX} 3 days after ischemia-reperfusion from WT (red squares) and p75NTR-/- mice (blue squares). **A**) Baseline dP/dt_{MAX} taken from WT and p75NTR-/- mice 3 days after sham or ischemia-reperfusion surgery. **B**) dP/dt_{MAX} after ganglionic block induced by i.v. infusion of hexamethonium (5mg/ kg) from WT and p75NTR-/- mice 3 days after sham or ischemia-reperfusion surgery. **C**) dP/dt_{MAX} in response to the β_1- adrenergic receptor agonist dobutamine (32 μg/ kg) from WT and p75NTR-/- mice 3 days after sham or ischemia-reperfusion surgery. **D**) dP/dt_{MAX} in response to tyramine (200 μg/ kg) from WT and p75NTR-/- mice 3 days after sham or ischemia-reperfusion surgery. (Mean ± SEM, *p< 0.05, n=6).

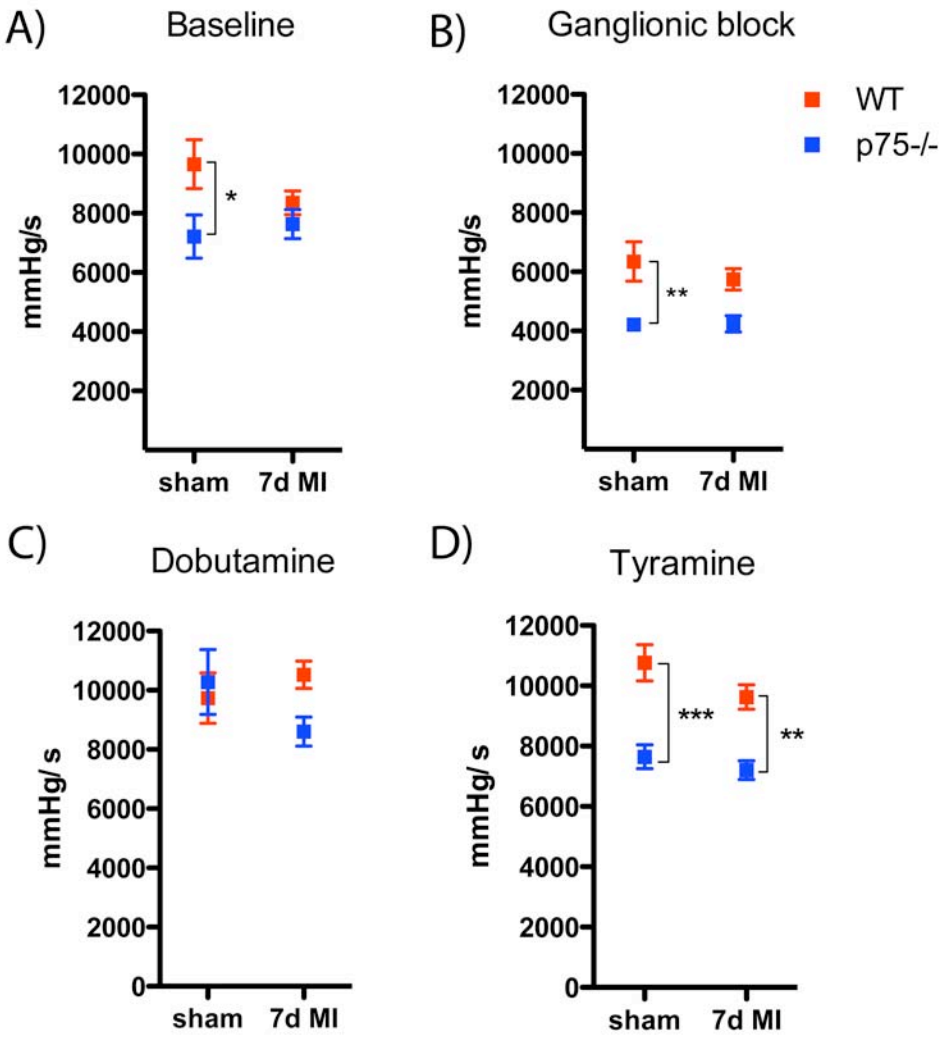

Figure B.4: dP/dt_{MAX} 7 days after ischemia-reperfusion from WT (red squares) and p75NTR-/- mice (blue squares). **A**) Baseline dP/dt_{MAX} taken from WT and p75NTR-/- mice 7 days after sham or ischemia-reperfusion surgery. **B**) dP/dt_{MAX} after ganglionic block induced by i.v. infusion of hexamethonium (5mg/ kg) from WT and p75NTR-/- mice 7 days after sham or ischemia-reperfusion surgery. **C**) dP/dt_{MAX} in response to the β_1- adrenergic receptor agonist dobutamine (32 μg/ kg) from WT and p75NTR-/- mice 7 days after sham or ischemia-reperfusion surgery. **D**) dP/dt_{MAX} in response to tyramine (200 μg/ kg) from WT and p75NTR-/- mice 7 days after sham or ischemia-reperfusion surgery. (Mean ± SEM, *p< 0.05, **p< 0.01, ***p< 0.001, n=4-6).

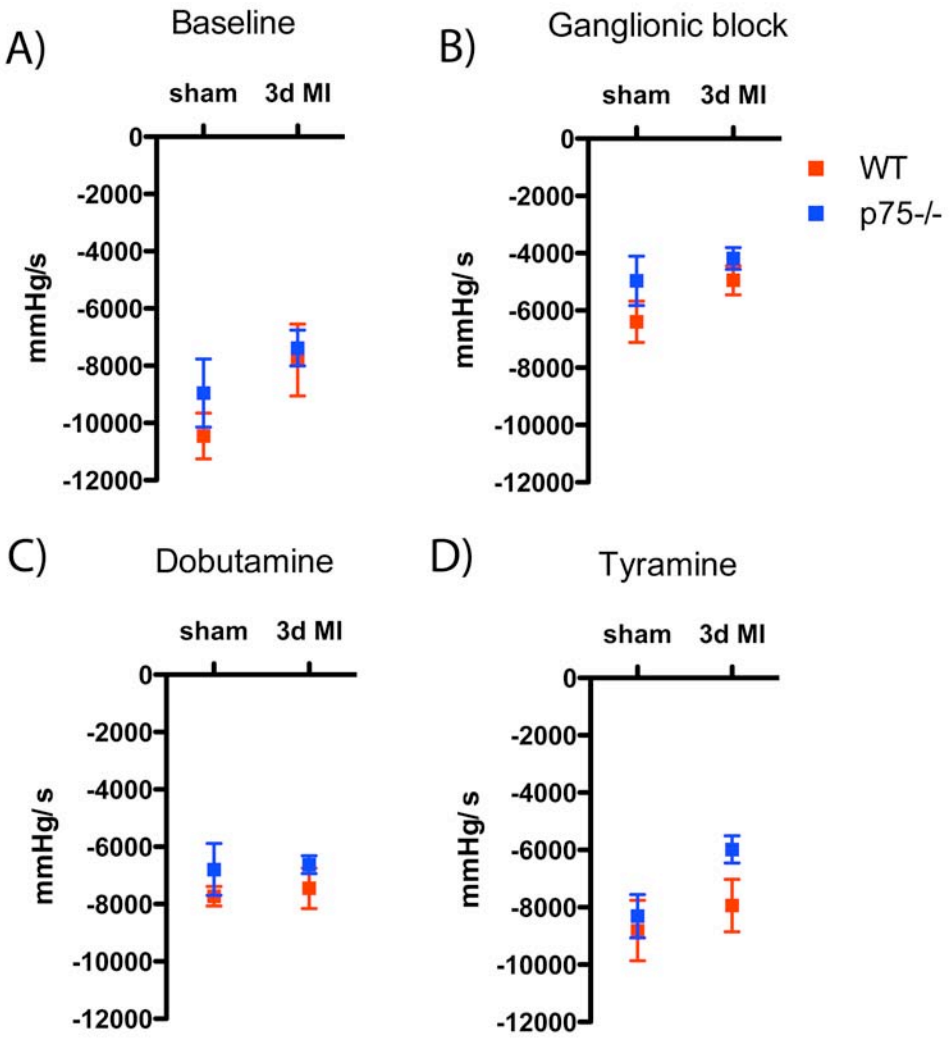

Figure B.5: dP/dt_{MIN} 3 days after ischemia-reperfusion from WT (red squares) and p75NTR-/- mice (blue squares). **A**) Baseline dP/dt_{MIN} taken from WT and p75NTR-/- mice 3 days after sham or ischemia-reperfusion surgery. **B**) dP/dt_{MIN} after ganglionic block induced by i.v. infusion of hexamethonium (5mg/ kg) from WT and p75NTR-/- mice 3 days after sham or ischemia-reperfusion surgery. **C**) dP/dt_{MIN} in response to the β_1- adrenergic receptor agonist dobutamine (32 μg/ kg) from WT and p75NTR-/- mice 3 days after sham or ischemia-reperfusion surgery. **D**) dP/dt_{MIN} in response to tyramine (200 μg/ kg) from WT and p75NTR-/- mice 3 days after sham or ischemia-reperfusion surgery. (Mean ± SEM, n=6).

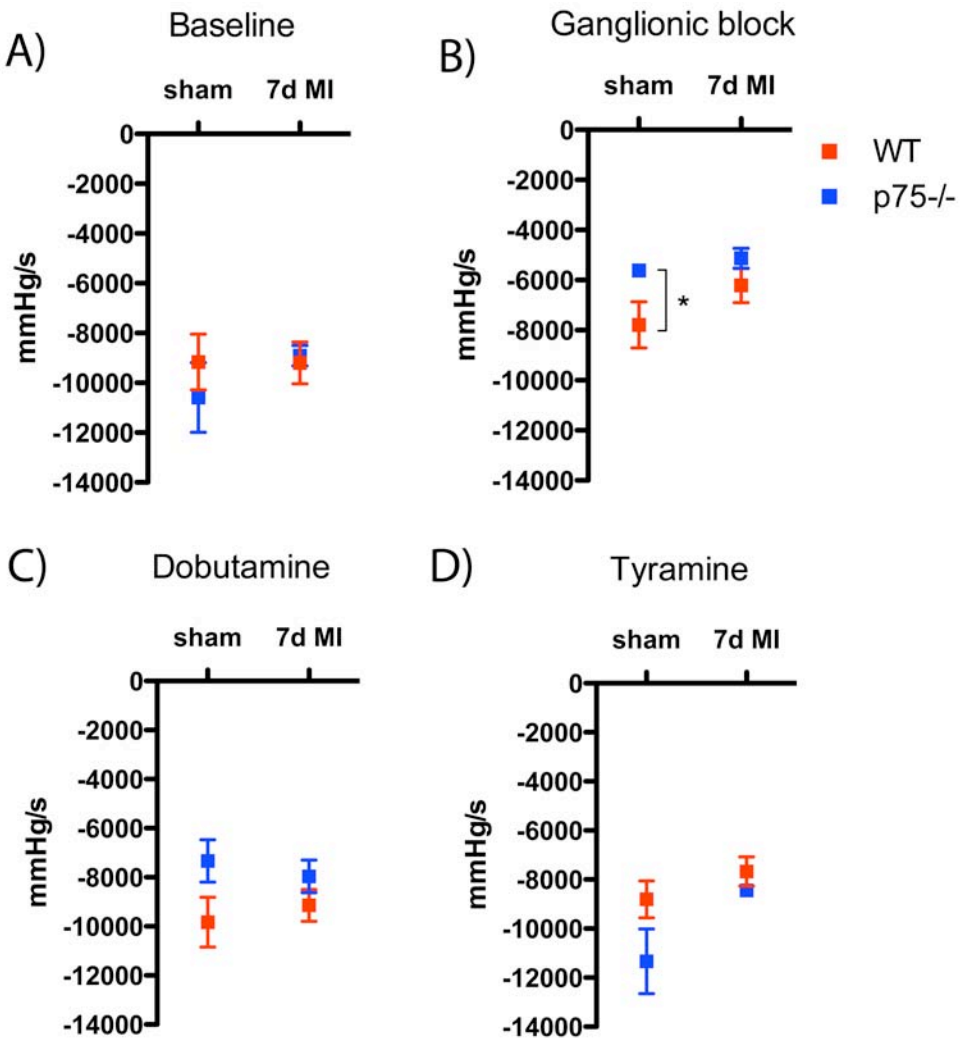

Figure B.6: dP/dt_{MIN} 7 days after ischemia-reperfusion from WT (red squares) and p75NTR-/- mice (blue squares). **A**) Baseline dP/dt_{MIN} taken from WT and p75NTR-/- mice 7 days after sham or ischemia-reperfusion surgery. **B**) dP/dt_{MIN} after ganglionic block induced by i.v. infusion of hexamethonium (5mg/ kg) from WT and p75NTR-/- mice 7 days after sham or ischemia-reperfusion surgery. **C**) dP/dt_{MIN} in response to the β_1- adrenergic receptor agonist dobutamine (32 μg/ kg) from WT and p75NTR-/- mice 7 days after sham or ischemia-reperfusion surgery. **D**) dP/dt_{MIN} in response to tyramine (200 μg/ kg) from WT and p75NTR-/- mice 7 days after sham or ischemia-reperfusion surgery. (Mean ± SEM, *p< 0.05, n=4-6).

Appendix C:

Dissection of Tissue for HPLC analysis: Following euthanasia, hearts were removed from the chest cavity of the mice and placed in saline. Any remaining blood in the heart was gently expelled with forceps. Hearts from sham and MI mice were dissected into four sections. First, the atria were removed. Next the base was separated from the ventricles at the point of ligation using a razor blade. The apex (bottom 1mm of tissue) was then removed and discarded. The LV was then dissected away from the RV, splitting the interventricular septum along the natural division of the muscle, which was identified visually. All dissected regions of the heart were immediately flash frozen and stored at -80°C until assayed.

HPLC: Norepinephrine was measured by high-performance liquid chromatography (HPLC) with electrochemical detection. Hearts were dissected as described above and frozen. The frozen hearts were pulverized using a ceramic mortar and pestle chilled on dry ice. The frozen tissue was weighed out in pre-weighed 1.5mL microcentrifuge tubes immediately followed by homogenization of the tissue in 250μL 0.1M perchloric acid containing 0.5μM of the internal standard, 3,4-Dihydroxybenzylamine (DHBA), to correct for sample recovery. The homogenates were centrifuged and the catechols were pre-purified by adsorption onto alumina as follows: 200μL of supernatant was neutralized with 1.0M Tris buffer, pH 8.6, and 15 mg acid-washed alumina was added. NE standards (0.25μM) were processed similarly. The alumina was

washed twice with mqH_2O and the catechols were desorbed with 100μL 0.1M perchloric acid. Fifty microliters of sample were injected onto the HPLC and the catecols were fractionated by reverse-phase HPLC on a C_{18} column (5μm, 4.5 mm x 15 cm) using a mobile phase that consisted of 75mM $NaH_2PO_4 \cdot H_2O$, 1.7mM sodium octane sulfonate, 0.01% triethylamine, and 3.0% acetonitrile, pH=3.0. A coulometric electrochemical detector was used (Coulochem III, ESA) with an electrode voltage set at 180mV, fullscale 200nA. Detection limits for NE were ~0.05 pmol with recoveries from the alumina extraction >60%. All data were analyzed using a two-way ANOVA with a Bonferroni post-test to compare across genotypes and treatment groups.

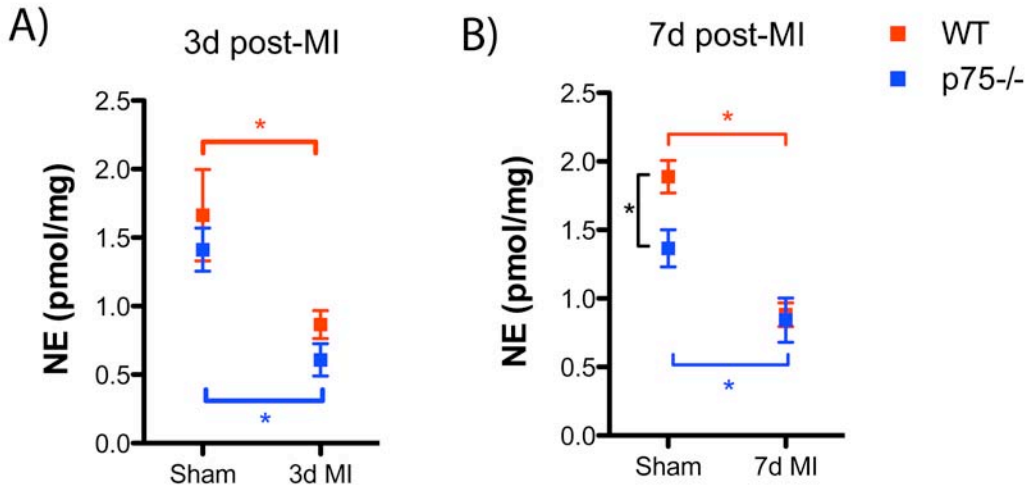

Figure C.1: Norepinephrine (NE) content in the left ventricle of WT (red squares) and p75NTR-/- mice (blue squares) 3 days **(A)** and 7 days **(B)** after sham or ischemia-reperfusion surgery, mean ± SEM, *p< 0.05, n=6.

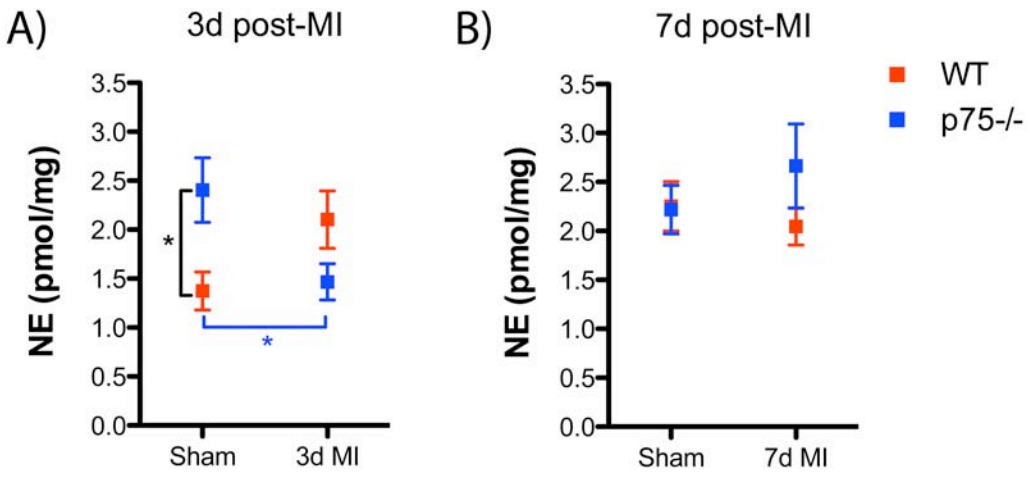

Figure C.2: Norepinephrine (NE) content in the right ventricle of WT (red squares) and p75NTR-/- mice (blue squares) 3 days **(A)** and 7 days **(B)** after sham or ischemia-reperfusion surgery, mean ± SEM, *p< 0.05, n=6.

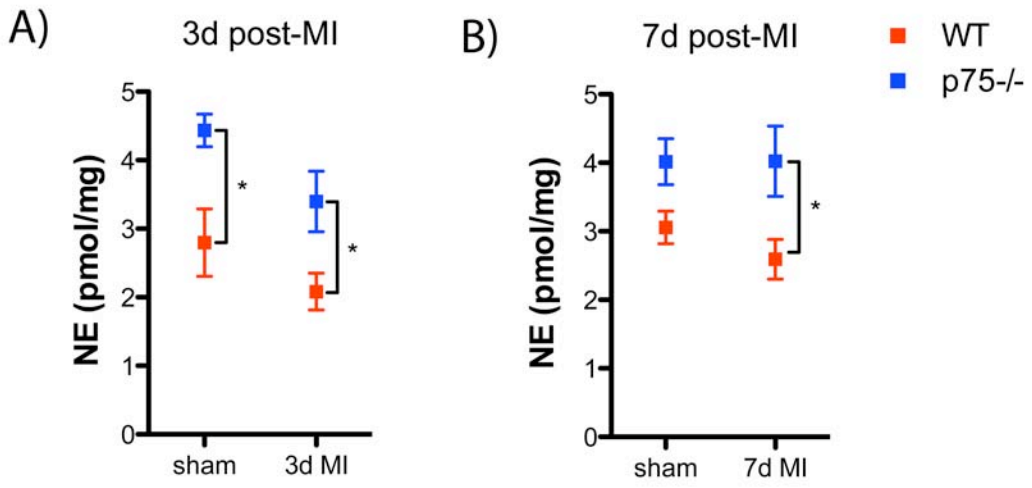

Figure C.3: Norepinephrine (NE) content in the base of WT (red squares) and p75NTR-/- mice (blue squares) 3 days **(A)** and 7 days **(B)** after sham or ischemia-reperfusion surgery, mean ± SEM, *p< 0.05, n=6.

References

AHA, 2009. American Heart Association. Heart Disease and Stroke Statistics-2009 Update. Vol., ed.^eds. Dallas, Texas: American Heart Association; 2009.

Aloyz, R.S., Bamji, S.X., Pozniak, C.D., Toma, J.G., Atwal, J., Kaplan, D.R., Miller, F.D., 1998. p53 is essential for developmental neuron death as regulated by the TrkA and p75 neurotrophin receptors. J Cell Biol. 143**,** 1691-703.

Angeletti, P.U., Levi-Montalcini, R., Caramia, F., 1971. Analysis of the effects of the antiserum to the nerve growth factor in adult mice. Brain Res. 27**,** 343-55.

Antzelevitch, C., Sicouri, S., Litovsky, S.H., Lukas, A., Krishnan, S.C., Di Diego, J.M., Gintant, G.A., Liu, D.W., 1991. Heterogeneity within the ventricular wall. Electrophysiology and pharmacology of epicardial, endocardial, and M cells. Circ Res. 69**,** 1427-49.

Aronow, W.S., Ahn, C., Mercando, A.D., Epstein, S., 1994. Circadian variation of sudden cardiac death or fatal myocardial infarction is abolished by propranolol in patients with heart disease and complex ventricular arrhythmias. Am J Cardiol. 74**,** 819-21.

Atwal, J.K., Massie, B., Miller, F.D., Kaplan, D.R., 2000. The TrkB-Shc site signals neuronal survival and local axon growth via MEK and P13-kinase. Neuron. 27**,** 265-77.

Backs, J., Haunstetter, A., Gerber, S.H., Metz, J., Borst, M.M., Strasser, R.H., Kubler, W., Haass, M., 2001. The neuronal norepinephrine transporter in experimental heart failure: evidence for a posttranscriptional downregulation. J Mol Cell Cardiol. 33**,** 461-72.

Bamji, S.X., Majdan, M., Pozniak, C.D., Belliveau, D.J., Aloyz, R., Kohn, J., Causing, C.G., Miller, F.D., 1998. The p75 neurotrophin receptor mediates neuronal apoptosis and is essential for naturally occurring sympathetic neuron death. J Cell Biol. 140**,** 911-23.

Bandtlow, C., Dechant, G., 2004. From cell death to neuronal regeneration, effects of the p75 neurotrophin receptor depend on interactions with partner subunits. Sci STKE. 2004**,** pe24.

Barber, M.J., Mueller, T.M., Henry, D.P., Felten, S.Y., Zipes, D.P., 1983. Transmural myocardial infarction in the dog produces sympathectomy in noninfarcted myocardium. Circulation. 67**,** 787-96.

Barde, Y.A., Edgar, D., Thoenen, H., 1982. Purification of a new neurotrophic factor from mammalian brain. EMBO J. 1**,** 549-53.

Belliveau, D.J., Krivko, I., Kohn, J., Lachance, C., Pozniak, C., Rusakov, D., Kaplan, D., Miller, F.D., 1997. NGF and neurotrophin-3 both activate TrkA on sympathetic neurons but differentially regulate survival and neuritogenesis. J Cell Biol. 136**,** 375-88.

Ben-Zvi, A., Ben-Gigi, L., Klein, H., Behar, O., 2007. Modulation of semaphorin3A activity by p75 neurotrophin receptor influences peripheral axon patterning. J Neurosci. 27**,** 13000-11.

Benedetti, M., Levi, A., Chao, M.V., 1993. Differential expression of nerve growth factor receptors leads to altered binding affinity and neurotrophin responsiveness. Proc Natl Acad Sci U S A. 90**,** 7859-63.

Berkemeier, L.R., Winslow, J.W., Kaplan, D.R., Nikolics, K., Goeddel, D.V., Rosenthal, A., 1991. Neurotrophin-5: a novel neurotrophic factor that activates trk and trkB. Neuron. 7**,** 857-66.

Bibel, M., Hoppe, E., Barde, Y.A., 1999. Biochemical and functional interactions between the neurotrophin receptors trk and p75NTR. EMBO J. 18**,** 616-22.

Bierl, M.A., Jones, E.E., Crutcher, K.A., Isaacson, L.G., 2005. 'Mature' nerve growth factor is a minor species in most peripheral tissues. Neurosci Lett. 380**,** 133-7.

Bjerre, B., Bjorklund, A., Mobley, W., Rosengren, E., 1975a. Short- and long-term effects of nerve growth factor on the sympathetic nervous system in the adult mouse. Brain Res. 94**,** 263-77.

Bjerre, B., Wiklund, L., Edwards, D.C., 1975b. A study of the de- and regenerative changes in the sympathetic nervous system of the adult mouse after treatment with the antiserum to nerve growth factor. Brain Res. 92**,** 257-78.

Blochl, A., Blochl, R., 2007. A cell-biological model of p75NTR signaling. J Neurochem. 102**,** 289-305.

Bonni, A., Ginty, D.D., Dudek, H., Greenberg, M.E., 1995. Serine 133-phosphorylated CREB induces transcription via a cooperative mechanism

that may confer specificity to neurotrophin signals. Mol Cell Neurosci. 6**,** 168-83.

Boudoulas, H., Karayannacos, P.E., Lewis, R.P., Leier, C.V., Vasko, J.S., 1982. Effect of afterload on left ventricular performance in experimental animals. Comparison of the pre-ejection period and other indices of left ventricular contractility. J Med. 13**,** 373-85.

Brann, A.B., Tcherpakov, M., Williams, I.M., Futerman, A.H., Fainzilber, M., 2002. Nerve growth factor-induced p75-mediated death of cultured hippocampal neurons is age-dependent and transduced through ceramide generated by neutral sphingomyelinase. J Biol Chem. 277**,** 9812-8.

Brennan, C., Rivas-Plata, K., Landis, S.C., 1999. The p75 neurotrophin receptor influences NT-3 responsiveness of sympathetic neurons in vivo. Nat Neurosci. 2**,** 699-705.

Bristow, M.R., Ginsburg, R., Umans, V., Fowler, M., Minobe, W., Rasmussen, R., Zera, P., Menlove, R., Shah, P., Jamieson, S., et al., 1986. Beta 1- and beta 2-adrenergic-receptor subpopulations in nonfailing and failing human ventricular myocardium: coupling of both receptor subtypes to muscle contraction and selective beta 1-receptor down-regulation in heart failure. Circ Res. 59**,** 297-309.

Bristow, M.R., Sandoval, A.B., Gilbert, E.M., Deisher, T., Minobe, W., Rasmussen, R., 1988. Myocardial alpha- and beta-adrenergic receptors in heart failure: is cardiac-derived norepinephrine the regulatory signal? Eur Heart J. 9 Suppl H**,** 35-40.

Bristow, M.R., 1997. Mechanism of action of beta-blocking agents in heart failure. Am J Cardiol. 80**,** 26L-40L.

Brunet, A., Bonni, A., Zigmond, M.J., Lin, M.Z., Juo, P., Hu, L.S., Anderson, M.J., Arden, K.C., Blenis, J., Greenberg, M.E., 1999. Akt promotes cell survival by phosphorylating and inhibiting a Forkhead transcription factor. Cell. 96**,** 857-68.

Brunet, S., Aimond, F., Li, H., Guo, W., Eldstrom, J., Fedida, D., Yamada, K.A., Nerbonne, J.M., 2004. Heterogeneous expression of repolarizing, voltage-gated K+ currents in adult mouse ventricles. J Physiol. 559**,** 103-20.

Bueker, E.D., 1948. Implantation of tumors in the hind limb field of the embryonic chick and the developmental response of the lumbosacral nervous system. Anat Rec. 102**,** 369-89.

Bullard, T.A., Protack, T.L., Aguilar, F., Bagwe, S., Massey, H.T., Blaxall, B.C., 2008. Identification of Nogo as a novel indicator of heart failure. Physiol Genomics. 32**,** 182-9.

Campenot, R.B., 1977. Local control of neurite development by nerve growth factor. Proc Natl Acad Sci U S A. 74**,** 4516-9.

Campenot, R.B., 1994. NGF and the local control of nerve terminal growth. J Neurobiol. 25**,** 599-611.

Cane, K.N., Anderson, C.R., 2009. Generating diversity: Mechanisms regulating the differentiation of autonomic neuron phenotypes. Auton Neurosci. 151**,** 17-29.

Cao, J.M., Chen, L.S., KenKnight, B.H., Ohara, T., Lee, M.H., Tsai, J., Lai, W.W., Karagueuzian, H.S., Wolf, P.L., Fishbein, M.C., Chen, P.S., 2000a. Nerve sprouting and sudden cardiac death. Circ Res. 86**,** 816-21.

Cao, J.M., Fishbein, M.C., Han, J.B., Lai, W.W., Lai, A.C., Wu, T.J., Czer, L., Wolf, P.L., Denton, T.A., Shintaku, I.P., Chen, P.S., Chen, L.S., 2000b. Relationship between regional cardiac hyperinnervation and ventricular arrhythmia. Circulation. 101**,** 1960-9.

Caporali, A., Pani, E., Horrevoets, A.J., Kraenkel, N., Oikawa, A., Sala-Newby, G.B., Meloni, M., Cristofaro, B., Graiani, G., Leroyer, A.S., Boulanger, C.M., Spinetti, G., Yoon, S.O., Madeddu, P., Emanueli, C., 2008. Neurotrophin p75 receptor (p75NTR) promotes endothelial cell apoptosis and inhibits angiogenesis: implications for diabetes-induced impaired neovascularization in ischemic limb muscles. Circ Res. 103**,** e15-26.

Caporali, A., Emanueli, C., 2009. Cardiovascular actions of neurotrophins. Physiol Rev. 89**,** 279-308.

Chao, M.V., Hempstead, B.L., 1995. p75 and Trk: a two-receptor system. Trends Neurosci. 18**,** 321-6.

Chao, M.V., 2003. Neurotrophins and their receptors: a convergence point for many signalling pathways. Nat Rev Neurosci. 4**,** 299-309.

Chun, L.L., Patterson, P.H., 1977. Role of nerve growth factor in the development of rat sympathetic neurons in vitro. I. Survival, growth, and differentiation of catecholamine production. J Cell Biol. 75**,** 694-704.

Cohen, S., Levi-Montalcini, R., Hamburger, V., 1954. A Nerve Growth-Stimulating Factor Isolated from Sarcom as 37 and 180. Proc Natl Acad Sci U S A. 40**,** 1014-8.

Cohen, S., Levi-Montalcini, R., 1956. A Nerve Growth-Stimulating Factor Isolated from Snake Venom. Proc Natl Acad Sci U S A. 42**,** 571-4.

Cohen, S., 1960. Purification of a Nerve-Growth Promoting Protein from the Mouse Salivary Gland and Its Neuro-Cytotoxic Antiserum. Proc Natl Acad Sci U S A. 46**,** 302-11.

Costantini, C., Weindruch, R., Della Valle, G., Puglielli, L., 2005a. A TrkA-to-p75NTR molecular switch activates amyloid beta-peptide generation during aging. Biochem J. 391**,** 59-67.

Costantini, C., Scrable, H., Puglielli, L., 2006. An aging pathway controls the TrkA to p75NTR receptor switch and amyloid beta-peptide generation. EMBO J. 25**,** 1997-2006.

Costantini, D.L., Arruda, E.P., Agarwal, P., Kim, K.H., Zhu, Y., Zhu, W., Lebel, M., Cheng, C.W., Park, C.Y., Pierce, S.A., Guerchicoff, A., Pollevick, G.D., Chan, T.Y., Kabir, M.G., Cheng, S.H., Husain, M., Antzelevitch, C., Srivastava, D., Gross, G.J., Hui, C.C., Backx, P.H., Bruneau, B.G., 2005b. The homeodomain transcription factor Irx5 establishes the mouse cardiac ventricular repolarization gradient. Cell. 123**,** 347-58.

Crick, S.J., Wharton, J., Sheppard, M.N., Royston, D., Yacoub, M.H., Anderson, R.H., Polak, J.M., 1994. Innervation of the human cardiac conduction

system. A quantitative immunohistochemical and histochemical study. Circulation. 89**,** 1697-708.

Crowley, C., Spencer, S.D., Nishimura, M.C., Chen, K.S., Pitts-Meek, S., Armanini, M.P., Ling, L.H., McMahon, S.B., Shelton, D.L., Levinson, A.D., et al., 1994. Mice lacking nerve growth factor display perinatal loss of sensory and sympathetic neurons yet develop basal forebrain cholinergic neurons. Cell. 76**,** 1001-11.

Cunningham, M.E., Greene, L.A., 1998. A function-structure model for NGF-activated TRK. EMBO J. 17**,** 7282-93.

Daniels, R.H., Hall, P.S., Bokoch, G.M., 1998. Membrane targeting of p21-activated kinase 1 (PAK1) induces neurite outgrowth from PC12 cells. EMBO J. 17**,** 754-64.

Datta, S.R., Dudek, H., Tao, X., Masters, S., Fu, H., Gotoh, Y., Greenberg, M.E., 1997. Akt phosphorylation of BAD couples survival signals to the cell-intrinsic death machinery. Cell. 91**,** 231-41.

Davies, A.M., 1994. Neurotrophic factors. Switching neurotrophin dependence. Curr Biol. 4**,** 273-6.

Davies, A.M., Minichiello, L., Klein, R., 1995. Developmental changes in NT3 signalling via TrkA and TrkB in embryonic neurons. EMBO J. 14**,** 4482-9.

de Chaves, E.P., Bussiere, M., MacInnis, B., Vance, D.E., Campenot, R.B., Vance, J.E., 2001. Ceramide inhibits axonal growth and nerve growth factor uptake without compromising the viability of sympathetic neurons. J Biol Chem. 276**,** 36207-14.

Delcroix, J.D., Valletta, J.S., Wu, C., Hunt, S.J., Kowal, A.S., Mobley, W.C., 2003. NGF signaling in sensory neurons: evidence that early endosomes carry NGF retrograde signals. Neuron. 39**,** 69-84.

Dhanoa, N.K., Krol, K.M., Jahed, A., Crutcher, K.A., Kawaja, M.D., 2006. Null mutations for exon III and exon IV of the p75 neurotrophin receptor gene enhance sympathetic sprouting in response to elevated levels of nerve growth factor in transgenic mice. Exp Neurol. 198**,** 416-26.

Dobaczewski, M., Gonzalez-Quesada, C., Frangogiannis, N.G., 2010. The extracellular matrix as a modulator of the inflammatory and reparative response following myocardial infarction. J Mol Cell Cardiol. 48**,** 504-11.

Dobaczewski, M., Bujak, M., Zymek, P., Ren, G., Entman, M.L., Frangogiannis, N.G., 2006. Extracellular matrix remodeling in canine and mouse myocardial infarcts. Cell Tissue Res. 324**,** 475-88.

Dobrowsky, R.T., Werner, M.H., Castellino, A.M., Chao, M.V., Hannun, Y.A., 1994. Activation of the sphingomyelin cycle through the low-affinity neurotrophin receptor. Science. 265**,** 1596-9.

Dobrowsky, R.T., Jenkins, G.M., Hannun, Y.A., 1995. Neurotrophins induce sphingomyelin hydrolysis. Modulation by co-expression of p75NTR with Trk receptors. J Biol Chem. 270**,** 22135-42.

Dobrowsky, R.T., Carter, B.D., 1998. Coupling of the p75 neurotrophin receptor to sphingolipid signaling. Ann N Y Acad Sci. 845**,** 32-45.

Dorian, P., 2005. Antiarrhythmic action of beta-blockers: potential mechanisms. J Cardiovasc Pharmacol Ther. 10 Suppl 1**,** S15-22.

Du, X.J., Cox, H.S., Dart, A.M., Esler, M.D., 1999. Sympathetic activation triggers ventricular arrhythmias in rat heart with chronic infarction and failure. Cardiovasc Res. 43**,** 919-29.

Ernfors, P., Lee, K.F., Jaenisch, R., 1994. Mice lacking brain-derived neurotrophic factor develop with sensory deficits. Nature. 368**,** 147-50.

Esposito, D., Patel, P., Stephens, R.M., Perez, P., Chao, M.V., Kaplan, D.R., Hempstead, B.L., 2001. The cytoplasmic and transmembrane domains of the p75 and Trk A receptors regulate high affinity binding to nerve growth factor. J Biol Chem. 276**,** 32687-95.

Estrach, S., Schmidt, S., Diriong, S., Penna, A., Blangy, A., Fort, P., Debant, A., 2002. The Human Rho-GEF trio and its target GTPase RhoG are involved in the NGF pathway, leading to neurite outgrowth. Curr Biol. 12**,** 307-12.

Fagan, A.M., Zhang, H., Landis, S., Smeyne, R.J., Silos-Santiago, I., Barbacid, M., 1996. TrkA, but not TrkC, receptors are essential for survival of sympathetic neurons in vivo. J Neurosci. 16**,** 6208-18.

Foreman, R.D., 1999. Mechanisms of cardiac pain. Annu Rev Physiol. 61**,** 143-67.

Frade, J.M., Rodriguez-Tebar, A., Barde, Y.A., 1996. Induction of cell death by endogenous nerve growth factor through its p75 receptor. Nature. 383**,** 166-8.

Francis, N., Farinas, I., Brennan, C., Rivas-Plata, K., Backus, C., Reichardt, L., Landis, S., 1999. NT-3, like NGF, is required for survival of sympathetic neurons, but not their precursors. Dev Biol. 210**,** 411-27.

Frangogiannis, N.G., 2006. Targeting the inflammatory response in healing myocardial infarcts. Curr Med Chem. 13**,** 1877-93.

Gau, Y.T., Liou, Y.J., Yu, Y.W., Chen, T.J., Lin, M.W., Tsai, S.J., Hong, C.J., 2008. Evidence for association between genetic variants of p75 neurotrophin receptor (p75NTR) gene and antidepressant treatment response in Chinese major depressive disorder. Am J Med Genet B Neuropsychiatr Genet. 147B**,** 594-9.

Geetha, T., Kenchappa, R.S., Wooten, M.W., Carter, B.D., 2005. TRAF6-mediated ubiquitination regulates nuclear translocation of NRIF, the p75 receptor interactor. EMBO J. 24**,** 3859-68.

Ghuran, A., Reid, F., La Rovere, M.T., Schmidt, G., Bigger, J.T., Jr., Camm, A.J., Schwartz, P.J., Malik, M., 2002. Heart rate turbulence-based predictors of fatal and nonfatal cardiac arrest (The Autonomic Tone and Reflexes After Myocardial Infarction substudy). Am J Cardiol. 89**,** 184-90.

Ginty, D.D., Bonni, A., Greenberg, M.E., 1994. Nerve growth factor activates a Ras-dependent protein kinase that stimulates c-fos transcription via phosphorylation of CREB. Cell. 77**,** 713-25.

Glebova, N.O., Ginty, D.D., 2004. Heterogeneous requirement of NGF for sympathetic target innervation in vivo. J Neurosci. 24**,** 743-51.

Glebova, N.O., Ginty, D.D., 2005. Growth and survival signals controlling sympathetic nervous system development. Annu Rev Neurosci. 28**,** 191-222.

Goodman, L.S., Hardman, J.G., Limbird, L.E., Gilman, A.G., 2001. Goodman & Gilman's the pharmacological basis of therapeutics, Vol., McGraw-Hill, New York.

Goridis, C., Rohrer, H., 2002. Specification of catecholaminergic and serotonergic neurons. Nat Rev Neurosci. 3**,** 531-41.

Graham, L.N., Smith, P.A., Stoker, J.B., Mackintosh, A.F., Mary, D.A., 2002. Time course of sympathetic neural hyperactivity after uncomplicated acute myocardial infarction. Circulation. 106**,** 793-7.

Graham, L.N., Smith, P.A., Huggett, R.J., Stoker, J.B., Mackintosh, A.F., Mary, D.A., 2004a. Sympathetic drive in anterior and inferior uncomplicated acute myocardial infarction. Circulation. 109**,** 2285-9.

Graham, L.N., Smith, P.A., Stoker, J.B., Mackintosh, A.F., Mary, D.A., 2004b. Sympathetic neural hyperactivity and its normalization following unstable angina and acute myocardial infarction. Clin Sci (Lond). 106**,** 605-11.

Grimes, M.L., Zhou, J., Beattie, E.C., Yuen, E.C., Hall, D.E., Valletta, J.S., Topp, K.S., LaVail, J.H., Bunnett, N.W., Mobley, W.C., 1996. Endocytosis of activated TrkA: evidence that nerve growth factor induces formation of signaling endosomes. J Neurosci. 16**,** 7950-64.

Habecker, B.A., Bilimoria, P., Linick, C., Gritman, K., Lorentz, C.U., Woodward, W., Birren, S.J., 2008. Regulation of cardiac innervation and function via the p75 neurotrophin receptor. Auton Neurosci. 140**,** 40-8.

Hallbook, F., Ibanez, C.F., Persson, H., 1991. Evolutionary studies of the nerve growth factor family reveal a novel member abundantly expressed in Xenopus ovary. Neuron. 6**,** 845-58.

Hamburger, V., Levi-Montalcini, R., 1949. Proliferation, differentiation and degeneration in the spinal ganglia of the chick embryo under normal and experimental conditions. J Exp Zool. 111**,** 457-501.

Hannila, S.S., Kawaja, M.D., 1999. Nerve growth factor-induced growth of sympathetic axons into the optic tract of mature mice is enhanced by an absence of p75NTR expression. J Neurobiol. 39**,** 51-66.

Hannila, S.S., Lawrance, G.M., Ross, G.M., Kawaja, M.D., 2004. TrkA and mitogen-activated protein kinase phosphorylation are enhanced in sympathetic neurons lacking functional p75 neurotrophin receptor expression. Eur J Neurosci. 19**,** 2903-8.

Hannila, S.S., Kawaja, M.D., 2005. Nerve growth factor-mediated collateral sprouting of central sensory axons into deafferentated regions of the dorsal horn is enhanced in the absence of the p75 neurotrophin receptor. J Comp Neurol. 486**,** 331-43.

Hasan, W., Jama, A., Donohue, T., Wernli, G., Onyszchuk, G., Al-Hafez, B., Bilgen, M., Smith, P.G., 2006. Sympathetic hyperinnervation and inflammatory cell NGF synthesis following myocardial infarction in rats. Brain Res. 1124**,** 142-54.

Haverkamp, W., Hindricks, G., Gulker, H., 1990. Antiarrhythmic properties of beta-blockers. J Cardiovasc Pharmacol. 16 Suppl 5**,** S29-32.

He, Z., Tessier-Lavigne, M., 1997. Neuropilin is a receptor for the axonal chemorepellent Semaphorin III. Cell. 90**,** 739-51.

Heerssen, H.M., Pazyra, M.F., Segal, R.A., 2004. Dynein motors transport activated Trks to promote survival of target-dependent neurons. Nat Neurosci. 7**,** 596-604.

Hempstead, B.L., Martin-Zanca, D., Kaplan, D.R., Parada, L.F., Chao, M.V., 1991. High-affinity NGF binding requires coexpression of the trk proto-oncogene and the low-affinity NGF receptor. Nature. 350**,** 678-83.

Hempstead, B.L., 2002. The many faces of p75NTR. Curr Opin Neurobiol. 12**,** 260-7.

Hendry, I.A., Stockel, K., Thoenen, H., Iversen, L.L., 1974. The retrograde axonal transport of nerve growth factor. Brain Res. 68**,** 103-21.

Henning, R.J., Sawmiller, D.R., 2001. Vasoactive intestinal peptide: cardiovascular effects. Cardiovasc Res. 49**,** 27-37.

Hiltunen, J.O., Laurikainen, A., Vakeva, A., Meri, S., Saarma, M., 2001. Nerve growth factor and brain-derived neurotrophic factor mRNAs are regulated in distinct cell populations of rat heart after ischaemia and reperfusion. J Pathol. 194**,** 247-53.

Hoard, J.L., Hoover, D.B., Mabe, A.M., Blakely, R.D., Feng, N., Paolocci, N., 2008. Cholinergic neurons of mouse intrinsic cardiac ganglia contain noradrenergic enzymes, norepinephrine transporters, and the neurotrophin receptors tropomyosin-related kinase A and p75. Neuroscience. 156**,** 129-42.

Hohn, A., Leibrock, J., Bailey, K., Barde, Y.A., 1990. Identification and characterization of a novel member of the nerve growth factor/brain-derived neurotrophic factor family. Nature. 344**,** 339-41.

Honma, Y., Araki, T., Gianino, S., Bruce, A., Heuckeroth, R., Johnson, E., Milbrandt, J., 2002. Artemin is a vascular-derived neurotropic factor for developing sympathetic neurons. Neuron. 35**,** 267-82.

Howard, M.J., 2005. Mechanisms and perspectives on differentiation of autonomic neurons. Dev Biol. 277**,** 271-86.

Huber, A.B., Weinmann, O., Brosamle, C., Oertle, T., Schwab, M.E., 2002. Patterns of Nogo mRNA and protein expression in the developing and adult rat and after CNS lesions. J Neurosci. 22**,** 3553-67.

Ibanez, C.F., 2007. Message in a bottle: long-range retrograde signaling in the nervous system. Trends Cell Biol. 17**,** 519-28.

Ieda, M., Fukuda, K., Hisaka, Y., Kimura, K., Kawaguchi, H., Fujita, J., Shimoda, K., Takeshita, E., Okano, H., Kurihara, Y., Kurihara, H., Ishida, J., Fukamizu, A., Federoff, H.J., Ogawa, S., 2004. Endothelin-1 regulates cardiac sympathetic innervation in the rodent heart by controlling nerve growth factor expression. J Clin Invest. 113**,** 876-84.

Ieda, M., Kanazawa, H., Ieda, Y., Kimura, K., Matsumura, K., Tomita, Y., Yagi, T., Onizuka, T., Shimoji, K., Ogawa, S., Makino, S., Sano, M., Fukuda, K., 2006. Nerve growth factor is critical for cardiac sensory innervation and rescues neuropathy in diabetic hearts. Circulation. 114**,** 2351-63.

Ieda, M., Kanazawa, H., Kimura, K., Hattori, F., Ieda, Y., Taniguchi, M., Lee, J.K., Matsumura, K., Tomita, Y., Miyoshi, S., Shimoda, K., Makino, S., Sano, M., Kodama, I., Ogawa, S., Fukuda, K., 2007. Sema3a maintains normal heart rhythm through sympathetic innervation patterning. Nat Med. 13**,** 604-12.

Inoue, H., Zipes, D.P., 1987. Results of sympathetic denervation in the canine heart: supersensitivity that may be arrhythmogenic. Circulation. 75**,** 877-87.

Inoue, H., Zipes, D.P., 1988. Time course of denervation of efferent sympathetic and vagal nerves after occlusion of the coronary artery in the canine heart. Circ Res. 62**,** 1111-20.

Jahed, A., Kawaja, M.D., 2005. The influences of p75 neurotrophin receptor and brain-derived neurotrophic factor in the sympathetic innervation of target tissues during murine postnatal development. Auton Neurosci. 118**,** 32-42.

Janes, R.D., Brandys, J.C., Hopkins, D.A., Johnstone, D.E., Murphy, D.A., Armour, J.A., 1986a. Anatomy of human extrinsic cardiac nerves and ganglia. Am J Cardiol. 57**,** 299-309.

Janes, R.D., Johnstone, D.E., Brandys, J.C., Armour, J.A., 1986b. Functional and anatomical variability of canine cardiac sympathetic efferent pathways: implications for regional denervation of the left ventricle. Can J Physiol Pharmacol. 64**,** 958-69.

Jiang, H., Lu, Z., Yu, Y., Zhao, D., Yang, B., Huang, C., 2007. Relationship between sympathetic nerve sprouting and repolarization dispersion at peri-infarct zone after myocardial infarction. Auton Neurosci. 134**,** 18-25.

Jing, S., Tapley, P., Barbacid, M., 1992. Nerve growth factor mediates signal transduction through trk homodimer receptors. Neuron. 9**,** 1067-79.

Johnson, D., Lanahan, A., Buck, C.R., Sehgal, A., Morgan, C., Mercer, E., Bothwell, M., Chao, M., 1986. Expression and structure of the human NGF receptor. Cell. 47**,** 545-54.

Jouven, X., Empana, J.P., Schwartz, P.J., Desnos, M., Courbon, D., Ducimetiere, P., 2005. Heart-rate profile during exercise as a predictor of sudden death. N Engl J Med. 352**,** 1951-8.

Jung, B.C., Dave, A.S., Tan, A.Y., Gholmieh, G., Zhou, S., Wang, D.C., Akingba, A.G., Fishbein, G.A., Montemagno, C., Lin, S.F., Chen, L.S., Chen, P.S., 2006. Circadian variations of stellate ganglion nerve activity in ambulatory dogs. Heart Rhythm. 3**,** 78-85.

Jung, K.M., Tan, S., Landman, N., Petrova, K., Murray, S., Lewis, R., Kim, P.K., Kim, D.S., Ryu, S.H., Chao, M.V., Kim, T.W., 2003. Regulated intramembrane proteolysis of the p75 neurotrophin receptor modulates its association with the TrkA receptor. J Biol Chem. 278**,** 42161-9.

Kammerling, J.J., Green, F.J., Watanabe, A.M., Inoue, H., Barber, M.J., Henry, D.P., Zipes, D.P., 1987. Denervation supersensitivity of refractoriness in noninfarcted areas apical to transmural myocardial infarction. Circulation. 76**,** 383-93.

Kanazawa, H., Ieda, M., Kimura, K., Arai, T., Kawaguchi-Manabe, H., Matsuhashi, T., Endo, J., Sano, M., Kawakami, T., Kimura, T., Monkawa, T., Hayashi, M., Iwanami, A., Okano, H., Okada, Y., Ishibashi-Ueda, H., Ogawa, S., Fukuda, K., 2010. Heart failure causes cholinergic transdifferentiation of cardiac sympathetic nerves via gp130-signaling cytokines in rodents. J Clin Invest. 120**,** 408-21.

Kaneko, S., Iwanami, A., Nakamura, M., Kishino, A., Kikuchi, K., Shibata, S., Okano, H.J., Ikegami, T., Moriya, A., Konishi, O., Nakayama, C., Kumagai, K., Kimura, T., Sato, Y., Goshima, Y., Taniguchi, M., Ito, M., He, Z., Toyama, Y., Okano, H., 2006. A selective Sema3A inhibitor enhances regenerative responses and functional recovery of the injured spinal cord. Nat Med. 12**,** 1380-9.

Kanning, K.C., Hudson, M., Amieux, P.S., Wiley, J.C., Bothwell, M., Schecterson, L.C., 2003. Proteolytic processing of the p75 neurotrophin receptor and two homologs generates C-terminal fragments with signaling capability. J Neurosci. 23**,** 5425-36.

Kaplan, D.R., Martin-Zanca, D., Parada, L.F., 1991. Tyrosine phosphorylation and tyrosine kinase activity of the trk proto-oncogene product induced by NGF. Nature. 350**,** 158-60.

Kaplan, D.R., Miller, F.D., 2000. Neurotrophin signal transduction in the nervous system. Curr Opin Neurobiol. 10**,** 381-91.

Kaplan, D.R., Miller, F.D., 2003. Axon growth inhibition: signals from the p75 neurotrophin receptor. Nat Neurosci. 6**,** 435-6.

Kaprielian, R., Sah, R., Nguyen, T., Wickenden, A.D., Backx, P.H., 2002. Myocardial infarction in rat eliminates regional heterogeneity of AP profiles, I(to) K(+) currents, and [Ca(2+)](i) transients. Am J Physiol Heart Circ Physiol. 283**,** H1157-68.

Karlsberg, R.P., Penkoske, P.A., Cryer, P.E., Corr, P.B., Roberts, R., 1979. Rapid activation of the sympathetic nervous system following coronary artery occlusion: relationship to infarct size, site, and haemodynamic impact. Cardiovasc Res. 13**,** 523-31.

Kawasaki, T., Bekku, Y., Suto, F., Kitsukawa, T., Taniguchi, M., Nagatsu, I., Nagatsu, T., Itoh, K., Yagi, T., Fujisawa, H., 2002. Requirement of neuropilin 1-mediated Sema3A signals in patterning of the sympathetic nervous system. Development. 129**,** 671-80.

Kaye, D.M., Vaddadi, G., Gruskin, S.L., Du, X.J., Esler, M.D., 2000. Reduced myocardial nerve growth factor expression in human and experimental heart failure. Circ Res. 86**,** E80-4.

Kaye, M.P., Wells, D.J., Tyce, G.M., 1979. Nerve growth factor-enhanced reinnervation of surgically denervated canine heart. Am J Physiol. 236**,** H624-8.

Kenchappa, R.S., Zampieri, N., Chao, M.V., Barker, P.A., Teng, H.K., Hempstead, B.L., Carter, B.D., 2006. Ligand-dependent cleavage of the P75 neurotrophin receptor is necessary for NRIF nuclear translocation and apoptosis in sympathetic neurons. Neuron. 50**,** 219-32.

Kimpinski, K., Jelinski, S., Mearow, K., 1999. The anti-p75 antibody, MC192, and brain-derived neurotrophic factor inhibit nerve growth factor-dependent neurite growth from adult sensory neurons. Neuroscience. 93**,** 253-63.

Kimura, K., Ieda, M., Kanazawa, H., Yagi, T., Tsunoda, M., Ninomiya, S., Kurosawa, H., Yoshimi, K., Mochizuki, H., Yamazaki, K., Ogawa, S., Fukuda, K., 2007. Cardiac sympathetic rejuvenation: a link between nerve function and cardiac hypertrophy. Circ Res. 100**,** 1755-64.

Kimura, K., Kanazawa, H., Ieda, M., Kawaguchi-Manabe, H., Miyake, Y., Yagi, T., Arai, T., Sano, M., Fukuda, K., 2010. Norepinephrine-induced nerve growth factor depletion causes cardiac sympathetic denervation in severe heart failure. Auton Neurosci.

Kiriazis, H., Du, X.J., Feng, X., Hotchkin, E., Marshall, T., Finch, S., Gao, X.M., Lambert, G., Choate, J.K., Kaye, D.M., 2005. Preserved left ventricular structure and function in mice with cardiac sympathetic hyperinnervation. Am J Physiol Heart Circ Physiol. 289**,** H1359-65.

Kjekshus, J., 1990. Arrhythmias and mortality in congestive heart failure. Am J Cardiol. 65**,** 42I-48I.

Klabunde, R.E., 2005. Cardiovascular physiology concepts, Vol., Lippincott Williams & Wilkins, Philadelphia.

Kleiger, R.E., Miller, J.P., Bigger, J.T., Jr., Moss, A.J., 1987. Decreased heart rate variability and its association with increased mortality after acute myocardial infarction. Am J Cardiol. 59**,** 256-62.

Klein, R., Jing, S.Q., Nanduri, V., O'Rourke, E., Barbacid, M., 1991. The trk proto-oncogene encodes a receptor for nerve growth factor. Cell. 65**,** 189-97.

Kohn, J., Aloyz, R.S., Toma, J.G., Haak-Frendscho, M., Miller, F.D., 1999. Functionally antagonistic interactions between the TrkA and p75 neurotrophin receptors regulate sympathetic neuron growth and target innervation. J Neurosci. 19**,** 5393-408.

Kokaia, Z., Andsberg, G., Martinez-Serrano, A., Lindvall, O., 1998. Focal cerebral ischemia in rats induces expression of P75 neurotrophin receptor in resistant striatal cholinergic neurons. Neuroscience. 84**,** 1113-25.

Kolodkin, A.L., Levengood, D.V., Rowe, E.G., Tai, Y.T., Giger, R.J., Ginty, D.D., 1997. Neuropilin is a semaphorin III receptor. Cell. 90**,** 753-62.

Korsching, S., Thoenen, H., 1983. Nerve growth factor in sympathetic ganglia and corresponding target organs of the rat: correlation with density of sympathetic innervation. Proc Natl Acad Sci U S A. 80**,** 3513-6.

Kreusser, M.M., Buss, S.J., Krebs, J., Kinscherf, R., Metz, J., Katus, H.A., Haass, M., Backs, J., 2008. Differential expression of cardiac neurotrophic factors and sympathetic nerve ending abnormalities within the failing heart. J Mol Cell Cardiol. 44**,** 380-7.

Krol, K.M., Crutcher, K.A., Kalisch, B.E., Rylett, R.J., Kawaja, M.D., 2000. Absence of p75(NTR) expression reduces nerve growth factor immunolocalization in cholinergic septal neurons. J Comp Neurol. 427**,** 54-66.

Kunugi, H., Hashimoto, R., Yoshida, M., Tatsumi, M., Kamijima, K., 2004. A missense polymorphism (S205L) of the low-affinity neurotrophin receptor p75NTR gene is associated with depressive disorder and attempted suicide. Am J Med Genet B Neuropsychiatr Genet. 129B**,** 44-6.

Kuo, H.C., Cheng, C.F., Clark, R.B., Lin, J.J., Lin, J.L., Hoshijima, M., Nguyen-Tran, V.T., Gu, Y., Ikeda, Y., Chu, P.H., Ross, J., Giles, W.R., Chien, K.R., 2001. A defect in the Kv channel-interacting protein 2 (KChIP2) gene leads to a complete loss of I(to) and confers susceptibility to ventricular tachycardia. Cell. 107**,** 801-13.

Kuruvilla, R., Ye, H., Ginty, D.D., 2000. Spatially and functionally distinct roles of the PI3-K effector pathway during NGF signaling in sympathetic neurons. Neuron. 27**,** 499-512.

Kuruvilla, R., Zweifel, L.S., Glebova, N.O., Lonze, B.E., Valdez, G., Ye, H., Ginty, D.D., 2004. A neurotrophin signaling cascade coordinates sympathetic neuron development through differential control of TrkA trafficking and retrograde signaling. Cell. 118**,** 243-55.

La Rovere, M.T., Specchia, G., Mortara, A., Schwartz, P.J., 1988. Baroreflex sensitivity, clinical correlates, and cardiovascular mortality among patients with a first myocardial infarction. A prospective study. Circulation. 78**,** 816-24.

La Rovere, M.T., Pinna, G.D., Hohnloser, S.H., Marcus, F.I., Mortara, A., Nohara, R., Bigger, J.T., Jr., Camm, A.J., Schwartz, P.J., 2001. Baroreflex sensitivity and heart rate variability in the identification of patients at risk

for life-threatening arrhythmias: implications for clinical trials. Circulation. 103**,** 2072-7.

Lampert, R., Rosenfeld, L., Batsford, W., Lee, F., McPherson, C., 1994. Circadian variation of sustained ventricular tachycardia in patients with coronary artery disease and implantable cardioverter-defibrillators. Circulation. 90**,** 241-7.

Lee, J.K., Zheng, B., 2008. Axon regeneration after spinal cord injury: insight from genetically modified mouse models. Restor Neurol Neurosci. 26**,** 175-82.

Lee, K.F., Li, E., Huber, L.J., Landis, S.C., Sharpe, A.H., Chao, M.V., Jaenisch, R., 1992. Targeted mutation of the gene encoding the low affinity NGF receptor p75 leads to deficits in the peripheral sensory nervous system. Cell. 69**,** 737-49.

Lee, K.F., Bachman, K., Landis, S., Jaenisch, R., 1994. Dependence on p75 for innervation of some sympathetic targets. Science. 263**,** 1447-9.

Lee, R., Kermani, P., Teng, K.K., Hempstead, B.L., 2001. Regulation of cell survival by secreted proneurotrophins. Science. 294**,** 1945-8.

Levi-Montalcini, R., Hamburger, V., 1951. Selective growth stimulating effects of mouse sarcoma on the sensory and sympathetic nervous system of the chick embryo. J Exp Zool. 116**,** 321-61.

Levi-Montalcini, R., 1952. Effects of mouse tumor transplantation on the nervous system. Ann N Y Acad Sci. 55**,** 330-44.

Levi-Montalcini, R., Meyer, H., Hamburger, V., 1954. In vitro experiments on the effects of mouse sarcomas 180 and 37 on the spinal and sympathetic ganglia of the chick embryo. Cancer Res. 14**,** 49-57.

Levi-Montalcini, R., Cohen, S., 1956. In Vitro and in Vivo Effects of a Nerve Growth-Stimulating Agent Isolated from Snake Venom. Proc Natl Acad Sci U S A. 42**,** 695-9.

Levi-Montalcini, R., Angeletti, P.U., 1966. Second symposium on catecholamines. Modification of sympathetic function. Immunosympathectomy. Pharmacol Rev. 18**,** 619-28.

Levi-Montalcini, R., 1987. The nerve growth factor 35 years later. Science. 237**,** 1154-62.

Lewin, G.R., Barde, Y.A., 1996. Physiology of the neurotrophins. Annu Rev Neurosci. 19**,** 289-317.

Li, S., Liu, B.P., Budel, S., Li, M., Ji, B., Walus, L., Li, W., Jirik, A., Rabacchi, S., Choi, E., Worley, D., Sah, D.W., Pepinsky, B., Lee, D., Relton, J., Strittmatter, S.M., 2004a. Blockade of Nogo-66, myelin-associated glycoprotein, and oligodendrocyte myelin glycoprotein by soluble Nogo-66 receptor promotes axonal sprouting and recovery after spinal injury. J Neurosci. 24**,** 10511-20.

Li, W., Knowlton, D., Van Winkle, D.M., Habecker, B.A., 2004b. Infarction alters both the distribution and noradrenergic properties of cardiac sympathetic neurons. Am J Physiol Heart Circ Physiol. 286**,** H2229-36.

Liang, C.S., Fan, T.H., Sullebarger, J.T., Sakamoto, S., 1989. Decreased adrenergic neuronal uptake activity in experimental right heart failure. A chamber-specific contributor to beta-adrenoceptor downregulation. J Clin Invest. 84**,** 1267-75.

Lim, Y.S., McLaughlin, T., Sung, T.C., Santiago, A., Lee, K.F., O'Leary, D.D., 2008. p75(NTR) mediates ephrin-A reverse signaling required for axon repulsion and mapping. Neuron. 59**,** 746-58.

Linggi, M.S., Burke, T.L., Williams, B.B., Harrington, A., Kraemer, R., Hempstead, B.L., Yoon, S.O., Carter, B.D., 2005. Neurotrophin receptor interacting factor (NRIF) is an essential mediator of apoptotic signaling by the p75 neurotrophin receptor. J Biol Chem. 280**,** 13801-8.

Lombardi, F., Verrier, R.L., Lown, B., 1983. Relationship between sympathetic neural activity, coronary dynamics, and vulnerability to ventricular fibrillation during myocardial ischemia and reperfusion. Am Heart J. 105**,** 958-65.

Long, J.B., Jay, S.M., Segal, S.S., Madri, J.A., 2009. VEGF-A and Semaphorin3A: modulators of vascular sympathetic innervation. Dev Biol. 334**,** 119-32.

Lonze, B.E., Riccio, A., Cohen, S., Ginty, D.D., 2002. Apoptosis, axonal growth defects, and degeneration of peripheral neurons in mice lacking CREB. Neuron. 34**,** 371-85.

Lopez-Sendon, J., Swedberg, K., McMurray, J., Tamargo, J., Maggioni, A.P., Dargie, H., Tendera, M., Waagstein, F., Kjekshus, J., Lechat, P., Torp-

Pedersen, C., 2004. Expert consensus document on beta-adrenergic receptor blockers. Eur Heart J. 25**,** 1341-62.

Lorentz, C.U., Alston, E.N., Belcik, J.T., Lindner, J.R., Giraud, G.D., Habecker, B.A., 2010. Heterogeneous ventricular sympathetic innervation, altered {beta} adrenergic receptor expression, and rhythm instability in mice lacking p75 neurotrophin receptor. Am J Physiol Heart Circ Physiol.

Lu, B., Pang, P.T., Woo, N.H., 2005. The yin and yang of neurotrophin action. Nat Rev Neurosci. 6**,** 603-14.

Lukas, A., Antzelevitch, C., 1993. Differences in the electrophysiological response of canine ventricular epicardium and endocardium to ischemia. Role of the transient outward current. Circulation. 88**,** 2903-15.

Luo, L., O'Leary, D.D., 2005. Axon retraction and degeneration in development and disease. Annu Rev Neurosci. 28**,** 127-56.

Mann, D.L., 1998. Basic mechanisms of disease progression in the failing heart: the role of excessive adrenergic drive. Prog Cardiovasc Dis. 41**,** 1-8.

Mansson-Broberg, A., Siddiqui, A.J., Genander, M., Grinnemo, K.H., Hao, X., Andersson, A.B., Wardell, E., Sylven, C., Corbascio, M., 2008. Modulation of ephrinB2 leads to increased angiogenesis in ischemic myocardium and endothelial cell proliferation. Biochem Biophys Res Commun. 373**,** 355-9.

Martin-Zanca, D., Hughes, S.H., Barbacid, M., 1986. A human oncogene formed by the fusion of truncated tropomyosin and protein tyrosine kinase sequences. Nature. 319**,** 743-8.

Martin-Zanca, D., Oskam, R., Mitra, G., Copeland, T., Barbacid, M., 1989. Molecular and biochemical characterization of the human trk proto-oncogene. Mol Cell Biol. 9**,** 24-33.

Martins, J.B., Zipes, D.P., 1980. Epicardial phenol interrupts refractory period responses to sympathetic but not vagal stimulation in canine left ventricular epicardium and endocardium. Circ Res. 47**,** 33-40.

Mason, D.T., 1969. Usefulness and limitations of the rate of rise of intraventricular pressure (dp-dt) in the evaluation of myocardial contractility in man. Am J Cardiol. 23**,** 516-27.

Mathew, T.C., Miller, F.D., 1990. Increased expression of T alpha 1 alpha-tubulin mRNA during collateral and NGF-induced sprouting of sympathetic neurons. Dev Biol. 141**,** 84-92.

Max, S.R., Rohrer, H., Otten, U., Thoenen, H., 1978. Nerve growth factor-mediated induction of tyrosine hydroxylase in rat superior cervical ganglia in vitro. J Biol Chem. 253**,** 8013-5.

Mazzoni, I.E., Said, F.A., Aloyz, R., Miller, F.D., Kaplan, D., 1999. Ras regulates sympathetic neuron survival by suppressing the p53-mediated cell death pathway. J Neurosci. 19**,** 9716-27.

McDonald, N.Q., Blundell, T.L., 1991. Crystallization and characterization of the high molecular weight form of nerve growth factor (7 S NGF). J Mol Biol. 219**,** 595-601.

McDonald, N.Q., Hendrickson, W.A., 1993. A structural superfamily of growth factors containing a cystine knot motif. Cell. 73**,** 421-4.

McGregor, S., Strauss, J., Bulgin, N., De Luca, V., George, C.J., Kovacs, M., Kennedy, J.L., 2007. p75(NTR) gene and suicide attempts in young adults with a history of childhood-onset mood disorder. Am J Med Genet B Neuropsychiatr Genet. 144B**,** 696-700.

Mi, S., Lee, X., Shao, Z., Thill, G., Ji, B., Relton, J., Levesque, M., Allaire, N., Perrin, S., Sands, B., Crowell, T., Cate, R.L., McCoy, J.M., Pepinsky, R.B., 2004. LINGO-1 is a component of the Nogo-66 receptor/p75 signaling complex. Nat Neurosci. 7**,** 221-8.

Minardo, J.D., Tuli, M.M., Mock, B.H., Weiner, R.E., Pride, H.P., Wellman, H.N., Zipes, D.P., 1988. Scintigraphic and electrophysiological evidence of canine myocardial sympathetic denervation and reinnervation produced by myocardial infarction or phenol application. Circulation. 78**,** 1008-19.

Mohrman, D.E., Heller, L.J., 2006. Cardiovascular physiology. In: Lange physiology series,. Vol., ed.^eds. Lange Medical Books/McGraw-Hill, New York.

Muller, J.E., Ludmer, P.L., Willich, S.N., Tofler, G.H., Aylmer, G., Klangos, I., Stone, P.H., 1987a. Circadian variation in the frequency of sudden cardiac death. Circulation. 75**,** 131-8.

Muller, J.E., Tofler, G.H., Willich, S.N., Stone, P.H., 1987b. Circadian variation of cardiovascular disease and sympathetic activity. J Cardiovasc Pharmacol. 10 Suppl 2**,** S104-9; discussion S110-1.

Nabauer, M., Beuckelmann, D.J., Uberfuhr, P., Steinbeck, G., 1996. Regional differences in current density and rate-dependent properties of the

transient outward current in subepicardial and subendocardial myocytes of human left ventricle. Circulation. 93**,** 168-77.

Nademanee, K., Taylor, R., Bailey, W.E., Rieders, D.E., Kosar, E.M., 2000. Treating electrical storm : sympathetic blockade versus advanced cardiac life support-guided therapy. Circulation. 102**,** 742-7.

Ng, Y.P., Cheung, Z.H., Ip, N.Y., 2006. STAT3 as a downstream mediator of Trk signaling and functions. J Biol Chem. 281**,** 15636-44.

NHLBI, 2008. National Heart Lung Blood Institute. Diseases and Conditions Index. http://www.nhlbi.nih.gov/health/dci/Diseases/HeartAttack/HeartAttack_Whatis.html.

Nian, M., Lee, P., Khaper, N., Liu, P., 2004. Inflammatory cytokines and postmyocardial infarction remodeling. Circ Res. 94**,** 1543-53.

Nusser, N., Gosmanova, E., Zheng, Y., Tigyi, G., 2002. Nerve growth factor signals through TrkA, phosphatidylinositol 3-kinase, and Rac1 to inactivate RhoA during the initiation of neuronal differentiation of PC12 cells. J Biol Chem. 277**,** 35840-6.

Nykjaer, A., Lee, R., Teng, K.K., Jansen, P., Madsen, P., Nielsen, M.S., Jacobsen, C., Kliemannel, M., Schwarz, E., Willnow, T.E., Hempstead, B.L., Petersen, C.M., 2004. Sortilin is essential for proNGF-induced neuronal cell death. Nature. 427**,** 843-8.

Nykjaer, A., Willnow, T.E., Petersen, C.M., 2005. p75NTR--live or let die. Curr Opin Neurobiol. 15**,** 49-57.

Oh, Y.S., Jong, A.Y., Kim, D.T., Li, H., Wang, C., Zemljic-Harpf, A., Ross, R.S., Fishbein, M.C., Chen, P.S., Chen, L.S., 2006. Spatial distribution of nerve sprouting after myocardial infarction in mice. Heart Rhythm. 3**,** 728-36.

Oppenheim, R.W., 1991. Cell death during development of the nervous system. Annu Rev Neurosci. 14**,** 453-501.

Orike, N., Thrasivoulou, C., Wrigley, A., Cowen, T., 2001. Differential regulation of survival and growth in adult sympathetic neurons: an in vitro study of neurotrophin responsiveness. J Neurobiol. 47**,** 295-305.

Pardini, B.J., Lund, D.D., Schmid, P.G., 1989. Organization of the sympathetic postganglionic innervation of the rat heart. J Auton Nerv Syst. 28**,** 193-201.

Park, K.J., Grosso, C.A., Aubert, I., Kaplan, D.R., Miller, F.D., 2010. p75NTR-dependent, myelin-mediated axonal degeneration regulates neural connectivity in the adult brain. Nat Neurosci.

Parrish, D.C., Gritman, K., Van Winkle, D.M., Woodward, W.R., Bader, M., Habecker, B.A., 2008. Postinfarct sympathetic hyperactivity differentially stimulates expression of tyrosine hydroxylase and norepinephrine transporter. Am J Physiol Heart Circ Physiol. 294**,** H99-H106.

Parrish, D.C., Alston, E.N., Rohrer, H., Nkadi, P., Woodward, W.R., Schutz, G., Habecker, B.A., 2009. Infarction-induced cytokines cause local depletion of tyrosine hydroxylase in cardiac sympathetic nerves. Exp Physiol. In Press.

Pearson, G., Robinson, F., Beers Gibson, T., Xu, B.E., Karandikar, M., Berman, K., Cobb, M.H., 2001. Mitogen-activated protein (MAP) kinase pathways: regulation and physiological functions. Endocr Rev. 22**,** 153-83.

Plo, I., Bono, F., Bezombes, C., Alam, A., Bruno, A., Laurent, G., 2004. Nerve growth factor-induced protein kinase C stimulation contributes to TrkA-dependent inhibition of p75 neurotrophin receptor sphingolipid signaling. J Neurosci Res. 77**,** 465-74.

Porter, K.E., Turner, N.A., 2009. Cardiac fibroblasts: at the heart of myocardial remodeling. Pharmacol Ther. 123**,** 255-78.

Prasad, A., Stone, G.W., Holmes, D.R., Gersh, B., 2009. Reperfusion injury, microvascular dysfunction, and cardioprotection: the "dark side" of reperfusion. Circulation. 120**,** 2105-12.

Pugazhenthi, S., Nesterova, A., Sable, C., Heidenreich, K.A., Boxer, L.M., Heasley, L.E., Reusch, J.E., 2000. Akt/protein kinase B up-regulates Bcl-2 expression through cAMP-response element-binding protein. J Biol Chem. 275**,** 10761-6.

Radeke, M.J., Misko, T.P., Hsu, C., Herzenberg, L.A., Shooter, E.M., 1987. Gene transfer and molecular cloning of the rat nerve growth factor receptor. Nature. 325**,** 593-7.

Ramos, A., Ho, W.C., Forte, S., Dickson, K., Boutilier, J., Favell, K., Barker, P.A., 2007. Hypo-osmolar stress induces p75NTR expression by activating Sp1-dependent transcription. J Neurosci. 27**,** 1498-506.

Randall, W.C., Szentivanyi, M., Pace, J.B., Wechsler, J.S., Kaye, M.P., 1968. Patterns of sympathetic nerve projections onto the canine heart. Circ Res. 22**,** 315-23.

Reichardt, L.F., 2006. Neurotrophin-regulated signalling pathways. Philos Trans R Soc Lond B Biol Sci. 361**,** 1545-64.

Riccio, A., Pierchala, B.A., Ciarallo, C.L., Ginty, D.D., 1997. An NGF-TrkA-mediated retrograde signal to transcription factor CREB in sympathetic neurons. Science. 277**,** 1097-100.

Riccio, A., Ahn, S., Davenport, C.M., Blendy, J.A., Ginty, D.D., 1999. Mediation by a CREB family transcription factor of NGF-dependent survival of sympathetic neurons. Science. 286**,** 2358-61.

Richardson, R.J., Grkovic, I., Allen, A.M., Anderson, C.R., 2006. Separate neurochemical classes of sympathetic postganglionic neurons project to the left ventricle of the rat heart. Cell Tissue Res. 324**,** 9-16.

Rockman, H.A., Koch, W.J., Lefkowitz, R.J., 2002. Seven-transmembrane-spanning receptors and heart function. Nature. 415**,** 206-12.

Rodriguez-Tebar, A., Dechant, G., Barde, Y.A., 1990. Binding of brain-derived neurotrophic factor to the nerve growth factor receptor. Neuron. 4**,** 487-92.

Rozanski, G.J., Xu, Z., Zhang, K., Patel, K.P., 1998. Altered K+ current of ventricular myocytes in rats with chronic myocardial infarction. Am J Physiol. 274**,** H259-65.

Rubart, M., Zipes, D.P., 2005. Mechanisms of sudden cardiac death. J Clin Invest. 115**,** 2305-15.

Rubin, E., 1985. Development of the rat superior cervical ganglion: ganglion cell maturation. J Neurosci. 5**,** 673-84.

Ruvolo, P.P., 2003. Intracellular signal transduction pathways activated by ceramide and its metabolites. Pharmacol Res. 47**,** 383-92.

Sanes, D.H., Reh, T.A., Harris, W.A., 2005. Development of the nervous system, Vol., Academic, London.

Scherrer-Crosbie, M., Rodrigues, A.C., Hataishi, R., Picard, M.H., 2007. Infarct size assessment in mice. Echocardiography. 24**,** 90-6.

Schmidt, A., Hall, A., 2002. Guanine nucleotide exchange factors for Rho GTPases: turning on the switch. Genes Dev. 16**,** 1587-609.

Schultz, H.D., Ustinova, E.E., 1998. Capsaicin receptors mediate free radical-induced activation of cardiac afferent endings. Cardiovasc Res. 38**,** 348-55.

Schwartz, P.J., Vanoli, E., Stramba-Badiale, M., De Ferrari, G.M., Billman, G.E., Foreman, R.D., 1988. Autonomic mechanisms and sudden death. New insights from analysis of baroreceptor reflexes in conscious dogs with and without a myocardial infarction. Circulation. 78**,** 969-79.

Seagard, J.L., Hopp, F.A., Bosnjak, Z.J., Osborn, J.L., Kampine, J.P., 1984. Sympathetic efferent nerve activity in conscious and isoflurane-anesthetized dogs. Anesthesiology. 61**,** 266-70.

Sebok, A., Nusser, N., Debreceni, B., Guo, Z., Santos, M.F., Szeberenyi, J., Tigyi, G., 1999. Different roles for RhoA during neurite initiation, elongation, and regeneration in PC12 cells. J Neurochem. 73**,** 949-60.

Sharma, V.K., Banerjee, S.P., 1977. Inhibition of [3H]norepinephrine uptake in peripheral organs of some mammalian species by ouabain. Eur J Pharmacol. 41**,** 417-29.

Singh, K.K., Park, K.J., Hong, E.J., Kramer, B.M., Greenberg, M.E., Kaplan, D.R., Miller, F.D., 2008. Developmental axon pruning mediated by BDNF-p75NTR-dependent axon degeneration. Nat Neurosci. 11**,** 649-58.

Smeyne, R.J., Klein, R., Schnapp, A., Long, L.K., Bryant, S., Lewin, A., Lira, S.A., Barbacid, M., 1994. Severe sensory and sympathetic neuropathies in mice carrying a disrupted Trk/NGF receptor gene. Nature. 368**,** 246-9.

Solomon, S.D., Zelenkofske, S., McMurray, J.J., Finn, P.V., Velazquez, E., Ertl, G., Harsanyi, A., Rouleau, J.L., Maggioni, A., Kober, L., White, H., Van de Werf, F., Pieper, K., Califf, R.M., Pfeffer, M.A., 2005. Sudden death in patients with myocardial infarction and left ventricular dysfunction, heart failure, or both. N Engl J Med. 352**,** 2581-8.

Song, X.Y., Zhong, J.H., Wang, X., Zhou, X.F., 2004. Suppression of p75NTR does not promote regeneration of injured spinal cord in mice. J Neurosci. 24**,** 542-6.

Squire, L.R., 2003. Fundamental neuroscience, Vol., Academic, San Diego, Calif. London.

Stanton, M.S., Tuli, M.M., Radtke, N.L., Heger, J.J., Miles, W.M., Mock, B.H., Burt, R.W., Wellman, H.N., Zipes, D.P., 1989. Regional sympathetic denervation after myocardial infarction in humans detected noninvasively using I-123-metaiodobenzylguanidine. J Am Coll Cardiol. 14**,** 1519-26.

Stevens, M.J., Raffel, D.M., Allman, K.C., Dayanikli, F., Ficaro, E., Sandford, T., Wieland, D.M., Pfeifer, M.A., Schwaiger, M., 1998. Cardiac sympathetic dysinnervation in diabetes: implications for enhanced cardiovascular risk. Circulation. 98**,** 961-8.

Stockel, K., Paravicini, U., Thoenen, H., 1974. Specificity of the retrograde axonal transport of nerve growth factor. Brain Res. 76**,** 413-21.

Tanelian, D.L., Barry, M.A., Johnston, S.A., Le, T., Smith, G.M., 1997. Semaphorin III can repulse and inhibit adult sensory afferents in vivo. Nat Med. 3**,** 1398-401.

Taniguchi, M., Yuasa, S., Fujisawa, H., Naruse, I., Saga, S., Mishina, M., Yagi, T., 1997. Disruption of semaphorin III/D gene causes severe abnormality in peripheral nerve projection. Neuron. 19**,** 519-30.

Tessarollo, L., Tsoulfas, P., Donovan, M.J., Palko, M.E., Blair-Flynn, J., Hempstead, B.L., Parada, L.F., 1997. Targeted deletion of all isoforms of the trkC gene suggests the use of alternate receptors by its ligand neurotrophin-3 in neuronal development and implicates trkC in normal cardiogenesis. Proc Natl Acad Sci U S A. 94**,** 14776-81.

Thoenen, H., Angeletti, P.U., Levi-Montalcini, R., Kettler, R., 1971. Selective induction by nerve growth factor of tyrosine hydroxylase and dopamine- -hydroxylase in the rat superior cervical ganglia. Proc Natl Acad Sci U S A. 68**,** 1598-602.

Thomas, D., Kiehn, J., Katus, H.A., Karle, C.A., 2004. Adrenergic regulation of the rapid component of the cardiac delayed rectifier potassium current,

I(Kr), and the underlying hERG ion channel. Basic Res Cardiol. 99**,** 279-87.

Torrent-Guasp, F., Buckberg, G.D., Clemente, C., Cox, J.L., Coghlan, H.C., Gharib, M., 2001. The structure and function of the helical heart and its buttress wrapping. I. The normal macroscopic structure of the heart. Semin Thorac Cardiovasc Surg. 13**,** 301-19.

Tsuji, H., Larson, M.G., Venditti, F.J., Jr., Manders, E.S., Evans, J.C., Feldman, C.L., Levy, D., 1996. Impact of reduced heart rate variability on risk for cardiac events. The Framingham Heart Study. Circulation. 94**,** 2850-5.

Tucker, W.K., Rackstein, A.D., Munson, E.S., 1974. Comparison of arrhythmic doses of adrenaline, metaraminol, ephedrine and phenylephrine during isoflurane and halothant anaesthesia in dogs. Br J Anaesth. 46**,** 392-6.

Ure, D.R., Campenot, R.B., 1997. Retrograde transport and steady-state distribution of 125I-nerve growth factor in rat sympathetic neurons in compartmented cultures. J Neurosci. 17**,** 1282-90.

Veeranna, Amin, N.D., Ahn, N.G., Jaffe, H., Winters, C.A., Grant, P., Pant, H.C., 1998. Mitogen-activated protein kinases (Erk1,2) phosphorylate Lys-Ser-Pro (KSP) repeats in neurofilament proteins NF-H and NF-M. J Neurosci. 18**,** 4008-21.

Volosin, M., Trotter, C., Cragnolini, A., Kenchappa, R.S., Light, M., Hempstead, B.L., Carter, B.D., Friedman, W.J., 2008. Induction of proneurotrophins and activation of p75NTR-mediated apoptosis via neurotrophin receptor-

interacting factor in hippocampal neurons after seizures. J Neurosci. 28**,** 9870-9.

Walker, M.J., Curtis, M.J., Hearse, D.J., Campbell, R.W., Janse, M.J., Yellon, D.M., Cobbe, S.M., Coker, S.J., Harness, J.B., Harron, D.W., et al., 1988. The Lambeth Conventions: guidelines for the study of arrhythmias in ischaemia infarction, and reperfusion. Cardiovasc Res. 22**,** 447-55.

Wallukat, G., 2002. The beta-adrenergic receptors. Herz. 27**,** 683-90.

Wang, Y., Cheng, J., Joyner, R.W., Wagner, M.B., Hill, J.A., 2006. Remodeling of early-phase repolarization: a mechanism of abnormal impulse conduction in heart failure. Circulation. 113**,** 1849-56.

Watson, F.L., Heerssen, H.M., Moheban, D.B., Lin, M.Z., Sauvageot, C.M., Bhattacharyya, A., Pomeroy, S.L., Segal, R.A., 1999. Rapid nuclear responses to target-derived neurotrophins require retrograde transport of ligand-receptor complex. J Neurosci. 19**,** 7889-900.

Watson, F.L., Heerssen, H.M., Bhattacharyya, A., Klesse, L., Lin, M.Z., Segal, R.A., 2001. Neurotrophins use the Erk5 pathway to mediate a retrograde survival response. Nat Neurosci. 4**,** 981-8.

Welcher, A.A., Bitler, C.M., Radeke, M.J., Shooter, E.M., 1991. Nerve growth factor binding domain of the nerve growth factor receptor. Proc Natl Acad Sci U S A. 88**,** 159-63.

WHO, 2009. World Health Organization. Fact Sheet No. 317. http://www.who.int/mediacentre/ factsheets/fs317/en.

Wong, S.T., Henley, J.R., Kanning, K.C., Huang, K.H., Bothwell, M., Poo, M.M., 2002. A p75(NTR) and Nogo receptor complex mediates repulsive signaling by myelin-associated glycoprotein. Nat Neurosci. 5**,** 1302-8.

Yamaguchi, Y., Katoh, H., Yasui, H., Mori, K., Negishi, M., 2001. RhoA inhibits the nerve growth factor-induced Rac1 activation through Rho-associated kinase-dependent pathway. J Biol Chem. 276**,** 18977-83.

Yamashita, T., Tucker, K.L., Barde, Y.A., 1999. Neurotrophin binding to the p75 receptor modulates Rho activity and axonal outgrowth. Neuron. 24**,** 585-93.

Yamashita, T., Higuchi, H., Tohyama, M., 2002. The p75 receptor transduces the signal from myelin-associated glycoprotein to Rho. J Cell Biol. 157**,** 565-70.

Yamashita, T., Tohyama, M., 2003. The p75 receptor acts as a displacement factor that releases Rho from Rho-GDI. Nat Neurosci. 6**,** 461-7.

Yan, H., Chao, M.V., 1991. Disruption of cysteine-rich repeats of the p75 nerve growth factor receptor leads to loss of ligand binding. J Biol Chem. 266**,** 12099-104.

Yang, J., Siao, C.J., Nagappan, G., Marinic, T., Jing, D., McGrath, K., Chen, Z.Y., Mark, W., Tessarollo, L., Lee, F.S., Lu, B., Hempstead, B.L., 2009. Neuronal release of proBDNF. Nat Neurosci. 12**,** 113-5.

Yaron, A., Huang, P.H., Cheng, H.J., Tessier-Lavigne, M., 2005. Differential requirement for Plexin-A3 and -A4 in mediating responses of sensory and sympathetic neurons to distinct class 3 Semaphorins. Neuron. 45**,** 513-23.

Yeiser, E.C., Rutkoski, N.J., Naito, A., Inoue, J., Carter, B.D., 2004. Neurotrophin signaling through the p75 receptor is deficient in traf6-/- mice. J Neurosci. 24**,** 10521-9.

Yen, L.D., Bennett, G.J., Ribeiro-da-Silva, A., 2006. Sympathetic sprouting and changes in nociceptive sensory innervation in the glabrous skin of the rat hind paw following partial peripheral nerve injury. J Comp Neurol. 495**,** 679-90.

Zampieri, N., Chao, M.V., 2006. Mechanisms of neurotrophin receptor signalling. Biochem Soc Trans. 34**,** 607-11.

Zhou, F.Q., Zhou, J., Dedhar, S., Wu, Y.H., Snider, W.D., 2004a. NGF-induced axon growth is mediated by localized inactivation of GSK-3beta and functions of the microtubule plus end binding protein APC. Neuron. 42**,** 897-912.

Zhou, S., Cao, J.M., Swissa, M., Gonzalez-Gomez, I., Chang, C.M., Chien, K., Miyauchi, Y., Fu, K.J., Yi, J., Asotra, K., Karagueuzian, H.S., Fishbein, M.C., Chen, P.S., Chen, L.S., 2004b. Low-affinity nerve growth factor receptor p75NTR immunoreactivity in the myocardium with sympathetic hyperinnervation. J Cardiovasc Electrophysiol. 15**,** 430-7.

Zhou, S., Chen, L.S., Miyauchi, Y., Miyauchi, M., Kar, S., Kangavari, S., Fishbein, M.C., Sharifi, B., Chen, P.S., 2004c. Mechanisms of cardiac nerve sprouting after myocardial infarction in dogs. Circ Res. 95**,** 76-83.

Zicha, S., Xiao, L., Stafford, S., Cha, T.J., Han, W., Varro, A., Nattel, S., 2004. Transmural expression of transient outward potassium current subunits in normal and failing canine and human hearts. J Physiol. 561**,** 735-48.

Zipes, D.P., 1990. Influence of myocardial ischemia and infarction on autonomic innervation of heart. Circulation. 82**,** 1095-105.

Zuurbier, C.J., Emons, V.M., Ince, C., 2002. Hemodynamics of anesthetized ventilated mouse models: aspects of anesthetics, fluid support, and strain. Am J Physiol Heart Circ Physiol. 282**,** H2099-105.

Zweifel, L.S., Kuruvilla, R., Ginty, D.D., 2005. Functions and mechanisms of retrograde neurotrophin signalling. Nat Rev Neurosci. 6**,** 615-25.